ON THE FORMATION OF CHOLESTEROL AUTOXIDATION PRODUCTS IN LIPID BILAYERS AND ELECTROPHILIC SECOSTEROLS DERIVED THEREFROM

By

Emily Lydia Schaefer

A thesis submitted to the Department of Chemistry and Biomolecular Sciences in conformity with the requirements for the degree of Master of Science in Chemistry

University of Ottawa

Ottawa, Ontario, Canada

June 2019

Abstract

Lipid peroxidation is believed to play a key role in the onset and progression of degenerative disease. Interestingly, although cholesterol is the most abundant lipid in the human body, our understanding of its autoxidation and subsequent decomposition is relatively limited. In fact, until recently, cholesterol-7-hydroperoxide was accepted as the only primary product of cholesterol autoxidation in organic solution, however, our group exhibited that the 4-, 5-, and 6-hydroperoxides are also formed. Although this work facilitated thorough investigation of the complexities of both H-atom abstraction and addition in cholesterol autoxidation in organic solution, it did not account for the dynamic environment of a cell membrane. Herein, we report on the product distribution of these primary autoxidation products in lipid bilayers and how antioxidant supplementation, H-bonding interactions, and concentration of polyunsaturated fatty acid (PUFA) substrate influence both the product distribution and efficiency of autoxidation. Indeed, not only does H-bonding of the 3β-OH of cholesterol appear to shut-down C4 H-atom abstraction, the absence of kinetic chol-5α-OOH product is likely due to the poor potency of α-tocopherol (α-TOH), also as a result of H-bonding with phosphate head group of lipid membrane phospholipids. Therefore, within a lipid membrane the 7-hydroperoxide products predominate, consistent with literature precedent, however the factors involved are more complex than previously understood.

Moreover, with the authentic cholesterol hydroperoxides in hand, we sought to determine if the different regioisomers exhibit different cytotoxicity. Glutathione peroxidases (GPXs) are cytoprotective enzymes that reduce harmful hydroperoxides to benign alcohols *in vivo*. Using RSL3, a small-molecule inhibitor for GPX4, we were able to sensitize mammalian cells to ferroptotic cell death via administration of our exogenously prepared chol-OOHs. Surprisingly,

we found that the toxicities of each of 7α-OOH, 6β-OOH and 5α-OOH were only marginally augmented by RSL3 treatment, suggesting that they do not substantially sensitize cells to ferroptosis, perhaps because their decomposition to lipid peroxidation chain-initiating species (i.e. alkoxyl radicals) is not particularly efficient. Instead their cytotoxicities may derive from other mechanisms, such as the induction of apoptosis. This inspired our investigation of the fate of lipid hydroperoxides *in vivo*, namely the secondary products of the predominant 7-hydroperoxide species.

Acid-catalyzed Hock fragmentation, known for the industrial synthesis of phenol and acetone from cumene or implication in the generation of 4-hydroxynonenal (4-HNE), of 5α- and 6β-OOH has been shown by our group to produce highly electrophilic secosterol species; we sought to investigate the same decomposition mechanism for 7α-OOH in light of our investigations in the lipid membrane. Interestingly, we found that Hock fragmentation of 7α-OOH does not exhibit products resulting from the anticipated O-vinyl oxocarbenium intermediate, rather, the mechanism appears to funnel through an α-epoxy carbenium to produce unprecedented A-ring cleavage and epoxide products. Herein, we describe our thorough analysis of this chol-7α-OOH Hock fragmentation and attempts to investigate the presence of these products in biological samples, similar to previous analyses of similar products in atherosclerotic plaque extracts.

The products isolated and characterized through this work have provided new mechanistic insight with regards to the primary and secondary oxidation products of cholesterol *in vivo*; through further development of these findings, we hope to provide a better understanding of the implications of cholesterol oxidation in the pathogenesis of atherosclerosis.

Acknowledgements

First and foremost, I would like to express immense gratitude to Dr. Derek Pratt for his patience, guidance, invaluable expertise, and support over the past few years. As a reflection of his dedication, excellent work ethic, and passion for science, the environment of his research group fosters these qualities. I have been fortunate to be able to pursue graduate studies under such a capable mentor.

I have also been fortunate to have had several other mentors that have afforded me the opportunity to pursue graduate studies. I would like to thank Mrs. Sarah Woods, Dr. Amanda Starr, Dr. Mariana Gomez-Smith, and Dr. Markus Griesser for their immense support as both a high school and undergraduate student at the beginning of my scientific career – my opportunities and successes today are a result of their immense support both personally and professionally.

Of course, I have had the opportunity to have worked with some of the most intelligent, hard-working, funny, and kind people I have known during my graduate career. I would like to thank Evan Haidasz, Bo Li, JP Chauvin, Omkar Zilka, Luke Farmer, Kareem Harrison, Katie Shirley, Anas Abou-Zaid, Mark Raycroft, Demar Pitter, Jia-Fei Poon, Pierre Faudot dit Bel, Spencer Short, Neill Penner, Dmitry Saraev, as well as the several undergraduate and visiting students I have had the pleasure of working with and getting to know over the past few years. Laughs shared at the bench, the desk, or over drinks will serve as some of my fondest memories of graduate school. I have learned from each and every one of you, and I am grateful for the opportunity to have gotten to know all of you. I also had the fantastic opportunity to mentor Melodie Mallais as an undergraduate student and have been proud to have witnessed her growth into an extremely competent chemist and trusted colleague; I look forward to hearing of all of your success in the future.

I would like to give particular acknowledgement to Nadia Zopyrus for her immense efforts that laid the foundation for our studies on Hock fragmentation. Additionally, I would also like to thank Zosia Zielinksi and Ron Shah for their excellent mentorship throughout my degree; I cannot thank either of you enough for your time and indispensable advice.

Finally, I would like to thank my parents for their unwavering love and support – without your encouragement, this would not have been possible.

Statement of Originality

I hereby certify that all of the work described in this thesis is the original work of the author, with exceptions for work performed by collaborators noted in the preface to each chapter. The work in this thesis draws upon a great deal of previously published research. Any published (or unpublished) work by others is cited and fully acknowledged within the references.

Emily L. Schaefer

Table of Contents

List of Figures

List of Schemes

List of Tables

List of Abbreviations

4-HNE	4-hydroxynonenal
13-HPODE	13-hydroperoxyoctadecadienoic acid
AAPH	2,2′-azobis(2-methylpropionamidine) dihydrochloride
ACAT	acyl-CoA:cholesterol acyltransferase
AO	antioxidant
APCI	atmospheric-pressure chemical ionization
α-TOH	α-tocopherol
BDE	bond dissociation enthalpy
BHT	butylated hydroxytoluene (2,6-di-*t*-butyl-4-methoxyphenol)
BTSFA	bis(trimethylsilyl) trifluoroacetamide
Bu_2cAMP	dibutyryl cyclic adenosine monophosphate (bucladesine)
chol	cholesterol
chol-OOH	cholesterol hydroperoxide
COSY	^{1}H-^{1}H Correlated Spectroscopy
DEPT	distortionless enhancement by polarization transfer
DMVN	2,2'-azobis(2,4-dimethylvaleronitrile)
DMEM	Dulbecco's modified Eagle's media
DNPH	2,4-dinitrophenylhydrazine
DPBS	Dulbecco's phosphate buffered saline
DTUN	di-tert-undecylhyponitrite
ETC	electron transport chain
ESI	electrospray ionization
FBS	fetal bovine serum

GPX	glutathione peroxidase
H2BC	heteronuclear two-bond correlation
HAT	hydrogen atom transfer
HDL	high density lipoprotein
HEK 293	human embryonic kidney cell line
HOCl	hypochlorous acid
HMBC	heteronuclear multiple bond correlation
HPLC	high performance liquid chromatography
HPODE	hydroperoxyoctadecadienoate
HSQC	heteronuclear single quantum correlation
INADEQUATE	incredible natural abundance double quantum transfer experiment
IPA	isopropanol
KIE	kinetic isotope effect
LDL	low density lipoprotein
LOX	lipoxygenase
NMR	nuclear magnetic resonance spectroscopy
NOESY	nuclear Overhauser effect spectroscopy
MβCD	methyl-β-cyclodextrin
MEFs	mouse embryonic fibroblasts (Pfa1 cells)
MEM	minimum essential media
MeOAMVN	2,2'-azobis(4-methoxy-2,4-dimethylvaleronitrile)
MPO	myeloperoxidase
MS	mass spectrometry
MS/MS	tandem mass spectrometry
m/z	mass-to-charge ratio

PBS	phosphate-buffered saline
PDA	photodiode array
PDI	polydispersity index
PhOx	phagocyte oxidase
PLPC	1-palmitoyl-2-linoleoylphosphatidylcholine
PMA	phorbol myristate acetate
PPh_3	triphenylphosphine
PSYCHE	pure shift yielded by chirp excitation
PUFA	polyunsaturated fatty acid
ROS	reactive oxygen species
RTA	radical-trapping antioxidant
SCP-2	sterol carrier protein-2
S_Hi	intramolecular homolytic substitution
SIR	selected ion recording
SOD	superoxide dismutase
SOTS-1	superoxide thermal source (di(4-carboxybenzyl) hyponitrite)
StARD1	steroidogenic acute regulatory protein
TCE	trichloroethylene
TIC	total ion chromatogram
UPLC	ultra performance liquid chromatography
UV-Vis	ultraviolet visualization

CHAPTER 1 Background and Significance

1.1 Lipid Peroxidation

Lipid peroxidation is the radical chain process by which lipids are oxidized by molecular oxygen. Generally, lipid peroxidation is believed to have a negative impact on our health; peroxidation of polyunsaturated fatty acids (PUFAs), in particular, has been implicated in carcinogenesis[1,2] diabetes,[3] and neurodegenerative diseases,[4] however, lipid peroxidation is perhaps most often associated with the pathogenesis of atherosclerosis and associated cardiovascular diseases.

Hydrocarbon autoxidation is typically discussed in the context of engine oils and other industrial processes; however, lipid peroxidation is simply hydrocarbon autoxidation in the context of biological membranes and thus, these two processes share the same general mechanism. In short, upon generation of an initiating radical species, hydrogen-atom (H-atom) abstraction occurs from a relatively labile position on a hydrocarbon chain to generate a carbon-centred radical. This radical species then rapidly reacts with oxygen at rates approaching diffusion-control to generate a peroxyl radical species, followed by H-atom abstraction from another molecule of hydrocarbon, propagating the chain reaction. Radical species generated may eventually encounter one another in solution leading to non-radical termination products, or they encounter a good H-atom donor that may break the propagating radical chain.

The general mechanism for lipid peroxidation can therefore be illustrated using the same key steps of a free radical chain reaction, however, environmental factors unique to oxidation in biological systems are highlighted herein.

Scheme 1.1 A general mechanism for the free-radical chain reactions involved in lipid peroxidation (L = lipid).

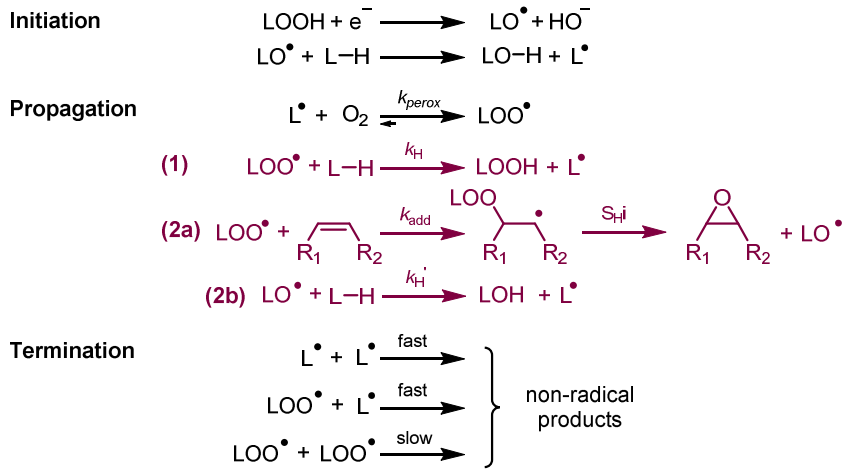

1.1.1 Initiation

In a biological system, initiation of lipid peroxidation can occur from a variety of endogenous or exogenous factors. Exogenous factors such as exposure to UV-light, ionizing radiation, and even exposure to ozone have all been proposed to initiate lipid peroxidation.[5–7] However, the endogenous generation of so-called reactive oxygen species (ROS) is believed to be particularly important. Of the myriad of compounds that are labeled 'ROS', hydroperoxyl radical (HOO•), the conjugate acid of superoxide ($O_2^{\bullet-}$), is arguably most important since it reacts with PUFAs much more rapidly than other substrates. However, it should be acknowledged that other 'ROS', such as hydroxyl radicals (HO•) or lipid alkoxyl radicals (LO•) derived from the reactions of hydrogen peroxide (H_2O_2) and/or lipid hydroperoxides with Fe^{2+}, are likely to also be important – especially at high concentrations of lipid hydroperoxides.[8]

The most significant source of ROS production occurs from the electron transport chain (ETC) of the inner mitochondrial membrane. Reduction of O_2 to $O_2^{\bullet-}$ as a consequence of electron leakage from the ETC is likely to occur at complex I (NADH dehydrogenase), complex III

(ubiquinone-cytochrome *c* reductase), or during electron shuttling by the semiquinone radical intermediate.[9,10] If superoxide is not oxidized back to molecular oxygen, it may react with nitric oxide to generate $ONOO^-$, or superoxide dismutase (SOD) can dismutate superoxide to hydrogen peroxide. Hydrogen peroxide can then either be detoxified to water and molecular oxygen by catalase or, via the Haber-Weiss process,[11] can generate a hydroxide ion and a highly reactive hydroxyl radical.

Scheme 1.2 Endogenous generation of ROS via electron leakage from complex I (NADH dehydrogenase) of the ETC. Adapted from Shadel and Horvath.[12]

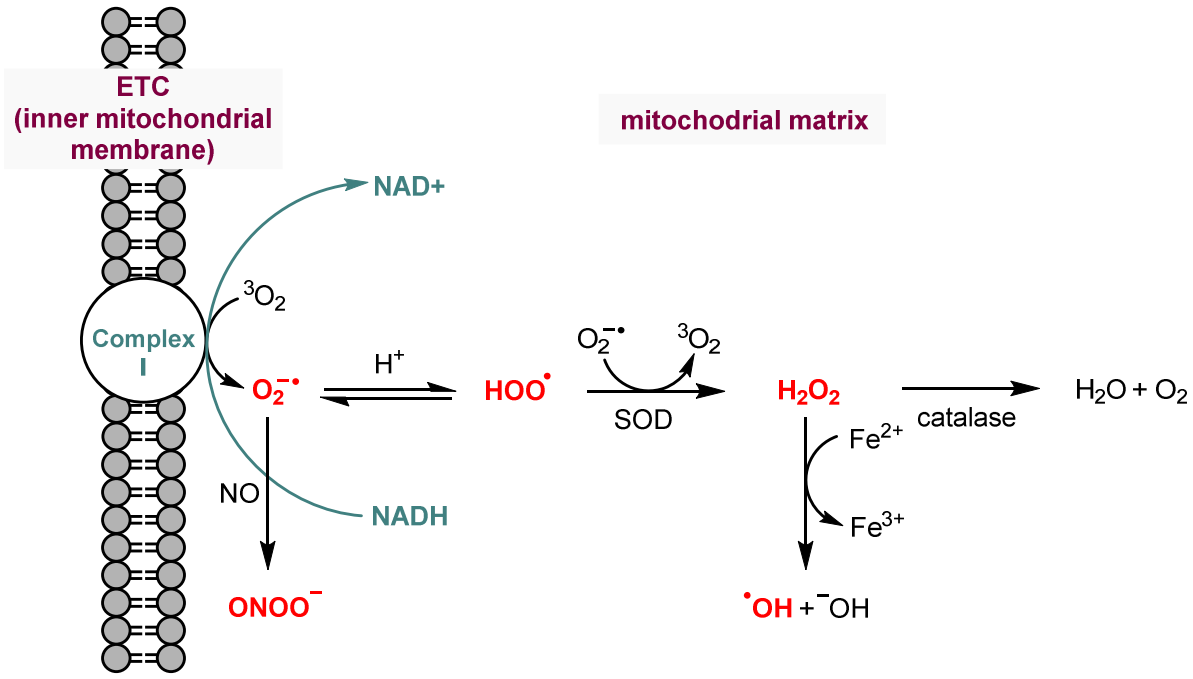

To initiate radical chain reactions for the purposes of *in vitro* studies, azo-initiators developed for the initiation of polymerization processes have been adopted as they allow for initiation at temperatures relevant to the experiment and provide a well-defined defined rate of initiation. For use in experiments that translate to biological models, lipid-soluble azo-initiators are often sought. To date, the most popular azo-initiator used in lipid oxidation experiments is

2,2'-azobis(4-methoxy-2,4-dimethylvaleronitrile) (MeOAMVN). Thermal decomposition of MeOAMVN occurs at physiologically relevant temperatures (37°C) with a sufficient half-life time and rate of decomposition to facilitate physiologically relevant experiments (**Scheme 1.3**).[13,14]

Scheme 1.3 Decomposition of lipid-soluble azo-initiator, MeOAMVN. Value obtained for ek_d determined in liposomes composed of soybean phosphatidylcholine and free cholesterol.[13]

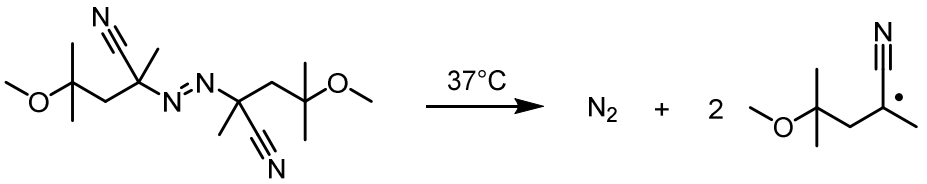

2,2'-azobis(4-methoxy-2,4-dimethylvaleronitrile)

MeOAMVN

ek_d = 3.3 X 10^{-6} s^{-1}; $t_{1/2}$ = 6 hours @ 37°C

1.1.2 Propagation

Upon generation of the initiating radical species, the free radical chain reaction is then propagated through rate-limiting abstraction of a labile hydrogen atom to generate a carbon-centred radical, subsequently followed by addition of molecular oxygen at near diffusion-controlled rates (k_{perox} = ~1.0 – 4.9 × 10^9 $M^{-1}s^{-1}$).[15] The resultant peroxyl radical (LOO•) is now the chain-carrying species as it can propagate the chain through abstraction of another labile H-atom or addition to an electron-rich double bond; incidentally, the steady-state concentration for LOO• is much higher than that of L• due to the rapid rate of oxygen addition relative to H-atom abstraction.[16]

When discussing the true oxidizability of a compound, it is important to consider both rate constant for propagation (k_p) and termination (k_t) for the substrate; the expression used to determine oxidizability is indicated in **eq. 1**.

$$\frac{k_p}{\sqrt{2k_t}} \quad (1)$$

As the rate-limiting step, the rate constant of propagation through H-atom abstraction from, or addition to, a substrate may be used as a relative measure of the oxidizability of one substrate compared to another.

Scheme 1.4 Bimolecular propagation rate constants for the H-atom abstraction of various lipid substrates. Values measured at 37°C in solution.[17]

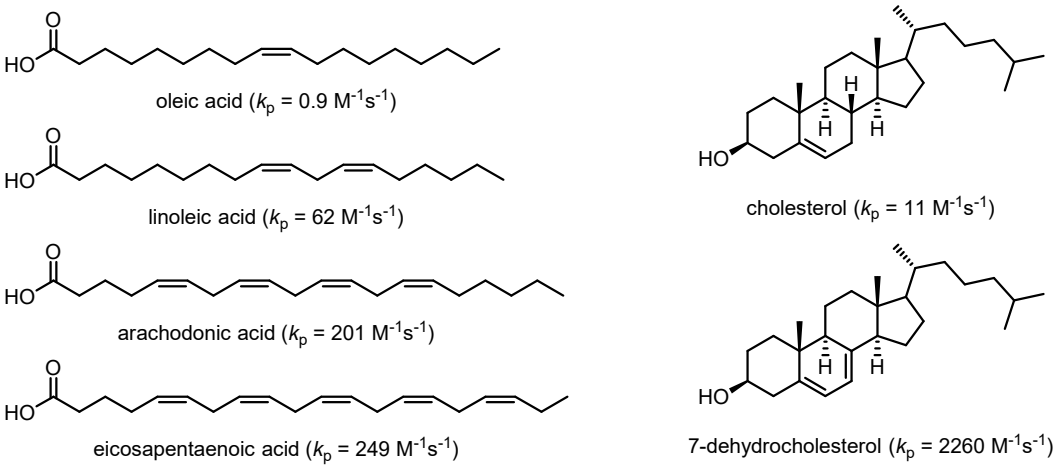

H-atom abstraction from mono- and poly-unsaturated substrates tends to be quite favourable due to the stability of the resulting allylic (or pentadienylic) radical species. In the case of PUFAs, the values for the bimolecular rate constants increase with the addition of each unsaturation; when comparing oleate and linoleate, the differences in their C-H bond dissociation energies of 10 kcal/mol is easily rationalized through the greater delocalization of the carbon-centered pentadienyl radical generated from H-atom abstraction of the bis-allylic position of linoleate.[18]

Scheme 1.5 Delocalized radical species generated upon H-atom abstraction from oleate, linoleate, cholesterol, and 7-dehydrocholesterol (7-DHC), respectively. H-atom abstraction from a single position on abbreviated scaffolds is shown for each compound, however, other positions are possible.

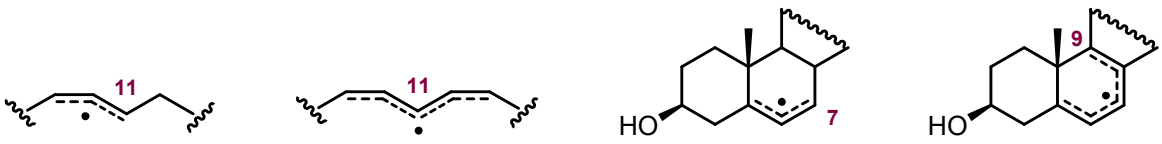

Additionally, delocalization of these allylic radical species affords a very diverse product distribution upon addition of molecular oxygen; peroxyl radicals generated therefrom will typically abstract a hydrogen atom to form their corresponding hydroperoxide, however, peroxyl radical species that are less stable undergo β-fragmentation, the reverse of oxygen addition, at a rate that is competitive with H-atom abstraction. Therefore, kinetic products can be selectively favoured in the presence of a good H-atom donor that competes with the rate of β-fragmentation of the peroxyl radical species. For example, in the case of linoleate autoxidation, products resulting from the addition of oxygen at the C11 position are not typically observed despite the high spin-density at this position,[19] however, in the presence of a good H-atom donor, such as α-tocopherol ($k_{inh} = 3.2 \times 10^6\ M^{-1}s^{-1}$ in styrene),[20] the rate of hydrogen atom transfer (HAT) is competitive with that of β-fragmentation ($k_\beta = 2.6 \times 10^6\ s^{-1}$), and so the kinetic C11-hydroperoxide product is observed.[21] Thermodynamic conjugated products are predominant in the absence of a good H-atom donor owing to the strength of their C-OO bond and low rate of β-fragmentation.[22] Notably, the ratio of kinetic versus thermodynamic hydroperoxyoctadecadienoate (HPODE) products has been used to determine the k_{inh} of antioxidants in lipid bilayers,[23,24] and as an indicator of the concentration of H-atom donors in biological media – particularly for that of α-tocopherol.[25–27]

Scheme 1.6 Partial mechanism of linoleate autoxidation and associated product distribution of HPODEs in the presence and absence of a good H-atom donor. Products arising from oxygen addition at C9 of the pentadienyl radical were excluded for brevity, but follow a similar mechanism with similar rate constants. Linoleate scaffold abbreviated for clarity. Adapted from Yin et al.[5]

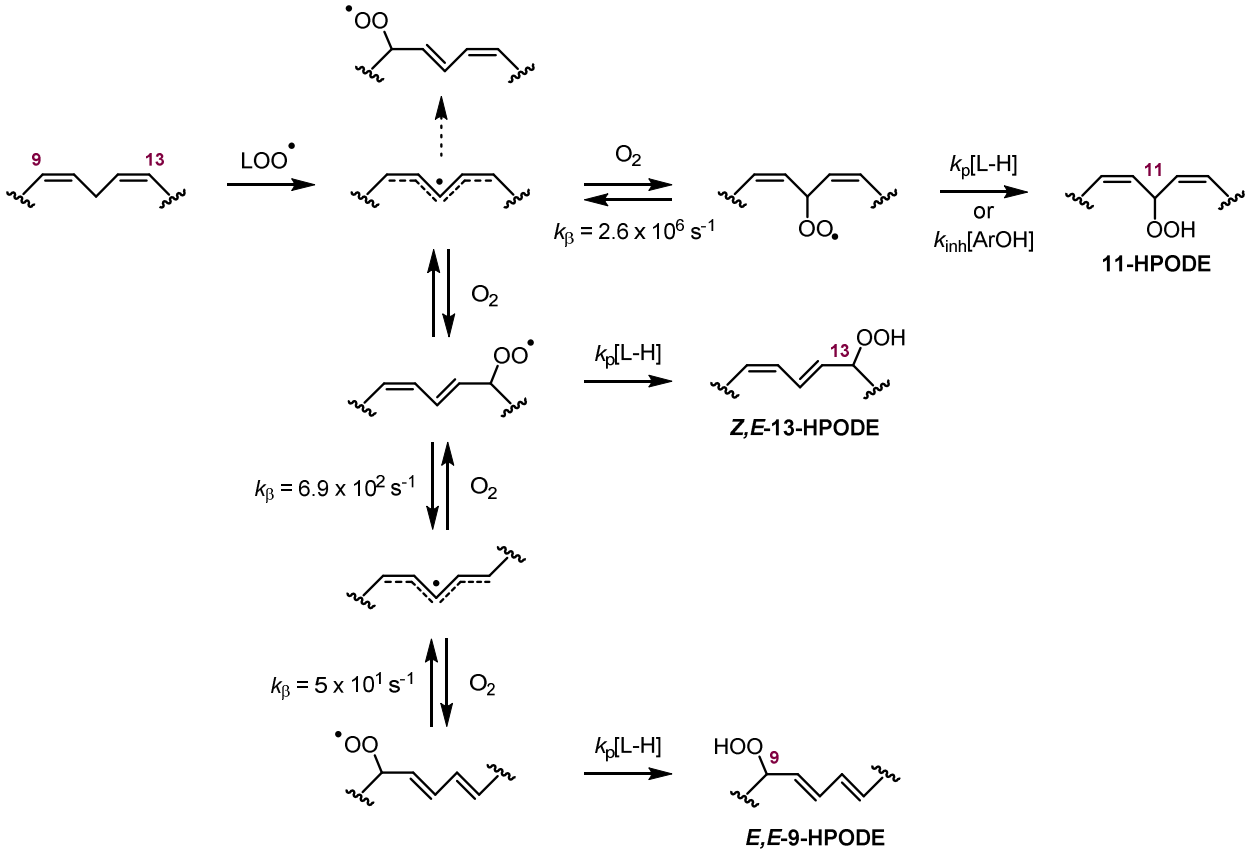

In addition to peroxyl radicals, other oxygen-centred radicals can serve as the chain-carrying species in propagation. Product distributions may be influenced by a phenomenon referred to as antioxidant-mediated peroxidation, where in cases of high antioxidant (AO) concentration, the AO actually acts as a prooxidant because the high steady-state concentration of AO-derived radical competes with the chain-carrying LOO• for propagation, such that the AO-derived radical becomes the chain-carrying species. Oxidation in low-density lipoprotein (LDL), an area rich in the lipid-soluble radical-trapping antioxidant (RTA) α-tocopherol (α-TOH), undergoes tocopherol-mediated peroxidation because the steady state concentration of the α-TO•

is much higher than that of the LOO•. This effect can be attenuated with the use of a co-antioxidant, such as water-soluble ascorbate or lipid-soluble ubiquinol.[28,29]

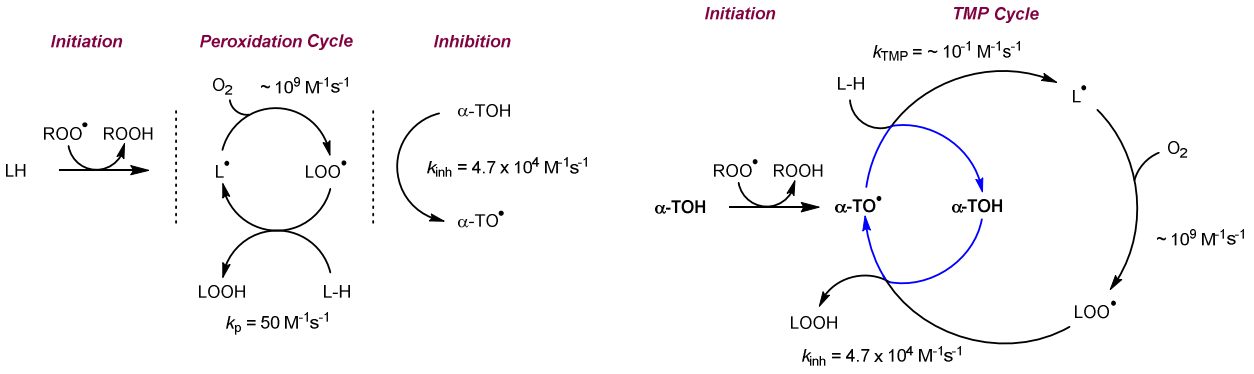

Figure 1.1 Inhibition of lipid peroxidation with α-TOH serving as an RTA (left) versus tocopherol-mediated peroxidation (TMP, right). The k_{inh} value for α-tocopherol was determined in PLPC liposomes at 37°C.[24] Adapted from Bowry and Stocker.[28]

Propagation does not occur via H-atom abstraction for all oxidizable substrates; substrates containing double bonds are also prone to undergo peroxyl radical addition to generate a carbon-centred radical. In the case of peroxyl radical addition, intramolecular homolytic substitution (S_Hi) resulting in epoxide formation is competitive with HAT in some substrates, and generation of an alkoxyl radical (RO•) may initiate another chain reaction.

Scheme 1.7 Peroxyl radical addition and subsequent S_Hi to generate an epoxide species and propagate the free radical chain reaction.

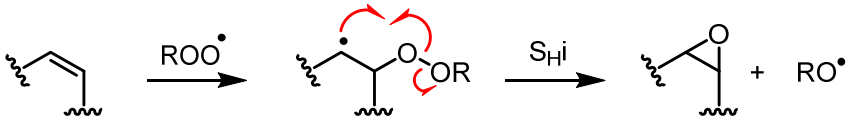

Peroxyl radicals themselves may also undergo intramolecular cyclization to form endoperoxide species with very interesting downstream products, perhaps most notably the isoprostanes generated from arachidonic acid oxidation.[30]

1.1.3 Termination

As shown in **Scheme 1.1**, termination occurs upon combination of two radical species to form non-radical products (NRPs), thus terminating the chain reaction. Although it is relatively unlikely that two radical species will encounter one another in solution given their extremely low concentration, the rate of radical-radical reactions are so rapid that they can be competitive with propagation. Values measured for k_t of secondary peroxyl radical species typically range from 10^6-10^7 $M^{-1}s^{-1}$,[31] making them several orders of magnitude larger than the aforementioned k_p values.

The rate of termination may also be enhanced by physical or environmental factors. For example, the biphasic character of a phospholipid membrane may enhance termination relative to homogenous solution due to the diffusion of the polar peroxyl radical moiety from the non-polar oxidizable interior to the inert polar interface, decreasing the efficiency for peroxyl-mediated propagation and increasing the chance of peroxyl-peroxyl encounter towards termination.[32] Overall, the system in which the chain reaction occurs will impact the general oxidizability of the substrate in question, and possibly the products that evolve therefrom.

Due to their relatively high steady-state concentration (compared to an alkyl radical), the most common proposed mechanism of termination of autoxidation is via reaction of two peroxyl radicals. This reaction is expected to proceed via Russell termination, as shown in **Scheme 1.8**, in which decomposition of the tetroxide intermediate evolves molecular oxygen, and carbonyl and alcohol moieties as NRPs.[33] Although these carbonyl and alcohol species are relatively innocuous compared to their hydroperoxide counterparts generated during propagation, their relative persistence can make them useful biomarkers of oxidative stress.

Scheme 1.8 Termination of two peroxyl radicals to generate non-radical products via Russel termination.

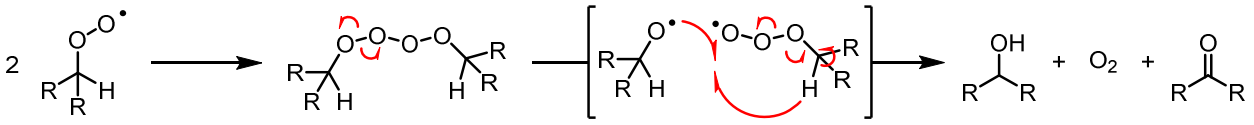

1.1.4 Inhibition of Lipid Peroxidation

Natural and designer RTAs have been used to inhibit or slow oxidation in biological and industrial contexts for decades. As aforementioned, inhibition of oxidation typically occurs at the propagation step of lipid peroxidation in which the chain-carrying peroxyl radical is intercepted by either H-atom abstraction from, or addition to, an AO, trapping the radical species and preventing further propagation; the AO responsible is referred to as a chain-breaking AO.[34] Nature's premier lipid-soluble RTA, α-TOH (Vitamin E), and the ubiquitous food additive, butylated hydroxytoluene (BHT), are generally the two most recognizable AOs, however, their relatively poor capacity for inhibition of oxidation for industrial (and even biological) use has led to the popularity of altered phenolic and diarylamine scaffolds as industrial standards for the inhibition of engine oil and lubricant degradation.[16,34,35]

More recently, ferrostatin-1 (Fer-1), liproxstatin-1 (Lip-1), and C_{15}-tetrahydronapthyridinol (C_{15}-THN) have been shown to serve as potent RTAs for the subversion of cell death mediated by lipid peroxidation.[36,37] Additionally, the capacity for these RTAs to subvert this cell death modality has been correlated with their potency as RTAs such that potent RTAs derived from industrial and pharmaceutical aminic RTA scaffolds such as diarylamine, phenoxazine, and phenothiazine have also been illustrated to inhibit lipid peroxidation in

mammalian cell models;[38,39] details on ferroptosis, the cell death modality in question, will be detailed in the forthcoming section.

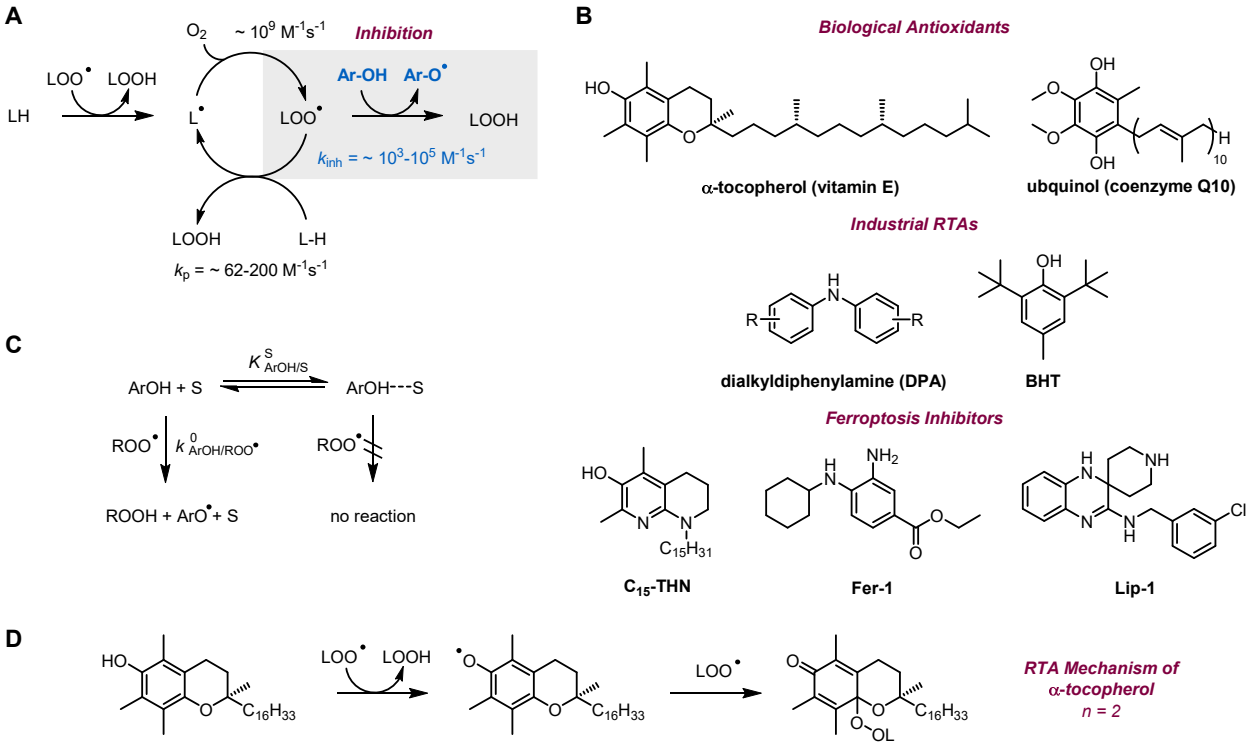

Figure 1.2 Inhibition of lipid peroxidation using RTAs. A general mechanism for inhibition (**A**), examples of some RTAs (**B**), the expression used to illustrate the impact of kinetic solvent effects on the efficacy of hydrogen atom abstraction by an AO (**C**), and the putative mechanism of radical trapping by α-TOH (**D**). $K^{S}_{ArOH/S}$ is the equilibrium constant for the formation of a hydrogen bond complex with the antioxidant, in this representation an aryl alcohol (ArOH), and the solvent (S), while $k^{0}_{ArOH/ROO•}$ is the rate constant for reaction of ROO• with non-hydrogen bonded ArOH.

The potency of an RTA is dependent upon several factors. Bond dissociation energy (BDE) of the X-H bond to undergo H-atom abstraction may serve as an indicator of potency of an RTA, however, this is not always indicative of the potential for subsequent addition of a peroxyl radical, nor does it consider environmental factors impacting HAT. In the context of lipid peroxidation, and particularly that of inhibition by α-TOH, kinetic solvent effects (KSE) induced by H-bonding capacity of the solvent can greatly influence the potency of an AO. As illustrated in **Figure 1.2C**,

the H-bonding acceptor (HBA) properties of the solvent can prevent H-atom abstraction by the peroxyl, preventing inhibition of oxidation by the RTA.[40] Therefore, an RTA that appears to be potent in organic solution with low HBA capacity may exhibit very different potency in aqueous solution or a lipid membrane.[38]

Although α-TOH is Nature's premier lipid-soluble RTA, it exhibits relatively poor reactivity as an RTA in comparison to most designer RTAs, particularly upon assessment in liposomal phospholipid membrane models. Relative values of k_{inh} determined by inhibited co-autoxidations of egg-phosphatidylcholine (egg PC) liposomes and STY-BODIPY reveal this stark contrast.[37,38,41]

A

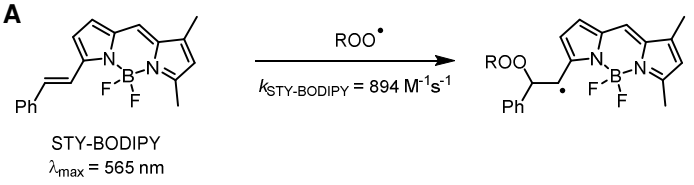

$$\frac{-\delta[\text{STY}-\text{BODIPY}]}{\delta t} = \frac{k_{\text{STY}-\text{BODIPY}}[\text{STY}-\text{BODIPY}]R_i}{nk_{inh}[\text{RTA}]} \qquad n = \frac{t_{inh} \times R_i}{[\text{RTA}]}$$

B

RTA	k_{inh} ($M^{-1}s^{-1}$)	*n*
α-TOH	(4.7 ± 0.4) x 10^3	2.0
Fer-1	(4.6 ± 0.8) x 10^4	3.1
Lip-1	(1.2 ± 0.1) x 10^4	3.5
C_{15}-THN	(9.3 ± 0.4) x 10^4	2.0
DTB-DPA	(2.5 ± 0.1) x 10^4	1.8
Phenothiazine	(2.1 ± 0.3) x 10^5	1.9
Phenoxazine	(4.5 ± 0.5) x 10^5	1.9

Figure 1.3 Inhibited co-autoxidations of STY-BODIPY in egg-PC liposomes at 37°C. Values for rate constants of inhibition are determined quantitatively through monitoring of the disappearance of signal at 565 nm upon oxidation of STY-BODIPY using the expression illustrated (**A**). Relative k_{inh} values are presented with their corresponding stoichiometries (**B**).[37,38]

Alteration and optimization of these RTA scaffolds have led to even more potent RTAs therapeutic potential in their ability to inhibit lipid peroxidation in mammalian cell models, namely to subvert ferroptotic cell death,[39,42] far exceeding the potency of naturally occurring α-TOH.

1.1.5 Ferroptosis: Accumulation of Phospholipid-Derived Hydroperoxides Resulting in Iron-Dependent Cell Death

Ferroptosis, an iron-dependent form of necrotic cell death, has been heavily associated recently in the pathogenesis of diseases in which lipid peroxidation is implicated. Ferroptotic cell death occurs upon the accumulation of (phospho)lipid-derived hydroperoxide species generated via free radical autoxidation or enzymatic oxidation, leading to eventual cell membrane degradation. This is characterized morphologically as cell swelling, which starkly contrasts the shrinking and blebbing observed during apoptotic cell death.[43]

Effective inhibition of ferroptosis has been observed through administration of RTAs to inhibit propagation and slow the accumulation of (phospho)lipid hydroperoxides; similarly, the use of iron chelators prevent the one-electron reduction of LOOH to LO• that can further propagate the chain.[44] Enzymatic oxidation of PUFAs by lipoxygenase (LOX) enzymes is attenuated by the administration of specific LOX inhibitors, however, it is interesting to note that most of these inhibitors display radical-trapping behaviour.[45]

For the purpose of mechanistic studies, ferroptotic cell death can be induced through a variety of methods, however, the most popular of these methods intervene in the reduction of (phospho)lipid hydroperoxides to their corresponding alcohols by the enzyme glutathioneperoxidase-4 (GPX4). Covalent inhibition of the active site selenol by the small molecule (1*S*,3*R*)-RSL3 is one of the most popular methods of inducing GPX4-mediated ferroptosis,[44] however, indirect depletion of glutathione through inhibition of the glutamate-cystine antiporter, system x_c^-, by the small molecule erastin[46] or inhibition of glutathione biosynthesis using buthionine sulfoximine (BSO)[47] are other possible methods.

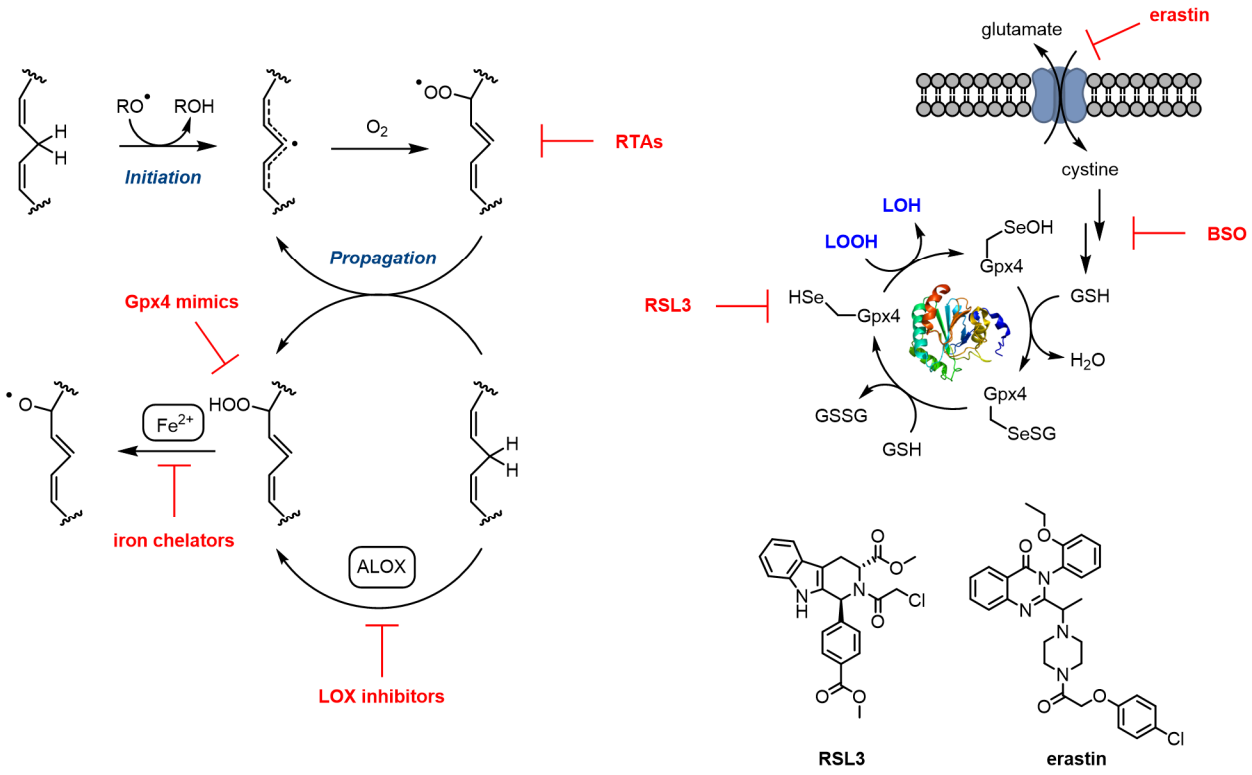

Figure 1.4 Accumulation of lipid-derived hydroperoxides generated via autoxidation and lipoxygenase-catalyzed oxidation of PUFAs (left) and the mechanism for enzymatic reduction of lipid-derived hydroperoxides by GPX4 (right). Possible sites of inhibition of either mechanism indicated in red. Adapted from Shah et al.[38]

Initial investigations of this cell death pathway originally suggested that enzymatic oxidation was the driving force of ferroptosis because inhibition of lipoxygenase enzymes was cytoprotective,[36,48] however, recent findings from our group have shown that inhibition of lipid peroxidation through the use of potent lipophilic RTAs slows ferroptotic cell death, suggesting that autoxidation is the major contributor to this process.[37,38,45] Interestingly, ferroptotic cell death appears to be independent of the nature of hydroperoxide species administered, suggesting that this unique cell death pathway may arise from autoxidation of lipids other than just PUFAs; this presents major implications for the accumulation of any lipid-derived hydroperoxides, including those derived from autoxidation of sterol molecules.

1.1.6 The Fate of Lipid Hydroperoxide Species In Vivo

Upon generation and accumulation of lipid hydroperoxide species, these relatively labile species may undergo decomposition to a variety of secondary autoxidation products. Possible fates of hydroperoxide species *in vivo* include reduction by GPX4 to their relatively innocuous corresponding alcohols,[49–51] dehydration to afford electrophilic ketone species,[25,52] one-electron reduction by iron to form alkoxyl or hydroxyl radicals capable of initiating further chain reactions or undergo intramolecular rearrangement,[53–55] and acid-catalyzed fragmentation to form labile lipid-derived electrophiles.[56–59] Despite some investigation of these fates, our understanding of the dominant mechanism of LOOH decomposition in different cell death processes, such as apoptosis or ferroptosis, is poorly understood. As previously noted, the most commonly detected biomarkers for lipid peroxidation include lipid-derived alcohols and ketones as they are relatively persistent compared to their more electrophilic aldehydic and epoxide counterparts, however, the inherent lability of their electrophilic counterparts not only makes them more difficult to detect, but also implies their rapid reactivity with biological nucleophiles is the source of their cytotoxicity.

Acid-catalyzed fragmentation, or "Hock" cleavage, of hydroperoxides to electrophilic carbonyl species has been invoked in industrial processes and in the evolution of secondary products of autoxidation *in vivo*. The first reported account of acid-catalyzed fragmentation of a hydroperoxide to generate two carbonyl fragments came from the lab of Heinrich Hock in 1936 in which cyclohexene hydroperoxide was shown to decompose to the carboxaldehyde upon treatment with sulfuric acid.[60,61]

Scheme 1.9 Decomposition of cyclohexene hydroperoxide to cyclopentanecarboxaldehyde under acid-catalyzed cleavage conditions. Adapted from Frimer.[62]

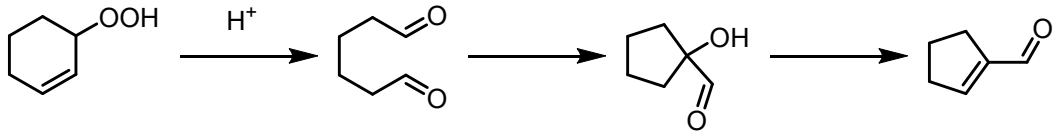

The latter steps can be easily explained through an internal aldol condensation of the hexane-1,6-dial followed by dehydration, however the cleavage to two carbonylic fragments requires rearrangement via migration of the vinylic substituent; this mechanism that has been shown to be applicable to several functional groups of different migratory aptitudes where cyclobutyl > aryl > vinyl > hydrogen > cyclopentyl ≃ cyclohexyl >> alkyl.[63] In the case of allylic hydroperoxides, the migrating group is typically vinylic. This is illustrated in the mechanism of acid-catalyzed fragmentation of cumene hydroperoxide in the industrial synthesis of acetone and phenol, termed the "cumene process".[64]

Scheme 1.10 Industrial synthesis of phenol and acetone through acid-catalyzed Hock fragmentation of cumene hydroperoxide.

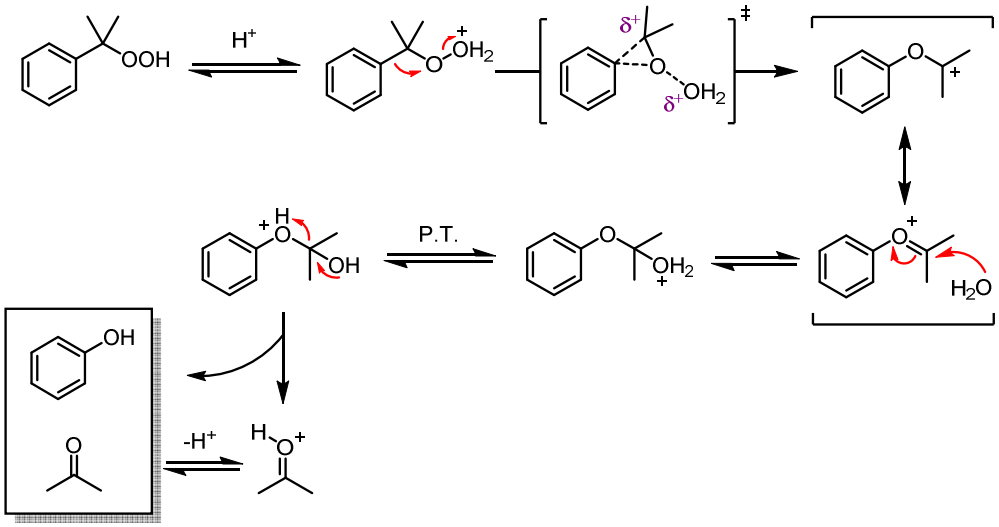

Evidence for Hock cleavage is also apparent in biological contexts – some of the most vilified electrophilic species are carbonylic compounds, typically aldehydes, that result from Hock

cleavage of primary lipid peroxidation products. Perhaps the most notorious is 4-hydroxy-2*E*-nonenal (4-HNE), a highly electrophilic α,β-unsaturated hydroxyalkenal which has been shown to impact cell signal transduction,[65] adduct to DNA-bases,[66] and participate in the pathogenesis of Alzheimer's disease, Parkinson's disease, atherosclerosis, and even cancer.[67] Although the pathological implications of 4-HNE were investigated heavily following its identification in 1980 as a secondary product of lipid peroxidation,[68] a mechanism of its formation was not identified until 2001 by Schneider et al as Hock cleavage of linoleate-derived hydroperoxides,[59,69] as shown in **Scheme 1.11**. Other potent aldehydes, including acrolein, malondialdehyde, and 4-hydroxyhexenal, have been suggested to form endogenously through Hock fragmentation of peroxidized polyunsaturated lipids.[70]

Scheme 1.11 Two proposed mechanistic routes to 4-HNE from linoleate autoxidation-derived 13-hydroperoxyoctadecadienoic acid (13-HPODE) via Hock fragmentation of the dihydroperoxy species. Adapted from Schneider et al.[59,69]

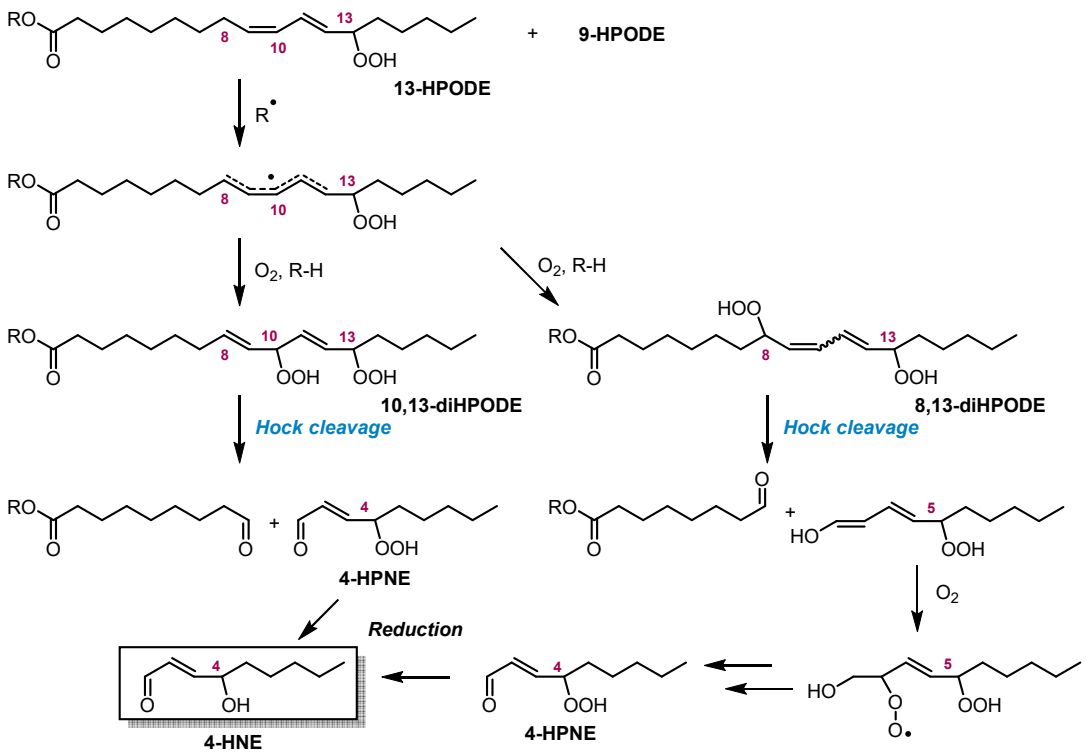

Alternatively, it is possible to form epoxide species from allylic hydroperoxides under similar acid-catalyzed conditions. Upon treatment with 0.1 M H_2SO_4 in 9:1 methanol:water, Gardner and coworkers observed an intramolecular rearrangement of 13-HPODE to a 12,13-epoxide species, rather than cleavage to the expected hexanal and dodecenoic acid product, followed by immediate capture of the carbocation by solvent,[58] as shown in **Scheme 1.12**. The resulting epoxide product predominates and comprises ~ 18 mol % of the recovered yield, however, some dihydroxy and hydroxy-methoxy solvolysis products are observed. Although this is not a true Hock *cleavage*, this alternative mechanism does present a possible route to other potent lipid-derived electrophilic species.

Scheme 1.12 Proposed mechanism for *trans*-epoxide formation via acid-catalyzed intramolecular rearrangement of 13-HPODE. Structures are abbreviated for clarity. Brackets include a postulated intermediate, but was not identified in preparative isolations. Adapted from Gardner et al.[58]

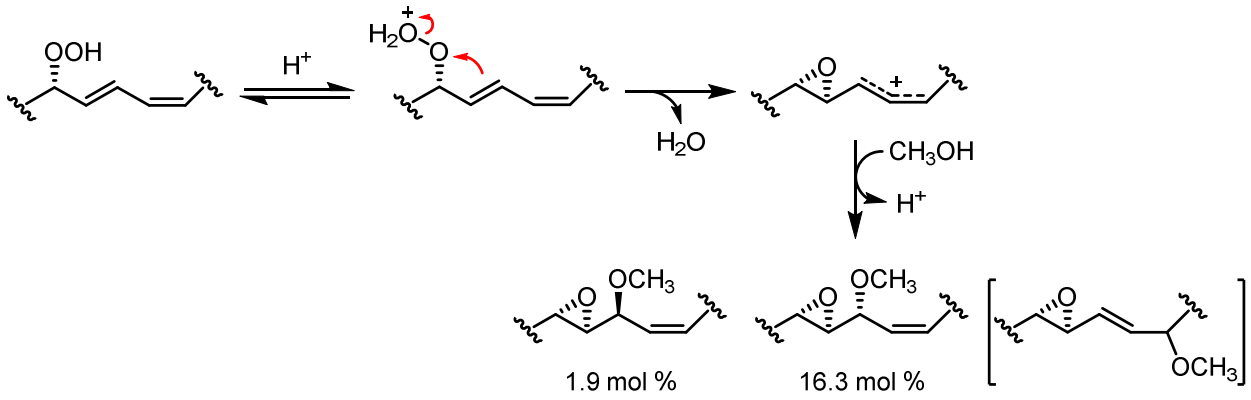

1.1.7 Role of Lipid-Derived Electrophiles in Mechanisms of Cell Death and Pathogenesis of Disease

Secondary autoxidation products, namely lipid-derived electrophiles, and their potential to covalently modify biological nucleophiles are a major factor implicating lipid peroxidation in the progression of atherosclerosis, Alzheimer's disease (AD), and Parkinson's disease (PD). Of the aforementioned lipid-derived electrophilic species, their electrophilic potential for reaction with

biological nucleophiles often dictates their potential cytotoxicity and association with disease pathogenesis. Aldehydes, often the most vilified of all lipid-derived electrophiles, are extremely prone to reaction with biological nucleophiles and can covalently modify nucleophilic moieties of proteins and nucleic acids in a similar manner to ketone and epoxide species.[71]

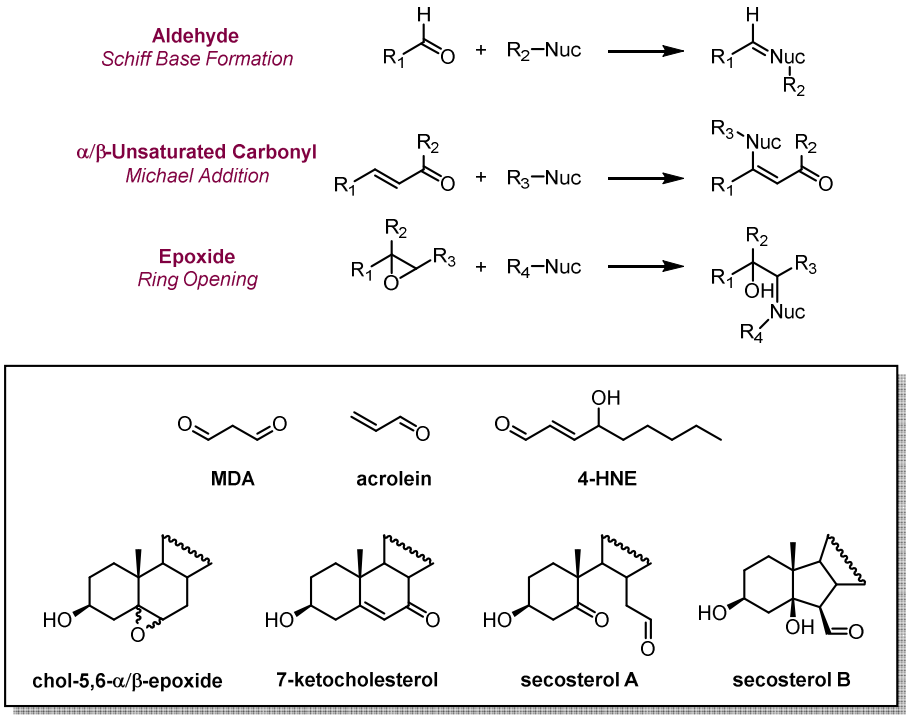

Figure 1.5 Potential reactivity of biological nucleophiles with lipid-derived electrophiles and examples of some lipid-derived electrophilic species. C and D rings of sterol scaffolds abbreviated for clarity.

Characterized by the deposition of plaques on the inside of arterial walls, atherosclerosis is one of the leading causes of heart attack and stroke. Formation of atherosclerotic plaques begins with the subendothelial accumulation of macrophages within the arterial wall to produce lesions referred to as fatty streaks. These particular macrophages are referred to as foam cells due to their "foamy" appearance from the accumulation of lipids (i.e. cholesterol, PUFAs, and triglycerides) within the cells. The resulting accumulation of foam cells within the arterial wall leads to

inflammation and formation of a plaque.[72] If the fibrous cap on the outside of the plaque is weakened, the plaque will rupture leading to thrombosis; in most cases of heart attack and stroke, the production of a thrombus due to the rupture of an atherosclerotic plaque is the direct cause of the infarction.[72–74] Additionally, it has been well established that the oxidative modification of LDL occurs *in vivo*[75–77] and this oxidized form of LDL (ox-LDL) has a much greater rate of uptake by macrophages than native LDL.[78] One of the first reports of the cytotoxic effects of ox-LDL suggests that oxidative modification occurs via a free radical mechanism, likely leading to the formation of primary and secondary autoxidation products.[79] Since this report, oxidation of LDL *in vivo* has been widely implicated; for example, oxidation of LDL by metal ions,[80] thiol,[81–83] superoxide,[84] and lipoxygenase[85,86] have all been reported.

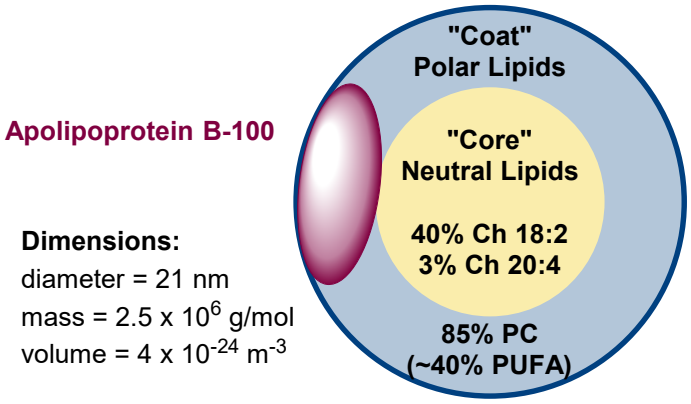

Figure 1.6 General components of a typical LDL particle. The non-polar oxidizable "core" typically consists of cholesterol esterified with linoleate (18:2) and arachidonate (20:4), while the polar outer "coat" consists of mainly polar phosphatidylcholine heads esterified to PUFAs, some triglycerides, and free cholesterol. Each particle contains an apolipoprotein B-100 moiety for stabilization of the structure. Adapted from Bowry and Ingold.[29]

At this time, there is still limited knowledge regarding the specific mechanism by which lipid peroxidation in LDL impacts the exacerbation or generation of atherosclerotic plaques, however,

several publications have implicated lipid-derived electrophiles for their reported proatherogenic effects.

In addition to cardiovascular disease, lipid-derived electrophiles have been implicated in neurodegenerative disease. AD is a poorly understood chronic neurodegenerative disease associated with symptoms such as memory loss, behavioural changes, problems with language, and lack of motivation. Inflammation triggered by the immune response to the binding of misfolded and aggregated proteins, such as amyloid-β, to receptors on astroglia and microglia appears to exacerbate disease progression, likely due to enhanced oxidative stress among other possible immune responses.[87] As such, the same covalent modification by lipid-derived electrophiles triggering aggregation of amyloid-β fibrils in atherosclerotic lesions has also been invoked to exacerbate amyloidogenesis in brain tissue.[88,89]

Although the mechanism by which lipid-derived electrophiles exacerbate the aforementioned disease pathologies is unclear, the reactivity of these molecules is suggestive of covalent modification of proteins and other biological nucleophiles. Further investigation of these compounds, and determination of the abundance of particular lipid-derived electrophiles in areas of disease pathology, will help to elucidate the role of lipid peroxidation in disease.

1.2 Cholesterol Autoxidation

Cholesterol, the most abundant lipid in the human body, comprises ~ 50 mol% of all lipids in the membranes of our cells.[90] In mammalian cell membranes, cholesterol is incorporated to maintain stability and fluidity;[91] other sterol lipids of a similar scaffold play a similar role in their respective species. Cholesterol also serves as the point of departure for the endogenous synthesis of steroid

hormones. For example, following conversion of cholesterol to pregnenolone by P_{450} enzymes, steroid hormones such as cortisol, progesterone, estradiol, and testosterone can be biosynthesized.[92]

Scheme 1.13 General structure and numbering assignment of a sterol scaffold (left), cholesterol (centre), and a 3-dimensional representation of cholesterol (right).

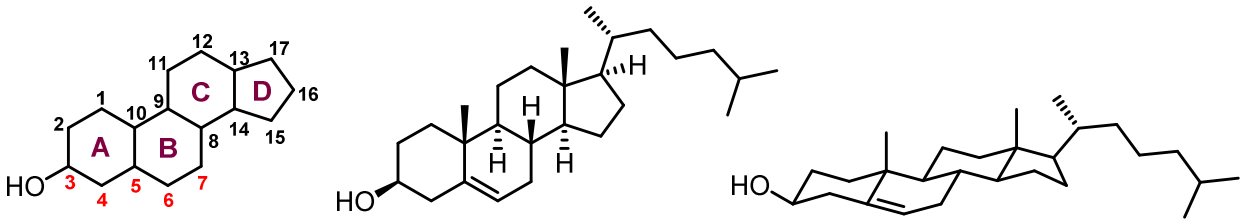

Although it is integral to the biosynthesis of hormones and maintenance of stability and fluidity in mammalian cell membranes, cholesterol is considered the most vilified of all lipids due to its abundance and susceptibility to oxidation. In comparison to PUFAs such as linoleate and arachidonate, monounsaturated cholesterol is much less oxidizable, however, its high concentration in the cell membrane compensates for its relatively low oxidizability. Resultant primary and secondary products of cholesterol autoxidation have been implicated in the pathogenesis of disease either as a proposed consequence of their decomposition or their detection in diseased tissue, much like their PUFA-derived counterparts.

Mechanisms for cholesterol autoxidation have appeared in the literature for the last 60 years, however, the complex product distribution was never fully realized until recently. Two possible routes for propagation of this free radical chain reaction and resultant products derived therefrom have been proposed and investigated: (1) H-atom abstraction from either the C4 or C7 positions to eventually generate hydroperoxide species or (2) addition to the $\Delta^{5,6}$ double bond followed by S_Hi to generate epoxide species.

Scheme 1.14 General representation of cholesterol autoxidation mediated by either H-atom abstraction or addition pathways in the propagation step. Adapted from Xu and Porter.[93]

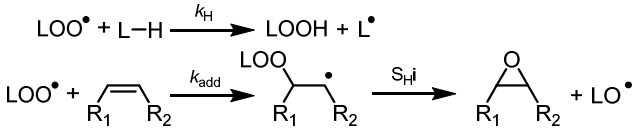

Interestingly, the most frequently observed oxysterol compounds are proposed to originate from C7 H-atom abstraction, and are products resulting from the rapid addition of molecular oxygen to the C7 position.[52,94,95] Namely, these products include the primary autoxidation product, cholesterol-7-hydroperoxide (chol-7-OOH), and the secondary products of its reduction, 7-hydroxycholesterol (chol-7-OH) and 7-ketocholesterol (7-keto);[96] chol-7-OH and 7-keto may also arise as a consequence of Russell termination of two chol-7-OO• radicals, similar to that shown in **Scheme 1.8.**[97] Although reaction of oxygen at the C5 position is possible, products of this character have never been observed *in vivo*, likely due to the rapid rate of β-fragmentation of the C5-peroxyl radical;[98] additionally, the C5 hydroperoxide has been shown to readily undergo Schenck rearrangement in non-polar solvents to the C7 hydroperoxide species.[99] However, minimal endogenous generation of chol-5α-OOH has typically been ascribed to oxidation by the high energy oxidant, singlet oxygen ($^1O_2$).[100–102]

Many researchers have speculated that abstraction of the C4 hydrogen atom is possible as the expected thermodynamic barrier to abstraction would likely be similar to that of C7-H abstraction, however, the resultant 4- and 6-hydroperoxide products had never been directly observed. Instead, chol-4α/β-OH have been observed *in vivo*, suggesting that these products do indeed arise from the reduction of their corresponding autoxidation-derived hydroperoxide.[103–106] Similarly, ketogenic oxysterols proposed to be a result of chol-6-OOH oxidation have also been observed *in vivo*.[100]

Scheme 1.15 Proposed mechanism of cholesterol autoxidation (c. 2011) based upon products isolated and observed from *in vivo* studies. Cholesterol scaffold abbreviated for clarity. Adapted from Yin et al.[5]

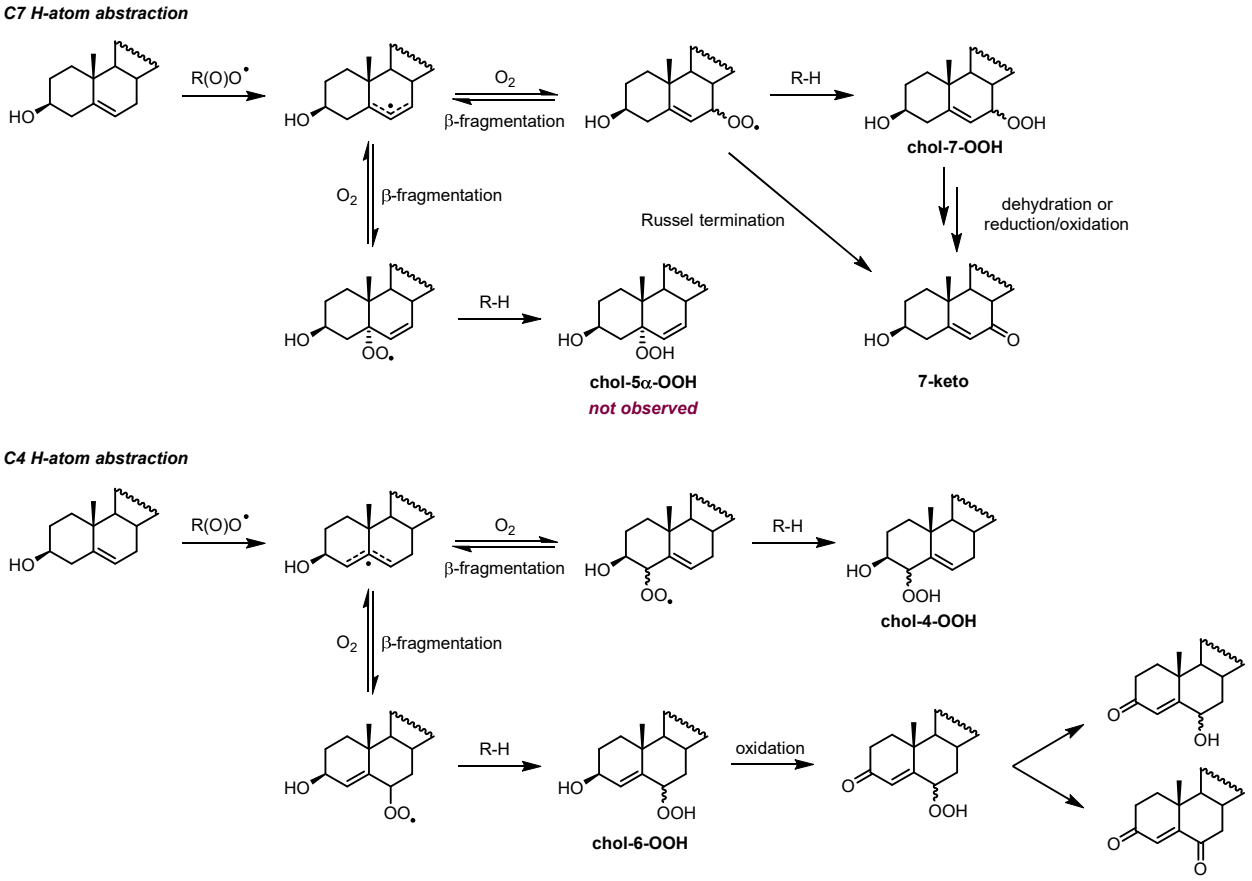

Recent investigations by our group[56,107] have provided a much more complete understanding of the mechanism for cholesterol autoxidation and will be detailed in Chapter 2.

1.3 On the Origin of Secosterols: The Fate of Cholesterol Hydroperoxide Species *In Vivo*

Upon autoxidation of cholesterol, the primary products generated decompose through a variety of mechanisms to form secondary products which are classically electrophilic in nature. Although hydroperoxide species themselves do not exhibit relevant reactivity, the lability of the species results in their relatively rapid decomposition. The aforementioned fates of lipid hydroperoxide species *in vivo* help to explain their role in the pathogenesis of disease, however, the origin of some

of the most deleterious of these species is still unclear. Herein, we detail the controversial proposed origin of the highly electrophilic secosterol species allegedly identified in atherosclerotic plaque and brain tissue, the alternative proposed mechanisms of their formation, and the other possible oxysterol species formed via similar mechanistic routes.

1.3.1 Debunking Endogenous Ozone

In a series of papers published in *Science* in the early 2000's,[108–110] a mechanistic pathway was proposed for the endogenous production of ozone through an antibody-catalyzed water-oxidation pathway in which ozone (O_3), or a trioxidic species of similar chemical signature, was produced as a by-product upon formation of hydrogen peroxide (H_2O_2) from singlet oxygen ($^1O_2^*$) and water.

Scheme 1.16 Proposed mechanism for the production of ozone in phagosomal bacterial killing and inflammation via an antibody-catalyzed water-oxidation pathway. Adapted from Babior et al.[111]

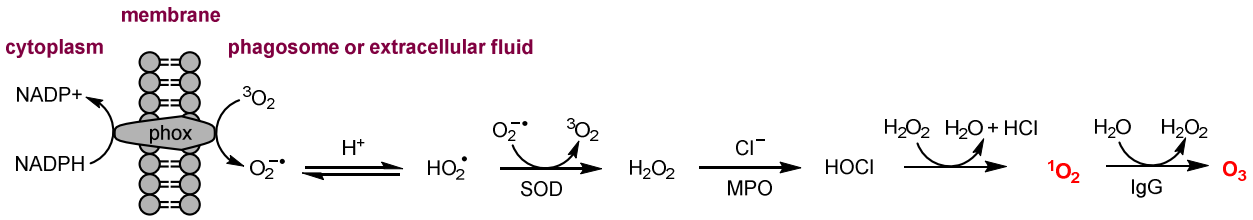

Endogenous production of singlet oxygen has been widely accepted to occur as part of phagocytic respiratory burst via the mechanism pictured in **Scheme 1.16**. Electron transfer from NADPH to triplet-state molecular oxygen ($^3O_2$) is mediated by NADPH oxidase, a transmembrane phagocyte oxidase system (phox), to generate the superoxide radical anion species ($O_2^{-\bullet}$).[112] Upon protonation, SOD mediates the rapid dismutation of $O_2^{-\bullet}$ to generate $^3O_2$ and H_2O_2. Myeloperoxidase (MPO) then oxidizes the chloride anion to hypochlorous acid (HOCl) using H_2O_2, the only mammalian enzyme known to be capable of catalyzing this reaction.[113,114] Excited-state singlet oxygen ($^1O_2$) is then ultimately generated from the reaction between HOCl and H_2O_2;[115,116] although it is not a free radical species, $^1O_2$ reacts rapidly with unsaturated lipids to

form products of similar character to that of autoxidation. Ultimately, antibody-catalyzed generation of H_2O_2 was proposed in which antibody-catalyzed water-oxidation serves as the electron source for reduction of $^1O_2$ to H_2O_3, an intermediate ultimately leading to H_2O_2,[108] however, the amount of H_2O_2 generated was found to be insufficient for the level of bacterial killing observed, proposing an "additional molecular species with a chemical signature similar to that of ozone" as the potent oxidant species responsible.[109]

Multiple reports have since investigated the unprecedented endogenous production of ozone in instances of inflammatory immune response,[109,111,117] including its potential role in the pathogenesis of atherosclerosis,[110] however, many researchers have expressed their reservations with the conclusions made in the foregoing work due to the lack of thorough mechanistic investigation and apparent circumstantial evidence.[118–120] In particular, many have had reservations concerning the findings that (1) cleavage of indigo carmine to generate isatin sulfonic acid and (2) cleavage of the $\Delta^{5,6}$ double bond of cholesterol to generate secosterol species are both exclusively mediated by ozone.

In consideration of (1), the authors detect the isotopically labeled products of indigo carmine ozonolysis by electrospray-ionization (ESI) mass spectrometry, in which incorporation of $H_2{}^{18}O$ provides distinct mass ions in negative mode of $[M\text{-}H]^-$ 228 and 230 for single and double incorporation of ^{18}O upon exchange with isotopic water, respectively.[109] Additionally, the authors note that $[M\text{-}H]^-$ of 230 is not detected upon oxidation of indigo carmine with $^1O_2$ and is therefore a unique chemical signature of ozonolysis. The proposed mechanism for ozonolysis of indigo carmine in the presence of $H_2{}^{18}O$, shown in

Figure 1.7A, shows formation of the primary ozonide and subsequent collapse to the Criegee intermediate whereby the incorporation of isotopic water and release of H_2O_2 occurs. However, very poorly resolved ESI-MS chromatograms and lack of additional mechanistic probing led others to study the oxidation of indigo carmine under similar conditions.

Soon thereafter, the endogenous ozone hypothesis is contested with evidence that the oxidation of indigo carmine by superoxide is indistinguishable from that by ozone based on isotopic incorporation from $H_2{}^{18}O$.[121] The proposed mechanism, shown in

Figure 1.7B, starts with one-electron reduction of indigo carmine by $O_2^{-\bullet}$ and subsequent reaction with another molecule of $O_2^{-\bullet}$ to generate a hydroperoxide. Hydrolysis of the hydroperoxide species by $H_2{}^{18}O$ liberates a molecule of isatin sulfonic acid and dioxindole sulfonate labelled with ^{18}O. The isotopically labelled dioxindole sulfonate can then autoxidize to generate the isotopically labelled isatin sulfonic acid species of $[M-H]^-$ 228 and exchange with $H_2{}^{18}O$ to give $[M-H]^-$ 230 – the same chemical signatures used as evidence of endogenous ozone.

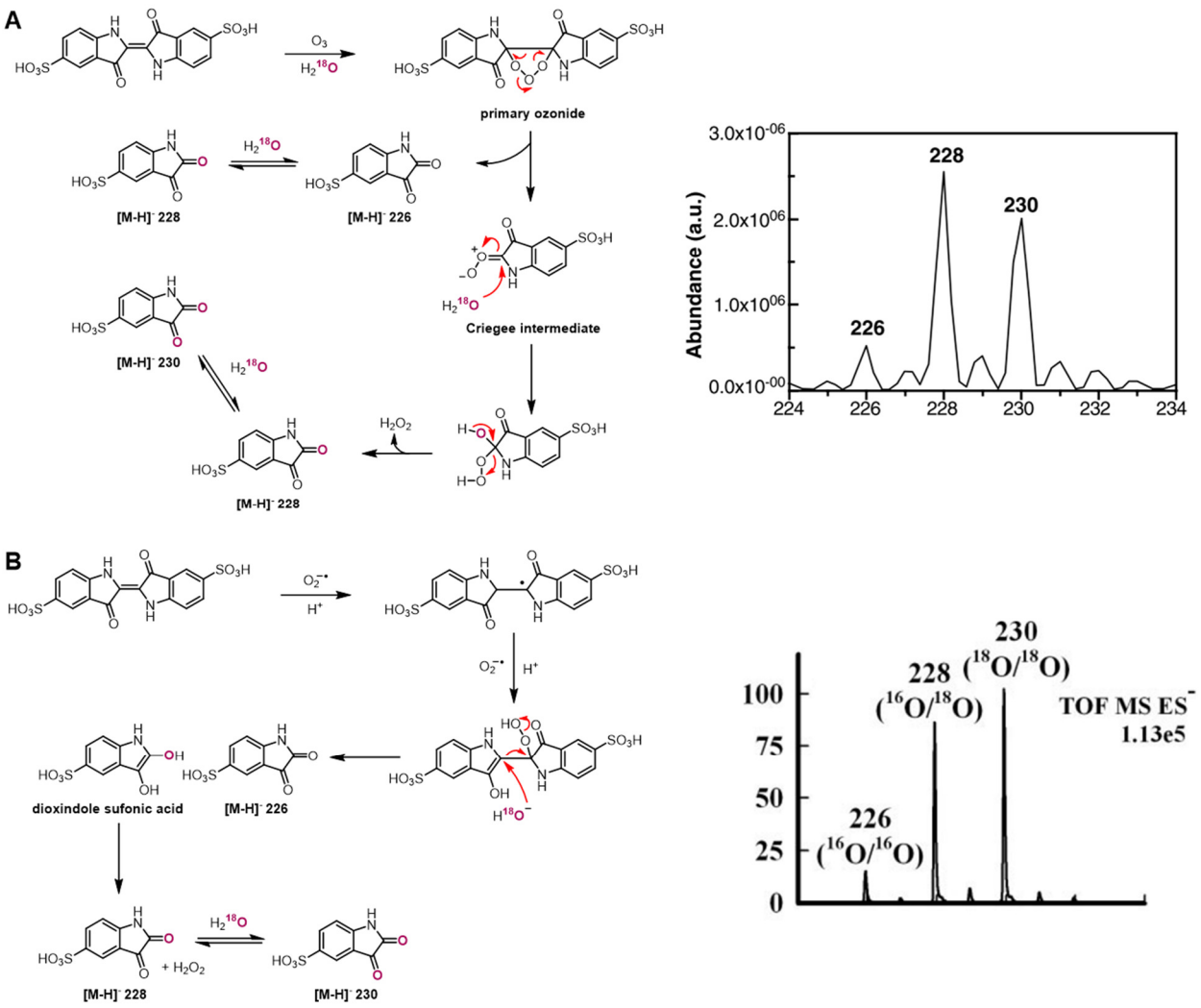

Figure 1.7 Proposed mechanism for cleavage of indigo carmine to isatin sulfonic acid mediated by (**A**) ozone[109] or (**B**) superoxide[121] in the presence of $H_2{}^{18}O$ with their corresponding representative negative mode ESI mass spectra.

A follow-up article in *Science* in 2003 brought forward some of the most impactful physiological implications of endogenous ozone: evidence for ozone-mediated cleavage of the $\Delta^{5,6}$-double bond of cholesterol to generate highly electrophilic aldehydic species in atherosclerotic plaque, termed atheronals.[110] In this work, the authors sought to determine if ozone is in fact produced as a result of inflammatory responses to the exacerbation of atherosclerosis and if any relevant ozonolysis products could be detected.

Previous work from Pryor et al described cholesterol ozonolysis products as possible biomarkers for atmospheric O_3 exposure due the high concentration of cholesterol in the lung lining fluid and its rapid reactivity with the oxidant in both organic and aqueous solution.[122] Additionally, they provided an indirect method for identification of these products through 2,4-dinitrophenylhydrazine (DNPH) derivatization of the aldehydic moieties. Ozonolysis products of cholesterol, termed "secosterols" for the cleavage of their B-ring, had been well characterized at this time,[122–125] however, a sensitive analytical method to detect and monitor their formation was missing. DNPH derivatization appends a UV-active hydrazone to a compound that is otherwise difficult to visualize and also enhances the stability of the compound for analysis. This was adapted for studies to trap highly electrophilic aldehydes of the secosterol species in atherosclerotic plaque for characterization by HPLC/ESI-MS.

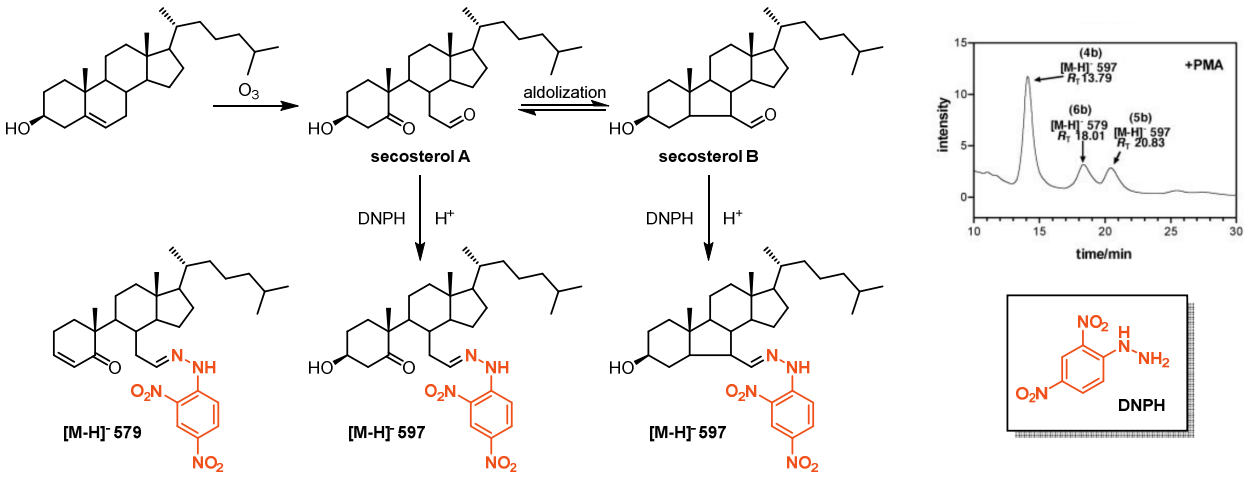

Figure 1.8 Cholesterol ozonolysis to the secoaldehyde (secosterol A) and aldol condensation to the carboxaldehyde (secosterol B) and subsequent DNPH derivatization of products to their respective hydrazone derivatives. Representative chromatogram of arterial plaque extract obtained on the right. Adapted from Wentworth *et al.*[110]

This study again invoked the use of indigo carmine as a chemical probe for ozone, and suggested that indigo carmine in the presence of plaque samples treated with phorbol myristate

acetate (PMA) to induce enhanced inflammatory response was indeed cleaved to isatin sulfonic acid through ozonolysis. Under this presumption, the high concentration of cholesterol within diseased arterial plaques would also undergo ozonolysis to generate secosterol species (now termed "atheronals"), as shown in **Figure 1.8**. These secosterol species were then presumably converted to their corresponding hydrazones via acid-catalyzed derivatization with DNPH before or after aldolization, and were indirectly characterized by HPLC/ESI-MS.

Similar to the reservations many researchers had regarding detection of endogenous ozone using indigo carmine as a chemical probe, the ozonolysis of cholesterol in diseased plaque was also met with controversy. Perhaps the most notable considerations were (1) atheronals are indirectly identified as hydrazone species through a transformation that requires a high concentration (0.1 M) of acid and (2) alternative routes using other potent oxidants were not proposed or evaluated as possible sources of these aldehydic species. Without these considerations, this oversight unveiled a division of questioning regarding the origin of these secosterol species and the presence of endogenous ozone itself. Were the secosterols observed a result of ozonolysis, or were they simply a consequence of the conditions by which they were derivatized? Is a different oxidant species responsible for cleavage of the $\Delta^{5,6}$ double bond, much like that of superoxide in the case of indigo carmine? These questions inspired the exploration for a simpler alternative mechanism utilizing oxidants with a higher likelihood to exist *in vivo*.

Brinkhorst, Nara, and Pratt provide such an alternative with their 2008 *JACS* article proposing cholesterol-5α-OOH, the major product of $^1O_2$ oxidation, undergoes acid-catalyzed Hock fragmentation to generate the same secosterol species identified in arterial plaque extracts.[57] This alternative mechanism suggests that the occurrence of the atheronals follows the same mechanistic route suggested to explain endogenous formation of 4-hydroxynonenal (4-HNE), or

they were a mere consequence of the acidic conditions under which they were derivatized for their identification. This route also invokes $^1O_2$ as the responsible oxidant species, the proposed precursor to endogenous O_3, and another species with evidence of *in vivo* generation.[115,116]

Upon photosensitization of O_2 to $^1O_2$, $^1O_2$ reacts with the $\Delta^{5,6}$ double bond of cholesterol via an ene-reaction with the proton at the 7-position to produce cholesterol-5α-OOH as the major product, or cholesterol-6β-OOH as the minor product upon reaction with the allylic proton at the 4-position. Additionally, allylic rearrangement of the 5α-OOH to the 7α/β-OOH occurs readily, rendering the 5α-OOH relatively transient, however, this is somewhat slowed in H-bond accepting solvents.[99]

Scheme 1.17 Ene-reaction of singlet oxygen with cholesterol to afford chol-5α-OOH (major) and chol-6β-OOH (minor). Allylic rearrangement of chol-5α-OOH to chol-7α/β-OOH is indicated on right.

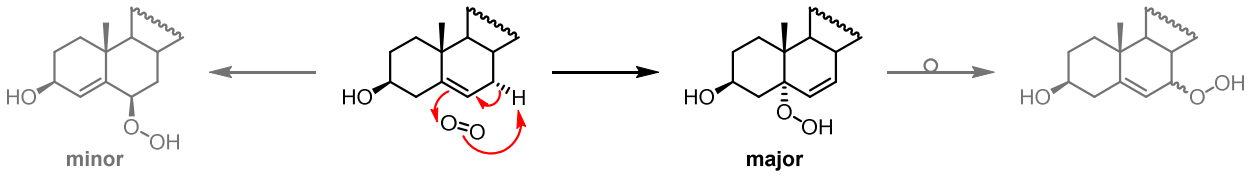

When subjected to acidic conditions, the quantitative product of 5α-OOH Hock fragmentation is the same aldolized product identified arterial plaque*:* secosterol B.

Scheme 1.18 Hock fragmentation of cholesterol-5α-OOH. Adapted from Brinkhorst *et al*.[57]

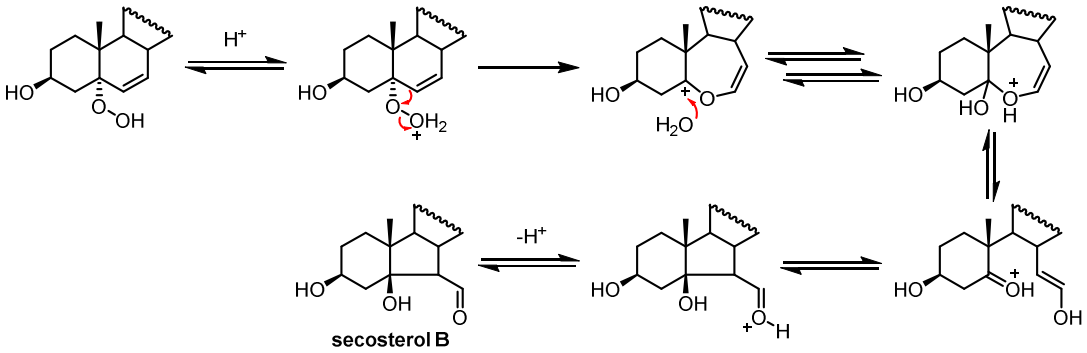

Simplicity of this precedented mechanism,[62] and familiarity of the mechanism of Hock fragmentation from its industrial use in acetone and phenol production,[64] made this an attractive alternative explanation for the generation of the atheronals. Additionally, the suggestion that singlet oxygen serves as the responsible oxidant was subsequently supported by Uemi et al.[126] Furthermore, acid-catalyzed Hock cleavage mechanism can occur for other cholesterol hydroperoxide species; this was highlighted by Zielinski and Pratt wherein chol-6β-OOH also undergoes Hock cleavage to generate secA and secB.[56] However, it is still unclear if the atheronals are truly formed *in vivo*, or are just a consequence of the acidic derivatization conditions.

Scheme 1.19 Hock fragmentation mechanism of cholesterol-6β-OOH to generate atheronals, secosterol A and B.

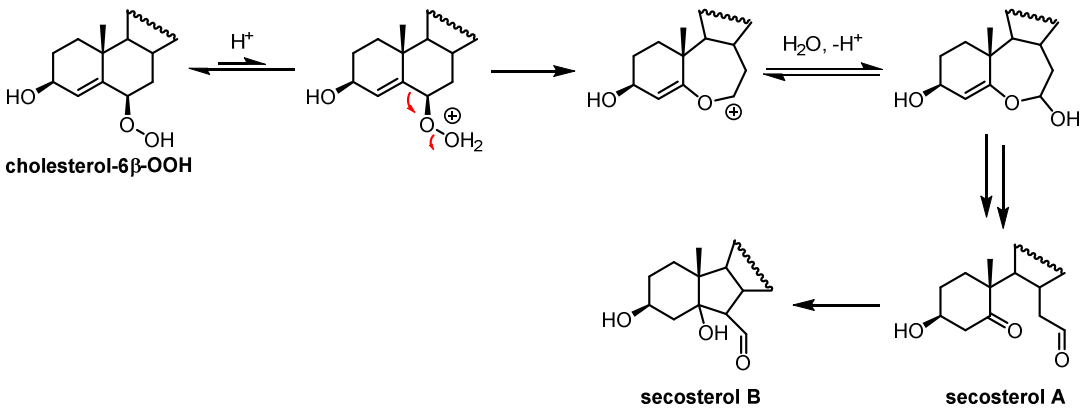

Originally termed atheronals for their indirect identification in human atherosclerotic plaque extracts,[121] secA and B have been since implicated in the degradation of macrophages leading to foam cell formation in the pathogenesis of atherosclerosis.[127] *In vitro* experiments suggest that the secosterols facilitate recruitment of macrophages to arterial tissue via chemotaxis, and that secB triggers monocyte differentiation to macrophage foam cells. It was later suggested that covalent modification via Schiff base formation of secA and B with lysine or N-terminal amino groups of human apolipoprotein C-II amyloid triggers aggregation leading to insoluble

amyloid-β fibrils in atherosclerotic lesions,[128] however, the mechanism for foam cell formation remains unclear.

The implication of cholesterol-derived atheronals in neurodegenerative diseases may be relatively limited, however, the potential impact of covalent modifications in brain tissue is of interest. Although most popularly associated with atherosclerosis, both secA and B have also been identified indirectly in brain tissue and have been implicated in the acceleration of amyloidogenesis involved in AD, PD, and Lewy-body dementia.[88,129] This is most often believed to occur upon covalent Schiff base formation with the terminal lysine residues of amyloid-β, triggering the aggregation of α-synuclein, or general protein misfolding. Interestingly, contrary to the vilification of atheronals due to their predisposition to trigger protein misfolding, one report had suggested that secB adduction actually inhibits the misfolding of a mutant prion protein fragment;[130] the group even suggests that secB, or a compound of a similar scaffold, may be considered as a potential therapeutic!

It is evident that there is no conclusive role for the atheronals *in vivo*, in addition to the possibility that the species themselves have been misidentified. Although it is apparent that Schiff base formation resulting in protein aggregation and misfolding is likely the predominant role of secosterols in the pathology of disease, some reports suggest that non-covalent pathways for secosterol-mediated protein aggregation are also possible.[88] Interestingly, apart from the LC/MS method developed by Windsor et al,[131] not one proteomic assay has been performed to assess the potential sites of covalent modification by the atheronals. Nonetheless, it is clear that lipid-derived electrophiles of this character have the potential to play a significant role in disease pathology, however, the mechanism by which they do so, and confirmation of their identity, remains indefinite.

1.4 Research Objectives

Our current understanding of the mechanism of the autoxidation of cholesterol, the most abundant lipid in the body, has only been fully realized based upon reports presented by our group within the last five years. For the first time, Zielinski and Pratt provide evidence for all expected products of symmetrical autoxidation of the $\Delta^{5,6}$-double bond, including products of addition and C7 and C4 H-atom abstraction; in the case of the 4-, 5-, and 6-hydroperoxide, (some of) these products had only ever been proposed, but never observed directly as products of autoxidation.[56,107]

This work probed the complexity of cholesterol autoxidation in organic solution; however, these mechanistic conclusions may not necessarily translate to the phospholipid cell membrane environment cholesterol inhabits *in vivo*. In this thesis, we explore the mechanism of cholesterol autoxidation in model lipid membrane systems and the influence that PUFA-derived chain-carrying species and steric constraints imposed by the orientation of cholesterol in an amphiphilic membrane system have on the product distribution. To study cholesterol oxidation products in these systems, sterol extracts were analyzed using an optimized LC/MS/MS method to accurately quantify hydroperoxide products following reduction to their corresponding alcohols. We analyze cholesterol autoxidation in two distinct phospholipid membrane systems, and provide a basis to investigate cholesterol autoxidation in other biological systems, including mammalian cells and LDL particles. Product distribution observed in these systems will provide insight regarding the dominant primary products of cholesterol autoxidation in relation to the cholesterol-derived species currently implicated in the pathogenesis of atherosclerosis. Investigation of the capacity of these species as substrates for GPX4 may also indicate their persistence relative to their PUFA-derived counterparts, indicating their relative contribution to ferroptotic cell death.

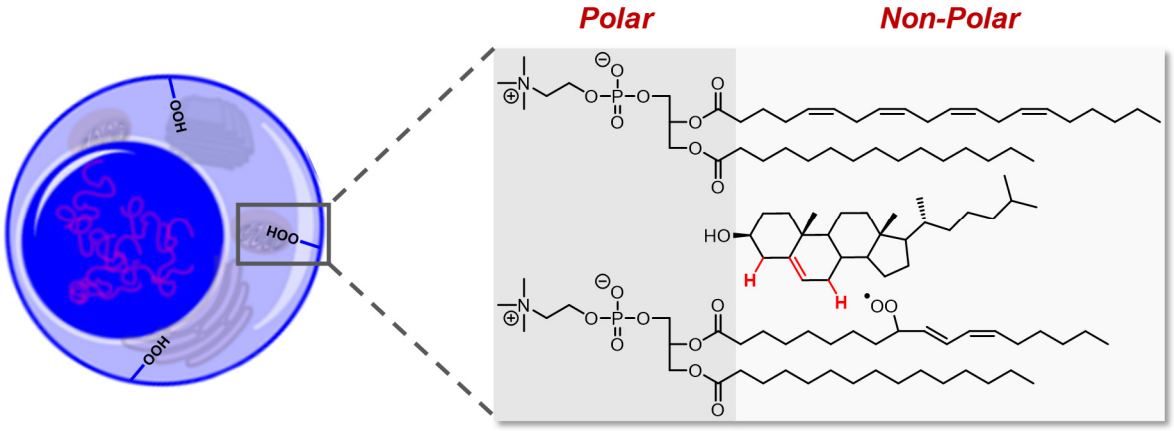

Figure 1.9 Model of potential anisotropy imparted by the phospholipid bilayer during cholesterol autoxidation.

Over the last 10 years, several members of our research group have sought to determine the true origin of the secosterol species and provide a more plausible explanation for the origin of secosterol products than oxidation by endogenous ozone.[108–110] Our investigations initially provided an ozone-free pathway to formation of the secosterols via acid-catalyzed Hock fragmentation of chol-5α-OOH,[57] however, generation of chol-5α-OOH *in vivo* invoked oxidation by a high energy oxidant, singlet oxygen. We subsequently showed that 5α-OOH could be formed via autoxidation, but only in the presence of a good H-atom donor. We also showed that chol-6β-OOH was shown to undergo Hock fragmentation and is formed simply by autooxidation, albeit in small amounts.[56] Alternatively, we sought to investigate the potential secondary products of chol-7-OOH: the predominant product of cholesterol autoxidation both *in vivo* and in organic solution. Hock fragmentation of chol-7-OOH is expected to generate electrophilic species of very similar spectroscopic character to those identified in atherosclerotic plaque extracts. Interestingly, investigations preceding those presented in this thesis revealed an epoxide product, potentially eluding to an epoxide intermediate in the mechanism of Hock fragmentation of this substrate.[132]

Herein, we expand on our preliminary efforts to elucidate the major product(s) derived from Hock fragmentation of chol-7-OOH and to examine their potential cytotoxicity compared against the atheronals and other oxysterol compounds. Additionally, our efforts to determine the origin of the secosterols resulted in our evaluation of the acidic conditions required for DNPH derivatization used for their original identification. Based upon these investigations, we will present evidence for the evolution of a series of novel aldehydic secosterol species via acid-catalyzed Hock fragmentation of cholesterol-7α-hydroperoxide that suggests that these species were likely *misidentified* as sec A and B in the initial studies presented. As such, we present an alternative set of secondary products of cholesterol autoxidation that would exhibit the same role in the pathology of atherosclerosis, Alzheimer's, and Parkinson's disease as the atheronals were proposed to exhibit.

Scheme 1.20 Proposed mechanism of cholesterol-7-hydroperoxide Hock fragmentation based upon products isolated and characterized during initial investigations.

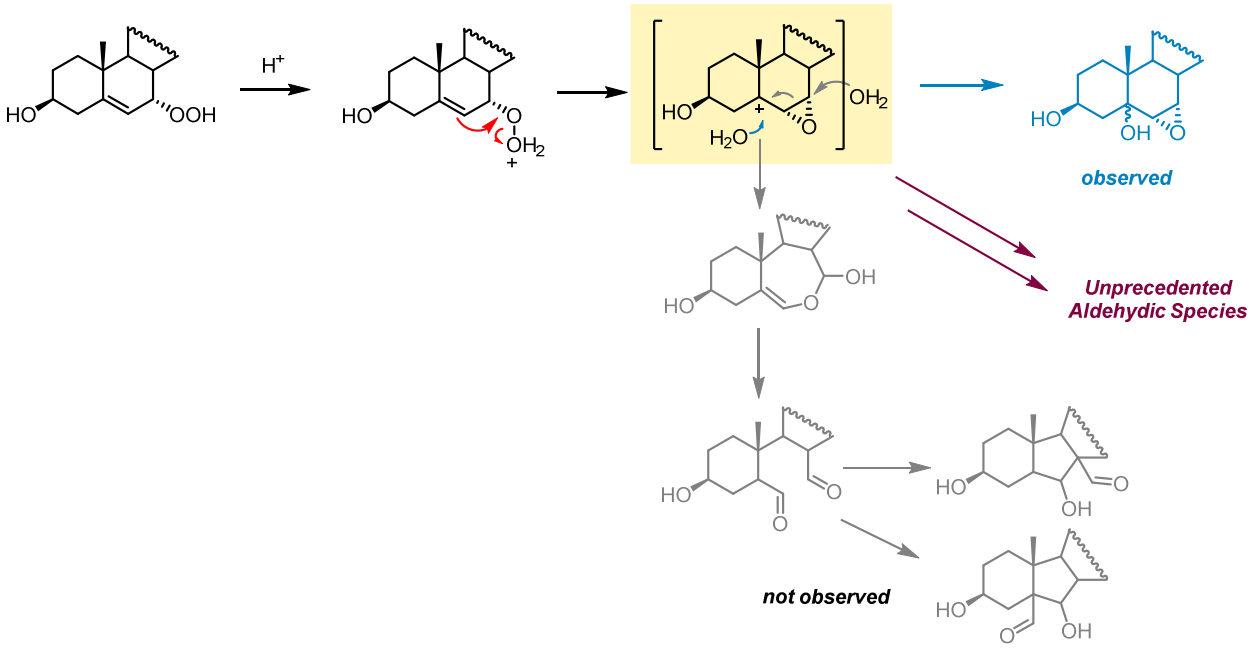

1.5 References

(1) Wu, R. P.; Hayashi, T.; Cottam, H. B.; Jin, G.; Yao, S.; Wu, C. C. N.; Rosenbach, M. D.; Corr, M.; Schwab, R. B.; Carson, D. A. *Proc. Natl. Acad. Sci. U. S. A.* **2010**, *107* (16), 7479–7484.

(2) Hammad, L. A.; Wu, G.; Saleh, M. M.; Klouckova, I.; Dobrolecki, L. E.; Hickey, R. J.; Schnaper, L.; Novotny, M. V.; Mechref, Y. *Rapid Commun. Mass Spectrom.* **2010**, *23* (6), 863–876.

(3) Silverstein, R. L.; Febbraio, M. *Sci. Signal.* **2009**, *2* (72), re3.

(4) Simonian, N. A.; Coyle, J. T. *Annu. Rev. Pharmacol. Toxicol.* **1996**, *36*, 83–106.

(5) Yin, H.; Xu, L.; Porter, N. A. *Chem. Rev.* **2011**, *111* (10), 5944–5972.

(6) Finkel, T.; Holbrook, N. J. *Nature* **2000**, *408* (6809), 239–247.

(7) Wang, K.; Bermúdez, E.; Pryor, W. A. *Steroids* **1993**, *58* (5), 225–229.

(8) Minotti, G.; Aust, S. D. *Lipids* **1992**, *27* (3), 219–226.

(9) Chen, Q.; Vazquez, E. J.; Moghaddas, S.; Hoppel, C. L.; Lesnefsky, E. J. *J. Biol. Chem.* **2003**, *278* (38), 36027–36031.

(10) Bochkov, V. N.; Oskolkova, O. V; Birukov, K. G.; Levonen, A.-L.; Binder, C. J.; Stöckl, J. *Antioxid. Redox Signal.* **2010**, *12* (8), 1009–1059.

(11) Haber, F.; Weiss, J. *Proc. R. Soc. London A Math. Phys. Eng. Sci.* **1934**, *147* (861), 332–351.

(12) Shadel, G. S.; Horvath, T. L. *Cell* **2015**, *163* (3), 560–569.

(13) Noguchi, N.; Yamashita, H.; Gotoh, N.; Yamamoto, Y.; Numano, R.; Niki, E. *Free Radic. Biol. Med.* **1997**, *24* (2), 259–268.

(14) Culbertson, S. M.; Vinqvist, M. R.; Barclay, L. R. C.; Porter, N. A. *J. Am. Chem. Soc.* **2001**, *123* (37), 8951–8960.

(15) Maillard, B.; Ingold, K. U.; Scaiano, J. C. *J. Am. Chem. Soc.* **1983**, *105* (15), 5095–5099.

(16) Ingold, K. U.; Pratt, D. A. *Chem. Rev.* **2014**, *114* (18), 9022–9046.

(17) Xu, L.; Davis, T. A.; Porter, N. A. *J. Am. Chem. Soc.* **2009**, *131* (36), 13037–13044.

(18) Porter, N. A.; Mills, K. A.; Carter, R. L. *J. Am. Chem. Soc.* **1994**, *116* (7), 6690–6696.

(19) Tallman, K. A.; Pratt, D. A.; Porter, N. A. *J. Am. Chem. Soc.* **2001**, *123* (47), 11827–11828.

(20) Burton, G. W.; Doba, T.; Gabe, E.; Hughes, L.; Lee, F. L.; Prasad, L.; Ingold, K. U. *J. Am. Chem. Soc.* **1985**, *107* (24), 7053–7065.

(21) Brash, A. R. *Lipids* **2000**, *35* (9), 947–952.

(22) Porter, N. A.; Weber, B. A.; Weenen, H.; Khan, J. A. *J. Am. Chem. Soc.* **1980**, *102* (17), 5597–5601.

(23) Barclay, L. R. C.; Antunes, F.; Egawa, Y.; McAllister, K. L.; Mukai, K.; Nishi, T.; Vinqvist, M. R. *Biochim. Biophys. Acta, Biomembr.* **1997**, *1328* (1), 1–12.

(24) Barclay, L. R. C.; Vinqvist, M. R.; Antunes, F.; Pinto, R. E. *J. Am. Chem. Soc.* **1997**, *119* (24), 5764–5765.

(25) Yoshida, Y.; Niki, E. *Free Radic. Res.* **2004**, *38* (8), 787–794.

(26) Yoshida, Y.; Hayakawa, M.; Habuchi, Y.; Niki, E. *Biochim. Biophys. Acta, Gen. Subj.* **2006**, *1760* (10), 1558–1568.

(27) Yoshida, Y.; Hayakawa, M.; Habuchi, Y.; Itoh, N.; Niki, E. *Lipids* **2007**, *42* (5), 463–472.

(28) Bowry, V. W.; Stocker, R. *J. Am. Chem. Soc.* **1993**, *115* (14), 6029–6044.

(29) Bowry, V. W.; Ingold, K. U. *Acc. Chem. Res.* **1999**, *32* (1), 27–34.

(30) Morrow, J. D.; Hill, K. E.; Burk, R. F.; Nammour, T. M.; Badr, K. F.; Roberts II., L. J. *Proc. Natl. Acad. Sci. U. S. A.* **1990**, *87* (23), 9383–9387.

(31) Howard, J. A.; Ingold, K. U. *Can. J. Chem.* **1966**, *44* (10), 1119–1130.

(32) Barclay, L. R. C.; Ingold, K. U. *J. Am. Chem. Soc.* **1981**, *103* (21), 6478–6485.

(33) Russell, G. A. *J. Am. Chem. Soc.* **1957**, *79*, 3871–3877.

(34) Li, B.; Pratt, D. A. *Free Radic. Biol. Med.* **2015**, *82*, 187–202.

(35) Hanthorn, J. J.; Haidasz, E.; Gebhardt, P.; Pratt, D. A. *Chem. Commun.* **2012**, *48* (81), 10141.

(36) Skouta, R.; Dixon, S. J.; Wang, J.; Dunn, D. E.; Orman, M.; Shimada, K.; Rosenberg, P. A.; Lo, D. C.; Weinberg, J. M.; Linkermann, A.; Stockwell, B. R. *J. Am. Chem. Soc.* **2014**, *136* (12), 4551–4556.

(37) Zilka, O.; Shah, R.; Li, B.; Friedmann Angeli, J. P.; Griesser, M.; Conrad, M.; Pratt, D. A. *ACS Cent. Sci.* **2017**, *3* (3), 232–243.

(38) Shah, R.; Margison, K.; Pratt, D. A. *ACS Chem. Biol.* **2017**, *12* (10), 2538–2545.

(39) Griesser, M.; Shah, R.; Van Kessel, A. T.; Zilka, O.; Haidasz, E. A.; Pratt, D. A. *J. Am. Chem. Soc.* **2018**, *140* (10), 3798–3808.

(40) Snelgrove, D. W.; Lusztyk, J.; Banks, J. T.; Mulder, P.; Ingold, K. U. *J. Am. Chem. Soc.* **2001**, *123* (3), 469–477.

(41) Shah, R.; Farmer, L. A.; Zilka, O.; Kessel, A. T. M. Van; Pratt, D. A. *ACS Cent. Sci.* **2019**,

Submitted.

(42) Farmer, L. A.; Haidasz, E. A.; Griesser, M.; Pratt, D. A. *J. Org. Chem.* **2017**, *82* (19), 10523–10536.

(43) Angeli, J. P. F.; Shah, R.; Pratt, D. A.; Conrad, M. *Trends Pharmacol. Sci.* **2017**, *38* (5), 489–498.

(44) Yang, W. S.; Stockwell, B. R. *Chem. Biol.* **2008**, *15* (3), 234–245.

(45) Shah, R.; Shchepinov, M. S.; Pratt, D. A. *ACS Cent. Sci.* **2018**, *4* (3), 387–396.

(46) Yagoda, N.; von Rechenberg, M.; Zaganjor, E.; Bauer, A. J.; Yang, W. S.; Fridman, D. J.; Wolpaw, A. J.; Smukste, I.; Peltier, J. M.; Boniface, J. J.; Smith, R.; Lessnick, S. L.; Sahasrabudhe, S.; Stockwell, B. R. *Nature* **2007**, *447* (7146), 865–869.

(47) Griffith, O. W.; Meister, A. *J. Biol. Chem.* **1979**, *254* (16), 7558–7560.

(48) Yang, W. S.; Kim, K. J.; Gaschler, M. M.; Patel, M.; Shchepinov, M. S.; Stockwell, B. R. *Proc. Natl. Acad. Sci. U. S. A.* **2016**, *113* (34), E4966–E4975.

(49) Thomas, J. P.; Geiger, P. G.; Maiorino, M.; Ursini, F.; Girotti, A. W. *Biochim. Biophys. Acta* **1990**, *1045*, 252–260.

(50) Friedmann Angeli, J. P.; Schneider, M.; Proneth, B.; Tyurina, Y. Y.; Tyurin, V. A.; Hammond, V. J.; Herbach, N.; Aichler, M.; Walch, A.; Eggenhofer, E.; Basavarajappa, D.; Radmark, O.; Kobayashi, S.; Seibt, T.; Beck, H.; Neff, F.; Esposito, I.; Wanke, R.; Foerster, H.; Yefremova, O.; Heinrichmeyer, M.; Bornkamm, G. W.; Geissler, E. K.; Thomas, S. B.; Stockwell, B. R.; O'Donnell, V. B.; Kagan, V. E.; Schick, J. A.; Conrad, M. *Nat. Cell Biol.* **2014**, *16* (12), 1180–1191.

(51) Korytowski, W.; Geiger, P. G.; Girotti, A. W. *Biochemistry* **1996**, *35*, 8670–8679.

(52) Brown, A. J.; Leong, S.-L.; Dean, R. T.; Jessup, W. *J. Lipid Res.* **1997**, *38* (9), 1730–1745.

(53) Lee, S. H.; Oe, T.; Arora, J. S.; Blair, I. A. *J. Mass Spectrom.* **2005**, *40* (5), 661–668.

(54) Girotti, A. W.; Korytowski, W. *Cell Biochem. Biophys.* **2017**, 1–7.

(55) Dixon, S. J.; Lemberg, K. M.; Lamprecht, M. R.; Skouta, R.; Zaitsev, E. M.; Gleason, C. E.; Patel, D. N.; Bauer, A. J.; Cantley, A. M.; Yang, W. S.; Morrison, B.; Stockwell, B. R. *Cell* **2012**, *149* (5), 1060–1072.

(56) Zielinski, Z. A. M.; Pratt, D. A. *J. Am. Chem. Soc.* **2016**, *138*, 6932–6935.

(57) Brinkhorst, J.; Nara, S. J. and; Pratt, D. A. *J. Am. Chem. Soc.* **2008**, *130* (37), 12224–12225.

(58) Gardner, H. W.; Weisleder, D.; Nelson, E. C. *J. Org. Chem.* **1984**, *49* (3), 508–515.

(59) Schneider, C.; Tallman, K. A.; Porter, N. A.; Brash, A. R. *J. Biol. Chem.* **2001**, *276* (24), 20831–20838.

(60) Hock, H.; Schrader, O. *Naturwissenschaften* **1936**, *24*, 159.

(61) Hock, H.; Ganicke, K. *Berichte der Dtsch. Chem. Gesellschaft [Abteilung] B Abhandlungen* **1938**, *71B*, 1430–1437.

(62) Frimer, A. A. *Chem. Rev.* **1979**, *79* (5), 359–387.

(63) Hiatt, R. In *Wiley-Interscience*; Swern, D., Ed., **1971**; Vol. 5, pp 79–80.

(64) Fortuin, J. P.; Waterman, H. I. *Chem. Eng. Sci.* **1953**, *2* (4), 182–192.

(65) Awasthi, Y. C.; Yang, Y.; Tiwari, N. K.; Patrick, B.; Sharma, A.; Li, J.; Awasthi, S. *Free Radic. Biol. Med.* **2004**, *37* (5), 607–619.

(66) Nair, J.; Barbin, A.; Velic, I.; Bartsch, H. *Mutat. Res. Fundam. Mol. Mech. Mutagen.* **1999**, *424* (1,2), 59–69.

(67) Negre-Salvayre, A.; Auge, N.; Ayala, V.; Basaga, H.; Boada, J.; Brenke, R.; Chapple, S.; Cohen, G.; Feher, J.; Grune, T.; Lengyel, G.; Mann, G. E.; Pamplona, R.; Poli, G.; Portero-Otin, M.; Riahi, Y.; Salvayre, R.; Sasson, S.; Serrano, J.; Shamni, O.; Siems, W.; Siow, R. C. M.; Wiswedel, I.; Zarkovic, K.; Zarkovic, N. *Free Radic. Res.* **2010**, *44* (10), 1125–1171.

(68) Benedetti, A.; Comporti, M.; Esterbauer, H. *Biochim. Biophys. Acta, Lipids Lipid Metab.* **1980**, *620* (2), 281–296.

(69) Schneider, C.; Boeglin, W. E.; Yin, H.; Stec, D. F.; Hachey, D. L.; Porter, N. A.; Brash, A. R. *Lipids* **2005**, *40* (11), 1155–1162.

(70) Esterbauer, H.; Schaur, R. J.; Zollner, H. *Free Radic. Biol. Med.* **1991**, *11* (1), 81–128.

(71) Windsor, K.; Genaro-Mattos, T. C.; Miyamoto, S.; Stec, D. F.; Kim, H.-Y. H.; Tallman, K. A.; Porter, N. A. *Chem. Res. Toxicol.* **2014**, *27* (10), 1757–1768.

(72) Lusis, A. J. *Nature* **2000**, *407*, 233–241.

(73) Ross, R. *Nature* **1993**, *362*, 801–809.

(74) Falk, E. *J. Am. Coll. Cardiol.* **2006**, *47* (8), C7-12.

(75) Palinski, W.; Rosenfeld, M. E.; Ylä-Herttuala, S.; Gurtner, G. C.; Socher, S. S.; Butler, S. W.; Parthasarathy, S.; Carew, T. E.; Steinberg, D.; Witztum, J. L. *Proc. Natl. Acad. Sci. U. S. A.* **1989**, *86* (4), 1372–1376.

(76) Ylä-Herttuala, S.; Palinski, W.; Rosenfeld, M. E.; Parthasarathy, S.; Carew, T. E.; Butler, S.; Witztum, J. L.; Steinberg, D. *J. Clin. Invest.* **1989**, *84* (4), 1086–1095.

(77) Witztum, J. L. *Lancet* **1994**, *344*, 793–795.

(78) Goldstein, J. L.; Ho, Y. K.; Basu, S. K.; Brown, M. S. *Proc. Natl. Acad. Sci. U. S. A.* **1979**, *76* (1), 333–337.

(79) Morel, D. W.; Hessler, J. R.; Chisolm, G. M. *J. Lipid Res.* **1983**, *24* (8), 1070–1076.

(80) Heinecke, J. W.; Rosen, H.; Chait, A. *J. Clin. Invest.* **1984**, *74*, 1890–1894.

(81) Heinecke, J. W.; Rosen, H.; Suzuki, L. A.; Chait, A. *J. Biol. Chem.* **1987**, *262* (21), 10098–10103.

(82) Heinecke, J. W.; Kawamura, M.; Suzuki, L.; Chait, A. *J. Lipid Res.* **1993**, *34*, 2051–2061.

(83) Sparrow, C. P.; Olszewski, J. *J. Lipid Res.* **1993**, *34* (7), 1219–1228.

(84) Cathcart, M. K.; McNally, A. K.; Morel, D. W.; Chisolm, G. M. *J. Immunol.* **1989**, *142* (6), 1963–1969.

(85) Ylä-Herttuala, S.; Rosenfeld, M. E.; Parthasarathy, S.; Sigal, E.; Sflrkioja, T.; Witztum, J. L.; Steinberg, D. *J. Clin. Invest.* **1991**, *87*, 1146–1152.

(86) Kühn, H.; Belkner, J.; Suzuki, H.; Yamamoto, S.; Kuhn, H.; Hiroshi, B.; Yamamotot, S. *J. Lipid Res.* **1994**, *35* (10), 1749–1759.

(87) Heneka, M. T.; Carson, M. J.; El Khoury, J.; Landreth, G. E.; Brosseron, F.; Feinstein, D. L.; Jacobs, A. H.; Wyss-Coray, T.; Vitorica, J.; Ransohoff, R. M.; Herrup, K.; Frautschy, S. A.; Finsen, B.; Brown, G. C.; Verkhratsky, A.; Yamanaka, K.; Koistinaho, J.; Latz, E.; Halle, A.; Petzold, G. C.; Town, T.; Morgan, D.; Shinohara, M. L.; Perry, V. H.; Holmes, C.; Bazan, N. G.; Brooks, D. J.; Hunot, S.; Joseph, B.; Deigendesch, N.; Garaschuk, O.; Boddeke, E.; Dinarello, C. A.; Breitner, J. C.; Cole, G. M.; Golenbock, D. T.; Kummer, M. P. *Lancet Neurol.* **2015**, *14* (4), 388–405.

(88) Bosco, D. A.; Fowler, D. M.; Zhang, Q.; Nieva, J.; Powers, E. T.; Wentworth, P.; Lerner, R. A.; Kelly, J. W. *Nat. Chem. Biol.* **2006**, *2*, 249–253.

(89) Bieschke, J.; Zhang, Q.; Bosco, D. A.; Lerner, R. A.; Powers, E. T.; Wentworth Jr., P.; Kelly, J. W. *Acc. Chem. Res.* **2006**, *39* (9), 611–619.

(90) van Meer, G.; Voelker, D. R.; Feigenson, G. W. *Nat. Rev. Mol. Cell Biol.* **2008**, *9* (2), 112–124.

(91) Bach, D.; Wachtel, E. *Biochim. Biophys. Acta - Biomembr.* **2003**, *1610* (2), 187–197.

(92) Hanukoglu, I. *J. Steroid Biochem. Mol. Biol.* **1992**, *43* (8), 779–804.

(93) Xu, L.; Porter, N. A. *Free Radic. Res.* **2015**, *49* (7), 835–849.

(94) Brown, A. J.; Jessup, W. *Atherosclerosis* **1999**, *142* (1), 1–28.

(95) Chisolm, G. M.; Ma, G.; Irwin, K. C.; Martin, L. L.; Gunderson, K. G.; Linberg, L. F.; Morel, D. W.; DiCorleto, P. E. *Proc. Natl. Acad. Sci. U. S. A.* **1994**, *91* (24), 11452–11456.

(96) Chang, Y. H.; Abdalla, D. S.; Sevanian, A. *Free Radic Biol Med* **1997**, *23* (2), 202–214.

(97) Howard, J. A.; Ingold, K. U. *J. Am. Chem. Soc.* **1968**, *90* (4), 1056–1058.

(98) Pratt, D. A.; Mills, J. H.; Porter, N. A. *J. Am. Chem. Soc.* **2003**, *125* (19), 5801–5810.

(99) Beckwith, A. L. J.; Davies, A. G.; Davidson, I. G. E.; Maccoll, A.; Mruzek, M. H. *J. Chem Soc. Perkin Trans. II* **1989**, *1* (4), 815–824.

(100) Smith, L. L. *Chem. Phys. Lipids* **1987**, *44*, 87–125.

(101) Kulig, M. J.; Smith, L. L. *J. Org. Chem.* **1973**, *38* (20), 3639–3642.

(102) Korytowski, W.; Bachowski, G. J.; Girotti, A. W. *Photochem. Photobiol.* **1992**, *56* (1), 1–8.

(103) Breuer, O. *J. Lipid Res.* **1995**, *36* (11), 2275–2281.

(104) Ansari, G. A. S.; Walker, R. D.; Smart, V. B.; Smith, L. L. *Food Chem. Toxicol.* **1982**, *20* (1), 35–41.

(105) Csiky, I. *J. Chromatogr.* **1982**, *241* (2), 381–389.

(106) Breuer, O.; Dzeletovic, S.; Lund, E.; Diczfalusy, U. *Biochim. Biophys. Acta, Lipids Lipid Metab.* **1996**, *1302* (2), 145–152.

(107) Zielinski, Z. A. M.; Pratt, D. A. *J. Am. Chem. Soc.* **2019**, *141* (7), 3047–3051.

(108) Wentworth Jr, P.; Jones, L. H.; Wentworth, A. D.; Zhu, X.; Larsen, N. A.; Wilson, I. A.; Xu, X.; Goddard III, W. A.; Janda, K. D.; Eschenmoser, A.; Lerner, R. A. *Science* **2001**, *293* (5536), 1806–1811.

(109) Wentworth, P.; McDunn, J. E.; Wentworth, A. D.; Takeuchi, C.; Nieva, J.; Jones, T.; Bautista, C.; Ruedi, J. M.; Gutierrez, A.; Janda, K. D.; Babior, B. M.; Eschenmoser, A.; Lerner, R. a. *Science* **2002**, *298* (5601), 2195–2199.

(110) Wentworth Jr., P.; Nieva, J.; Takeuchi, C.; Galve, R.; Wentworth, A. D.; Dilley, R. B.; DeLaria, G. A.; Saven, A.; Babior, B. M.; Janda, K. D.; Eschenmoser, A.; Lerner, R. A. *Science* **2003**, *302* (5647), 1053–1056.

(111) Babior, B. M.; Takeuchi, C.; Ruedi, J.; Gutierrez, A.; Wentworth Jr., P. *Proc. Natl. Acad. Sci. U. S. A.* **2003**, *100* (6), 3031–3034.

(112) Allen, R. C.; Stjernholm, R. L.; Steele, R. H. *Biochem. Biophys. Res. Commun.* **1972**, *47* (4), 679–684.

(113) Gaut, J. P.; Yeh, G. C.; Tran, H. D.; Byun, J.; Henderson, J. P.; Richter, G. M.; Brennan, M.-L.; Lusis, A. J.; Belaaouaj, A.; Hotchkiss, R. S.; Heinecke, J. W. *Proc. Natl. Acad. Sci. U. S. A.* **2001**, *98* (21), 11961–11966.

(114) Harrison, J. E.; Schultz, J. *J. Biol. Chem.* **1976**, *251* (5), 1371–1374.

(115) Steinbeck, M. J.; Khan, A. U.; Karnovsky, M. J. *J. Biol. Chem.* **1992**, *267* (19), 13425–13433.

(116) Steinbeck, M. J.; Khan, A. U.; Karnovsky, M. J. *J. Biol. Chem.* **1993**, *268* (21), 15649–15654.

(117) Wentworth Jr., P.; Wentworth, A. D.; Zhu, X.; Wilson, I. A.; Janda, K. D.; Eschenmoser, A.; Lerner, R. A. *Proc. Natl. Acad. Sci. U. S. A.* **2003**, *100* (4), 1490–1493.

(118) Sies, H. *Angew. Chemie - Int. Ed.* **2004**, *43* (27), 3514–3515.

(119) Smith, L. L. *Free Radic. Biol. Med.* **2004**, *37* (3), 318–324.

(120) Pryor, W. W. A.; Houk, K. K. N.; Foote, C. S.; Fukuto, J. M.; Ignarro, L. J.; Squadrito, G. L.; Davies, K. J. A. *Am. J. Physiol. Regul. Integr. Comp. Physiol.* **2006**, *291* (3), R491-511.

(121) Kettle, A. J.; Clark, B. M.; Winterbourn, C. C. *J. Biol. Chem.* **2004**, *279* (18), 18521–18525.

(122) Wang, K.; Bermudez, E.; Pryor, W. A. *Steroids* **1993**, *58* (5), 225–229.

(123) Gumulka, J.; Smith, L. L. *J. Am. Chem. Soc.* **1983**, *105* (7), 1972–1979.

(124) Cornforth, J. W.; Hunter, G. D.; Popjak, G. *Biochem. J.* **1953**, *54*, 590–597.

(125) Paryzek, Z.; Martynow, J.; Swoboda, W. *J. Chem. Soc. Perkin Trans. 1 Org. Bio-Organic Chem.* **1990**, No. 4, 1222–1223.

(126) Uemi, M.; Ronsein, G. E.; Miyamoto, S.; Medeiros, M. H. G.; Di Mascio, P. *Chem. Res. Toxicol.* **2009**, *22* (5), 875–884.

(127) Takeuchi, C.; Galvé, R.; Nieva, J.; Witter, D. P.; Wentworth, A. D.; Troseth, R. P.; Lerner, R. A.; Wentworth, P. *Biochemistry* **2006**, *45* (23), 7162–7170.

(128) Stewart, C. R.; Wilson, L. M.; Zhang, Q.; Chi, |; Pham, L. L.; Waddington, L. J.; Staples, M. K.; Stapleton, D.; Kelly, J. W.; Howlett, G. J. *Biochemistry* **2007**, *46*, 5552–5561.

(129) Zhang, Q.; Powers, E. T.; Nieva, J.; Huff, M. E.; Dendle, M. A.; Bieschke, J.; Glabe, C. G.; Eschenmoser, A.; Wentworth Jr., P.; Lerner, R. A.; Kelly, J. W. *Proc. Natl. Acad. Sci. U. S. A.* **2004**, *101* (14), 4752–4757.

(130) Scheinost, J. C.; Witter, D. P.; Boldt, G. E.; Offer, J.; Wentworth Jr., P. *Angew. Chemie, Int. Ed.* **2009**, *48* (50), 9469–9472, S9469/1-S9469/14.

(131) Windsor, K.; Genaro-Mattos, T. C.; Miyamoto, S.; Stec, D. F.; Kim, H.-Y. H.; Tallman, K. A.; Porter, N. A. *Chem. Res. Toxicol.* **2014**, *27*, 1757–1768.

(132) Nadia Zopyrus. On the Origin of Secosterols upon Oxidation of Cholesterol, University of Ottawa, 2017.

2.1 Introduction

In 2016, Zielinski and Pratt published a communication addressing their recent re-examination of the long-standing dogma that cholesterol autoxidation affords one sole major product, chol-7-OOH, and instead show that it is possible to afford at least three other hydroperoxide species and their corresponding epimers,[1] as shown in **Scheme 2.1**. These findings contrasted the assumption that some cholesterol oxidation products could be used as exclusive biomarkers for endogenous oxidants. One of the most notable examples being chol-5α-OOH and the presumption that it is exclusively a product of oxidation by singlet oxygen. This work was the first time 4-, 5-, or 6-hydroperoxide had ever been directly observed as products of cholesterol autoxidation via H-atom abstraction from the two allylic positions.

Scheme 2.1 Putative mechanism of cholesterol autoxidation. Adapted from Zielinski and Pratt.[1]

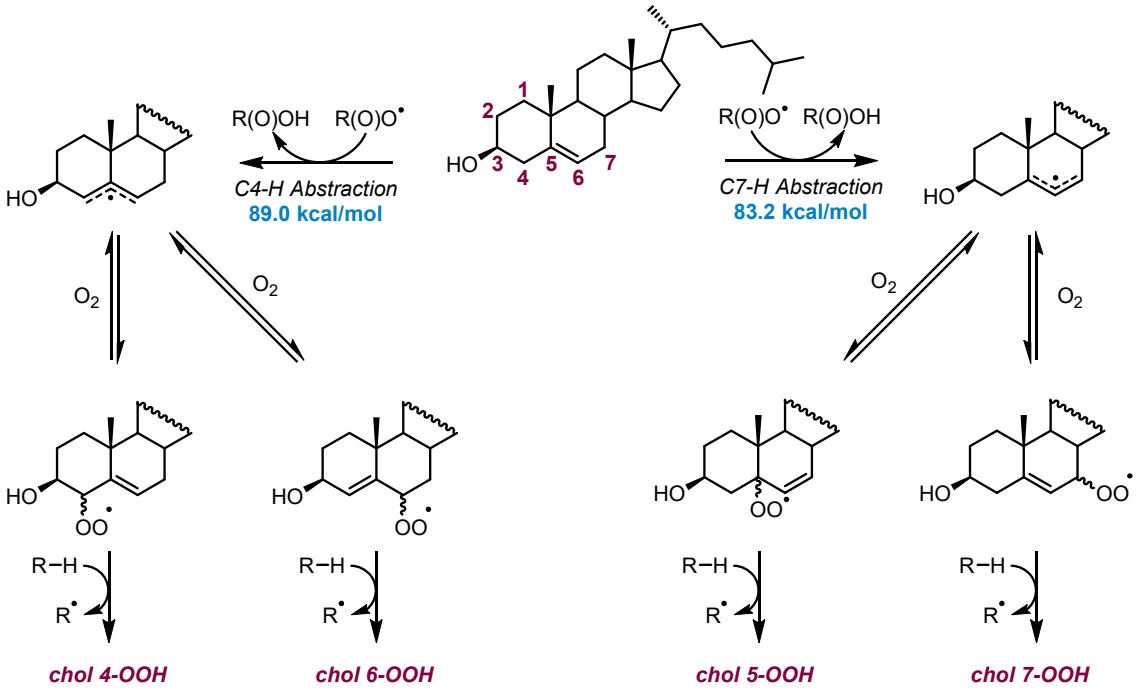

Analogous to the observation of C-11 kinetic products from linoleate autoxidation,[2] the observation of chol-5α-OOH was surprising considering the lability of the 5α-OO• and its tendency to undergo rapid β-fragmentation, however, the presence of a good H-atom donor can trap this species before it undergoes β-fragmentation to favour addition of O_2 at the C7-position. Because k_H for BDMP is of similar magnitude to the k_β for the C-5 peroxyl radical species, the 5α-OO• is trapped and 5α-OOH is generated in quantifiable amounts.

Scheme 2.2 Kinetic control of cholesterol autoxidation in the presence of a good H-atom donor, BDMP. Expression included within used for determination of k_β. Adapted from Zielinski et al.[1]

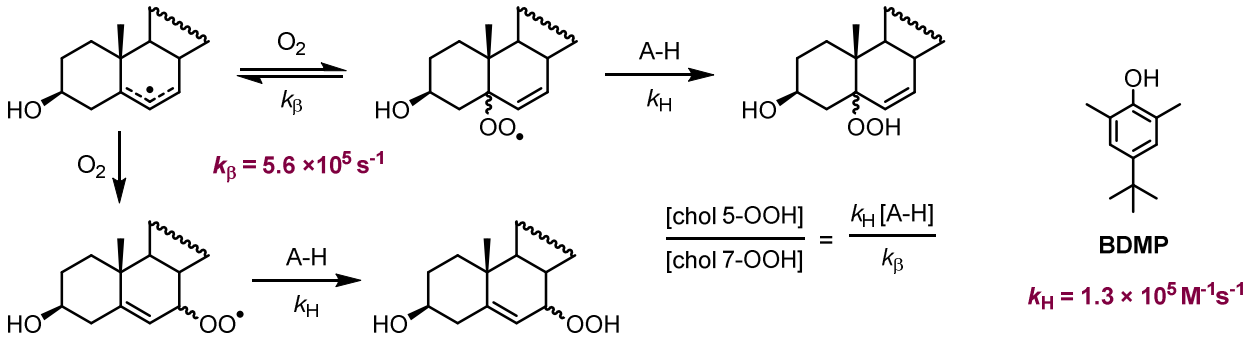

It is interesting to note that *in vivo* this process is likely facilitated by lipid-soluble RTAs, such as α-TOH, and may provide an alternative source for endogenous chol-5α-OOH.

Furthermore, the large ratio of chol-4-OH in the product distribution was surprising considering that the BDE for H-atom abstraction from the C4 position is 89.0 kcal/mol versus the lower 83.2 kcal/mol for the C7 position. However, CBS-QB3 calculations illustrate that the enthalpic barrier for C4 H-atom abstraction is lowered due to hydrogen bonding of the 3β-OH with the internal oxygen atom of the chain carrying peroxyl radical species, as shown in **Scheme 2.3.**

Scheme 2.3 Transition state structures for the H-atom abstraction from the C4 and C7 positions and their associated enthalpic barriers as calculated by CBS-QB3. Adapted from Zielinski et al.[1]

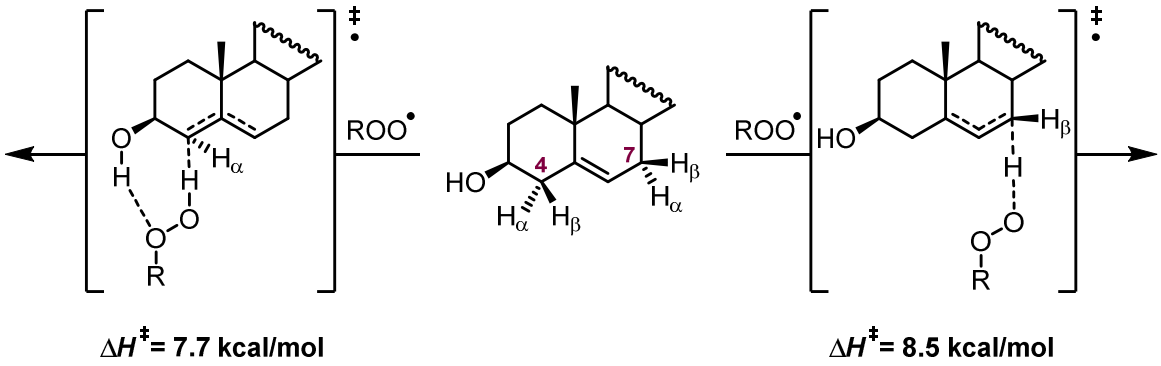

Fundamental concepts demonstrated here present numerous unforeseen considerations related to the products resulting from cholesterol autoxidation. Never before had chol-4- or 6-OOH been seriously considered to be formed in significant amounts *in vivo*, and the chol-5α-OOH had only ever been observed as a product of the high-energy oxidant, singlet oxygen. Zielinski and Pratt also note that both the chol-5- and 6-OOH can undergo acid-catalyzed Hock fragmentation to highly electrophilic secosterol species that have famously been implicated in the pathogenesis of cardiovascular disease, cancer, and neurodegeneration; their origin had controversially been credited exclusively to reaction with endogenous ozone,[3] however, this study suggests that these species likely derive from reaction with aerobic oxygen – a much simpler explanation.

A continuation of the aforementioned work by Zielinski and Pratt explores not only the products of H-atom abstraction by the chain-carrying peroxyl radical, but emphasizes the complexity of cholesterol autoxidation through exploration of the competing addition pathway and the products derived therefrom - the 5,6-α/β-epoxide species.[4] Ketone dehydration products of the aforementioned 4-, 6-, and 7-hydroperoxide species are also quantified using an updated HPLC APCI$^+$-MS/MS method. Additionally, the effects on product distribution following esterification

or deuteration of cholesterol are also explored to further probe the mechanistic attributes discussed in their 2016 report.

Peroxyl radical addition to the $\Delta^{5,6}$ double bond, the competitive pathway to H-atom abstraction of allylic hydrogen atoms in autoxidation, is expected to occur at the least sterically hindered C6 position, followed by subsequent S_Hi of an alkoxyl radical to afford the α- or β-epoxide. Rapid addition of oxygen to the resultant C5 radical prior to epoxide formation is also possible and can result in dimeric or oligomeric species, as shown in **Scheme 2.4.**

Scheme 2.4 Mechanism for the chain-carrying peroxyl radical addition to the $\Delta^{5,6}$ double bond of cholesterol to form epoxide species and other possible oligomeric products. Adapted from Zielinski et al.[4]

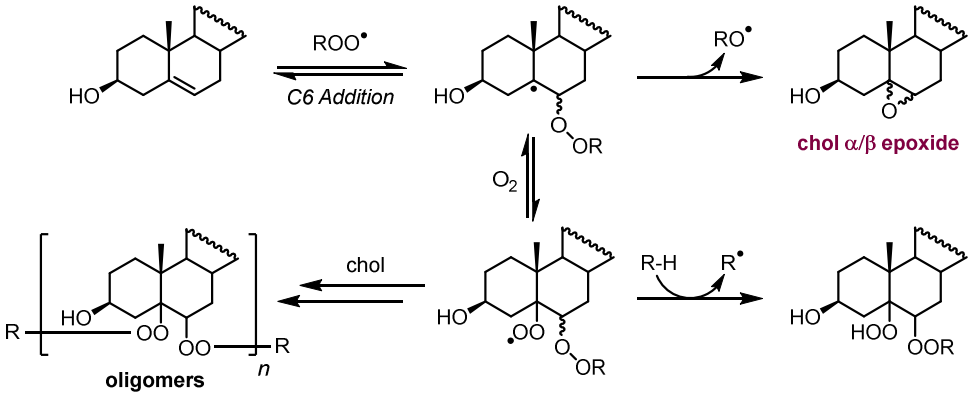

The epoxide species quantified using this updated method are shown to comprise ~ 15 % of the product distribution in an autoxidation in the absence of H-atom donor, suggesting that the addition pathway is competitive with H-atom transfer (HAT).

Using the enthalpic barrier values calculated from their computational models, the authors were able to calculate rate constants for each potential route. HAT from the C7-position is calculated to be the fastest ($k_{HAT\text{-}C7}$ = 24 $M^{-1}s^{-1}$) whilst abstraction at the C4-position is much slower ($k_{HAT\text{-}C4}$ = 0.96 $M^{-1}s^{-1}$). Surprisingly, addition to the C6 position of the $\Delta^{5,6}$ double bond (k_{epox} = 19

$M^{-1}s^{-1}$) is competitive with HAT from C7; with respect to the predominance of hydroperoxide products in their product distribution, this similarity in computed rates prompted the authors to investigate whether tunneling may play a role in the HAT pathway. Utilizing fully deuterated 2,2,4,4,7,7-d_6-cholesterol, cholesterol autoxidation with isotope substitution could be performed to determine a kinetic isotope effect (KIE).

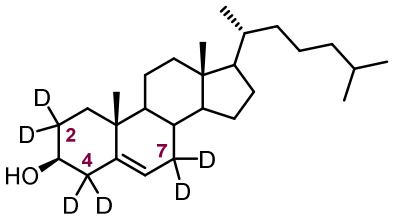

The estimated very large KIE value of $k_H/k_D = 20$ supports that tunneling does indeed contribute to the HAT pathway and provides rationale for the large contribution of H-atom abstraction products to the overall product distribution.

Mechanistic insights from the foregoing work highlight that ratio and product distribution of cholesterol autoxidation products and associated ratios are not necessarily indicative of the means by which it was generated; these ratios and distributions can be easily influenced by the presence of H-atom donor and are highly dependent upon their environment or the conditions under which they were isolated. Autoxidation is also highlighted as a possible source for chol-5α-OOH and chol-6α/β-OOH, emphasizing that high energy oxidants are not required to form these primary hydroperoxide species.

Contrasting the mechanism in organic solution, cholesterol autoxidation efficiency and product distribution within a phospholipid bilayer is expected to be influenced by the conformational constraint imposed by the polarity of the surrounding phospholipids, hydrogen bonding interactions with the surrounding phospholipids, and the nature of the propagating radical

species. Hydrophilic and hydrophobic regions of the membrane enforce anisotropy on cholesterol molecules due to their amphiphilic nature and H-bonding interactions with the surround phospholipids. Ubiquitous in cell membranes, cholesterol comprises ~ 50 mol% of all lipids in human cell membranes,[5] however, the remaining lipids are comprised of phospholipid esters of PUFAs that exhibit much higher oxidizability than cholesterol. Although present at a much lower concentration than cholesterol, the oxidizability of these PUFAs is competitive with that of oxidation of cholesterol, as indicated by their respective bimolecular propagation rate constants (for example, $k_p = 62\ M^{-1}s^{-1}$ for linoleate and $k_p = 201\ M^{-1}s^{-1}$ for arachidonate compared to $k_p = 11\ M^{-1}s^{-1}$ for cholesterol).[6] As such, the nature of the propagating radical during *in vivo* cholesterol autoxidation is most likely PUFA-derived.

To probe the influence of a phospholipid membrane environment on cholesterol autoxidation and resultant product distribution, we have autoxidized cholesterol within liposomal membrane systems of different lipid composition, followed by sterol extraction and subsequent analysis using the normal-phase HPLC-APCI$^+$-MS/MS method developed for the identification and quantification of cholesterol autoxidation products described in the aforementioned work. This provides an interesting opportunity to analyze the distribution of these products in various *in vitro* physiological models. Following recent work from Zielinski and Pratt,[1,4] we currently have a very thorough understanding of the mechanism of cholesterol autoxidation in organic solution, however, these new mechanistic insights have yet to be investigated in a physiologically-relevant context.

2.2 Results

2.2.1 Development of an HPLC-APCI$^+$/MS/MS Method for the Determination of Cholesterol Autoxidation Products in Phospholipid Membranes

Cholesterol was co-autoxidized in the presence of PUFAs in liposomal membrane systems prepared using either egg-phosphatidylcholine (egg-PC) or soy lecithin (soy LC) in phosphate-buffered saline (PBS) buffer. A composition of 43.5 mol% chol in phospholipid was used in all assays based upon previous liposomal studies,[7,8] such that small unilamellar vesicles (SUVs) were prepared containing 2 mM phospholipid and 1.54 mM cholesterol in 2 mL of PBS for autoxidations; SUV liposomal preparations were measured at 133 nm (PDI = 0.180) in diameter by dynamic light scattering. Upon preparation of cholesterol-loaded liposomes, autoxidation was initiated using the lipid-soluble azo-initiator MeOAMVN at 37°C and left to proceed for 16 hours. Oxidations were then quenched with a solution containing BHT and PPh_3 in order to terminate the free radical chain reaction and reduce any hydroperoxides to their corresponding alcohols, respectively. Cholesterol-derived oxidation products were extracted using a modified Bligh-Dyer approach,[9] and passed through silica-based Sep-Pak cartridges to remove remaining phospholipids prior to analysis. Sterol extracts were analyzed by normal-phase HPLC-APCI$^+$/MS/MS and UV detection with deuterated internal standards for accurate quantification of the chromatographically separated products. The approach is summarized in **Scheme 2.5**.

Scheme 2.5 General workflow for the preparation and analysis of cholesterol-PUFA co-autoxidations in egg-PC liposomes.

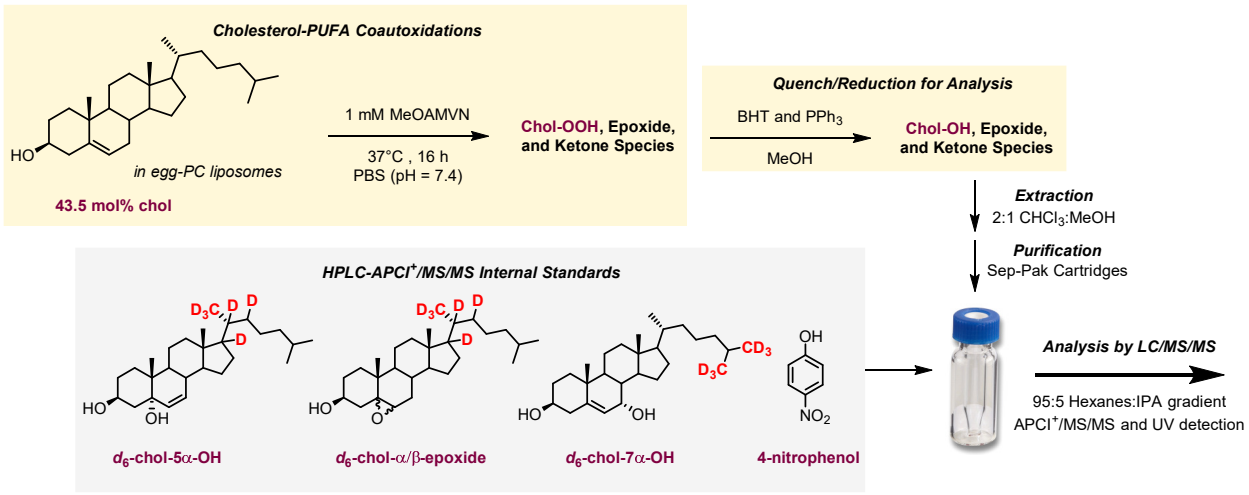

Using this approach, we were able to quantify the following products of cholesterol autoxidation: chol-4α-, 4β-, 5α-, 6α-, 6β-, 7β-, 7α-OH, chol-5,6-α/β-epoxide, and 4-, 6-, and 7-ketocholesterol, and a set of representative chromatograms appear in **Scheme 2.6**.

Scheme 2.6 Cholesterol autoxidation products quantified by normal-phase HPLC-APCI$^+$/MS/MS (**A**) and representative chromatograms for the detection of the cholesterol autoxidation products separated using a 95:5 hexanes:IPA gradient and quantified by APCI$^+$-MS/MS (**B**).

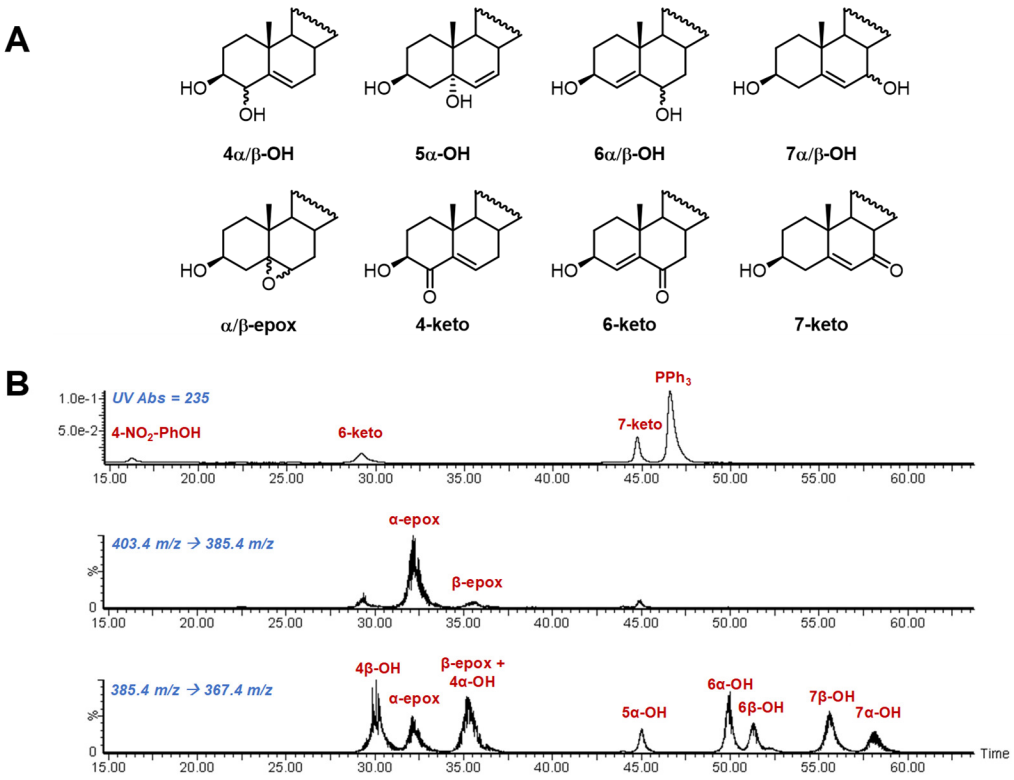

Quantification of the products first required determination of the efficiency with which they were extracted from the autoxidation samples. Extraction efficiency, expressed as a percentage of material recovered following extraction, was evaluated through the extraction of known amounts of each authentic standard (50 μM) from egg-PC liposomes subjected to the same extraction procedure used in the corresponding autoxidation experiments. The extracted authentic standards were then quantified by normal-phase (95:5 hexanes:isopropanol gradient) HPLC-APCI$^+$-MS/MS and UV detection with respect to deuterated chol standards and 4-nitrophenol, respectively. As described by Zielinski and Pratt,[4] these deuterated standards have unique MS/MS transitions such that they are detected independently of the alcohols and epoxides of interest. Although the cholesterol diols and cholesterol epoxides exhibit the same MS/MS transition (384.5

m/z → 367.4 *m/z*) of $[M+H-H_2O]^+$ → $[M+H-2H_2O]^+$, and the chol-4α-OH and β-epox happen to coelute, the α/β-epoxides can be accurately quantified as they also exhibit a unique transition independent of the diols (403.4 *m/z* → 385.4 *m/z*) of $[M+H]^+$ → $[M+H-H_2O]^+$. A representative set of chromatograms for each of the channels monitored during detection is shown in **Figure 2.1**. Ionization efficiency for each authentic standard is applied as a correction factor using the same values as previously reported.

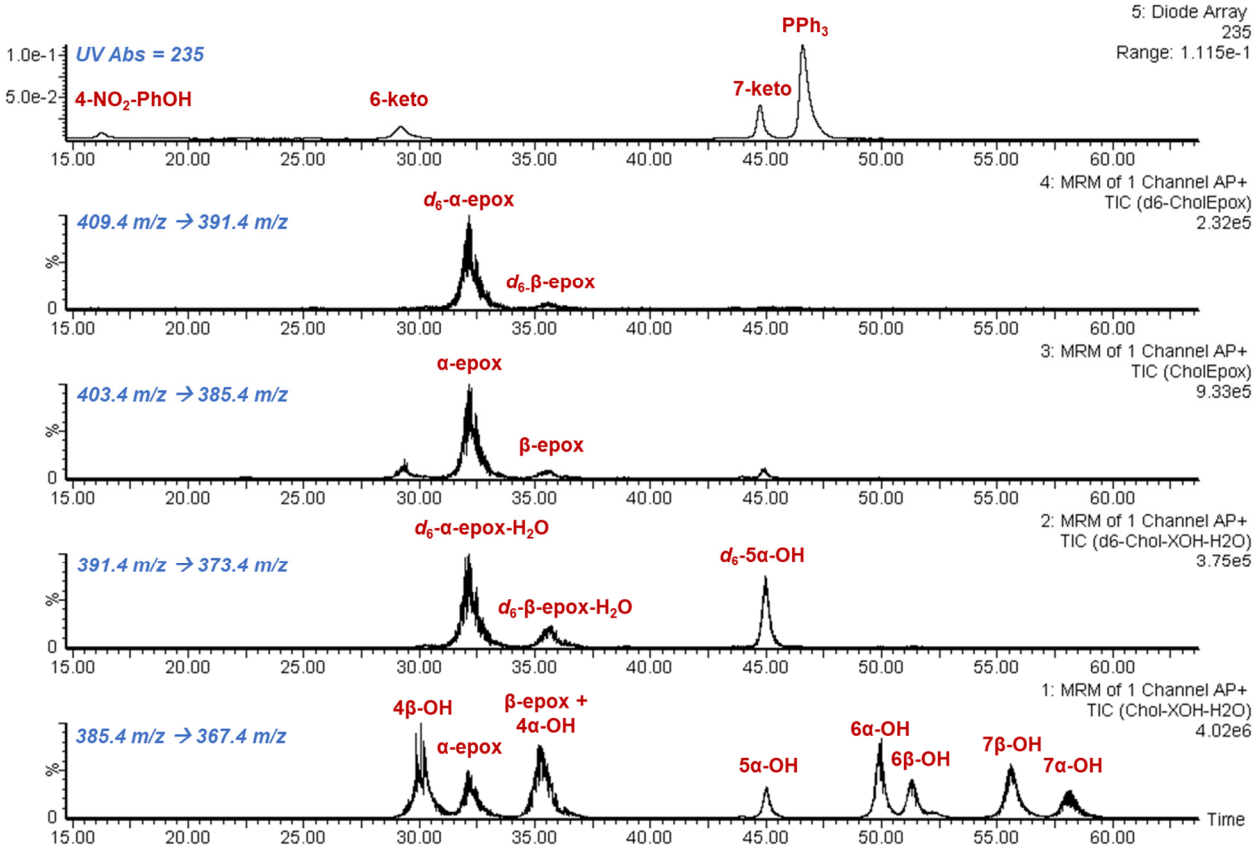

Figure 2.1 Representative HPLC-APCI$^+$/MS/MS chromatograms for all authentic standards following their extraction from egg-PC liposomes and the internal standards utilized for their quantification.

Although most compounds were exhibited extraction efficiencies near 100%, the 4β-, 7α-, and 7β-OH diols consistently exhibited extraction efficiency values much greater than 100%.

Replacement of the corona pin of the MS ion source improved the signal-to-noise ratio in the chromatograms, which improved some of the extraction efficiency values, however, it did not completely resolve the issue. In an attempt to minimize the impact of spurious signals on the integration of these peaks for quantification of these compounds relative to the d_6-5α-OH internal standard used in our previous work, we explored the use of d_6-7α-OH as an internal standard. An example of the clear difference in response exhibited by the TQ detector at ~ 46 minutes where the d_6-5α-OH elutes versus ~ 60 minutes where the d_6-7α-OH and protiated 7α-OH elute is highlighted in **Figure 2.2B**.

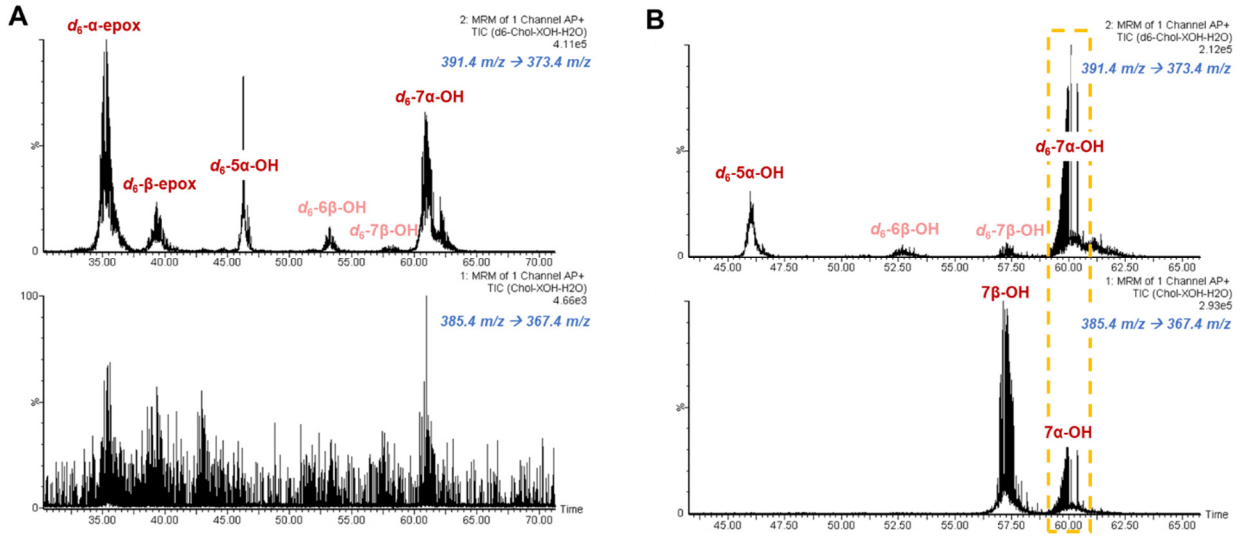

Figure 2.2 Representative HPLC-APCI$^+$/MS/MS chromatograms of all deuterated authentic standards of chol-d_6-α-epoxide, d_6-β-epoxide, d_6-5α-OH, and d_6-7α-OH (**A**) and a comparative representation of the protiated 7α/β-OH diols compared to the d_6-5α-OH, and d_6-7α-OH standards (**B**). Small amounts of d_6-6β-OH and d_6-7β-OH present as minor products of synthesis of the d_6-7α-OH by photooxidation and subsequent rearrangement, respectively. MS/MS transitions corresponding to 391.4 *m/z* → 373.4 *m/z* (top) and 385.4 *m/z* → 367.4 *m/z* (bottom).

With the authentic d_6-7α-OH in hand (synthesized by Z. A. M. Zielinski; photo-oxidation of deuterated cholesterol resulted in formation of some inseparable minor products as indicated in **Figure 2.2**), we determined the accuracy for quantification of the [chol-7-OH] when using d_6-7α-

OH as an internal standard as compared to d_6-5α-OH. The results are shown in **Figure 2.3**, indicating that the d_6-7α-OH internal standard provides a more accurate quantitation of the chol 7-OHs.

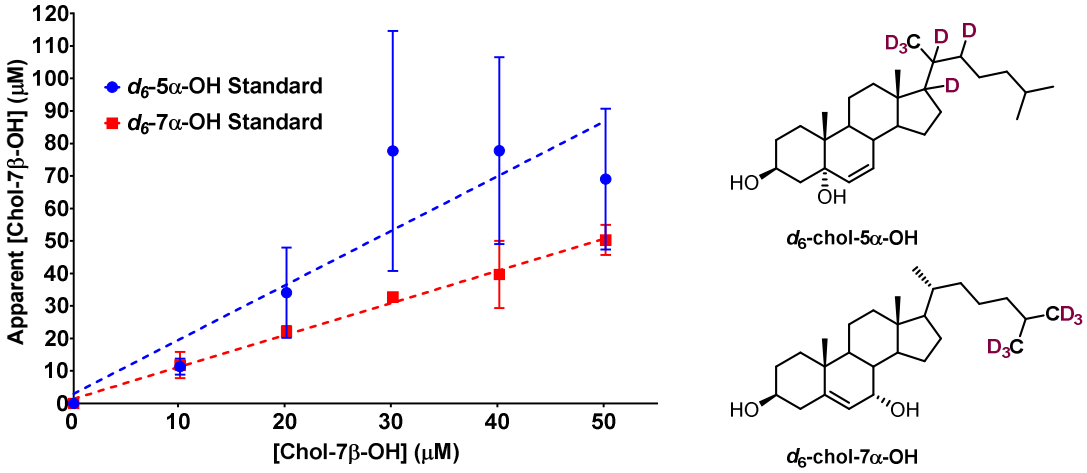

Figure 2.3 Standard curve for [chol-7β-OH] values calculated relative to 20 μM d_6-5α-OH (●) versus 25 μM d_6-7α-OH (■).

Towards resolving similar issues for the quantification of the 4β-OH following extraction, we sought to investigate whether we could establish a standard curve for the 4β-OH diol specific to its quantification following extraction. Although similar to the issues experienced with the 7α/β-OH, the extraction efficiency values for the 4β-OH appear to be *extremely* high relative to the other diols (~ 2000 %). This issue may have been resolved using a deuterated 4β-OH standard as well, however, these values seemed abnormally high even when the response from the TQ detector was normal. Therefore, we suspected that this issue must be a consequence of the extraction of this compound from a liposomal membrane, however, we did not have an explanation for why this may be the case. Nevertheless, an extraction-based standard curve was performed in which egg-PC liposomes were prepared to contain 0, 7.5, 10, 20, 22.5, 30, 37.5, 40, or 50 μM chol-4β-OH and chol-4α-OH, followed by the aforementioned extraction procedure. HPLC-APCI$^+$-MS/MS

analysis was performed with 20 µM d_6-5α-OH, 20 µM d_6-α-epoxide, and 5.6 µM d_6-β-epoxide as internal standards. Interestingly, the response factor calculated from the slope as shown in **Figure 2.5B** of 3.556 indicates that extraction of the 4β-OH is indeed over-estimated as a consequence of extraction. Replacement of the Sunfire silica HPLC column (100Å, 5 µm, 4.6 mm X 250 mm) for the foregoing experiments permitted separation of the β-epoxide and 4α-OH, resulting in almost perfect estimation of the [4α-OH] after extraction, as shown by the response factor of 0.9694 in **Figure 2.5B.**

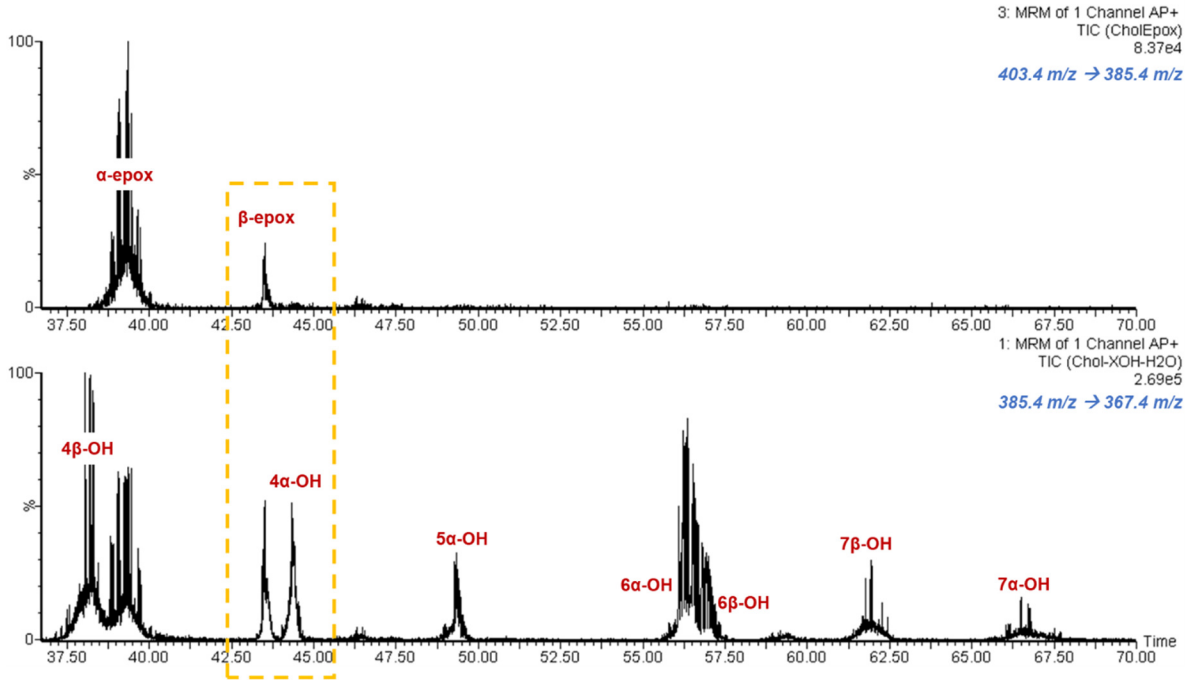

Figure 2.4 Representative HPLC-APCI$^+$/MS/MS chromatograms of protiated epoxide and diol standards following replacement of the Sunfire silica HPLC column (100Å, 5 µm, 4.6 mm X 250 mm) facilitated separation of the β-epoxide and 4α-OH in the 385.4 *m/z* → 367.4 *m/z* transition channel.

Although application of the calculated response factor to correct the extraction efficiency value for 4β-OH significantly reduced this value, the value still appeared to be greatly overestimated, as shown in **Figure 2.5A.**

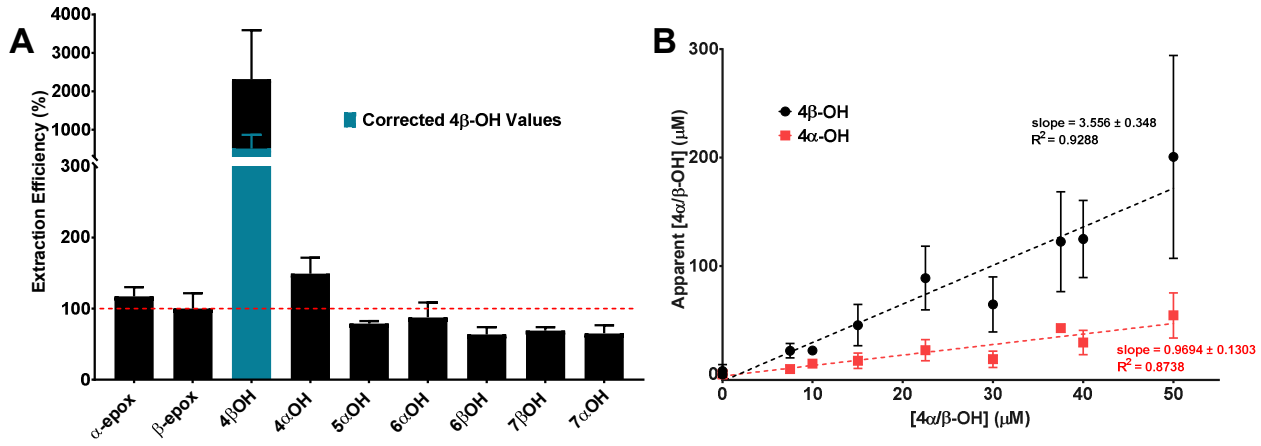

Figure 2.5 Extraction efficiency values for cholesterol α-epox, β-epox, 4β-OH (corrected), 4α-OH, 5α-OH, 6α-OH, 6β-OH, 7β-OH, and 7α-OH standards extracted from egg-PC liposome preparations (**A**) and the corresponding extraction efficiency standard curve prepared for chol-4α-(■) and β-OH (●) to account for their high response upon extraction from egg-PC liposomes (**B**). Correction factor from **B** for 4β-OH (3.556) was applied to provide the corrected 4β-OH values.

Table 2.1 Extraction efficiency values obtained for α-epox, β-epox, 4β-OH (corrected), 4α-OH, 5α-OH, 6α-OH, 6β-OH, 7β-OH, and 7α-OH standards extracted from egg-phosphatidylcholine liposomes.

	α-epox	**β-epox**	**4βOH**	**4αOH**	**5αOH**	**6αOH**	**6βOH**	**7βOH**	**7αOH**
Extraction Efficiency (%)	117.0	99.9	509.0[a]	96.9[b]	78.9	87.8	63.6	68.9	65.3

[a] *Extraction based response factor of 3.556 applied to correct value*
[b] *Used as response factor in lieu of original value due to separation of 4αOH from β-epox now permitted using a new HPLC column*

2.2.2 Cholesterol Autoxidation Products in Liposomes of Egg Phosphatidylcholine

To model cholesterol autoxidation in a phospholipid bilayer, cholesterol-loaded liposomes composed of egg-PC were prepared. Egg-PC is on average composed of ~15% linoleate with the remaining composition attributed to relatively non-reactive lipids such as monounsaturated oleate and saturated fatty acids such as stearate. Product distribution was assessed in the absence and presence of the lipid-soluble RTA α-tocopherol (k_{inh} = 4.7 x 10^3 $M^{-1}s^{-1}$ in egg-PC liposomes at

37°C)[10] to assess the influence of a biologically-relevant H-atom donor on the kinetics of products generated.

Cholesterol-loaded liposomes were prepared from 2 mM egg-PC, 1.54 mM cholesterol, and 0, 10, 25, 50, 75, or 100 µM α-tocopherol in PBS buffer (pH = 7.4). Liposomes containing different concentrations of α-TOH were measured between 109-131 nm with little change in their polydispersity index (PDI). Autoxidation was initiated with 1 mM MeOAMVN at 37°C and the samples were left open to air for 16 hours with stirring. Reactions were quenched with 4 mM BHT and 4 mM PPh_3, extracted, and then subsequently purified using silica Sep-Pak cartridges. The resulting sterol extracts were analyzed by HPLC-APCI$^+$/MS/MS and UV detection and quantified relative to 100 µM 4-NO_2PhOH, 20 µM d_6-5α-OH, 20 µM d_6-α-epoxide, 5.6 µM d_6-β-epoxide, and 25 µM d_6-7α-OH internal standards. A representative chromatogram is shown in **Figure 2.6** and relevant data is summarized in **Figure 2.7**.

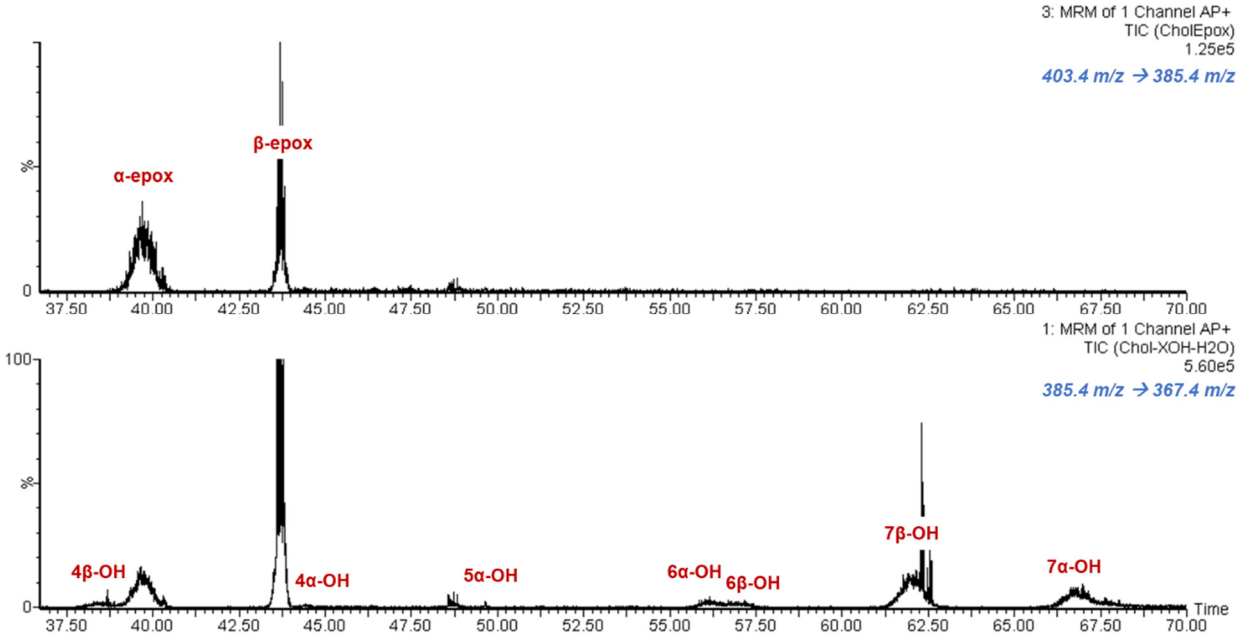

Figure 2.6 Representative HPLC-APCI$^+$-MS/MS chromatograms of epoxide and diol products extracted following uninhibited autoxidation of cholesterol-loaded egg-PC liposomes.

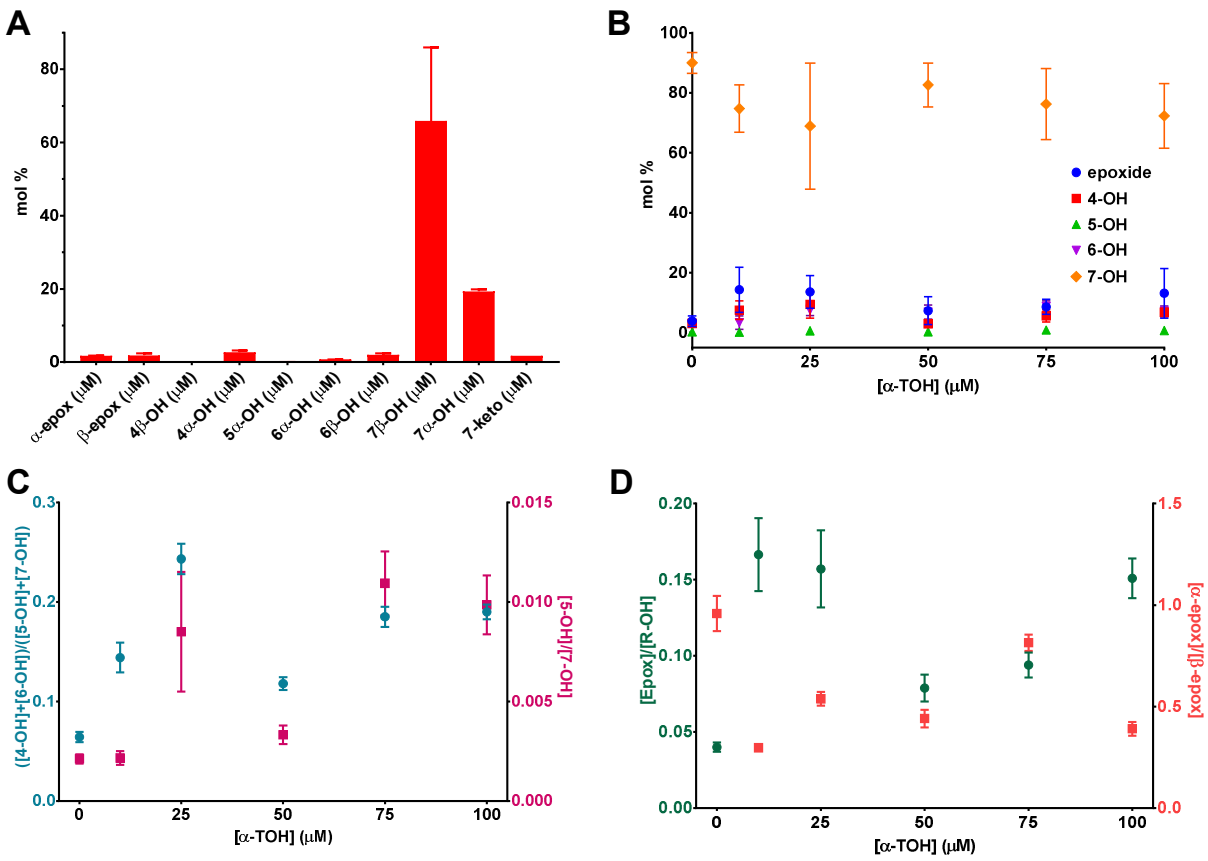

Figure 2.7 Product distribution resulting from cholesterol autoxidation in egg-PC liposomes and the effect of increasing [α-TOH]. Uninhibited cholesterol oxidation product distribution for each isomer and resultant product (**A**), influence of increasing [α-TOH] on overall product distribution (**B**), ratio of C4-H versus C7-H atom abstraction products compared against formation of C5 versus C7 hydroperoxide product (**C**), and ratio of epoxide versus H-atom abstraction products compared against formation of α- versus β-epoxide product (**D**).

It is clear that cholesterol autoxidation within this lipid bilayer model elicits chol-7-OH as the major product, particularly the β-epimer; predominance of the β-epimer is consistent with previous reports of analyses of sterol extracts of *in vivo* sources.[11–13] Interestingly, in contrast with observations made in homogenous solution, incorporation of α-TOH did not affect the product distribution to any significant extent.

2.2.3 Cholesterol Autoxidation Products in Liposomes of Soy Lecithin

To model cholesterol autoxidation in a phospholipid bilayer containing higher levels of more oxidizable polyunsaturated lipids, cholesterol-loaded liposomes composed of soy lecithin were prepared. Soy lecithin is on average composed of ~ 64% linoleate with the remaining composition attributed to relatively non-reactive lipids such as monounsaturated oleate and other saturated fatty acids. Product distribution was assessed for comparison to the less oxidizable egg PC system.

Cholesterol-loaded liposomes were prepared containing 2 mM soy lecithin and 1.54 mM cholesterol in PBS buffer (pH = 7.4). Autoxidation, extraction, and purification were carried out in the same manner as described for cholesterol-loaded egg-PC liposomes. A representative chromatogram is shown in **Figure 2.8** and relevant data displayed in **Figure 2.9.**

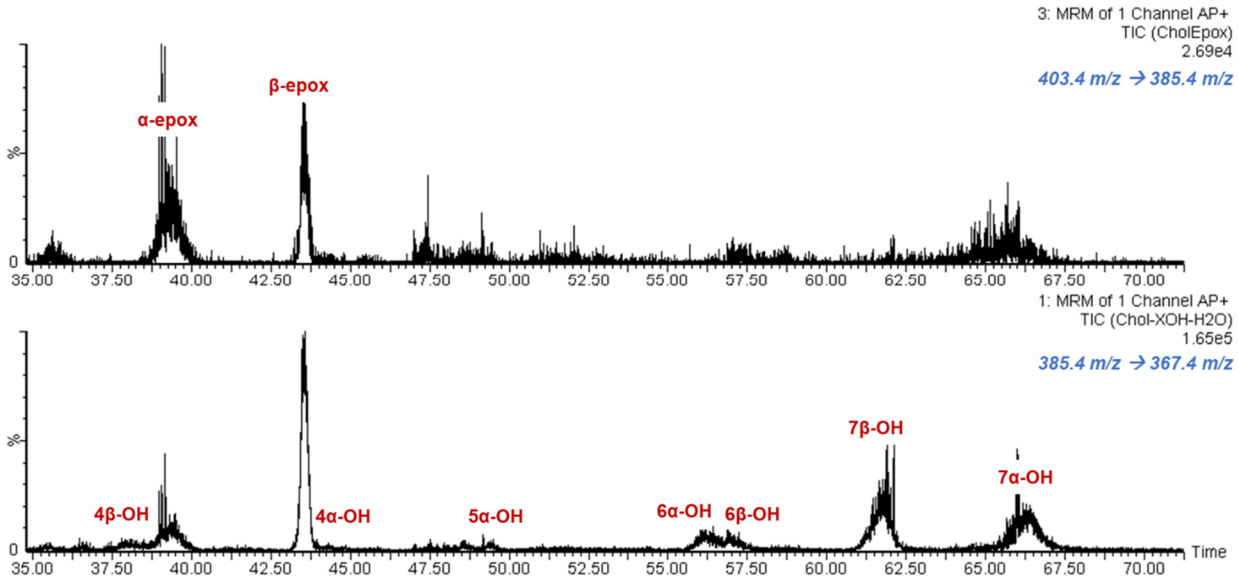

Figure 2.8 Representative HPLC-APCI$^+$/MS/MS chromatograms of epoxide and diol products extracted following uninhibited autoxidation of cholesterol-loaded soy lecithin liposomes.

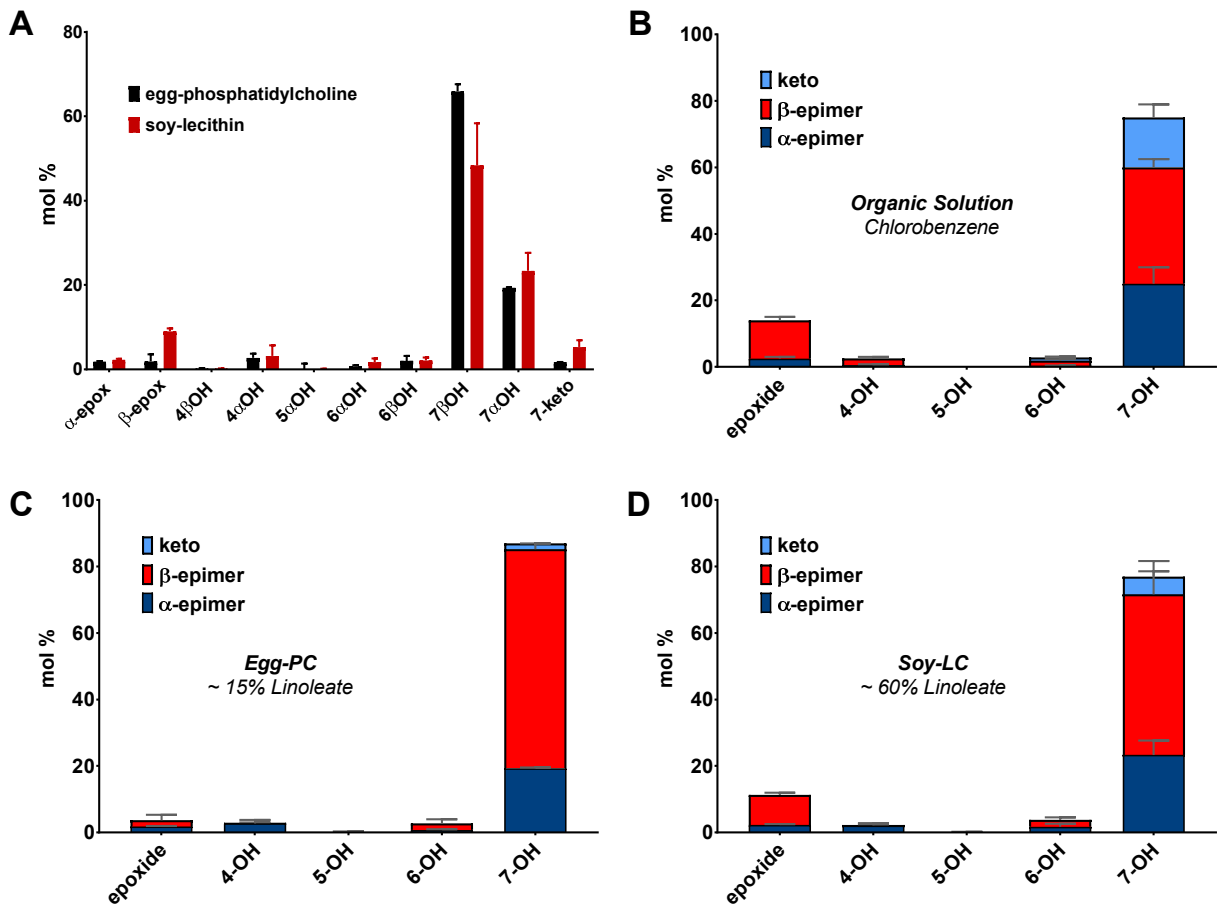

Figure 2.9 Product distribution of cholesterol autoxidation in model phospholipid membranes and comparison to that observed in organic solution. Direct comparison of cholesterol co-autoxidations in egg-phosphatidylcholine and soy lecithin model membrane systems (**A**), product distribution of cholesterol autoxidation carried out in chlorobenzene (performed by Z. A. M. Zielinski;[4] 0.5 M cholesterol, initiated by 20 mM MeOAMVN, oxidized at 37°C for 16 h) (**B**), product distribution of cholesterol autoxidation in cholesterol-loaded egg-PC liposomes (**C**) and soy lecithin liposomes (**D**) performed as previously described.

Interestingly, besides oxidation occurring within a phospholipid bilayer for both egg-PC and soy lecithin liposomal systems, product distribution favouring oxidation of the C7 position closely resembles that of oxidation in organic solution. Comparison of cholesterol autoxidations in egg-PC versus soy lecithin liposome systems appears to show some favouring for epoxide products in the system with higher susceptibility to oxidation, however the systems both show very

similar product distribution. Additionally, although the concentration detected is relatively low, cholesterol autoxidation products never directly observed *in vivo* (4α/β-OOH) are detected in our *in vitro* models.

2.2.4 Cholesterol Autoxidation Products in Human Embryonic Kidney Cells

To attempt to model cholesterol autoxidation in the phospholipid bilayer of a cell membrane, human embryonic kidney (HEK 293) cells were supplemented with cholesterol and ferroptotic cell death was induced using the small-molecule GPX4 inhibitor, (1*S*,3*R*)-RSL3. In the absence of RSL3 treatment, we were unable to observe quantifiable product, likely due to the inadequate accumulation of hydroperoxide. Additionally, cells were also supplemented with exogenous cholesterol as we were unable to observe quantifiable product without supplementation. PUFA and cholesterol composition of HEK 293 cells does not appear to be very well characterized, however, one study reports that linoleate and arachidonate compose ~ 50 % and ~ 20 % of all lipid quantified in their assay, respectively,[14] whilst cholesterol has been shown to comprise ~ 20 %.[15] Product distribution was assessed for comparison to our much less complex liposomal systems.

Methods for induction of ferroptosis and subsequent extraction for analysis were modelled after a method developed by our group for the analysis of phospholipid hydroperoxide products in ferroptotic cell death systems.[16] HEK 293 cells were cultured to confluency and supplemented with 50 μM cholesterol for overnight incubation at 37°C to allow for diffusion of cholesterol into the cell membrane. The media was then removed and the plate was washed with PBS buffer (pH = 7.4) to remove any free cholesterol that did not diffuse into the cells. Ferroptosis was then induced using fresh media containing 5 μM RSL3 and was left to incubate for 6 hours at 37 °C. After 6 hours, cells were harvested and flash frozen immediately until analysis. Similar to our

liposomal system, the cells were treated with BHT and PPh_3 to terminate any remaining free radical chain reactions and reduce the hydroperoxides to their corresponding alcohols, respectively. Although methanol is sufficient for disruption of liposomal membranes, sonication was used to encourage complete destruction of the cell membrane for efficient extraction. Sterol products were extracted using chloroform and brine and separation was encouraged by centrifugation. Following extraction, sterol extracts were purified using silica Sep-Pak cartridges prior to analysis. Sterol extracts were then analyzed by normal-phase HPLC-APCI$^+$/MS/MS and UV detection; a representative chromatogram is shown in **Figure 2.10**.

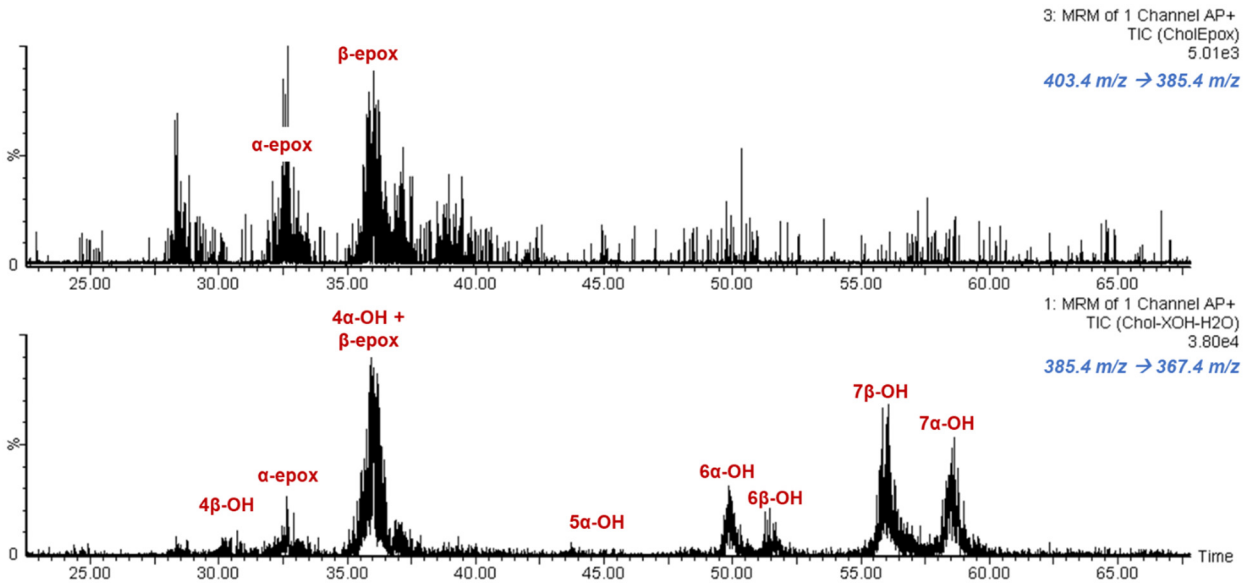

Figure 2.10 Representative HPLC-APCI$^+$/MS/MS chromatograms of cholesterol epoxide and diol products extracted from HEK 293 cells following RSL3-induced ferroptotic cell death.

Unfortunately, the concentration of products extracted from HEK 293 cells, even with supplementation of exogenous cholesterol, were too low to accurately quantify the concentration of most products. Attempts to enhance the scale of the experiment using larger plates for cell growth did not improve the resolution of products drastically and only led to difficulty in purification by Sep-Pak cartridge and eventual overloading of our preparative HPLC column.

Therefore, analysis of product distribution can only be made qualitatively based upon low recovery of sterol extracts, however, the qualitative product ratios are still of interest. Of particular note, 6α- and 6β-OOH species are present in observable amounts considering their absence in previous assays. Unsurprisingly, C7 oxidation products appear to be predominant as observed in all other assays performed by our group and is consistent with previous reports from the literature.

2.2.5 Cytotoxicities of Cholesterol Hydroperoxides

With the authentic cholesterol-5α-, 6β-, and 7α-OOH in hand (obtained preparatively from photo-oxidation, much higher yielding than autoxidation for these isomers), we were able to evaluate the potential for cholesterol hydroperoxides to sensitize cells to ferroptotic cell death. Our understanding of the product distribution of cholesterol autoxidation in our *in vitro* model systems enabled us to assess the translation of the actual cytotoxic potential of the hydroperoxide species upon their generation *in vivo* and their capacity to serve as substrates for detoxification by GPX4.

Covalent modification of the active site selenol of GPX4 by RSL3 prevents reduction of lipid derived hydroperoxides to their corresponding alcohols, leading to accumulation of hydroperoxides and eventual ferroptotic cell death - for the purpose of this assay, RSL3-mediated inhibition of GPX4 allows for the assessment of the natural ability of the cell to detoxify exogenously administered cholesterol hydroperoxide species. In our initial attempts to explore the cytotoxicity of these compounds, we used the mammalian cell line HEK 293 as this cell line has a known susceptibility for sensitization to ferroptotic cell death, and could be easily transfected for future assays. HEK 293 cells were treated with 0.25 μM RSL3 for 30 minutes and subsequently treated with the corresponding chol-OOH species. Following administration of the chol-OOH species, the cells were incubated for an additional 5 hours and cell viability was then assessed by AquaBluer assay. Over the course of 6 hours, control experiments showed treatment of HEK 293

cells with 0.25 μM RSL3 under the same conditions induced death of ~ 5 % of cells. Coinciding experiments were performed in the absence of RSL3 treatment to generally assess the cytotoxicity of the chol-OOH species under our experimental conditions.

Chol-OOH species were administered to cells using liposomes as the delivery vehicle due to their poor solubility in aqueous media. Liposomes were prepared containing 2:1:1 egg-PC:cholesterol:chol-OOH where the concentration reported herein corresponds solely to the amount of chol-OOH within the liposomes prepared. Control experiments in which HEK 293 cells are treated with egg-PC-cholesterol liposomes prepared without chol-OOH show no cytotoxicity under the same conditions. This indirect delivery method does appear to induce cytotoxicity, however, the TC_{50} values determined may be artificially high due to the inefficiency of diffusion of the chol-OOH species from the liposome vesicle to the cell membrane. Nevertheless, the result of this assay provides informative trends with regards to the relative cytotoxicity of each isomer to one another as shown in **Figure 2.11**.

Interestingly, the 6β-OOH appears to exhibit the lowest cytotoxicity (TC_{50} = 126.8 μM), however, upon RSL3-mediated inhibition of GPX4 coupled with addition of 6β-OOH, it appears that the cells experience a drastic reduction in cell viability (TC_{50} = 50.0 μM) suggesting that 6β-OOH is a very good substrate for GPX4 and is reduced efficiently to 6β-OH by the unmodified enzyme. In the case of 5α-OOH and 7α-OOH, both compounds appear to be relatively cytotoxic to cells under normal conditions (TC_{50} = 16.8 and 24.5 μM, respectively), however, RSL3-mediated inhibition of GPX4 does not appear to drastically reduce cell viability (TC_{50} = 11.8 and 17.5 μM, respectively) compared to observations for 6β-OOH, suggesting that 5α-OOH and 7α-OOH are relatively poor substrates for GPX4. This trend in cytotoxicity (potency to induce cell death: 6β-OOH << 7α-OOH < 5α-OOH) and ability of GPX4 to reduce the hydroperoxide to its

corresponding alcohol (as a substrate for GPX4: 6β-OOH > 7α-OOH ≈ 5α-OOH) is consistent with similar experiments previously reported.[17,18]

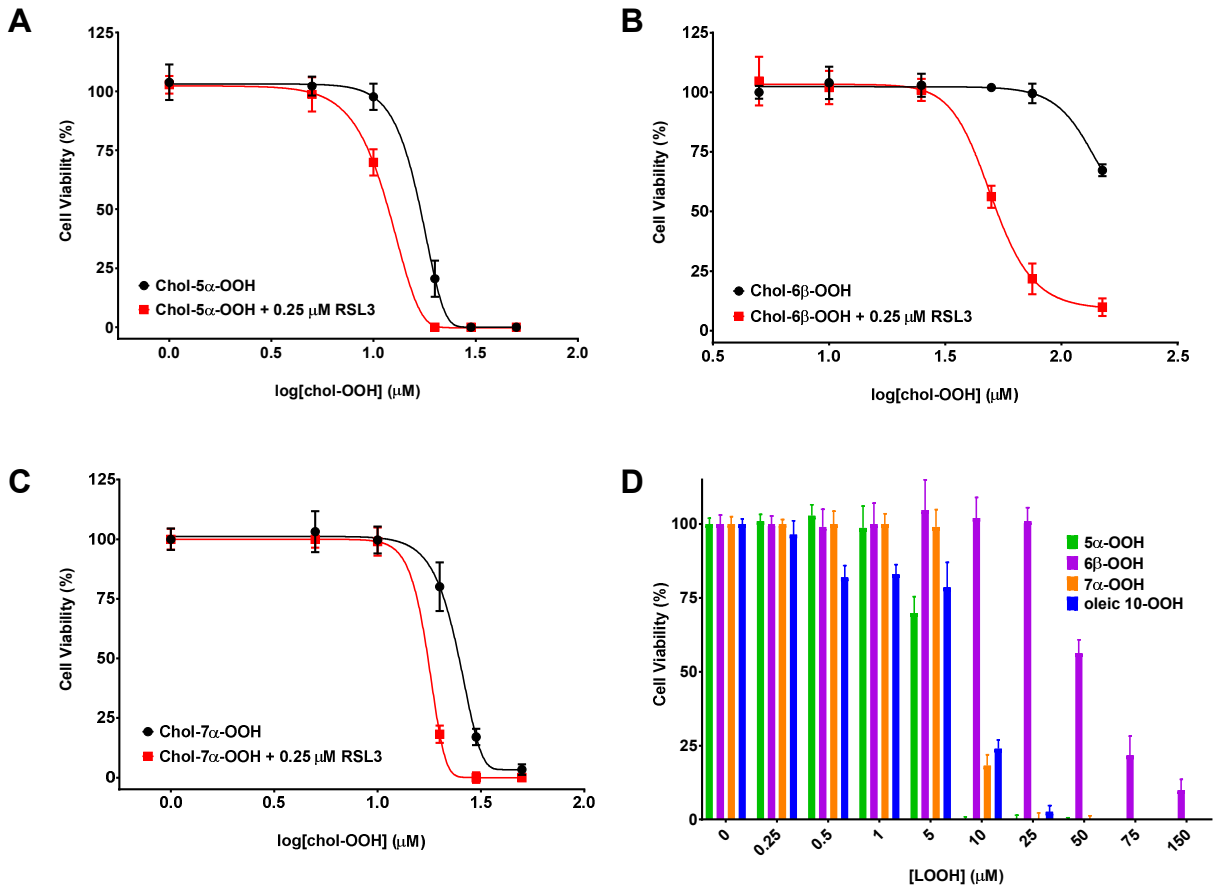

Figure 2.11 Effect of RSL3-mediated inhibition of GPX4 on the cytotoxicity of cholesterol 5α-OOH (**A**), 6β-OOH (**B**), and 7α-OOH (**C**) in HEK 293 cells and a comparison of the sensitization of HEK 293 cells to ferroptosis with 0.25 μM RSL3 in the presence of various concentrations of exogenously prepared hydroperoxides: 5α-OOH (green), 6β-OOH (purple), 7α-OOH (orange), and oleic 10-OOH (blue) (**D**). HEK 293 cells were sensitized to ferroptosis using 0.25 μM RSL3 and chol-OOH compounds were administered in liposomes composed of 2:1:1 cholesterol:egg-PC:chol-OOH. Cytotoxicity was assessed after 5 hours by AquaBluer assay.

Analogous experiments were performed to corroborate our results in a Pfa1 mouse embryonic fibroblast (MEF) cell line, which are highly sensitive to ferroptosis.[19] As such, we anticipated that in this system a lower concentration of chol-OOH, particularly the notoriously insoluble 6β-OOH, would be required to induce cell death allowing for direct addition of the

compound rather than delivery using a liposomal vesicle as the vehicle. Experiments were carried out as described as those performed in HEK 293 cells, however a slightly lower concentration of RSL3 (0.1 μM) was required and chol-OOHs were directly administered to cells dissolved in EtOH such that the final EtOH concentration in media was < 1%; control experiments did not show toxicity upon administration of media containing 1% EtOH.

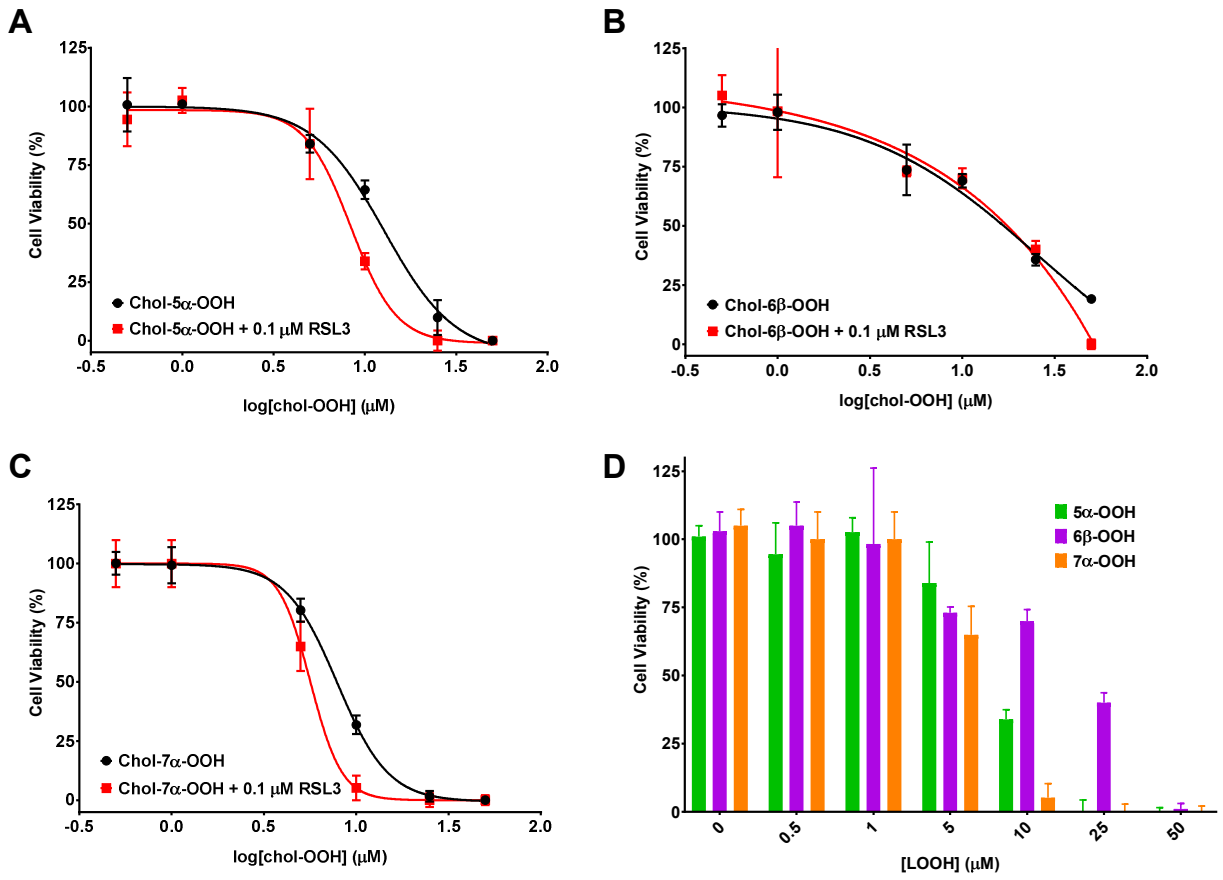

Figure 2.12 Effect of RSL3-mediated inhibition of GPX4 on the cytotoxicity of cholesterol 5α-OOH (**A**), 6β-OOH (**B**), and 7α-OOH (**C**) in Pfa1 cells. Sensitization of Pfa1 cells to ferroptosis with 0.1 μM RSL3 in the presence of various concentrations of exogenously prepared hydroperoxides: 5α-OOH (green), 6β-OOH (purple), and 7α-OOH (orange) (**D**). Pfa1 cells were sensitized to ferroptosis using 0.1 μM RSL3 and chol-OOH products were administered directly in 1% EtOH. Cytotoxicity was assessed after 5 hours by AquaBluer assay.

Under these conditions, we do observe a reduction in the TC_{50} values for each compound, reflecting the higher sensitivity of Pfa1 cells. However, the same trends observed in our HEK 293 system do not seem to hold true in this case. In this system, 6β-OOH remains least cytotoxic (TC_{50} = 25.5 μM) compared to 7α-OOH and 5α-OOH (TC_{50} = 7.8 ± 0.6 and 12.7 ± 1.6 μM, respectively), however, the aforementioned values show that the 7α-OOH is the most cytotoxic, contrasting our other observations. Additionally, the difference is not as pronounced between treatment of cells sensitized to ferroptosis using RSL3 to those that are treated only with the chol-OOH species; for direct comparison, these values are displayed in **Table 2.2.**

Table 2.2 Comparison of TC_{50} values (μM) for the treatment of HEK 293 and Pfa1 cells with cholesterol-5α-, 6β-, and 7α-OOH in the absence or presence of RSL3. In HEK 293 cell experiments, chol-OOHs were administered in liposomes composed of 2:1:1 cholesterol:egg-PC:chol-OOH and in Pfa1 cell experiments, chol-OOHs were administered directly in 1% EtOH. Data represent the mean ± SD for three independent experiments ($P < 0.001$ for 6β-OOH in HEK 293 cells between untreated and treated with 0.25 μM RSL3 TC_{50} values as determined by one-way ANOVA, all other values were not significant (i.e. $P > 0.05$)).

	HEK 293 Cells		***Pfa1 Cells***	
Chol-OOH Species	**Untreated**	**Treated with 0.25 μM RSL3**	**Untreated**	**Treated with 0.1 μM RSL3**
5α-OOH	16.8 ± 2.3	11.8 ± 1.9	12.7 ± 1.6	8.3 ± 1.1
6β-OOH	126.8 ± 11.7	50.0 ± 3.4	25.5 ± 4.5	20.0 ± 6.0
7α-OOH	24.5 ± 1.2	17.5 ± 2.0	7.8 ± 0.6	5.6 ± 0.4

Although the method of direct delivery versus liposomal theoretically allows for more rapid incorporation of the chol-OOH species into the cell membrane, it is possible that chol-OOH administered in this way experience similar barriers to diffusion into the phospholipid bilayer. We attempted several different precedented approaches to enhance uptake or exchange of chol-OOH including transfection with sterol carrier protein-2 (SCP-2),[20,21] treatment with dibutyryl cAMP (Bu_2cAMP) to upregulate steroidogenic acute regulatory protein (StARD1),[22] and treatment with methyl-β-cyclodextrin (MβCD) for the efflux of cholesterol to encourage uptake of the chol-OOH

species,[23] however, none of these approaches appeared to improve the resolution of the assays. Nevertheless, the results of these assays provide general trends for the toxicity of chol hydroperoxide species in addition to suggesting which compounds may be deleterious *in vivo* due to their potential to be detoxified by GPX4, combined with their inherent toxicity. Directly compared to an oleate-derived hydroperoxide, and assays of other hydroperoxide species under similar conditions,[16] it is suggestive that chol-derived hydroperoxides sensitize cells to ferroptosis.

2.3 Discussion

Cholesterol, the most abundant lipid in the human body, undergoes autoxidation to produce a myriad of cholesterol hydroperoxide species that decompose to generate deleterious electrophilic oxysterol species. Until recently, cholesterol autoxidation was believed to afford a limited range of products - namely 7α/β-OOH, cholesterol-5,6-epoxides, and 7-ketocholesterol. However, Zielinski and Pratt provided the first evidence of formation of 5α-OOH and 6α/β-OOH from the autoxidation of cholesterol, products that had only ever been observed as a consequence of singlet oxygen oxidation *in vivo*, and the first ever direct observation of 4α/β-OOH. This report presented a new opportunity to study the generation of primary hydroperoxide products of cholesterol autoxidation in biological model systems and compare the product distribution relative to that observed in organic solution as well as previous reports. Methods previously used to study cholesterol autoxidation in liposomal model membrane systems have only detected a limited scope of cholesterol autoxidation products or the influence cholesterol has on the oxidation of surrounding PUFAs.[7,24,25] With a method developed for the separation and detection of these unexplored cholesterol autoxidation products in hand, we were able to probe the influence the phospholipid membrane imparted on product distribution and comment on the role these

previously unknown oxidation products may have on the perceived toxicity of cholesterol in disease states.

With regards to the overall product distribution of cholesterol autoxidation in a phospholipid membrane, we utilized liposomal preparations of differing lipid composition for the co-autoxidation of cholesterol. For this assay, egg-PC and soy lecithin phospholipids were utilized due to the large disparity in their linoleate content (15% versus 60%, respectively). Interestingly, the general product distribution appears to coincide with that of cholesterol autoxidation within a liposome versus in organic solution. This observation is interesting as it implies that our attempts to model cholesterol autoxidation in organic solution, and some of the mechanistic conclusions we have made therefrom, provide an accurate estimation of the expected product distribution; however, we had anticipated that autoxidation of cholesterol within an anisotropic medium such as a lipid membrane may impart more influence on product distribution than what was observed. Primarily, predisposed orientation of cholesterol imposed by the polarity of the phospholipid bilayer was hypothesized to impart positional selectivity for H-atom abstraction from the C7 position at the expense of the C4 position based upon the proximity of a linoleate-derived peroxyl radical relative to the cholesterol molecule. Referring to a rather simple representation of the orientation of cholesterol relative to phospholipids in the membrane, cholesterol is positioned such that the 3β-OH can hydrogen bond with an oxygen of the phosphate head group in what is represented as a highly ordered system in **Scheme 2.7**.[26–28]

Scheme 2.7 Hypothetical positioning of cholesterol in a simplified phospholipid membrane system relative to a linoleate-derived peroxyl radical.

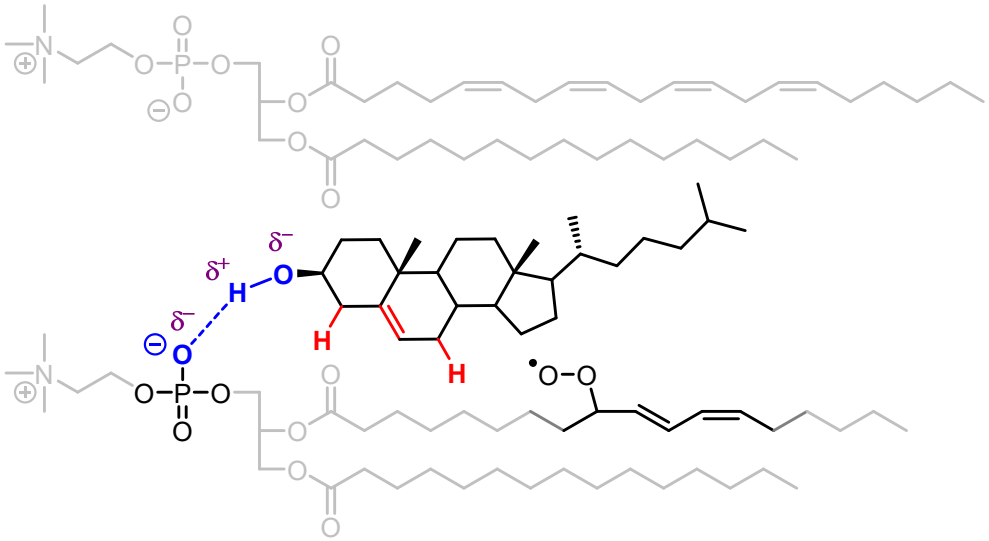

This schematic is highly suggestive of positional selectivity for C7 H-atom abstraction at the expense of C4 H-atom abstraction, which is supported in part by our data: C7 H-atom abstraction products compose ~ 90 % of the product distribution of oxidation of cholesterol in egg-PC liposomes in the absence of an H-atom donor. Although the C7 product is also favoured in organic solution, its dominance in the product distribution relative to the other possible products is not as pronounced as what is observed in a liposomal model, and could potentially be attributed to selectivity for the C7 position.

Interestingly, the oxidation of cholesterol in soy lecithin liposomes, a highly oxidizable system due to its high linoleate composition relative to egg-PC, more closely resembles that of oxidation in organic solution as it exhibits ~ 80 % C7 H-atom abstraction products and a significantly higher contribution of epoxide products (a ratio of 23:1 H-atom abstraction versus addition products in egg-PC compared to 8:1 in soy lecithin), suggesting that peroxyl radical addition plays a larger role in a lipid membrane with a higher concentration of linoleate. Increased fluidity of the membrane and a higher steady state concentration of linoleate-derived peroxyl

radical relative likely contribute to increased accessibility to the $\Delta^{5,6}$-double bond for addition. Relative to a cholesterol-derived peroxyl, PUFA-derived peroxyls are significantly less hindered and therefore more likely to facilitate addition reactions, as illustrated in **Scheme 2.8B**. Our observation that cholesterol autoxidation in chlorobenzene affords a similar ratio of H-atom abstraction versus addition products (5:1) as observed in soy lecithin (8:1) is understood when we compare the unhindered nature of the initiator-derived radical serving as the chain-carrying species to a linoleate-derived peroxyl.

Scheme 2.8 Nature of the propagating radical species and relative steric hinderance for H-atom abstraction (**A**) and addition (**B**) of initiator-, cholesterol-, and linoleate-derived peroxyl radicals. The initiator-derived peroxyl represents the species generated upon decomposition of MeOAMVN to an alkyl radical followed by immediate reaction with oxygen.

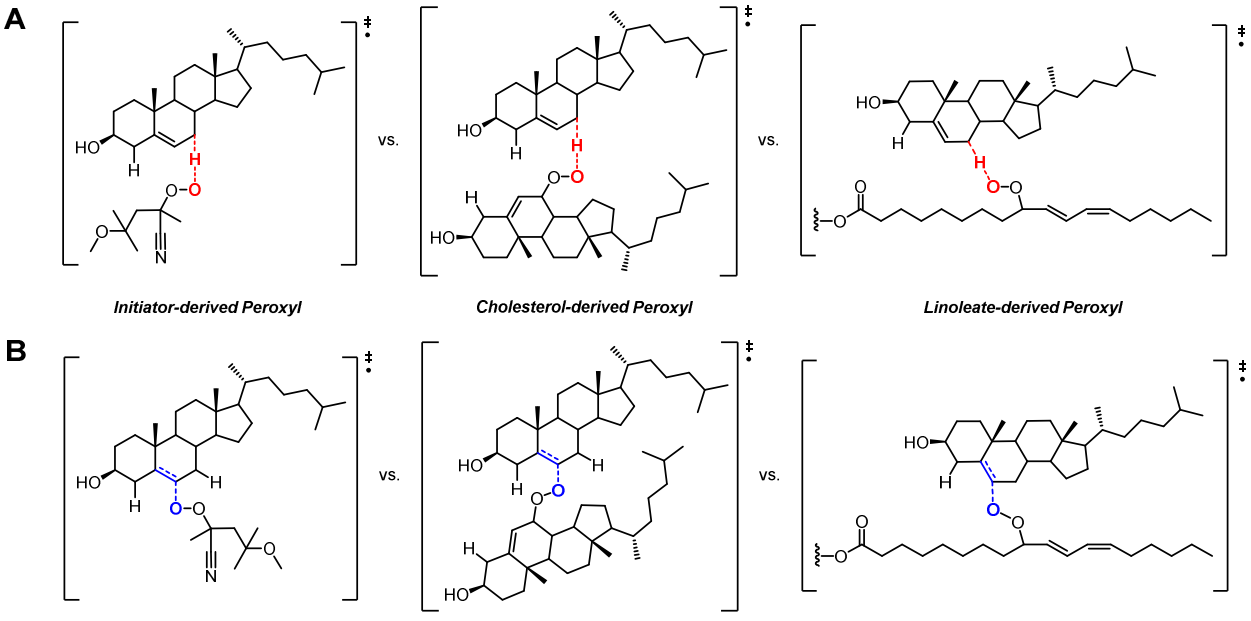

Beyond the restricted orientation of cholesterol and its proximity to the propagating radical species, hydrogen bonding effects imparted by the surrounding phospholipids may also contribute to the predominance of 7-hydroperoxide products. As illustrated in **Scheme 2.7**, H-bonding is most likely to occur between the 3β-OH and the phosphate head group of the neighbouring phospholipid, restricting the availability for H-bonding with the internal oxygen of the propagating

peroxyl radical species. As described in our previous reports,[1,4] H-bonding of the internal oxygen atom of the approaching peroxyl lowered the enthalpic barrier for C4 H-atom abstraction such that 4- and 6-hydroperoxide species were observed in significant quantities. It is interesting that in our system in which H-bonding with the 3β-OH can no longer occur, we observe near-insignificant amounts of the 4- and 6-hydroperoxide species. If H-bonding no longer facilitates the reaction, it is likely that the disparity between the BDE values calculated for abstraction from the C4 and C7 positions truly reflect the enthalpic barrier to abstraction.

Scheme 2.9 Proposed transition state structures for H-atom abstraction from the C4 and C7 positions for cholesterol autoxidation in a lipid bilayer. Consideration of H-bonding of the 3β-OH with the phosphate head group is included with particular emphasis on the inability for the 3β-OH to H-bond with the internal oxygen of the approaching peroxyl during C4 H-atom abstraction.

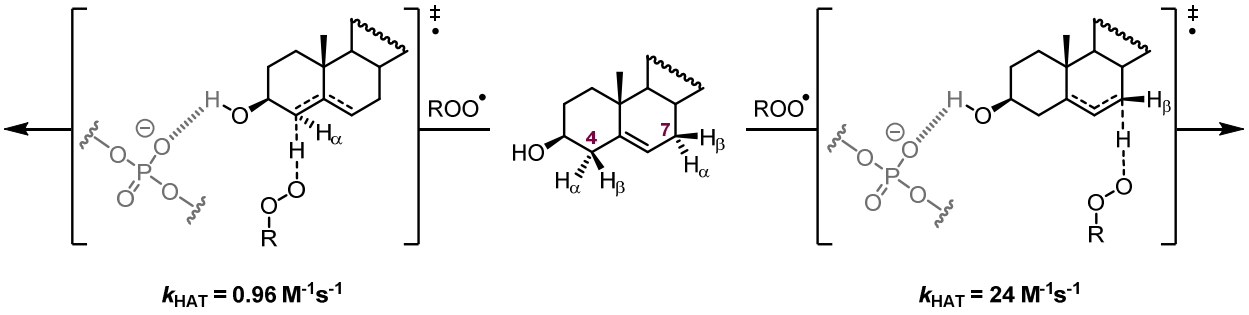

Although our previous work regarding cholesteryl acetate autoxidation resulted in very little difference in product distribution despite a similar prevention of H-bonding interaction the approaching peroxyl, it was suggested that the orientation of the approaching peroxyl radical was adjusted such that secondary orbital interactions with the $\Delta^{5,6}$ double bond could still occur, facilitating abstraction at this position. It is difficult to predict the freedom of the approaching linoleate-derived peroxyl radical to permit secondary orbital interaction with the $\Delta^{5,6}$-double bond, however, it is likely that a combination of inability to H-bond with the 3β-OH and restriction in approach of the propagating species that serves to effectively enhance the barrier to C4 H-atom

abstraction in a membrane model system such that the 4- and 6-hydroperoxide species are produced in relatively low amounts.

Our attempts to model the presence of a good H-atom donor on the product distribution invoked the use of different concentrations of α-tocopherol to trap the kinetic 5α-OO• product during cholesterol autoxidation in a lipid membrane analogous to the product analyses of linoleate autoxidation[29] and cholesterol autoxidation in organic solution.[1,4] It is recognized in several reports that the effectiveness of α-tocopherol as an H-atom donor for peroxyl radical trapping decreases dramatically in the lipid membrane compared to that observed organic solution.[30–32] The k_{inh} of α-TOH in chlorobenzene is reflective of a relatively good H-atom donor at 3.2 x 10^6 $M^{-1}s^{-1}$,[33] particularly when compared to the k_{inh} = 4.7 x 10^3 $M^{-1}s^{-1}$ calculated in egg PC liposomes.[10,32] The poor potency of α-TOH as an H-atom donor in a lipid bilayer, due to the H-bonding of the phenolic H-atom with the phosphate head group,[32] was reflected by the lack of any dependence on the [α-TOH] in the observed cholesterol autoxidation product distribution. Interestingly, this is contrary to our previous reports where increased [BDMP] led to trapping of the kinetic 5α-OOH product, however the k_{inh} value for BDMP in chlorobenzene (k_{inh} = 1.3 x 10^5 $M^{-1}s^{-1}$) was competitive with k_β = 5.6 x 10^5 for oxygen addition at the C5 position, permitting trapping of this kinetic product at high [BDMP]. Even at high [α-TOH], the k_{inh} value for α-TOH is too low to compete with the rate of β-fragmentation, as shown in **Scheme 2.10**, and therefore rationalizes why 5α-OOH is not observed upon oxidation of cholesterol in a lipid membrane. Interestingly, this suggests that the kinetic products of cholesterol autoxidation may not be of significance *in vivo*.

Scheme 2.10 Relatively poor k_{inh} value for α-tocopherol in egg-phosphatidylcholine liposomes[10] is not competitive with the k_β value[1] to trap the kinetic product of cholesterol autoxidation, cholesterol-5α-OOH.

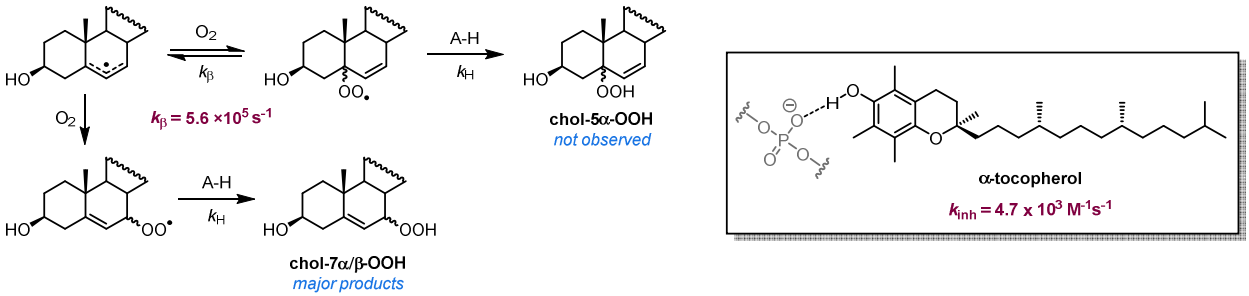

In terms of the kinetic behaviour of the reaction in a liposomal system, it appears that unlike the oxidation of cholesterol alone in organic solution, the efficiency of propagation in the presence of highly oxidizable PUFAs facilitates efficient propagation of free radical chain reactions. In a lipid membrane, this is likely a consequence of two major factors: the high effective concentration of cholesterol as it is confined in a relatively strict orientation exclusively within the lipid membrane space, and the high oxidizability of the PUFA chains of the surrounding lipid membrane relative to that of cholesterol. In our recent report,[4] the value calculated for chain length (R_p/R_i) of cholesterol autoxidation in chlorobenzene was found to be 0.9, suggesting that the reaction was stoichiometric due to direct reactions of small initiator-derived radicals with cholesterol *in lieu* of reaction with sterically-encumbered cholesterol-derived peroxyls. Interestingly, analogous experiments performed by Barclay and coworkers measure R_p using oxygen consumption in chlorobenzene and observe calculated chain length values of ~ 5.[34] These experiments are performed at a similar concentration of cholesterol (0.56 M vs. 0.5 M, respectively) and initiator (20.1 mM azobis-2,4-dimethylvaleronitrile (DMVN) used *in lieu* of 20 mM MeOAMVN). This appears to suggest that our assay is unable to quantify a portion of the oxidation products formed, suggesting that oligomerized products are formed that are not resolvable by our method; these products are likely of interest since they are unlikely to be detoxified by GPX4. Therefore, it is

likely that the use of quantification of products to calculate the kinetic chain length is useful relative to our experiments in organic solution, however, oxygen consumption experiments provide a more accurate representation of the actual chain length.

Using the quantification of cholesterol oxidation products generated in a liposomal membrane model system, we observe a much more efficient chain reaction relative to our measurements in chlorobenzene when comparing the values obtained for the kinetic chain length (R_p/R_i) in both systems. High concentrations of highly oxidizable species that can serve as more efficient chain-carriers than cholesterol-derived peroxyl radicals greatly improve the capacity for free radical chain propagation. Under autoxidation conditions, linoleate competes with cholesterol for oxidation due to its high oxidizability as indicated by its high propagation rate constant (k_p = 62 $M^{-1}s^{-1}$ versus 11 $M^{-1}s^{-1}$ for cholesterol) and relatively high concentration within both egg-PC and soy lecithin liposomes. Relative to the partial rate factor of cholesterol in both liposome systems (k_p[chol] = (11 $M^{-1}s^{-1}$)(1.54 mM) = 0.017 s^{-1}), the contribution of linoleate in egg PC liposomes (k_p[linoleate] = (62 $M^{-1}s^{-1}$)(0.33 mM) = 0.019 s^{-1}) is competitive, however, the contribution of linoleate in soy lecithin liposomes (k_p[linoleate] = (62 $M^{-1}s^{-1}$)(1.28 mM) = 0.080 s^{-1}) is much greater, greatly outcompeting cholesterol as the potential chain-carrying species. Considering the nature of linoleate as the propagating radical species, as illustrated in **Scheme 2.8**, we would expect the efficiency of propagation to be much greater in soy lecithin liposomes wherein linoleate-derived peroxyls predominate. Moreover, generation of a propagating species so close to its reactive partner increases the efficiency of propagation by effectively eliminating much of the entropic barrier to H-atom abstraction, as modelled in **Scheme 2.7**.

As expected, we do observe more efficient propagation in our lipid membrane models than in organic solution with chain length values calculated to be ~ 3; although this is reflective of the

enhanced efficiency of propagation in a lipid membrane relative to organic solution, we had anticipated a larger disparity between this value and that observed in organic solution. In combination with the aforementioned high oxidizability of linoleate and proximity of the propagating species to its substrate, the confinement of cholesterol to the lipid membrane space also increases its effective concentration relative to that of organic solution. Accounting for only the volume of the lipid space, the effective concentration of cholesterol in our liposomal preparation is closer to 0.62 M rather than 1.54 mM in aqueous buffer as we have reported; relative to the 0.5 M used for autoxidation in chlorobenzene and all other parameters remaining the same, it is surprising that the value for chain length is not significantly higher. Nevertheless, this reflects the facilitation of propagation directly compared to the inefficiency observed in organic solution under our experimental conditions and using our analytical methods.

$$x = \frac{[prod]/t}{2ek_d[In]} = \frac{R_p}{R_i}$$

Equation 2.1 Estimation of chain lengths (x) for free radical chain cholesterol autoxidation reactions in phospholipid membranes. Total amount of products ([prod] = [chol-OH] + [chol-epox] + [ketochol]) over the autoxidation time period (t) is divided by the concentration of MeOAMVN (In) and the known ek_d value[35] for MeOAMVN at 37°C in 2:1 soy-lecithin:cholesterol liposomes. Value for [prod] does not account for the products of linoleate oxidation as those products were not quantified, and so the chain length is only truly representative of the contribution of cholesterol to the overall chain reaction.

Table 2.3 Estimated chain lengths for cholesterol autoxidation in different phospholipid membrane systems at various time points under typical autoxidation conditions.

	x
Cholesterol – Chlorobenzene (16 hours)[4]	0.9 ± 0.1
Cholesterol – Egg-PC Liposomes (16 hours)	2.62 ± 0.6
Cholesterol – Egg-PC Liposomes (4 hours)	2.31 ± 0.5
Cholesterol – Soy-Lecithin Liposomes (16 hours)	3.73 ± 0.9

In reference to the values obtained between liposomes composed of egg-PC versus soy lecithin, as reported in **Table 2.3**, it is not surprising that we observe higher chain length values for soy lecithin given its aforementioned high concentration of linoleate. We were also concerned that the nature of the oxidation may change over the course of our reaction due to gradual decomposition of the initiator ($t_{1/2}$ = 6.1 h),[35] however, similar values for the chain length and comparative product distributions in egg-PC liposomes at both the 4- and 16-hour time points supports that the rate of initiation after 16 hours is relatively constant.

Overall, product quantification as a method of determining kinetic chain length is informative regarding the quantity and nature of cholesterol oxidation products that are formed - information that can not otherwise be obtained using oxygen consumption or PUFA oxidation product monitoring alone. Much like their PUFA-derived counterparts, cholesterol has a high potential to decompose to deleterious electrophiles; matched with the abundancy of cholesterol in the lipid membrane, the accumulation of primary cholesterol hydroperoxides species is inevitable regardless of low oxidizability. A combination of our method for cholesterol oxidation product quantification and total oxidation of the liposomal system would serve well towards a better understanding of the influence of cholesterol on the efficiency of propagation, as well as to provide more accurate kinetic values for comparison of cholesterol oxidation in different model liposomal systems. In order to do so, we would have to be able to quantify both PUFA-derived and cholesterol-derived hydroperoxide species, an experiment that does not appear to have ever been performed; the closest of which was performed to assess the contribution of cholesterol based upon detection of cholesterol-7α-OH, a parameter that does not take the other primary hydroperoxide products into consideration.[36,37]

An alternative proposition that is perhaps less cumbersome than oxygen consumption experiments would be the adaptation of a method previously reported from our group for the measurement of global hydroperoxide concentration;[38] this high-throughput microplate method utilizes a fluorogenic coumarin-triarylphosphine probe to monitor evolution of hydroperoxides through oxidation of the probe and reduction of the lipid-derived hydroperoxide to its corresponding alcohol analogous to the mechanism exhibited for reduction by triphenylphosphine.[39] This would facilitate the non-selective measurement of both cholesterol and PUFA derived hydroperoxide species generated in different liposomal systems with the use of minimal material, allowing us to easily assess the effect cholesterol has on the rate of propagation.

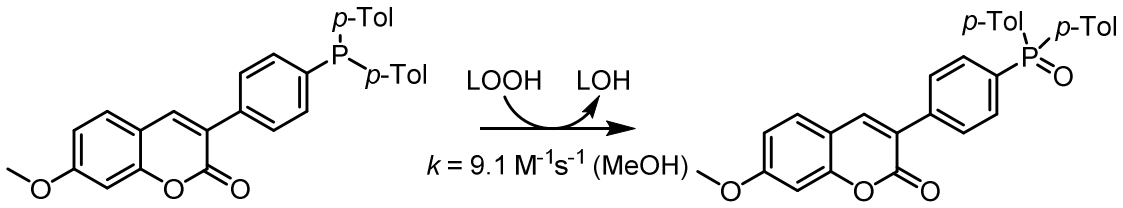

Scheme 2.11 Oxidation of a fluorogenic coumarin-triarylphosphine probe by a lipid-derived hydroperoxide species followed by subsequent reduction of the hydroperoxide to its corresponding alcohol. Adapted from Shah and Pratt.[38]

Future experiments may include measurement of chain length and the efficiency of propagation of autoxidation in liposomal systems containing different concentrations of cholesterol in tandem with our APCI$^+$-HPLC/MS/MS method for the precise quantification and identification of primary cholesterol hydroperoxides. The only consideration this assay neglects to make is the contribution and measurement of secondary autoxidation products that result from the decomposition of the hydroperoxides such as epoxides, ketones, or even aldehydes; this may also help to explain the disparity between our measurements of chain length in organic solution through product quantification versus oxygen consumption. It may also be useful to assess cholesterol

autoxidation in non-oxidizable phospholipids to inform the true potential of cholesterol-derived peroxyl radicals alone to propagate in a lipid membrane and to compare our results with those previously measured using oxygen consumption.[34]

In combination with the aforementioned experiments, it would also be of interest to explore different sources of initiating radicals and their effect on the product distribution. Although MeOAMVN serves as a good comparative model of initiation for comparison to literature-precedented autoxidations, and our previous work,[1,4] it may not be entirely representative of the generation of initiating radical species *in vivo*. Endogenous formation of initiating radicals are typically either sourced from leakage of the ETC of the mitochondria in the form of ROS such as $O_2^{\bullet-}$, HO•, or HOO•,[40] all of which are aqueous soluble in nature, or from iron-catalyzed decomposition of hydroperoxide to alkoxyl radicals that are contained within the internal lipophilic component of the membrane. It may be of interest to assess initiation in our system using an aqueous-soluble initiator such as 2,2′-azobis(2-methylpropionamidine) dihydrochloride (AAPH) or even di(4-carboxybenzyl)hyponitrite (SOTS-1), a superoxide generator,[41] to model surface-predominant initiation by aqueous soluble ROS. Perhaps most interestingly, our recent development of a new lipophilic alkoxyl radical initiator, di-tert-undecylhyponitrite (DTUN),[32] would serve as an excellent model for internal initiation of lipid peroxidation for the purposes of studying cholesterol autoxidation in a system reflective of ferroptotic cell death.

Unfortunately, quantification of cholesterol autoxidation products in mammalian cells was complicated by the relatively low amount of material isolated from extraction from cultured mammalian cells. Initial attempts to extract cholesterol autoxidation products from HEK 293 cells did not yield material sufficient for detection using our $APCI^+$/MS/MS method. This was presumed to be due to the relatively low contribution of cholesterol to the total lipid in the membrane at ~ 20

% in HEK 293 cells.[15] Simple supplementation of the cells with exogenous cholesterol did not initially appear to yield more hydroperoxide product upon quantification of the products, nor did it appear to have any subsequent impact on the viability of the cells. In light of this, we determined that perhaps a ferroptotic cell model in which RSL3-inhibition of GPX4 would facilitate accumulation of hydroperoxides. Unfortunately, we were unable to obtain sufficient cholesterol hydroperoxide products with the aforementioned adjustments to observe any more than near-baseline peaks. Subsequent attempts were made to increase the number of cells used in our assay; however, we reached the limit of solubility of the extracted product without any improvement in the yield of cholesterol hydroperoxide product. Nevertheless, consistent with our observations in both homogenous organic solution and phospholipid bilayers, it is clear that the C7 oxidation products predominate over products at any other position and 7β-OOH is also slightly favoured over the 7α-OOH species. The predominance of 7β-OOH is also consistent with reports that have previously extracted cholesterol oxidation products from oxidized LDL and human atherosclerotic plaque tissue.[11,13] Based upon the predominance of the 7-hydroperoxides in both liposomal and cellular models, forthcoming work will illustrate our investigations into the fate of these species *in vivo* (see Chapter 3).

The implication of hydroperoxide species in the initiation and execution of ferroptotic cell death prompted our evaluation of the capacity of the different isomers of cholesterol hydroperoxide to sensitize cells to ferroptosis induced by the GPX4 inhibitor RSL3. We surmised that although cholesterol-derived hydroperoxides may be formed to a lesser extent than PUFA-derived hydroperoxides due to their lower inherent oxidizability, they may sensitize cells to ferroptosis to a greater extent due to slower detoxification by GPX4. In fact, using selenium-depletion experiments to knock-out GPX4, Girotti and coworkers had reported that 5α-OOH < 6α-OOH ≈

7α/7β-OOH < 6β-OOH in terms of their reducibility by GPX4.[18] Additionally, they had reported that the reduction of cholesterol-derived hydroperoxides by GPX4 was slower than those derived from PUFAs,[42] suggesting that cholesterol hydroperoxides may be more persistent. Interestingly, we found that, similarly, 5α-OOH ≈ 7α-OOH < oleic 10-OOH << 6β-OOH in terms of reducibility by GPX4. Although the design of our assay is unique, the general trend in cytotoxicity and substrate potential is consistent with previous reports.[18,43,44] However, most surprisingly, we found that the toxicities of each of 7α-OOH, 6β-OOH and 5α-OOH were only marginally augmented by RSL3 treatment, suggesting that they do not significantly sensitize cells to ferroptosis, perhaps because their decomposition to lipid peroxidation chain-initiating species (i.e. alkoxyl radicals) is not particularly efficient. Instead their cytotoxicities may derive from other mechanisms, such as the induction of apoptosis. Indeed, we have reported that both 5α-OOH and 6β-OOH can undergo Hock fragmentation to generate electrophilic secosterol aldehydic products,[1,45] which may be the cytotoxic species in question.[46–49] If the 5α-OOH and 6β-OOH do generate the same secondary decomposition products (i.e. secosterols), it is surprising that we do not observe similar toxicity upon administration of these two primary autoxidation species if this is in fact the mechanism by which they induce cell death. Ongoing efforts to expand these investigations to include the other relevant isomers (6α-OOH, 7β-OOH and perhaps the 4α/β-OOHs) are underway.

Compared to the products of peroxyl radical addition, the weak electrophilicity and cytotoxicity of the 5,6-epoxide species[50] is likely not to significantly contribute to the overall deleterious effects of cholesterol autoxidation compared to products of H-atom abstraction, however, this remains to be explored. We have made attempts to study the relative toxicity of H-atom abstraction products versus addition products using 2,2,4,4,7,7-d_6-cholesterol; with deuteration at both the C4 and C7 positions, H-atom abstraction should be shut-down and addition

will exclusively occur, permitting the investigation of the contribution of addition products to the deleterious effects of cholesterol autoxidation. Unfortunately, we were unable to resolve any meaningful differences between treatment with this species and protiated cholesterol as they exhibited equivalent toxicity. This was thought to be due to insufficient replacement and uptake of either protiated or deuterated cholesterol and attempts to resolve these differences through encouragement of cholesterol uptake are currently under investigation.

2.4 Conclusions

In summary, our investigations of the product distribution and reaction kinetics of cholesterol autoxidation in model phospholipid liposomal membrane systems have provided insight regarding the likely mechanism *in vivo* and rationale for the predominance of cholesterol 7-hydroperoxide species in biological tissue, despite some of our most recent findings in organic solution. Absence of the kinetic 5α-OOH product upon increasing the [α-TOH] provides direct evidence for the relatively poor capacity for α-TOH to serve as a good H-atom donor in a lipid membrane, as well as the potential impact H-bonding interactions of RTAs may have towards influencing lipid peroxidation product distribution in a lipid membrane. H-bonding interactions of the 3β-OH with the phosphate head group also appeared to prevent C4 H-atom abstraction as the approaching internal peroxyl radical can no longer H-bond with the 3β-OH to lower the entropic barrier to abstraction. A combination of these two H-bonding interactions appear to explain the predominance of chol-7-OOH species as they essentially eliminate the formation of significant amounts of chol-4α/β, 5α, or 6α/β-OOH.

Investigations towards a better understanding of the addition products are currently underway, however, our results suggest that the steric hinderance of the propagating radical will dictate whether addition is favourable. Our results suggest that areas rich in unsaturation where unhindered PUFA-derived peroxyls are the chain-carrying species are more likely to exhibit a higher contribution of addition products. Propagation is also seemingly much more efficient in these systems when compared with cholesterol autoxidation in organic solution based upon chain length values calculated using the total number of products quantified using our $APCI^+$/MS/MS method. Relative to previous methods used to evaluate cholesterol autoxidation in a lipid membrane, this method is informative regarding both the quantity and nature of the oxidation products formed rather than a global value of oxidation.

In terms of the related cytotoxic effects of cholesterol autoxidation products, we evaluated the relative toxicities of these compounds in a ferroptotic cell death model. Our results supported previous observations that detoxification of cholesterol-derived hydroperoxides by GPX4 is slower relative to PUFA-derived hydroperoxides, however, that had yet to be shown exclusively for a broad range of chol-OOHs in a ferroptotic model. Additionally, the toxicities the chol-OOHs assayed were only marginally augmented by RSL3 treatment, suggesting that they do not significantly sensitize cells to ferroptosis, and that their cytotoxicity derives from other mechanisms, such as the induction of apoptosis. Decomposition of the most predominant species, cholesterol 7-hydroperoxide, and the electrophilic products formed therefrom, may serve to explain the deleterious effects associated with cholesterol autoxidation.

2.5 Experimental

All chemicals and solvents were purchased from Sigma Aldrich Co. LLC and used as received, unless otherwise stated. Cholesterol (92%) was purified to >99% by the well precedented method of bromination/debromination to remove other sterol impurities.[51] The >99% cholesterol was then freshly recrystallized from methanol prior to each experiment to remove trace oxidation product impurities. MeOAMVN[35] was purchased from Wako Pure Chemical Industries, Ltd. and used as received. BHT and PPh_3 were recrystallized from hexanes prior to use. 17,20,21,21,21,22-d_6-5α-hydroxycholesterol and 17,20,21,21,21,22-d_6-cholesterol-5,6-epoxide were graciously provided by Z. A. M. Zielinski; synthesized as described in our recent report.[4] (1*R*,3*S*)-RSL3 was synthesized according to literature procedures.[19,52] MEM media with/without phenol red, Dulbecco's phosphate buffered saline (DPBS), fetal bovine serum (FBS), penicillin-streptomycin, and AquaBluer were purchased from commercial sources and used as received.

Synthesis of 5α-, 6β-, and 7α-hydroperoxycholesterol (chol-5α-, 6β-, and 7α-OOH): Prepared by photo-oxidation of cholesterol as previously described,[53,54] species were separated and isolated by preparative HPLC (1 mL/min; 95:5 MeOH:H_2O; XBridge Prep C18, 5 µm, 10 X 150 mm). Analytical data in accordance to those reported in literature.[53] ***Cholesterol-5α-OOH***: ^{1}H-NMR (400 MHz; $CDCl_3$): δ 7.05 (s, 1H), 5.83 (dd, J = 10.0, 2.1 Hz, 1H), 5.60 (dd, J = 10.0, 2.7 Hz, 1H), 4.11 (tt, J = 10.8, 5.4 Hz, 1H), 2.39 (ddd, J = 13.2, 5.1, 1.7 Hz, 1H), 1.93 (td, J = 26.0, 9.9 Hz, 7H), 1.73 (t, J = 13.1 Hz, 4H), 1.57-1.45 (m, 11H), 1.38-1.11 (m, 9H), 1.00 (t, J = 9.5 Hz, 2H), 0.95-0.85 (m, 12H), 0.69 (s, 6H). ***Cholesterol-6β-OOH***: ^{1}H-NMR (400 MHz; $CDCl_3$): δ 7.69 (s, 1H), 5.65 (t, J = 1.5 Hz, 1H), 4.33 (dd, J = 4.0, 2.3 Hz, 1H), 4.21-4.17 (m, 1H), 2.07-1.98 (m, 3H), 1.81-1.08 (m, 36H), 1.04-0.92 (m, 3H), 0.90 (d, J = 6.5 Hz, 4H), 0.86 (dd, J = 6.6, 1.8 Hz, 8H), 0.74 (ddd, J = 22.1, 10.8, 4.9 Hz, 2H), 0.68 (s, 3H)**.** ***Cholesterol-7α-OOH***: ^{1}H-NMR (400 MHz;

$CDCl_3$): δ 7.71 (s, 1H), 5.72 (dd, J = 5.0, 1.8 Hz, 1H), 4.16 (td, J = 4.7, 1.6 Hz, 1H), 3.66-3.58 (m, 1H), 2.44-2.28 (m, 2H), 1.97 (dt, J = 8.7, 4.1 Hz, 1H), 1.92-1.82 (m, 4H), 1.62 (td, J = 11.5, 4.6 Hz, 3H), 1.53-1.45 (m, 5H), 1.42-1.27 (m, 7H), 1.20-1.10 (m, 9H), 0.99 (s, 3H), 0.92 (d, J = 6.5 Hz, 3H), 0.86 (dd, J = 6.6, 1.9 Hz, 6H), 0.66 (s, 3H).

Synthesis of trans-10-hydroperoxyoctadec-8-enoic acid (oleic-10-OOH): Prepared by photo-oxidation of oleic acid as previously described,[55] purified by silica gel flash column (50% EtOAc in hexanes). Analytical data in accordance to those reported in literature.[55] ^{1}H-NMR (400 MHz; $CDCl_3$): δ 5.75 (dq, J = 15.2, 7.6 Hz, 1H), 5.36 (dddt, J = 15.3, 8.4, 3.4, 1.6 Hz, 1H), 4.26 (q, J = 7.4 Hz, 1H), 2.34 (td, J = 7.5, 2.8 Hz, 2H), 2.07 (dd, J = 14.4, 7.7 Hz, 2H), 1.63 (dq, J = 12.2, 6.4 Hz, 3H), 1.41-1.25 (broad m, 23H), 0.87 (td, J = 6.8, 1.8 Hz, 3H).

Synthesis of 26,26,26,27,27,27-d_6-cholesterol (d_6-chol): Prepared as previously described[56] (however, the compound is also commercially available). Synthesis carried out by Z. A. M. Zielinski. ^{1}H-NMR (400 MHz; $CDCl_3$): δ 5.35 (t, J = 2.7 Hz, 1H), 3.52 (tt, J = 10.7, 5.1 Hz, 1H), 2.32-2.20 (m, 2H), 2.04-1.94 (m, 2H), 1.86-1.78 (m, 3H), 1.49-1.05 (m, 17H), 1.01 (s, 3H), 0.97-0.88 (m, 4H), 0.83 (dd, J = 9.7, 6.6Hz, 2H), 0.68 (s, 3H).

Synthesis of 26,26,26,27,27,27-d_6-7α-hydroxycholesterol (d_6-chol-7α-OH): Photo-oxidation of d_6-chol analogous to that described for cholesterol[53] afforded d_6-chol-5α-OOH. 30 mg (0.114 mmol) of d_6-chol-5α-OOH was dissolved in chloroform and stirred overnight at RT to facilitate rearrangement to the d_6-chol-7α-OOH. 30 mg of PPh_3 was then added dissolved in 1 mL of IPA to reduce the hydroperoxide to its corresponding alcohol. The mixture was stirred for 2 hours and was subsequently concentrated by rotary evaporation. The resulting crude material was purified by silica gel preparatory TLC (20% EtOAc in hexanes). Analytical data is in accordance to those

reported in literature.[57] Synthesis carried out by Z. A. M. Zielinski. Note that the signals corresponding to C26 and C27 are not observed in the ^{13}C NMR presumably due to broadening caused by their coupling with three D-atoms each. White solid; ^{1}H-NMR (400 MHz; $CDCl_3$): δ 5.61 (dd, J = 5.2, 1.7 Hz, 1H), 3.85 (t, J = 2.9 Hz, 1H), 3.59 (tt, J = 10.7, 5.1 Hz, 1H), 2.37-2.25 (m, 2H), 2.03-1.84 (m, 5H), 1.74-1.67 (m, 2H), 1.54-0.99 (m, 33H), 0.92 (d, J = 6.5 Hz, 6H), 0.68 (s, 3H), 0.07 (s, 1H). ^{13}C NMR (151 MHz; $CDCl_3$): δ 146.4, 124.0, 71.5, 65.5, 56.0, 49.6, 42.40, 42.28, 42.15, 39.5, 39.3, 37.65, 37.54, 37.1, 36.3, 35.9, 31.5, 28.4, 27.7, 24.4, 23.9, 20.9, 18.9, 18.4, 11.8.

Preparation of Egg-PC and Soy-Lecithin Liposomes: For each type of cholesterol-loaded liposome autoxidation experiment, a bulk stock liposomal solution was prepared at 26 mM phospholipid, 20 mM cholesterol and the corresponding concentration of α-tocopherol (0, 167, 333, 500, or 667 μM) such that replicate autoxidations and extractions could be performed from the same preparation. As such, 20 mg of egg-PC (MW ≈ 768 g/mol) or soy-lecithin (MW ≈ 776 g/mol), 7.8 mg cholesterol, and the corresponding amount of α-tocopherol (from a 10 mM stock prepared in $CHCl_3$, either 0, 16.7, 33.3, 50.0, or 66.7 μL is added to the corresponding vial) were combined in a vial, dissolved in chloroform to form a homogenous mixture, followed subsequently by evaporation of chloroform with N_2 to form a thin film on the wall of the vial. To ensure complete evaporation of organic solvent, lipid/antioxidant mixtures were left under reduced pressure for an hour. Upon solvent removal, each lipid/AO mixture is reconstituted in 1 mL of 10 mM PBS (prepared in ultrapure Milli-Q water, pH = 7.4) and is subsequently subjected to 10 sonication-freeze-thaw cycles to induce micelle formation. Each 1 mL lipid/antioxidant mixture is then extruded through a 100 nm polycarbonate membrane (Avestin) 25 times to ensure the formation

of uniform unilamellar vesicles. Stock lipid/antioxidant preparations are used for autoxidation experiments on the same day of their preparation.

Autoxidation of Cholesterol-Loaded Liposomes: From the 1 mL of bulk cholesterol-loaded liposome preparations (26 mM phospholipid, 20 mM cholesterol, and 0, 167, 333, 500, or 667 μM α-tocopherol), 150 μL for each replicate is diluted with 10 mM PBS (pH = 7.4) to a total volume of 2 mL in a 4 mL vial such that the final concentration for oxidation is 2 mM phospholipid, 1.54 mM cholesterol, and either 0, 10, 25, 50, 75, or 100 μM α-tocopherol. Each individual type of liposomal preparation is oxidized in triplicate from the same bulk preparation for comparison of extraction following oxidation. To initiate oxidation, 20 μL of a 100 mM stock of MeOAMVN in benzene is added. Each vial was loosely capped and incubated at 37°C for 16 hours with stirring. Upon completion, each solution is quenched with 2 mL of 4 mM BHT and 4 mM PPh_3 in 2:1 $CHCl_3$:MeOH in preparation for extraction.

Sterol Extraction from Egg-PC and Soy-Lecithin Liposomes: Following quenching, the entire solution is transferred from the 4 mL vial to a 10 mL screw-capped test tube for efficient extraction. 1 mL of 0.9 % NaCl in distilled water is added to each sample followed by vigorous vortexing for ~ 5 seconds to ensure complete destruction of the liposomal membrane. Mixtures are spun-down for ~ 3 minutes to encourage separation of the organic and aqueous layer. A thin, disposable needle and syringe is used to remove the organic layer and transfer to another test tube for solvent removal without disturbing the turbid aqueous layer. Extraction is repeated twice more with the addition of 5 mL of $CHCl_3$ to the aqueous layer followed by vortexing (~ 5 s), spin-down (~ 30 s), and subsequent combination of the organic layer with the other organic extracts. Solvent is removed from all samples simultaneously under reduced pressure using a Labconco CentriVap Vacuum Concentrator until solvent is completely removed. To ensure complete removal of $CHCl_3$, samples

are left to dry under reduced pressure in a desiccator overnight. For purification of sterols from remaining phospholipids, residues are reconstituted in 1 mL of 95:5 hexanes:IPA and are applied to SiliaPrep™ SPE Cartridges (silica-based, 200 mg, 3 mL, 40-63 μm, 60 Å) pre-treated with 3 column volumes of IPA, washed with 3 column volumes of hexanes, and subsequently eluted with 3 column volumes of Et_2O. Solvent is again removed under reduced pressure using by CentriVap until solvent is completely removed and left to dry under reduced pressure in a desiccator for ~ 1 hour. Sterol extracts were stored at - 20°C until analysis.

Cell Culture: Both HEK 293 and Pfa1 cell lines were cultured at 37 °C in a 5% CO_2 atmosphere. HEK 293 cells were cultured in MEM with 10% FBS, 1% 100× non-essential amino acid solution, 1 mM sodium pyruvate and 1% penicillin-streptomycin. Cells were passaged by dissociation with 0.05% trypsin and 0.2% EDTA every two to three days. Pfa1 cells were cultured in DMEM with 10% FBS, 1% 100× non-essential amino acid solution, 1 mM sodium pyruvate and 1% penicillin-streptomycin. All cell experiments were carried out at a minimum of three biological replicates.

Generation of Cholesterol Hydroperoxides in Mammalian Cells under Ferroptotic Cell Death Conditions: HEK 293 cells were cultured to confluency on 150 mm cell culture plates. Media is aspirated and replaced with 10 mL of MEM containing 50 μM of exogenous cholesterol for overnight incubation at 37°C. Media is again aspirated and the cells are subsequently washed with PBS buffer (pH = 7.4) prior to RSL3 treatment. Ferroptosis was induced with the addition of 5 μM RSL3 in 10 mL MEM and was left to incubate for 6 hours at 37 °C. After 6 hours, cells were removed from the plate using a cell scraper, transferred to a 50 mL centrifuge tube, and subsequently flash frozen in liquid N_2 and stored at – 80°C until extraction. Analogous control experiments were performed in the absence of RSL3 treatment and in the absence of exogenous cholesterol and yielded no quantifiable oxidation products.

Sterol Extraction from HEK 293 Mammalian Cells: Upon thawing, the cells are immediately quenched 5 mL of MeOH containing 1 mg/mL BHT and PPh_3. To ensure complete destruction of the cellular membrane, a probe sonicator was used to induce 1 second pulses of ultrasonication for 1 minute on ice. For sterol extraction, 10 mL $CHCl_3$ and 1 mL of 0.9 % NaCl in H_2O is added to each sample followed by vigorous vortexing for ~ 10 seconds. To ensure sufficient mixing, samples are left to shake for 1 hour on a shaker. Samples are subsequently centrifuged at 3000 rpm for ~ 20 minutes or until the separation of the organic and aqueous layer is observed and the formation of a thin layer of protein is formed. A thin, disposable needle and syringe is used to remove the organic layer and transfer to another test tube for solvent removal without disturbing the turbid aqueous or protein layer. Extraction is repeated twice more with the addition of 5 mL of $CHCl_3$ to the aqueous layer followed by vortexing (~ 30 s), centrifuge (~ 20 min), and subsequent combination of the organic layer with the other organic extracts. Solvent is removed from all samples simultaneously under reduced pressure using a Labconco CentriVap vacuum concentrator until solvent is completely removed. To ensure complete removal of $CHCl_3$, samples are left to dry under reduced pressure in a desiccator overnight. For purification of sterols from remaining phospholipids, residues are reconstituted in 1 mL of 95:5 hexanes:IPA and are applied to SiliaPrep™ SPE Cartridges (silica-based, 200 mg, 3 mL, 40-63 μm, 60 Å) pre-treated with 3 column volumes of IPA, washed with 3 column volumes of hexanes, and subsequently eluted with 3 column volumes of Et_2O. Solvent is again removed under reduced pressure using by CentriVap until solvent is completely removed and left to dry under reduced pressure in a desiccator for ~ 1 hour. Sterol extracts were stored at -20°C until analysis.

HPLC-APCI-MS/MS Analysis: Following extraction from a liposomal or cellular medium, sterol extracts were combined with the following internal standards (standards prepared at 1 mM in

chlorobenzene): 10 µL 4-nitrophenol (100 µM), 6 µL d_6-chol-5,6-epoxide (20 µM α-epox, 5.6 µM β-epox), 4 µL of d_6-chol-5α-OH (20 µM), and 5µL of d_6-chol-7α-OH (25 µM; added unless otherwise stated). Upon addition of internal standards, total volume was brought to 100 µL with chlorobenzene for analysis. 10 µL of this dilution was injected onto a normal phase HPLC column (SunFire 5 µm silica; 4.6 mm × 250 mm) and eluted with the following gradient of hexane:isopropanol (IPA) at a flow rate of 1.5 mL/min: 99:1 to 98:2 over 30 minutes, 98:2 from 30 to 40 minutes, 98:2 to 95:5 from 40 to 41 minutes, 95:5 from 41 to 49 minutes, 95:5 to 99:1 from 49 to 50 minutes, and 99:1 from 50 to 60 minutes. APCI-MS/MS detection in positive ion mode was used for the MS/MS transitions: 403.4 m/z → 385.4 m/z and 385.4 m/z → 367.4 m/z, for chol epoxides and alcohols, respectively; as well as 409.4 m/z → 391.4 m/z and 391.4 m/z → 373.4 m/z for d_6-chol epoxides and alcohols, respectively. The settings for mass spectral analysis were as follows: corona current 2 µA; cone voltage 25 V; source temperature 150°C; APCI probe temperature 500°C; desolvation gas flow 600 L/hr; cone gas flow 20 L/hr; collision gas flow 0.2 mL/min; collision energy 15 eV. Simultaneous UV detection was carried out by photodiode array, and the 7-ketocholesterol was detected at 234 nm relative to 4-nitrophenol as internal standard.

Sensitization to Ferroptosis Induced by Sub-Lethal Concentration of (1S,3R)-RSL3 and Subsequent Treatment with Lipid Hydroperoxides: HEK 293 or Pfa1 cells (3,000 in 100 µL) were seeded in 96-well plates and cultured overnight. The next day the media was removed, the cells were washed with PBS and the cells were suspended in new media containing (1*S*, 3*R*)-RSL3 (0.25 µM for HEK 293, 0.1 µM for Pfa1) for 30 minutes before addition of cholesterol hydroperoxide species. Cholesterol hydroperoxides were administered incorporated in egg-PC liposomes (HEK 293) or in dissolved in EtOH (Pfa1). Liposomes were prepared according to the same protocol reported above containing 2:1:1 egg-PC:cholesterol:chol-OOH with a concentration of 1.5 mM

cholesterol hydroperoxide that is diluted with PBS (pH 7.4) to achieve the concentration administered to cells. Control experiments in which HEK 293 cells are treated with egg-PC-cholesterol liposomes prepared without chol-OOH show no cytotoxicity under the same conditions. Cell viability was assessed ~ 5 hours later using the AquaBluer assay (MultiTarget Pharmaceuticals, LLC) according to the manufacturer's instructions. Cell viability was calculated by normalizing the data to untreated controls. Experiments are carried out with six-technical replicates (n = 6 wells of a 96-well plate) and performed independently with a minimum of three biological replicates. Control experiments performed using the vehicles for administration in the absence of the administered compounds resulted in an insignificant reduction in cell viability relative to the untreated controls. Treatment of cells with sublethal concentrations of RSL3 denoted above also result in negligible cytotoxicity.

2.6 References

(1) Zielinski, Z. A. M.; Pratt, D. A. *J. Am. Chem. Soc.* **2016**, *138* (22), 6932–6935.

(2) Tallman, K. A.; Pratt, D. A.; Porter, N. A. *J. Am. Chem. Soc.* **2001**, *123* (47), 11827–11828.

(3) Wentworth Jr., P.; Nieva, J.; Takeuchi, C.; Galve, R.; Wentworth, A. D.; Dilley, R. B.; DeLaria, G. A.; Saven, A.; Babior, B. M.; Janda, K. D.; Eschenmoser, A.; Lerner, R. A. *Science* **2003**, *302* (5647), 1053–1056.

(4) Zielinski, Z. A. M.; Pratt, D. A. *J. Am. Chem. Soc.* **2019**, *141* (7), 3047–3051.

(5) van Meer, G.; Voelker, D. R.; Feigenson, G. W. *Nat. Rev. Mol. Cell Biol.* **2008**, *9* (2), 112–124.

(6) Yin, H.; Xu, L.; Porter, N. A. *Chem. Rev.* **2011**, *111* (10), 5944–5972.

(7) Sevanian, A.; McLeod, L. L. *Lipids* **1987**, *22* (9), 627–636.

(8) Mosca, M.; Ceglie, A.; Ambrosone, L. *Chem. Phys. Lipids* **2011**, *164* (2), 158–165.

(9) Bligh, E. G.; Dyer, W. J. *Can. J. Biochem. Physiol.* **1959**, *37* (8), 911–917.

(10) Zilka, O.; Shah, R.; Li, B.; Friedmann Angeli, J. P.; Griesser, M.; Conrad, M.; Pratt, D. A. *ACS Cent. Sci.* **2017**, *3* (3), 232–243.

(11) Brown, A. J.; Leong, S.-L.; Dean, R. T.; Jessup, W. *J. Lipid Res.* **1997**, *38* (9), 1730–1745.

(12) Garcia-Cruset, S.; Carpenter, K. L. H.; Guardiola, F.; Mitchinson, M. J. *Free Radic. Res.* **1999**, *30* (5), 341–350.

(13) Chisolm, G. M.; Ma, G.; Irwin, K. C.; Martin, L. L.; Gunderson, K. G.; Linberg, L. F.; Morel, D. W.; DiCorleto, P. E. *Proc. Natl. Acad. Sci. U. S. A.* **1994**, *91* (24), 11452–11456.

(14) Zhu, G.; Ou, Q.; Zhang, T.; Jiang, X.; Sun, G.; Zhang, N.; Wang, K.; Fang, H.; Wang, M.; Sun, J.; Ge, T. *PLoS One* **2013**, *8* (12), e84871/1-e84871/6, 6 pp.

(15) Dawaliby, R.; Trubbia, C.; Delporte, C.; Noyon, C.; Ruysschaert, J.-M.; Van Antwerpen, P.; Govaerts, C. *J. Biol. Chem.* **2016**, *291* (7), 3658–3667.

(16) Shah, R.; Shchepinov, M. S.; Pratt, D. A. *ACS Cent. Sci.* **2018**, *4* (3), 387–396.

(17) Geiger, P. G.; Korytowski, W.; Girotti, A. W. *Photochem. Photobiol.* **1995**, *62* (3), 580–587.

(18) Korytowski, W.; Geiger, P. G.; Girotti, A. W. *Biochemistry* **1996**, *35*, 8670–8679.

(19) Friedmann Angeli, J. P.; Schneider, M.; Proneth, B.; Tyurina, Y. Y.; Tyurin, V. A.; Hammond, V. J.; Herbach, N.; Aichler, M.; Walch, A.; Eggenhofer, E.; Basavarajappa, D.; Radmark, O.; Kobayashi, S.; Seibt, T.; Beck, H.; Neff, F.; Esposito, I.; Wanke, R.; Foerster,

H.; Yefremova, O.; Heinrichmeyer, M.; Bornkamm, G. W.; Geissler, E. K.; Thomas, S. B.; Stockwell, B. R.; O'Donnell, V. B.; Kagan, V. E.; Schick, J. A.; Conrad, M. *Nat. Cell Biol.* **2014**, *16* (12), 1180–1191.

(20) Vila, A.; Levchenko, V. V; Korytowski, W.; Girotti, A. W. *Biochemistry* **2004**, *43* (39), 12592–12605.

(21) Kriska, T.; Pilat, A.; Schmitt, J. C.; Girotti, A. W. *J. Lipid Res.* **2010**, *51*, 3174–3184.

(22) Korytowski, W.; Wawak, K.; Pabisz, P.; Schmitt, J. C.; Chadwick, A. C.; Sahoo, D.; Girotti, A. W. **2015**.

(23) Yancey, P. G.; Rodrigueza, W. V; Kilsdonk, E. P. C.; Stoudt, G. W.; Johnson, W. J.; Phillips, M. C.; Rothblat, G. H. *J. Biol. Chem.* **1996**, *271* (27), 16026–16034.

(24) Weenen, H.; Porter, N. A. *J. Am. Chem. Soc.* **1982**, *104* (19), 5216–5221.

(25) Smith, L. L. *Chem. Phys. Lipids* **1987**, *44*, 87–125.

(26) Brockerhoff, H. *Lipids* **1974**, *9* (9), 645–650.

(27) Dufourc, E. J.; Parish, E. J.; Chitrakorn, S.; Smith, I. C. P. *Biochemistry* **1984**, *23* (25), 6062–6071.

(28) Ermilova, I.; Lyubartsev, A. P. *Soft Matter* **2019**, *15* (1), 78–93.

(29) Porter, N. A.; Weber, B. A.; Weenen, H.; Khan, J. A. *J. Am. Chem. Soc.* **1980**, *102* (17), 5597–5601.

(30) Barclay, L. R. C.; Vinqvist, M. R.; Antunes, F.; Pinto, R. E. *J. Am. Chem. Soc.* **1997**, *119* (24), 5764–5765.

(31) Culbertson, S. M.; Antunes, F.; Havrilla, C. M.; Milne, G. L.; Porter, N. A. *Chem. Res. Toxicol.* **2002**, *15* (6), 870–876.

(32) Shah, R.; Farmer, L. A.; Zilka, O.; Kessel, A. T. M. Van; Pratt, D. A. *ACS Cent. Sci.* **2019**, Submitted.

(33) Burton, G. W.; Doba, T.; Gabe, E.; Hughes, L.; Lee, F. L.; Prasad, L.; Ingold, K. U. *J. Am. Chem. Soc.* **1985**, *107* (24), 7053–7065.

(34) Barclay, L. R. C.; Cameron, R. C.; Forrest, B. J.; Locke, S. J.; Nigam, R.; Vinqvist, M. R. *Biochim. Biophys. Acta, Lipids Lipid Metab.* **1990**, *1047* (3), 255–263.

(35) Noguchi, N.; Yamashita, H.; Gotoh, N.; Yamamoto, Y.; Numano, R.; Niki, E. *Free Radic. Biol. Med.* **1997**, *24* (2), 259–268.

(36) Yoshida, Y.; Niki, E. *J. Oleo Sci.* **2008**, *57* (7), 407–414.

(37) Saito, Y.; Yoshida, Y.; Niki, E. *FEBS Lett.* **2007**, *581* (22), 4349–4354.

(38) Shah, R.; Pratt, D. A. *J. Org. Chem.* **2016**, *81* (15), 6649–6656.

(39) Hiatt, R.; Smythe, R. J.; McColeman, C. *Can. J. Chem.* **1971**, *49* (10), 1707–1711.

(40) Shadel, G. S.; Horvath, T. L. *Cell* **2015**, *163* (3), 560–569.

(41) Ingold, K. U.; Paul, T.; Young, M. J.; Doiron, L. *J. Am. Chem. Soc.* **1997**, *119* (50), 12364–12365.

(42) Thomas, J. P.; Geiger, P. G.; Maiorino, M.; Ursini, F.; Girotti, A. W. *Biochim. Biophys. Acta* **1990**, *1045*, 252–260.

(43) Korytowski, W.; Bachowski, G. J.; Girotti, A. W. *Photochem. Photobiol.* **1992**, *56*, 1–8.

(44) Hurst, R.; Korytowski, W.; Kriska, T.; Esworthy, R. S.; Chu, F.-F.; Girotti, A. W. *Free Radic. Biol. Med.* **1997**, *31* (9), 1051–1065.

(45) Brinkhorst, J.; Nara, S. J. and; Pratt, D. A. *J. Am. Chem. Soc.* **2008**, *130* (37), 12224–12225.

(46) Takeuchi, C.; Galvé, R.; Nieva, J.; Witter, D. P.; Wentworth, A. D.; Troseth, R. P.; Lerner, R. A.; Wentworth, P. *Biochemistry* **2006**, *45* (23), 7162–7170.

(47) Bieschke, J.; Zhang, Q.; Bosco, D. A.; Lerner, R. A.; Powers, E. T.; Wentworth Jr., P.; Kelly, J. W. *Acc. Chem. Res.* **2006**, *39* (9), 611–619.

(48) Bosco, D. A.; Fowler, D. M.; Zhang, Q.; Nieva, J.; Powers, E. T.; Wentworth, P.; Lerner, R. A.; Kelly, J. W. *Nat. Chem. Biol.* **2006**, *2*, 249–253.

(49) Zhang, Q.; Powers, E. T.; Nieva, J.; Huff, M. E.; Dendle, M. A.; Bieschke, J.; Glabe, C. G.; Eschenmoser, A.; Wentworth Jr., P.; Lerner, R. A.; Kelly, J. W. *Proc. Natl. Acad. Sci. U. S. A.* **2004**, *101* (14), 4752–4757.

(50) Paillasse, M. R.; Saffon, N.; Gornitzka, H.; Silvente-Poirot, S.; Poirot, M.; de Medina, P. *J. Lipid Res.* **2012**, *53* (4), 718–725.

(51) Fieser, L. F. *J. Am. Chem. Soc.* **1953**, *75*, 542l – 2.

(52) Yang, W. S.; SriRamaratnam, R.; Welsch, M. E.; Shimada, K.; Skouta, R.; Viswanathan, V. S.; Cheah, J. H.; Clemons, P. A.; Shamji, A. F.; Clish, C. B.; Brown, L. M.; Girotti, A. W.; Cornish, V. W.; Schreiber, S. L.; Stockwell, B. R. *Cell* **2014**, *156* (1), 317–331.

(53) Beckwith, A. L. J.; Davies, A. G.; Davidson, I. G. E.; Maccoll, A.; Mruzek, M. H. *J. Chem Soc. Perkin Trans. II* **1989**, *1* (4), 815–824.

(54) Ronsein, G. E.; Prado, F. M.; Mansano, F. V; Oliveira, M. C. B.; Medeiros, M. H. G.; Miyamoto, S.; Di Mascio, P. *Anal. Chem.* **2010**, *82* (17), 7293–7301.

(55) Porter, N. A.; Wujek, J. S. *J. Org. Chem.* **1987**, *52* (23), 5085–5089.

(56) Holm, T.; Crossland, I. *J. Labelled Comp. Radiopharm.* **1996**, *38* (9), 803–808.

(57) Li, S.; Pang, J.; Wilson, W. K.; Schroepfer, G. J. *Chem. Phys. Lipids* **1999**, *99*, 33–71.

2.7 Appendix

^{1}H NMR (400 MHz, $CDCl_3$)

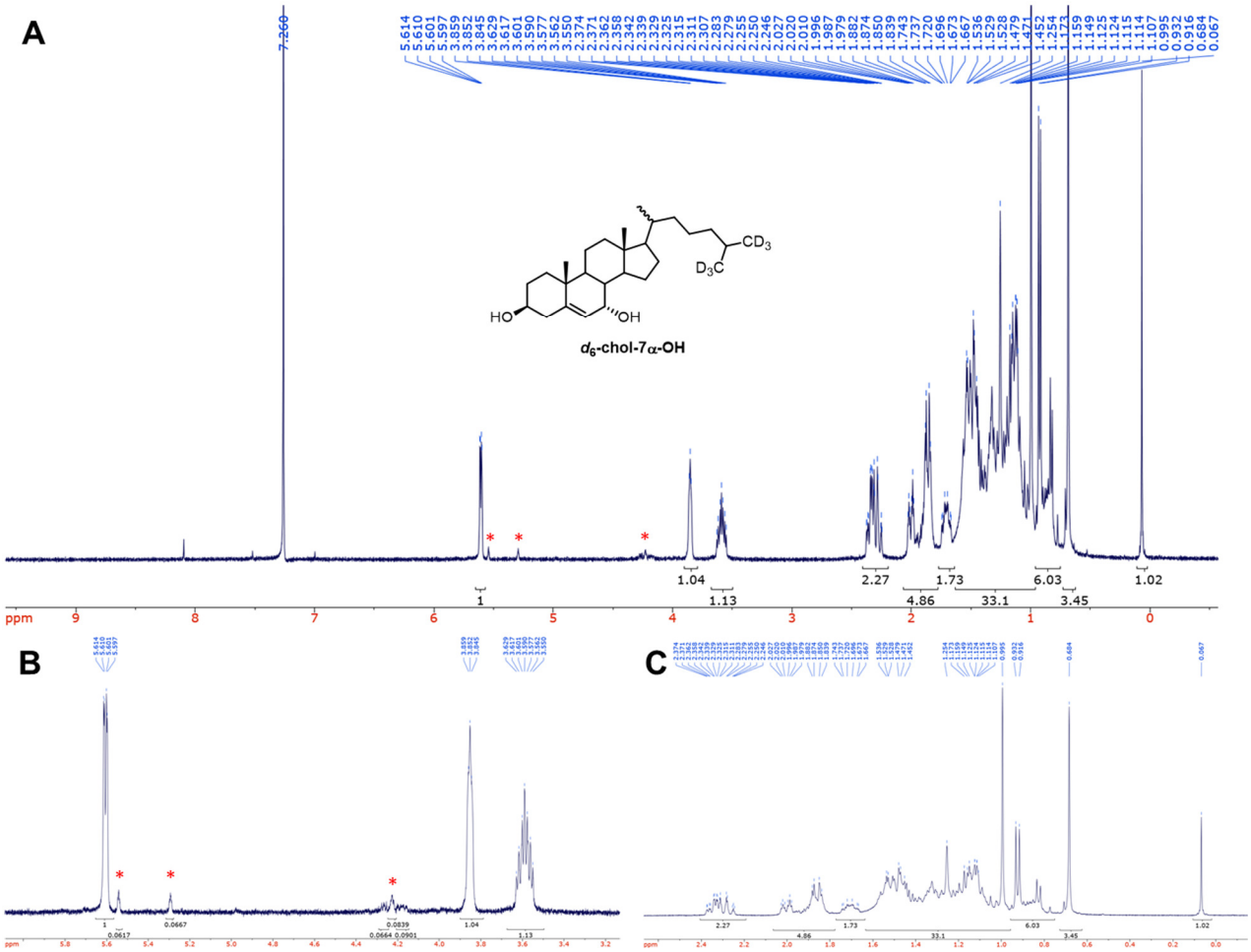

Figure 2.13 ^{1}H NMR spectrum of d_6-chol-7α-OH (**A**) and expansions of 3.0-6.0 ppm (**B**) and 0.0-3.0 ppm (**C**). Peaks corresponding to the minor stereoisomer, d_6-chol-7β-OH, or d_6-chol-6β-OH are indicated with asterisks (*).

^{13}C NMR (150 MHz, $CDCl_3$)

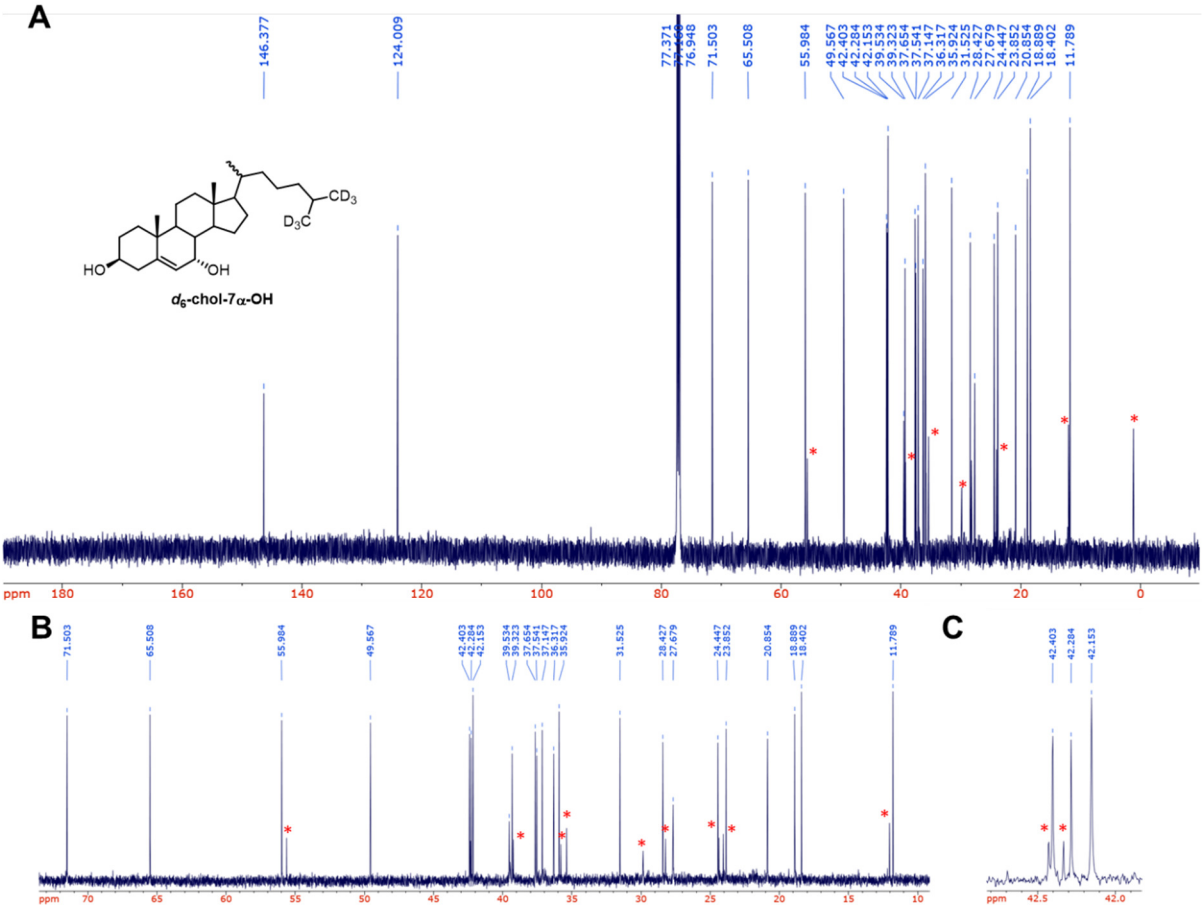

Figure 2.14 ^{13}C NMR spectrum of d_6-chol-7a-OH (**A**) and expansions of 10-75 ppm (**B**) and 41.5-43 ppm (**C**). Peaks corresponding to the minor stereoisomer, d_6-chol-7β-OH, or d_6-chol-6β-OH are indicated with asterisks (*).

CHAPTER 3 Acid-Catalyzed Hock Fragmentation of Cholesterol 7-Hydroperoxide

3.1 Introduction

Lipid peroxidation has been invoked as the source of many deleterious electrophiles implicated in the pathology of disease. Although the mechanisms which underlie the formation of the primary hydroperoxide species that arise in lipid peroxidation are well understood and have been extensively investigated for lipid species such as oleate,[1] linoleate,[2] arachidonate,[3] cholesterol[4,5] and 7-dehydrocholesterol,[6] the mechanism(s) by which they are subsequently converted into lipid-derived electrophiles remains unclear. Given the comparatively slow detoxification of cholesterol-derived hydroperoxides by glutathione peroxidase 4 (GPX4),[7] and the abundance of cholesterol in lipid bilayers and rafts, electrophile formation therefrom could be particularly relevant. Nevertheless, to date, electrophiles derived from polyunsaturated fatty acids, such as 4-HNE, acrolein, and MDA, have been far more intensely investigated. They have been proposed to be sourced from acid-catalyzed Hock fragmentation of their parent PUFA-derived hydroperoxide species,[8,9] or possibly via one-electron reduction by Fe^{2+} or acid-catalyzed intramolecular cyclization to epoxide products that themselves may eventually decompose to aldehydic species.[10,11]

Scheme 3.1 Potential mechanisms for electrophile generation from lipid-derived hydroperoxide species.

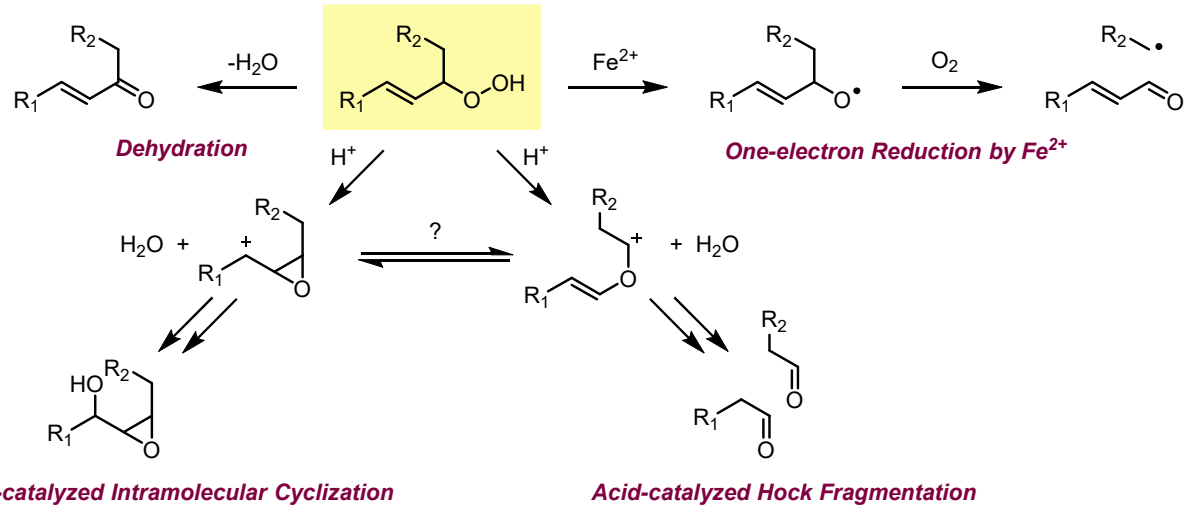

Interestingly, an analogous mechanism for decomposition of cholesterol-derived primary hydroperoxides had not been explored until our group proposed Hock fragmentation of chol-5α-OOH, the product of the reaction of $^1O_2$ with cholesterol, to yield the cholesterol-derived secoaldehyde species, secosterols A and B.[12] This provided an alternative mechanism for the formation of secA and secB, which had previously been proposed to arise *in vivo* from reaction with endogenous ozone generated during inflammatory response.[13] We subsequently showed that chol-6-OOH can also undergo Hock fragmentation to afford secA and secB.[4] Thus, these compounds can form in the absence of high energy oxidants such as ozone and singlet oxygen. Of course, it must be acknowledged that secA and secB are generally identified following derivatization conditions under which the precursor hydroperoxides undergo Hock fragmentation, and so their physiological relevance remains a matter of debate.[14–19]

Cholesterol 7-hydroperoxide isomers are the most abundant of the primary cholesterol autoxidation products based upon previous work,[20–23] and our own studies,[4,5] suggesting that secondary products derived therefrom may be of physiological relevance; this is evident in the

omnipresence of 7-ketocholesterol (7-keto) in contexts undergoing oxidative stress.[24–28] This suggests that decomposition of chol-7-OOH does occur in these locations, as evidenced by 7-keto as a persistent biomarker, however, decomposition may occur through mechanisms other than dehydration to form products that are much more electrophilic than 7-keto, perhaps making them more difficult to detect.

Of particular interest is the decomposition of chol-7-OOH by acid-catalyzed Hock fragmentation. This is underscored by the aforementioned fact that electrophilic species, such as secA and secB, are often detected as hydrazones under acidic derivatization conditions. Although the putative Hock fragmentation mechanism does not yield secA and B, it is possible that the aldehydic products generated will share similar spectroscopic characteristics to that of the atheronals, including the same mass ion; these products may serve as an alternative explanation for the detection of proposed ozone-derived secosterols.

Scheme 3.2 Putative mechanism for the Hock fragmentation of cholesterol 5α-, 6β-, and 7α-hydroperoxides.

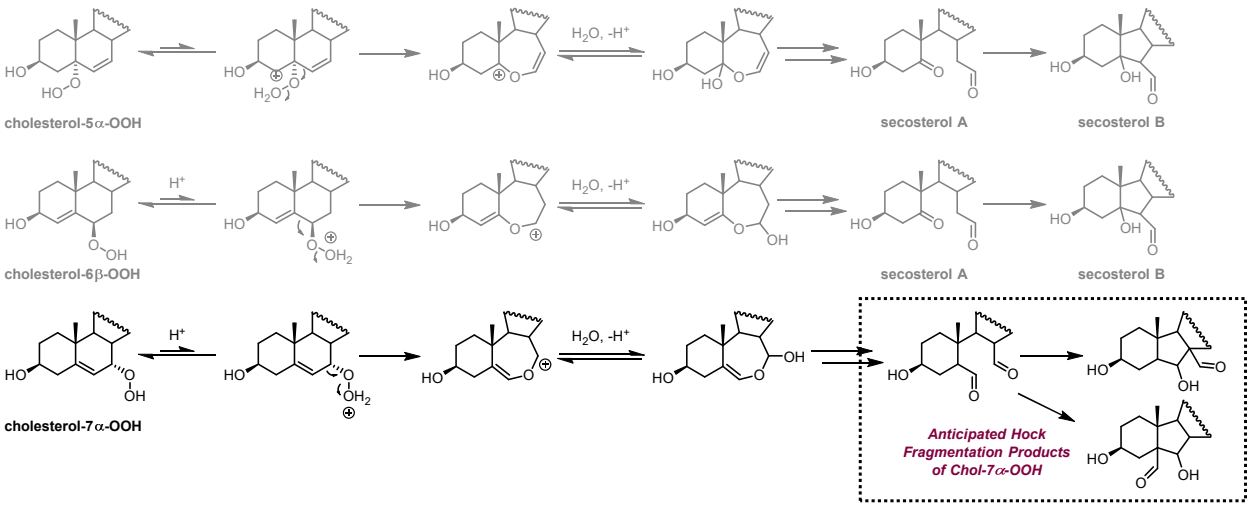

Surprisingly, preliminary efforts made by Nadia Zopyrus to study the Hock fragmentation of chol-7α-OOH yielded no indication of the anticipated Hock fragmentation products, and instead

provided evidence for the unprecedented 6,7-epoxide products shown in **Scheme 3.3**.[29] Herein, we describe our efforts to follow up this observation, which include the identification of the other major products as well as our efforts to understand the mechanisms underlying their formation.

Scheme 3.3 Unexpected 6,7-epoxy-5-hydroxy (or methoxy) products arising in the acid-catalyzed rearrangement of chol-7α-OOH (in methanol). The initially anticipated products, shown in grey, were not observed. Adapted from Zopyrus.[29]

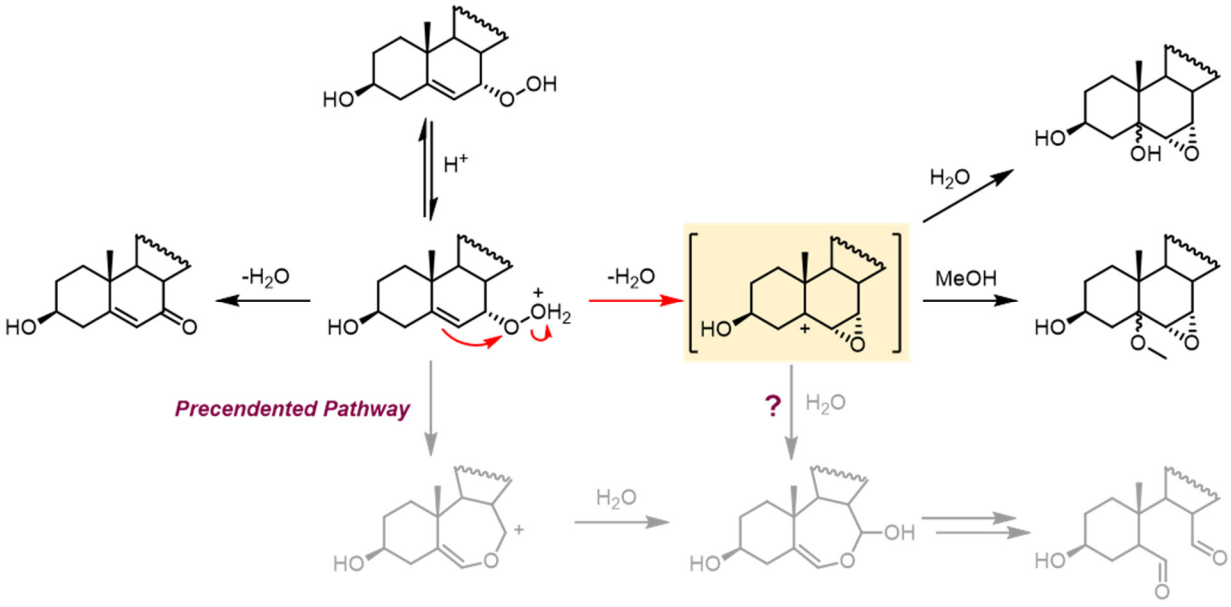

3.2 Results

3.2.1 Products of Hock Fragmentation of Cholesterol-7α-Hydroperoxide in Organic Solution

Although chol-7β-OOH is the biologically-predominant 7-OOH isomer, chol-7α-OOH was used for the purposes of our mechanistic investigations due to the synthetic challenges faced in attempts to generate 7β-OOH on a preparative scale. Epimerization of chol-7α-OOH to 7β-OOH via extensive stirring in $CHCl_3$ is the only reported synthesis for this isomer,[30] however, only trace amounts of the 7β-OOH product are afforded following several days of stirring and both inseparable 7-keto and 7α-OH form within the same amount of time. Chol-7α-OOH was prepared

as previously described and subjected to typical derivatization conditions used to identify lipid-derived electrophiles, i.e. 200 μM of 2,4-dinitrophenylhydrazine (DNPH) in methanol containing 100 mM HCl.[13] Interestingly, we found that the majority of the mass balance comprised products which lacked DNPH-derived hydrazones. Thus, subsequent experiments were carried out in the absence of DNPH. As expected, 7-ketocholesterol, a dehydration product of chol-7α-OOH and a classic biomarker for cholesterol oxidation, was identified as one of the major products. The isolation, purification, and characterization of the other products proved difficult, even with the use of a multitude of ^{1}H and ^{13}C NMR analyses, as these novel products bore unfamiliar and unique moieties when compared against reported cholesterol-derived oxysterol products. Fortunately, crystallization of one of the unknown products was successful, revealing an unprecedented epoxide species, 6α,7α-epoxy-5β-methoxy-cholestane-3β-ol (5β-OMe-epox).[29] Spectroscopic characterization of this epoxide species facilitated elucidation of another unknown as the α-epimer of this species, 6α,7α-epoxy-5α-methoxy-cholestane-3β-ol (5α-OMe-epox), which co-eluted as a ~ 1:1 mixture with 7-ketocholesterol. Although the 5β-OMe-epox (~45%), 5α-OMe-epox (~15%), and 7-keotcholesterol (~15%) comprised the majority of the mass balance, several uncharacterized products remained.

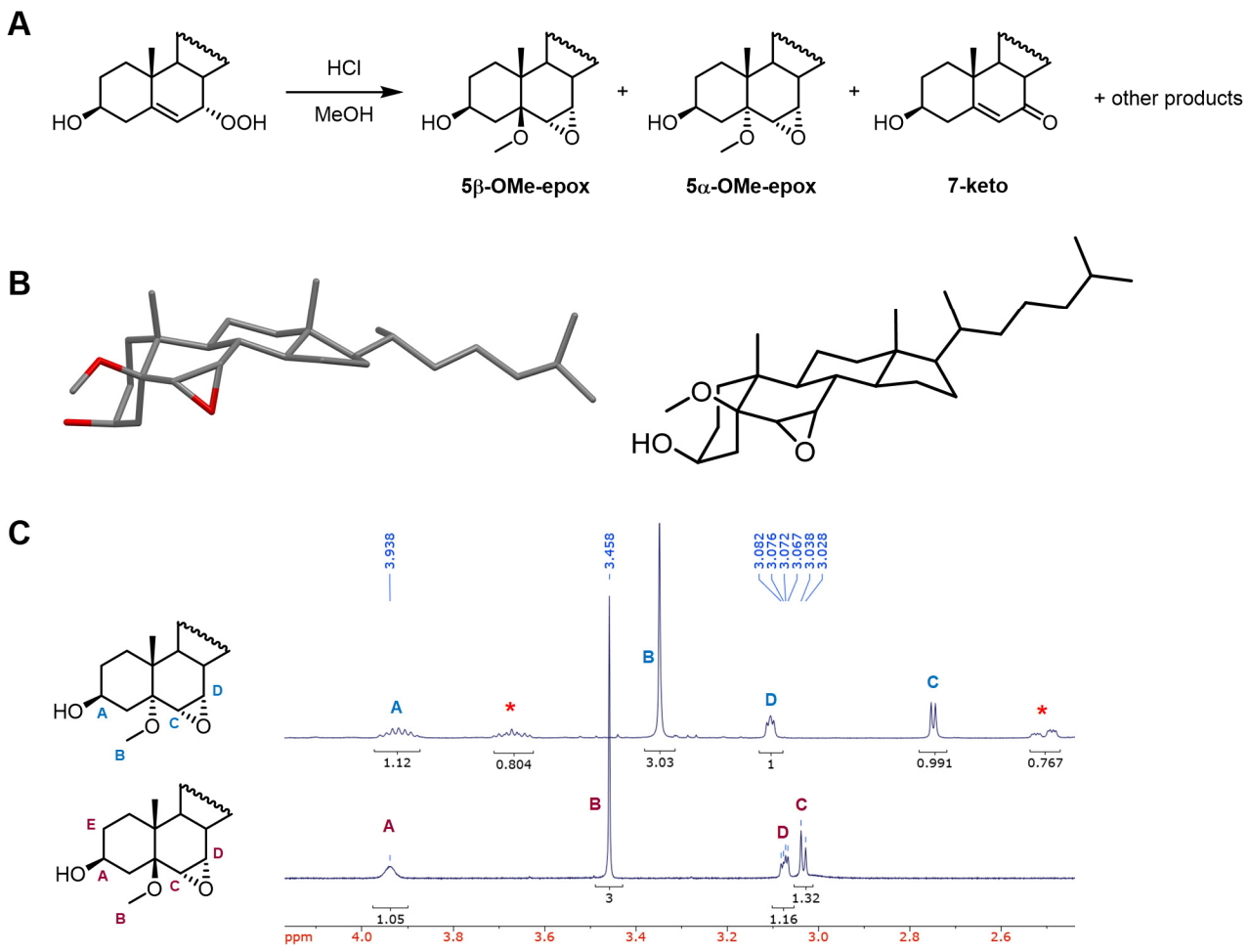

Figure 3.1 Representative scheme and product characterization for Hock fragmentation of chol-7α-OOH in methanol as the participating solvent. Reagents and characterized products are illustrated (**A**) in addition to the crystal structure used for characterization of 5β-OMe-epox (**B**) and the corresponding ^{1}H NMR spectra for both α and β epimers of the epoxide species (**C**). Crystal data and structure refinement obtained at 200 K at a wavelength of 0.71073 Å with an orthorhombic crystal system. 5α-OMe-epox isolated as a mixture with 7-keto, indicated by a red asterisk (*). ^{1}H NMR spectra recorded at 400 MHz relative to $CDCl_3$.

Given the expectation of aldehydic products arising from Hock fragmentation, we anticipated that a non-participating solvent in which water would serve as the only possible nucleophilic source would simplify the product distribution. Thus, chol-7α-OOH at 50 mM in acetone saturated with water was subjected to acid-catalyzed Hock fragmentation by addition of HCl to a final concentration of 100 mM to mimic the concentration utilized for DNPH

derivatization. Although a diverse mixture of products was formed, four products were predominant upon visualization by TLC. As we had anticipated, upon separation and isolation of these products by silica gel flash chromatography, the product mixture consisted of alcoholic analogs of the epoxide species observed in methanol, 6α,7α-epoxycholestane-5α- and 5β,3β-diol (5α- and 5β-OH-epoxide), an unfamiliar aldehydic species, and a convoluted mixture of what are presumed to be polar poly-hydroxy products. Interestingly, no 7-ketocholesterol was formed under these conditions. Crystals were successfully grown for the 5β-OH-epox via vapour diffusion using a binary solvent system of benzene and hexanes to a diameter of ~ 1 mm sufficient to solve for an X-ray crystal structure; this structure helped support our proposed assignments based upon the characteristic "roofing" peaks observed in our ^{1}H NMR spectra for both epoxide isomers and facilitated comparison to the characterization of the structures in the literature – products that had only previously been synthesized under harsh oxidation conditions.[31,32]

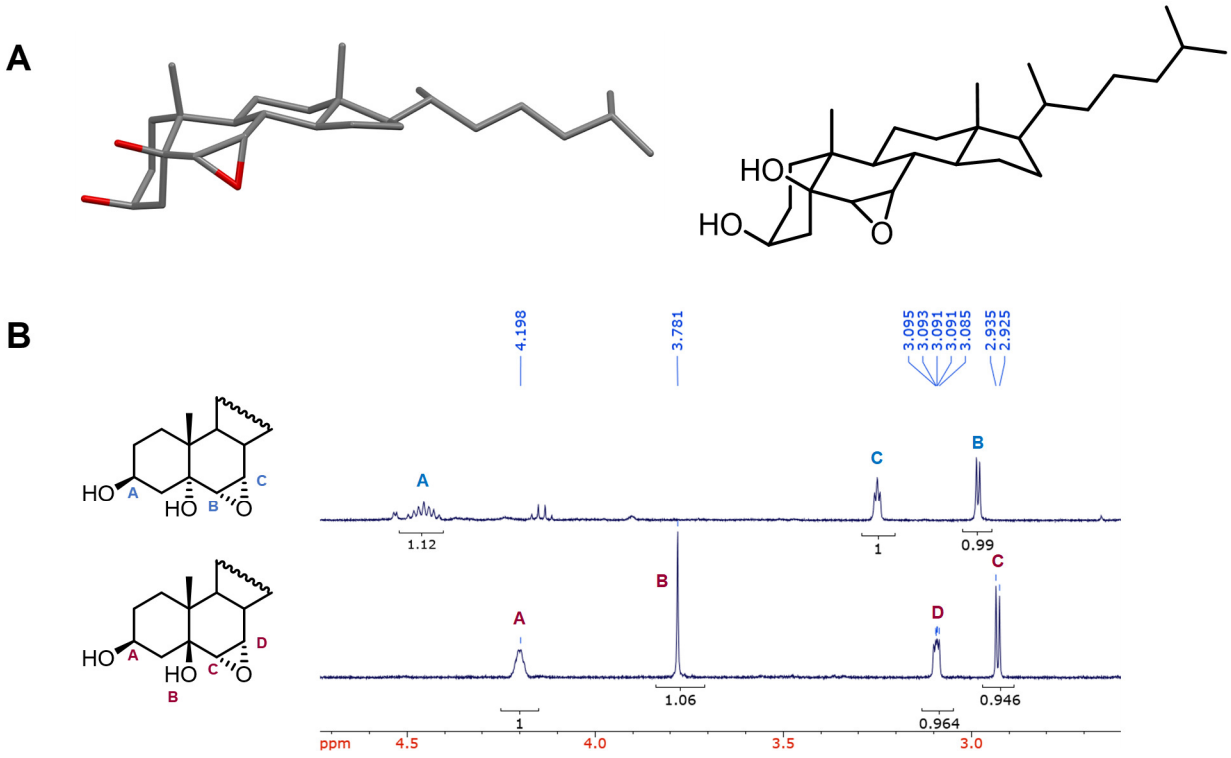

Figure 3.2 Representative characterization data for Hock fragmentation products of chol-7α-OOH in acetone/H_2O. The X-ray crystal structure used for characterization of 5β-OH-epox (**A**) and the corresponding ^{1}H NMR spectra for both α and β epimers of the epoxide species (**B**). Crystal data and structure refinement obtained at 200 K at a wavelength of 0.71073 Å with an orthorhombic crystal system. ^{1}H NMR spectra recorded at 400 MHz relative to $CDCl_3$.

The structure of the aldehydic species isolated as the major product of this reaction proved difficult to elucidate, primarily due to the presence of several unfamiliar upfield signals in the ^{1}H NMR spectrum (i.e. B, C, D, and E in **Figure 3.3A**). Unlike the 5β-OH-epox, we were unable to obtain a crystal structure of this compound; upon characterization of the compound, it became abundantly clear that the lack of defined structure likely prevented tight packing of the compound to facilitate crystallization. As such, we relied heavily on a comprehensive set of one and two-dimensional NMR experiments (**Figure 3.3**) and mass spectrometry (**Figure 3.4**) to determine the structure. Our proposed assignments and key representative spectra are illustrated in **Figure 3.3,** however, complete spectra without assignments are provided at the end of this chapter.

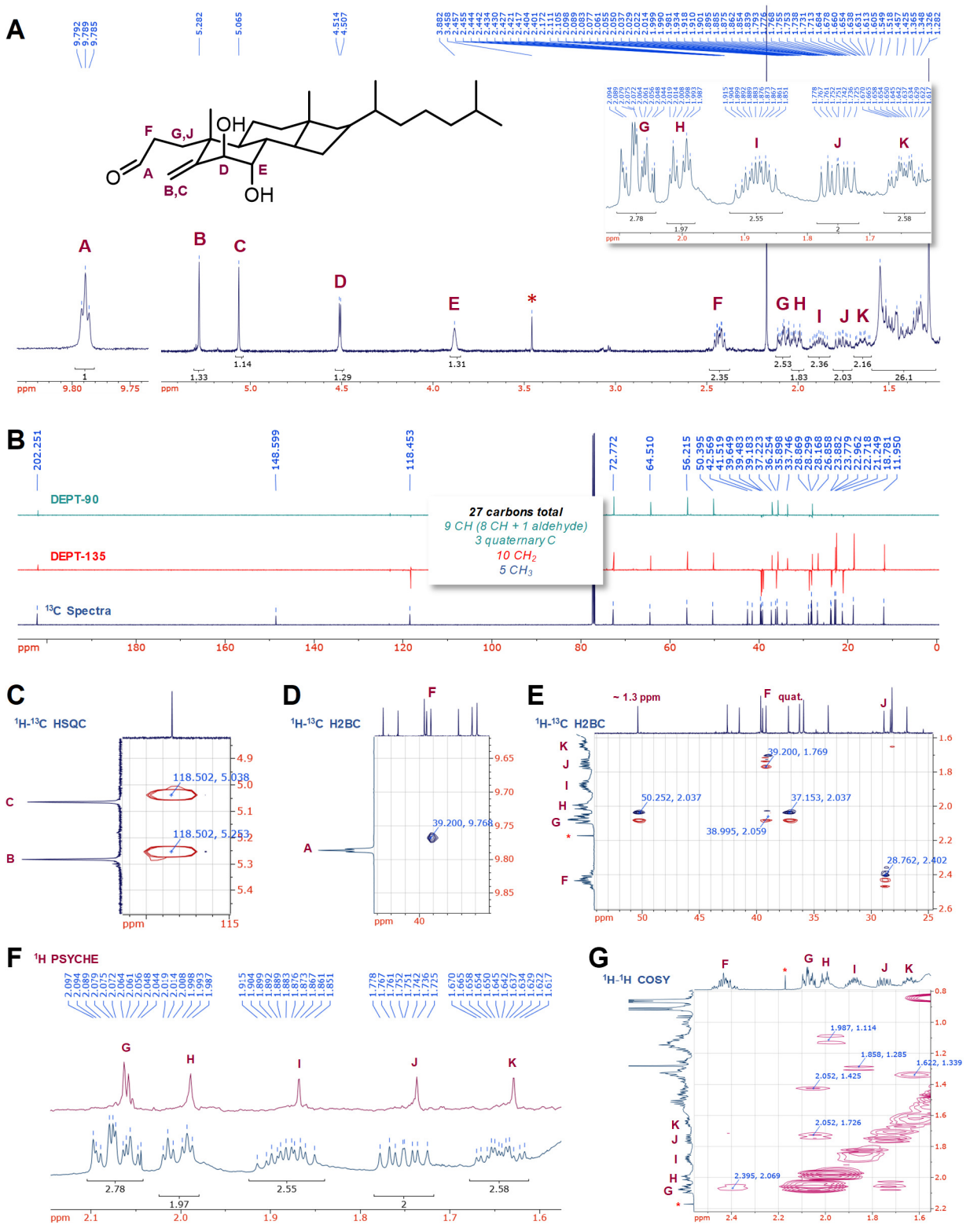

Figure 3.3 Characteristic ^{1}H, ^{13}C, and 2-D NMR spectra and assignments of 3,4-*seco*-6β,7α-diol. Spectra recorded at 600 MHz and 151 MHz for ^{1}H and ^{13}C, respectively, relative to $CDCl_3$.

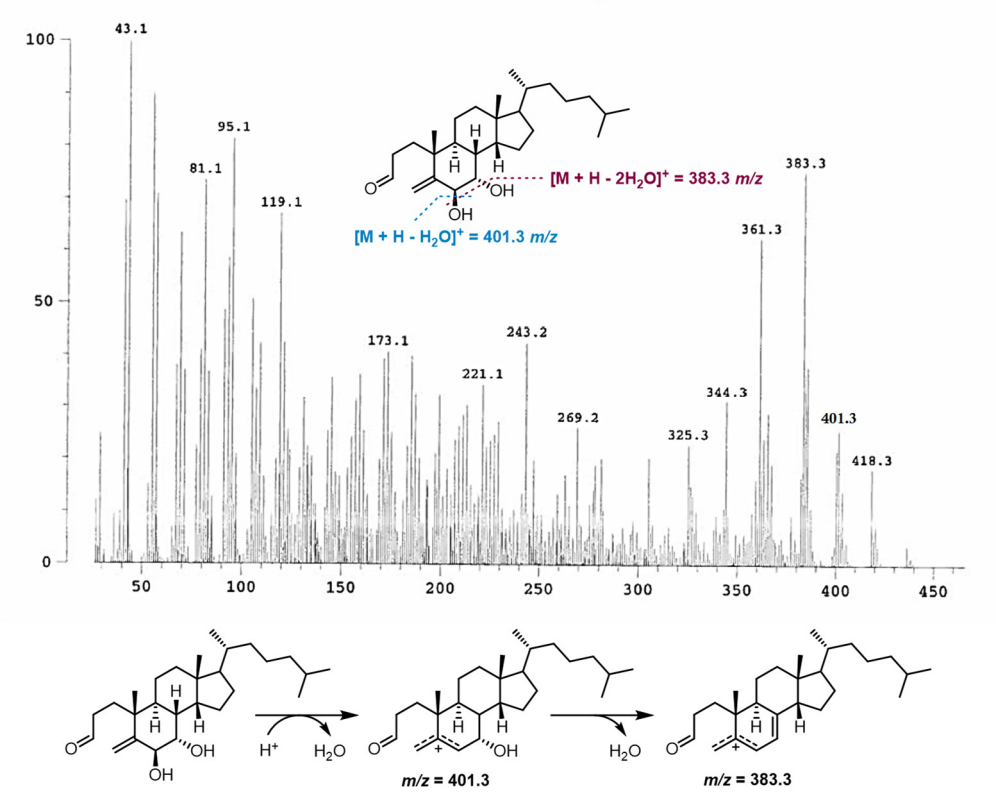

Figure 3.4 Electron impact mass spectrum and corresponding proposed fragmentation pattern obtained for the authentic 3,4-*seco*-6β,7α-diol.

From the ^{1}H NMR spectra, an aldehydic proton was evident based upon the shift and integration of the triplet peak at 9.79 ppm (**A**), however, although we observe very well-defined splitting patterns for the deshielded singlet, doublet, triplet, and several multiplet peaks, we were unable to make confident assignments for these peaks without more information. This is in part due to the convolution of the shielded protons of the sterol scaffold, as shown in **Figure 3.3A**.

^{13}C NMR spectra, including DEPT-135 and DEPT-90 experiments for the identification of the CH_2 and CH systems, respectively, pictured in **Figure 3.3B** were used in combination with a ^{1}H-^{13}C heteronuclear single-quantum coherence (HSQC) experiment pictured in **Figure 3.3C** to illustrate that both singlets at 5.28 (**B**) and 5.07 ppm (**C**) were coupled to the same carbon atom at

118.45 ppm; this is also supported in the DEPT-135 spectra as the corresponding negative signal at 188.45 ppm indicates this carbon atom is a CH_2.

Perhaps one of the most useful 2D NMR experiments used to elucidate our structure was the heteronuclear two-bond correlation (H2BC) experiment.[33] Similar to that of a heteronuclear multiple bond correlation (HMBC) experiment, H2BC presents the ^{1}H-^{13}C correlation through two bonds, reducing the amount of signal observed compared to the correlations through multiple bonds shown in HMBC, simplifying the spectra for assignment of the scaffold. Compared to a 2D ^{13}C-^{13}C incredible natural abundance double quantum transfer experiment (INADEQUATE) typically used for the assignment of a complex carbon backbone, H2BC is advantageous as it requires much less instrument time and relies on the proton signal, facilitating the use of less material, while still providing crucial information regarding the connections of carbon atoms to one another in the scaffold. Using a combination of the strong coupling observed by ^{1}H-^{1}H correlation spectroscopy (COSY) and the through two-bond correlation observed by ^{1}H-^{13}C H2BC illustrated in **Figure 3.3D**, we were able to confidently assign a connection between our aldehyde with a ^{1}H shift of 9.79 ppm (**A**) and the multiplet with complex splitting at 2.44 ppm (**F**).

Furthermore, the H2BC spectra shown in **Figure 3.3E** facilitated assignment of the connection between the CH_2 at 2.44 ppm (**F**) to the diastereotopic protons represented by the doublet of quartets at 1.75 ppm (**J**) and the complex splitting pattern at 2.08 ppm (**G**), continuing to help elucidate the backbone structure of our scaffold. Interestingly, although the splitting pattern at 2.08 ppm (**G**) appears to be relatively complex, we are able to use a combination of HSQC and pure shift yielded by chirp excitation (PSYCHE), a sensitive method that permits suppression of homonuclear spin-spin couplings to produce a single unique ^{1}H signal for each chemically unique site,[34] to determine that this signal splitting pattern represents the overlap of at least two unique

spin systems; for the region of 1.5-2.2 ppm, a stark contrast of single spin systems versus the multiple spin systems observed for the complex splitting pattern at 2.08 ppm (**G**) is clearly indicated in **Figure 3.3F**. Therefore, the multiple connections between the protons at 2.08 ppm (**G**) that did not seem to align with the correlations observed by ^{1}H-^{1}H COSY can be explained based upon the overlapping of two different spin systems. We were able to then rationalize the observed ^{1}H-^{1}H coupling between 2.08 ppm (**G**) and the spin system at both 3.88 ppm (**E**) and 1.75 ppm (**J**) even though we were unable to determine a means to connect the spin systems at 3.88 ppm (**E**) and 1.75 ppm (**J**) themselves.

Upon electron impact (EI) mass spectral analysis, the sequential loss of two water molecules from our parent compound supported the assignment of a diol moiety, supporting the assignment made by ^{1}H NMR. To achieve the fragmented ions observed in the spectra shown in **Figure 3.4**, we propose that the compound undergoes initial protonation followed by the loss of a water molecule, and then subsequent loss of a second water molecule. Considering the inclusion of an aldehyde moiety, this fragmentation pattern is highly suggestive of a diol moiety between the C6 and C7 positions. With regards to the assignment of the stereochemistry at this position, the ^{1}H-^{1}H coupling constant of 3 Hz between the protons at 4.51 ppm (**D**) and 3.88 ppm (**E**) is indicative of two adjacent equatorial protons, suggesting that the corresponding alcohols are anti with respect to one another. To achieve the most stable chair structure with an anti assignment at this position, we propose an assignment of 6β-OH and 7α-OH for the diol moiety.

3.2.2 On the Origin of the 3,4-seco-6β,7α-diol

To provide additional support for our characterization of the novel and thoroughly unexpected sterol A-ring cleavage product, we synthesized an isotopologue of cholesterol-7α-OOH to enable direct tracking of the atoms involved in the fragmentation by ^{1}H NMR and mass spectrometry. In

particular, we sought to deuterate the C4 position, since these protons are expected to comprise the characteristic exomethylene protons in our final secosterol product.

Following a modified synthesis originally carried out by Diekman and Djerassi,[35] 2,2,4,4-d_4-cholesterol was prepared as in **Scheme 3.4**. This approach required initial deconjugation of Δ^4-cholesten-3-one with potassium *tert*-butoxide followed by subsequent addition of *tert*-butanol-OD such that the enolate formed upon deconjugation would become deuterated through exchange at the C2 and C4 positions adjacent to the original ketone; quenching of the reaction using acetic acid-D aided in maintaining a high level of deuterium incorporation. Particular care was required to ensure glassware used in this preparation were completely evacuated of oxygen to prevent premature formation of oxidation products, and absent of water to prevent loss of deuterium. The deconjugated 2,2,4,4-d_4-3-cholesterone was then reduced to the corresponding alcohol via lithium aluminum hydride-mediated reduction of the corresponding ketone to the alcohol, affording the authentic 2,2,4,4-d_4-cholesterol (d_4-chol) in 59% yield. We were fortunate enough to have essentially complete incorporation of deuterium at both the C2 and C4 position, as evidenced by ^{1}H, ^{13}C NMR and mass spectra, however, complete deuteration was not necessarily required for our proposed experiments.

Scheme 3.4 Synthesis of 2,2,4,4-d_4-cholesterol, 2,2,4,4-d_4-cholesterol-7α-OOH, and d_4-3,4-*seco*-6α,7β-diol.

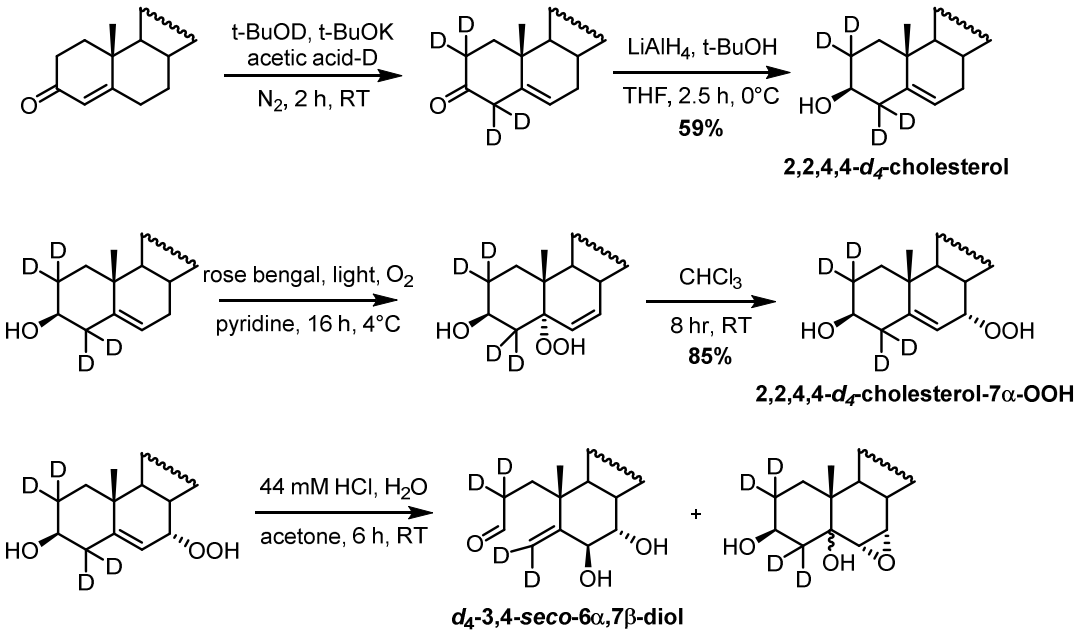

With the authentic d_4-chol in hand, we were able to follow the same synthetic steps used to synthesize chol-7α-OOH to afford 2,2,4,4-d_4-chol-7α-OOH (d_4-chol-7α-OOH). Once again, ^{1}H, ^{13}C NMR and mass spectra all suggested complete deuteration of the final product following photo-oxidation and rearrangement. As expected, d_4-chol-7α-OOH subjected to 50 mM HCl in acetone saturated with water afforded the d_4-3,4-*seco*-6α,7β-diol at 35 % yield and with a product mixture that mirrored that obtained with the protiated material. However, the exomethylene proton signals of the d_4-3,4-*seco*-6α,7β-diol at 5.23 and 5.03 ppm were almost completely supressed – indicating that they originated as protons from either C2 or C4. Some retention in signal for the peak at 2.40 ppm suggested that some exchange, albeit minor, occurred at this position; provided that H/D exchange appears to be considerably higher for this position, this suggests that the signal at 2.40 ppm originated as protons at the C2 position given that H/D exchange likely occurs as a consequence of acid-catalyzed enolization of the aldehyde.

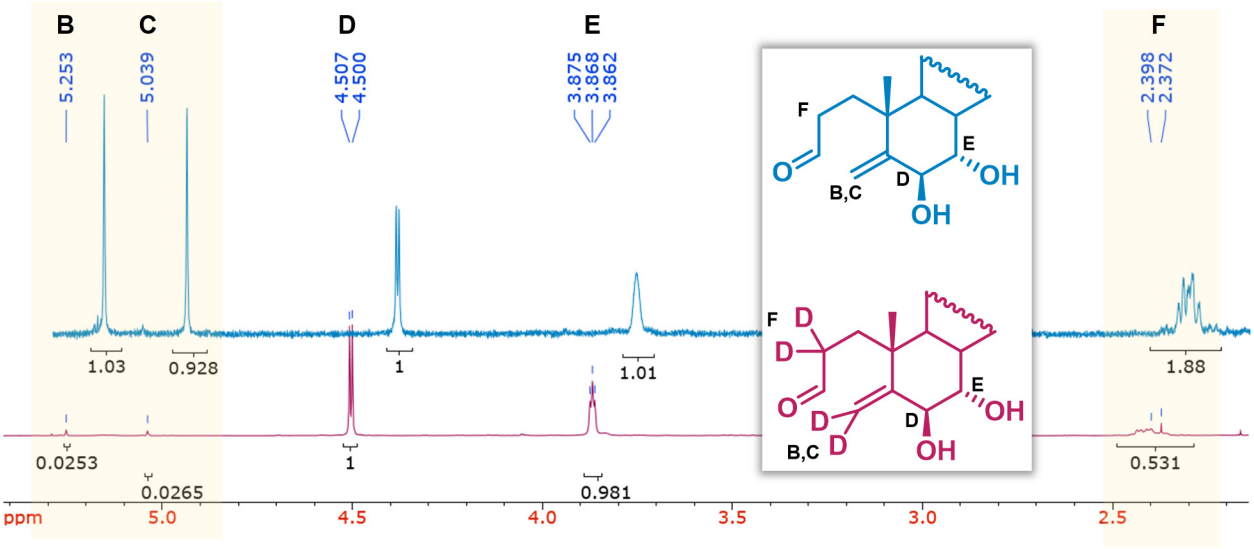

Figure 3.5 Direct comparison from 3.6-5.5 ppm of the ^{1}H NMR spectra for the protiated (blue) and deuterated (pink) 3,4-*seco*-6β,7α-diol. Areas in which deuteration has resulted in an absence of signal are highlighted in yellow. Spectra recorded at 400 MHz relative to $CDCl_3$; horizontal offset of 0.1 ppm applied to the overlay of the spectra of the protiated compound for clarity.

3.2.3 Product Profiling in the Hock Fragmentation of Cholesterol-7α-Hydroperoxide

To confirm that fragmentation of chol-7α-OOH was acid-catalyzed, and to evaluate the stabilities of the fragmentation products to the reaction conditions, ^{1}H NMR experiments were performed to monitor product evolution over time. A range of acid concentrations spanning three orders of magnitude were investigated (0.005, 0.01, 0.1 and 1 M HCl), holding the chol-7α-OOH concentration constant at 50 mM in acetone-d_6 containing 11.1 mM trichloroethylene (TCE) as an internal standard. Resulting consumption of chol-7α-OOH and corresponding product evolution are shown in **Figure 3.6**.

Although some convolution is present in the 3.0 – 4.5 ppm region of the spectra at late stages of the reaction, presumably due to the evolution of poly-hydroxy products, we are able to quantify the 3,4-*seco*-6β,7α-diol and the 5α- and 5β-OH epoxide epimers easily as their

characteristic peaks are located downfield and upfield, respectively, relative to this region, permitting reliable quantification. Signals corresponding to the isolated and characterized products observed during the reaction are highlighted in the spectrum provided in **Figure 3.6E**.

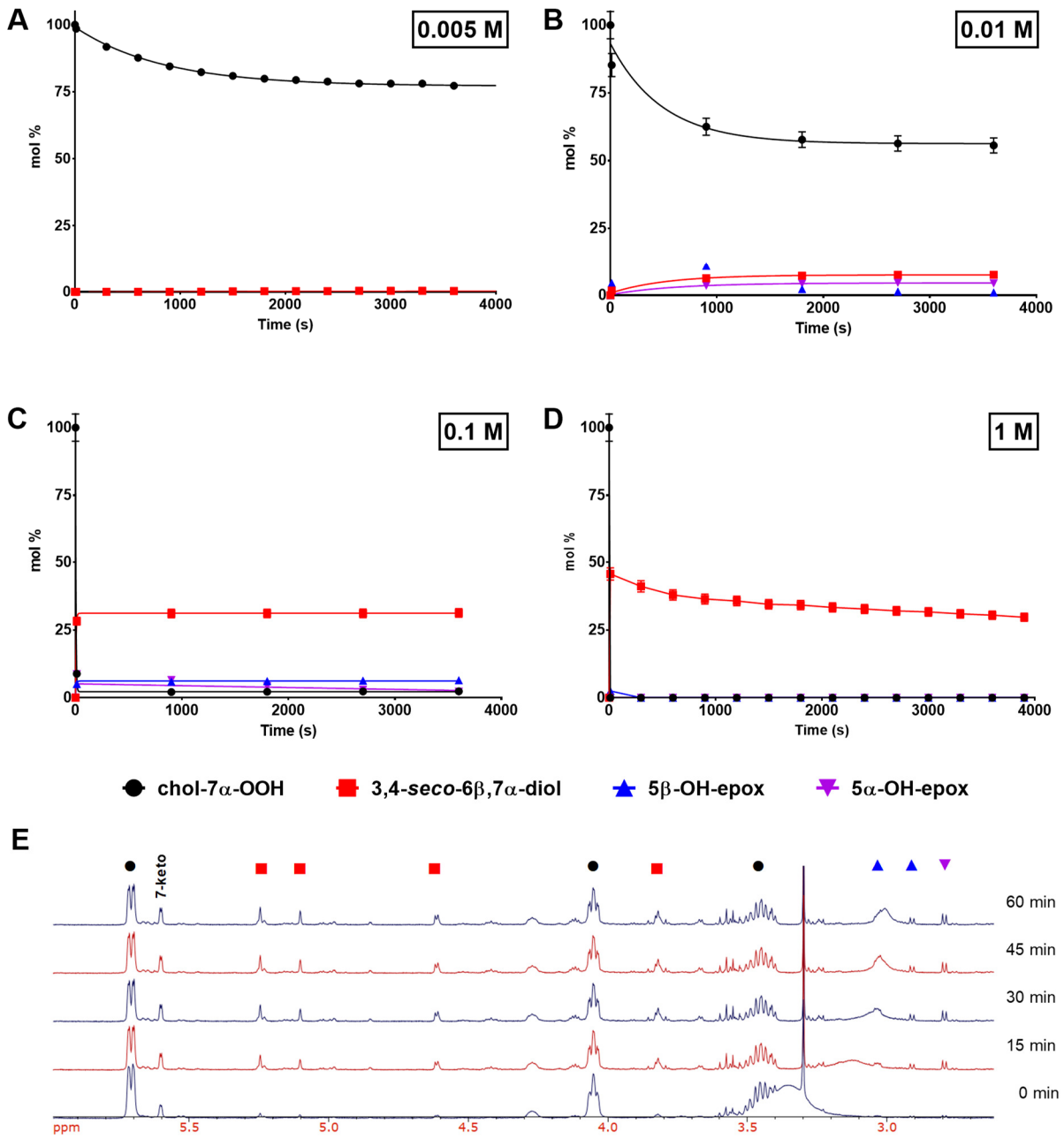

Figure 3.6 ^{1}H NMR monitoring the Hock fragmentation of chol-7α-OOH (50 mM) in the presence of 0.005 M (**A**), 0.01 M (**B**), 0.1 M (**C**), and 1 M (**D**) HCl in acetone-d_6. Chol-7α-OOH

(●) decomposition and product evolution of 3,4-*seco*-6β,7α-diol (■), 5β-OH epoxide (▲), and 5α-OH epoxide (▼) were measured. Representative spectra of 0.01 M HCl for time points spanning the first hour of the reaction with our proposed assignment of the mixture are presented (**E**). 7-ketocholesterol is denoted as a contaminant of the starting material, but does not increase in concentration throughout the course of the monitored reaction. Spectra recorded at 300 MHz every 15 minutes for 10 hours at 64 scans per spectra collected; 11.1 mM TCE utilized as an internal standard.

Interestingly, 0.1 M HCl used to facilitate DNPH derivatization is coincidentally optimal to yield the largest amount of 3,4-*seco*-6β,7α-diol. At other concentrations assessed, either starting material is not consumed enough to evaluate or the conditions are too harsh such that the of 3,4-*seco*-6β,7α-diol itself appears to decompose after extended exposure. Additionally, evolution of 3,4-*seco*-6β,7α-diol occurs almost instantly and appears to persist without decomposition throughout the time course of the reaction. This speaks to the robustness of this material under relatively harsh conditions – a surprising phenomena considering the perceived electrophilicity of the aldehydic moiety.

Perhaps one of the most notable issues observed with this method of quantification is the inability to fully account for the mass balance of the products resulting from the reaction. Using 0.1 M HCl as a model for its efficient product consumption and lack of product degradation, we can highlight the inability to account for the full mass balance. Although 3,4-*seco*-6β,7α-diol is the apparent major product, this only accounts for ~ 30 % of the products evolved in consideration that the starting material is completely consumed. Given that the 5α- and 5β-OH-epoxides compose less than 10 % of the products evolved, and also appear to degrade over the course of the reaction, we proposed that the epoxide isomers may be opening to their corresponding tetra-hydroxy products in the presence of water given the presence of several broad multiplets around 4.0 ppm, likely contributing to a large portion of the mass balance.

Unfortunately, we were unable to preparatively separate and isolate any of these proposed tetra-hydroxy products, however, we were able to subject the authentic 5β-OH epoxide to the same reaction conditions in an effort to provide evidence that the epoxide hydrolysis products contribute to the unaccounted portion of the mass balance. Interestingly, we were able to observe what we propose are tetra-hydroxy products of the 5β-OH epoxide within the region of 3.0 to 4.5 ppm, and what are likely to make up the majority of the mass balance at later stages of the reaction based upon the convolution in this region after treatment with 0.1 M HCl. As illustrated in **Figure 3.7**, we propose that the two possible tetra-hydroxy products are generated from the 5β-OH-epoxide alone and that near complete decomposition of the epoxide species occurs within an hour of subjection to these conditions.

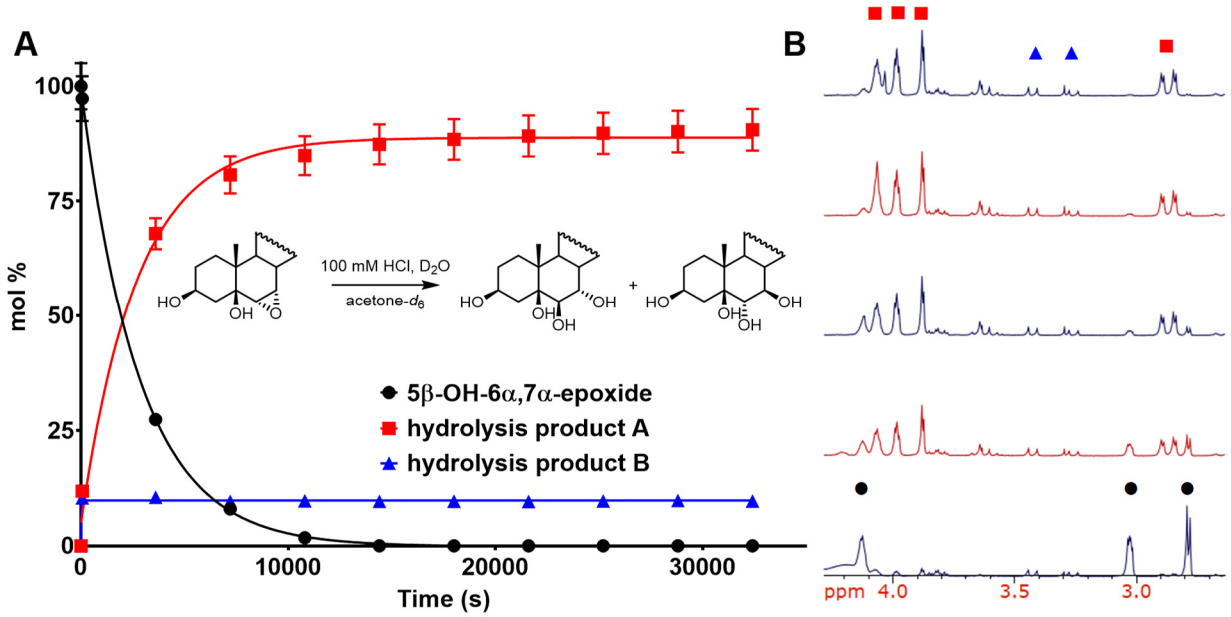

Figure 3.7 ^{1}H NMR monitoring of the hydrolysis of chol-5β-hydroxy-6α,7α-epoxide subjected to 100 mM HCl over time (**A**) and a sample of the corresponding representative spectra from 2.5 to 4.5 ppm (**B**). 5β-OH-epoxide (●) decomposition and product evolution of unknown hydrolysis products A (■), and B (▲) were measured. Spectra were recorded at 300 MHz relative to acetone-d_6 every hour for 10 hours at 64 scans per spectra collected; peaks integrated relative to trichloroethylene (TCE) as an internal standard.

Despite great efforts, individual components of the highly polar mixture of tetra-hydroxy compounds were extremely difficult to isolate following silica gel flash chromatography, however we were able to clearly identify the evolution of one distinct tetra-hydroxy species that composed ~ 90 % of the product resulting from hydrolysis (**product A**). We tentatively assign the structure of this compound to the 3β,5β,6β,7α-tetrahydroxy cholesterol based upon the known assignments of the stereochemistry of the diol moiety of 3,4-*seco*-6β,7α-diol and the expectation that hydrolysis will likely occur favourably in the same manner. A second minor product was also identified (**product B**) which we also tentatively identify as opening of the epoxide to afford the 6α,7β isomer of the tetra-hydroxy compound, however, with little product afforded in the reaction, it is difficult to identify distinct peaks corresponding to this product. Nevertheless, these findings helped rationalize the portions of the mass balance we were unable to account for.

Following attempts to isolate the products from a preparative scale mixture of the chol-7α-OOH subjected to 0.1 M HCl in acetone, we can now deconvolute the mixture afforded. Although the major product appears to be the 3,4-*seco*-6α,7α-diol, there is a diverse mixture of epoxide isomers apparent between 2.5-4.0 ppm, as illustrated in **Figure 3.8**, evidenced by their characteristic "roofing" peaks. Both the 5α- and 5β-OH α-epoxide isomers identified are easily confirmed based upon their characterization from the literature,[31,32] and our own spectroscopic data, however, we were unable to isolate the other apparent minor epoxide product (**yellow**) for thorough characterization and were unable to make comparison to any available literature source to identify this product. Interestingly, it does exhibit the same roofing peak character as the other epoxide species, however it appears that the polarity of the molecule has been influenced such that the shift of the C6 and C7 protons has reversed relative to the other species; this initially implied that dehydration possible occurs on the A-ring to afford an alkene at either the $\Delta^{3,4}$ or $\Delta^{4,5}$ positions,

however, no such alkene peaks were present in the isolated product. We have therefore tentatively assigned this unknown minor product as the 5α-OH-6β,7β-epoxide isomer as this characterization preserves the epoxide moiety and does not match the reported characterization for the 5β-OH-6β,7β-epoxide.[31]

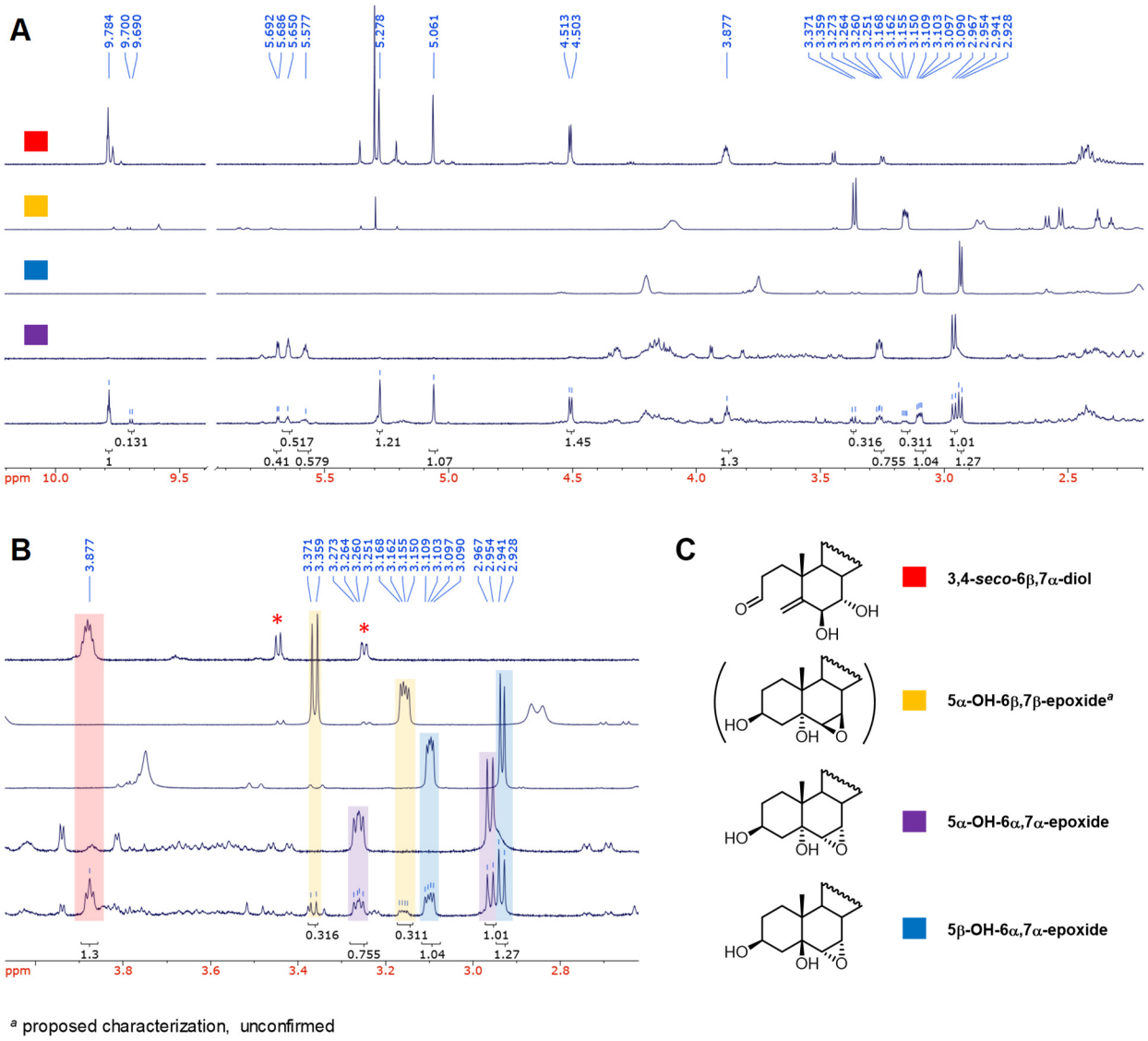

Figure 3.8 Deconvolution of known products formed following Hock fragmentation of chol-7α-OOH. A representative spectrum of the product mixture formed following treatment of chol-7α-OOH with 0.01 M HCl in acetone for 1 hour is overlaid with representative spectra of the products successfully separated from this mixture via silica gel flash chromatography (**A**). Components of the convoluted mixture identified are highlighted (**B**) and their proposed or confirmed

characterization is provided (**C**). Peaks marked with an asterisk (*) correspond to the 3,4-*seco*-6α,7α-epoxide. Spectra were recorded at 400 MHz relative to $CDCl_3$.

To probe the mechanism of this fragmentation further, we sought to compare product evolution in solvent systems of participating and non-participating nature. Using kinetic ^{1}H NMR, we monitored fragmentation of chol-7α-OOH in 0.1 M HCl administered in D_2O over the course of 10 hours in acetone-d_6, chloroform-*d*, and methanol-d_4.

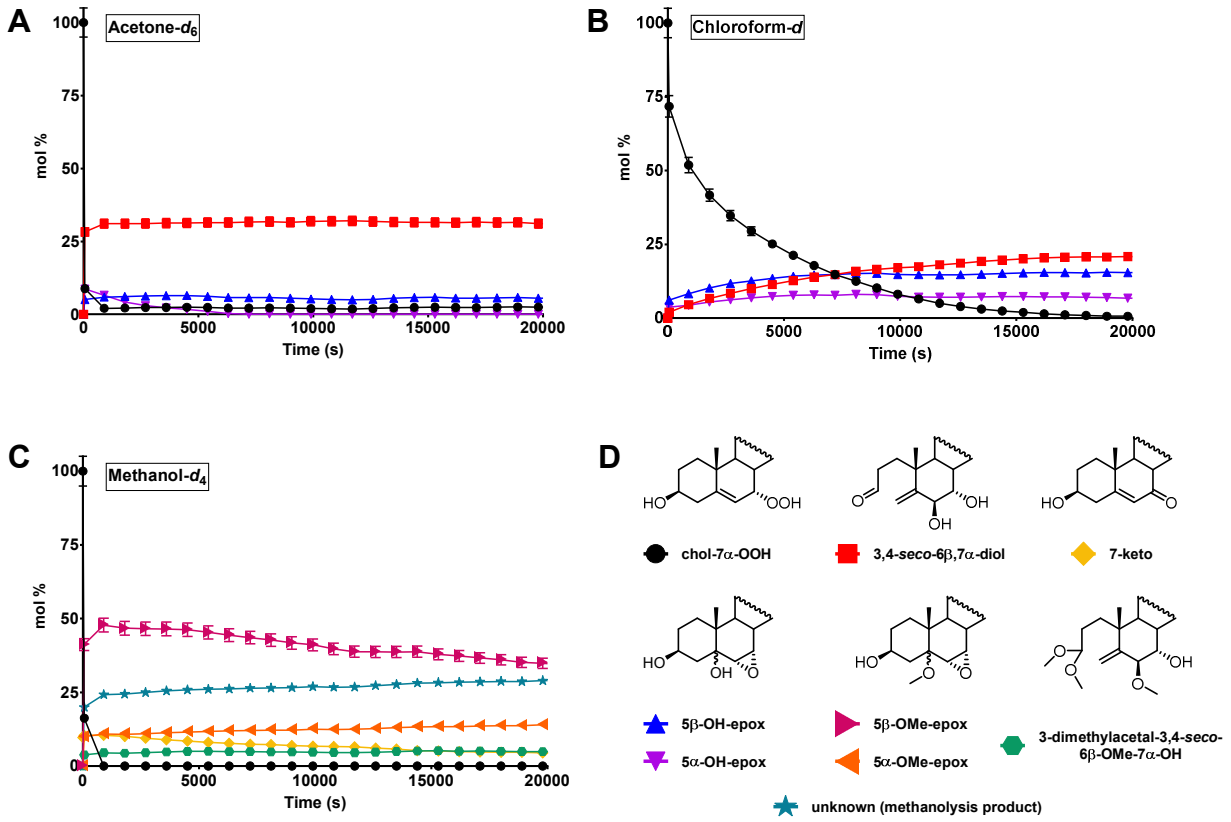

Figure 3.9 Qualitative ^{1}H NMR monitoring of the product evolution arising from Hock fragmentation of chol-7α-OOH with 0.1 M HCl in acetone-d_6 (**A**), chloroform-*d* (**B**), and methanol-d_4 (**C**). Chol-7α-OOH (●) decomposition and product evolution of 3,4-*seco*-6β,7α-diol (■), 7-keto (◆), 5β-OH epoxide (▲), 5α-OH epoxide (▼), 5β-OMe epoxide (▶), and 5α-OMe epoxide (◀), 3-dimethylacetal-3,4-*seco*-6β-OMe-7α-OH (⬣), and an unknown methanolysis product (★) were measured. Structures of the compound of interest are presented (**D**). Spectra were recorded at 300 MHz relative to acetone-d_6, chloroform-*d*, or methanol-d_4 every 15 minutes for 10 hours at 64 scans per spectra collected; TCE utilized as an internal standard.

Each solvent system provides a slightly different environment based upon the miscibility of water and the participating nature of the solvent itself. Acetone serves as a non-participating system in which water is the active nucleophile; this model is likely the most representative in organic solution of a product profile of what may be observed *in vivo*. Chloroform is also non-participating in nature, however, poor miscibility of water appears to alter the product profile and rate of decomposition of chol-7α-OOH significantly.

In contrast to non-participating solvent, the reaction in participating alcoholic solvent (i.e. methanol) may not provide a product profile that is representative of the *in vivo* products formed, however, products resulting from the reaction in methanol would help to identify products that form as a consequence of DNPH derivatization in ethanol. As previously reported by our group,[29] the analogous methoxy epoxide species are observed as a consequence of Hock fragmentation in the absence of DNPH, however, no such aldehydic species are formed. In the case of our attempts to qualitatively monitor the reaction by ^{1}H NMR, we observe the same product profile as had been reported in our past work. However, with the information we now have regarding the formation of the 3,4-*seco*-6β,7α-diol, we can now identify products contained in our mixture that we had not been able to before to help rationalize the absence of aldehydic species under these conditions.

Although we had suspected that the lack of an aldehydic product may simply reflect the formation of an acetal, it was difficult to distinguish these peaks from the rest of the mixture without the knowledge of the structural character we now have. It is evident now that although ~ 60 % of the product mixture is composed of the 5β-OMe and 5α-OMe epoxide products, as shown in **Figure 3.9C**, the absence of 3,4-*seco*-6β,7α-diol is likely a consequence of the participating nature of the methanolic solvent readily forming a dimethyl acetal with the highly electrophilic aldehyde. This has since been identified as one of the previously unknown compounds isolated as

a mixture by silica gel flash chromatography with the 5β-OMe epoxide species, as shown in **Figure 3.10**. The lack of free aldehyde in the sample, and the predominance of non-aldehydic products of acid-catalyzed fragmentation underlies why little hydrazone is formed when chol 7-OOH is subjected to typical DNPH derivatization conditions.

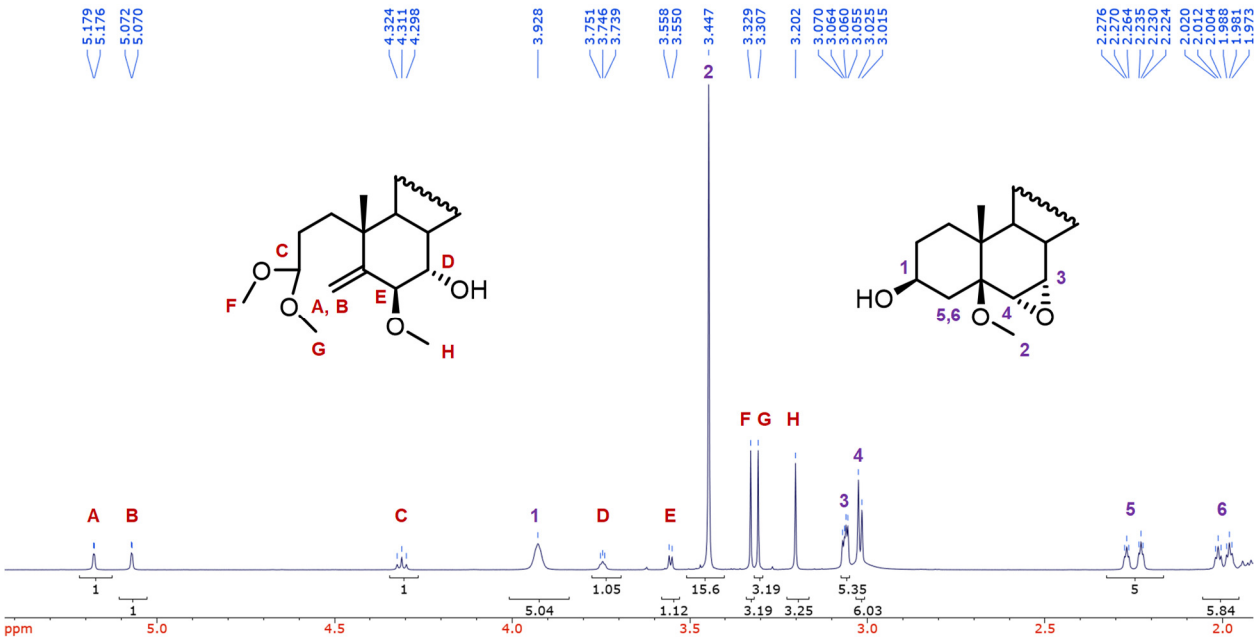

Figure 3.10 ^{1}H NMR spectra of a 3-dimethylacetal-3,4-*seco*-6β-OMe-7α-cholestanol and 5β-OMe epoxide mixture isolated preparatively by silica gel flash chromatography and their corresponding proposed assignments. Spectra were recorded at 400 MHz relative to $CDCl_3$.

Additional mass balance is likely to consist of products resulting from methanolysis of the epoxide, as indicated by quantification of the unknown methanolysis product in **Figure 3.9C**.

3.2.4 Product Profiling in the Hock Fragmentation of Cholesteryl Acetate-7α-Hydroperoxide

Our final mechanistic exploration by ^{1}H NMR sought to probe the importance of the free 3β-OH in the mechanism of Hock fragmentation of chol-7α-OOH, particularly for the formation of the 3,4-*seco*-6β,7α-diol. Therefore, cholesteryl acetate-7α-OOH was synthesized by photo-oxidation of cholesteryl acetate analogous to the method used to afford chol-7α-OOH. This acetylated form

of our primary autoxidation product serves as an excellent model for Hock fragmentation of esterified chol-7α-OOH, the form in which it would likely exist in oxidized LDL.

Cholesteryl acetate-7α-OOH was subjected to 0.1 M HCl administered in D_2O in acetone-d_6 analogous to the aforementioned experiments performed for chol-7α-OOH. Solubility of both the free and esterified 7α-OOH were very similar and would therefore have not impacted the product distribution observed. Indeed, we do observe a very different product distribution wherein the 3,4-*seco*-6β,7α-diol product comprises only ~ 5 % of the mixture compared to the near 30 % 5β/α-OH epoxide species prior to hydrolysis of these species; the ratio of 3,4-*seco*-6β,7α-diol to 5β/α-OH epoxide species is ~ 1:6 which is in stark contrast to the ~ 6:1 ratio observed for Hock fragmentation of free chol-7α-OOH. We also observe the rapid evolution of a presumed hydrolysis product of one of the epoxide isomers based upon comparison to the hydrolysis product evolved with free chol-7α-OOH. Although cholesteryl acetate appeared to maintain hydrolytic stability when subjected to the same acidic conditions, it is likely that the relatively small amount of 3,4-*seco*-6β,7α-diol forms as a result of some hydrolysis of the acetate. Nevertheless, the observation that esterified chol-7α-OOH does not readily evolve to form 3,4-*seco*-6β,7α-diol, unlike its free 3β-OH counterpart, is informative towards our understanding of the potential impact of Hock fragmentation in areas esterified cholesterol oxidation products *in vivo*.

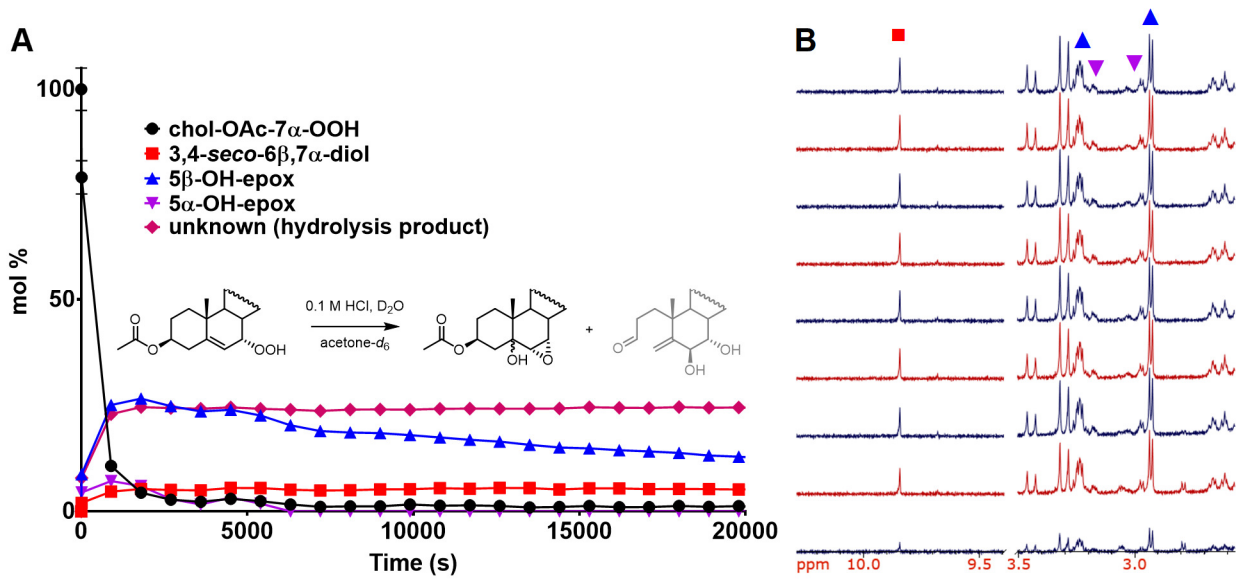

Figure 3.11 Qualitative ^{1}H NMR monitoring of the product evolution arising from Hock fragmentation of cholesteryl acetate-7α-OOH with 0.1 M HCl in acetone-d_6 (**A**) and a representative ^{1}H NMR spectra and a sample of the corresponding representative spectra from 2.5 to 3.5 ppm and 9.5 to 10.5 ppm (**B**). Chol-OAc-7α-OOH (●) decomposition and product evolution of 3,4-*seco*-6β,7α-diol (■), 5β-OH epoxide (▲), 5α-OH epoxide (▼), and an unknown hydrolysis product (◆) reliably measured. Spectra were recorded at 300 MHz relative to acetone-d_6 every 15 minutes for 8 hours at 64 scans per spectra collected; TCE utilized as an internal standard.

3.2.5 Hock Fragmentation of Cholesterol-7α-Hydroperoxide Under DNPH Derivatization Conditions: Product Identification by HPLC/UV-Vis and NMR Spectroscopy

With the product distribution arising from the acid-catalyzed fragmentation of chol-7α-OOH in the absence of DNPH largely characterized, we sought to translate our insights to enable characterization of the products formed under typical (acidic) DNPH derivatization conditions. Due to the poor solubility and spectral complexity upon inclusion of DNPH, we were unable to accurately monitor reactions under derivatization conditions by ^{1}H NMR. However, DNPH-derived hydrazones are easily monitored by UV-Vis detection at λ_{max} ~ 360 nm following their separation by HPLC. Authentic standards of the DNPH-derived hydrazones of 3,4-*seco*-6β,7α-diol and 7-ketocholesterol were synthesized (along with derivatized testosterone as an internal

standard) and compared to cholesterol-7α-OOH subjected to 0.1 M HCl and 200 μM DNPH in EtOH. Indeed, we found that derivatized 3,4-*seco*-6β,7α-diol shared the same retention time as the major derivatized product peak at 24 minutes and derivatized 7-keto shared the same retention time as the peak at 41 minutes, as illustrated in **Figure 3.12**. Secosterols A and B (secA and B), the known aldehydic sterols derived from ozonolysis of cholesterol and Hock fragmentation of chol 5- and 6-OOH, were also synthesized for comparison. Interestingly, we found that derivatized secA eluted at the same retention time as the minor peak at 17.5 min and derivatized secB eluted at the same retention time as the major peak at 24 min attributed to the derivatized 3,4-*seco*-6β,7α-diol!

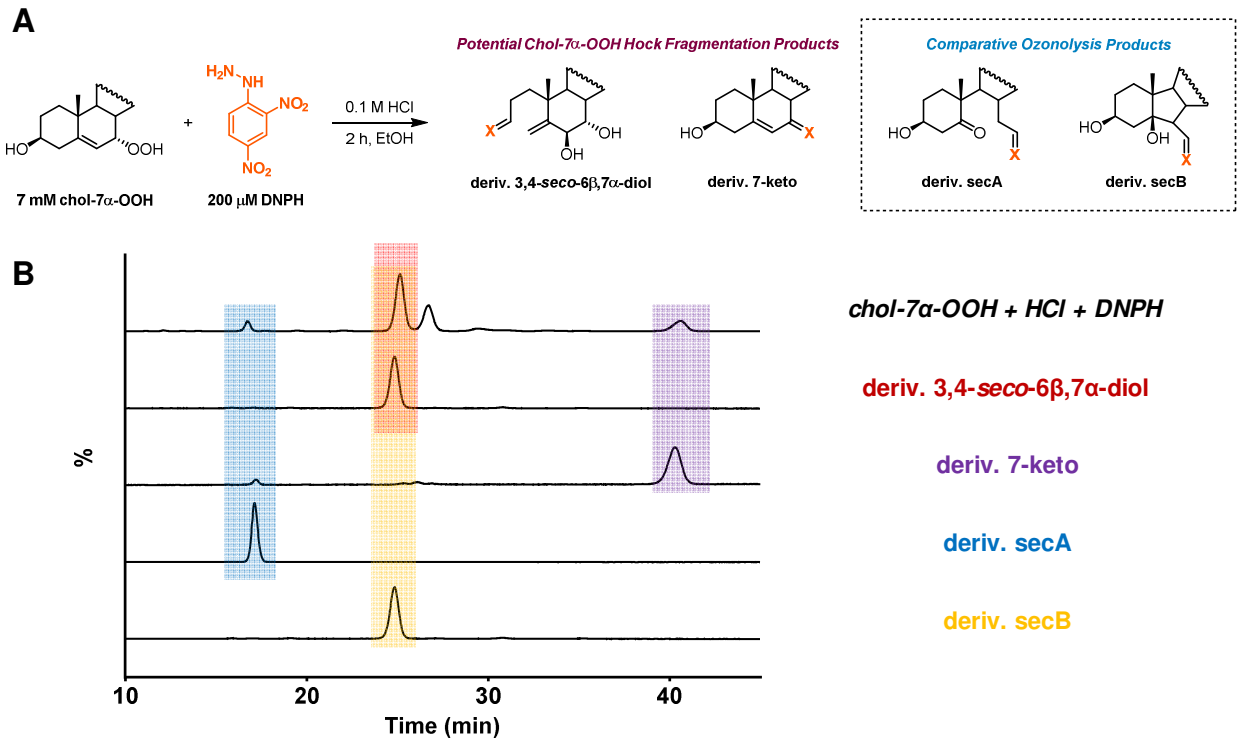

Figure 3.12 Proposed products of Hock fragmentation of chol-7α-OOH under acidic DNPH derivatization conditions (**A**) and representative HPLC chromatograms chol-7α-OOH subjected to the described DNPH derivatization conditions compared to authentic derivatized hydrazone standards of 3,4-*seco*-6β,7α-diol, 7-ketocholesterol, secosterol A, and secosterol B, (**B**). 5 μL of each sample in ethanol was injected onto a 4.6 × 150 mm Atlantis C18 reverse-phase HPLC

column with a flow rate of 1 mL/min of 75:20:5 ACN:MeOH:H_2O. Visualized by UV-Vis detection at 360 nm.

Although this observation suggested that chol-7α-OOH likely fragments under acidic DNPH derivatization conditions, we sought to probe the nature of these products further to confirm their identity, particularly for the uncharacterized peaks. Therefore, we subjected chol-7α-OOH to the same DNPH derivatization conditions described above on a preparative scale and utilized preparative HPLC to separate and isolate the compounds for characterization. To our surprise, the ^{1}H NMR spectra of these products did not match any of the chol-7α-OOH Hock fragmentation products identified in the absence of DNPH, with the exception of 7-keto, however, they appeared to be of similar secosterol character. Proposed assignments for each of the isolated products, as illustrated in **Figure 3.13**, were based upon comparisons to the ^{1}H NMR spectra of underivatized compounds of similar nature to be described herein.

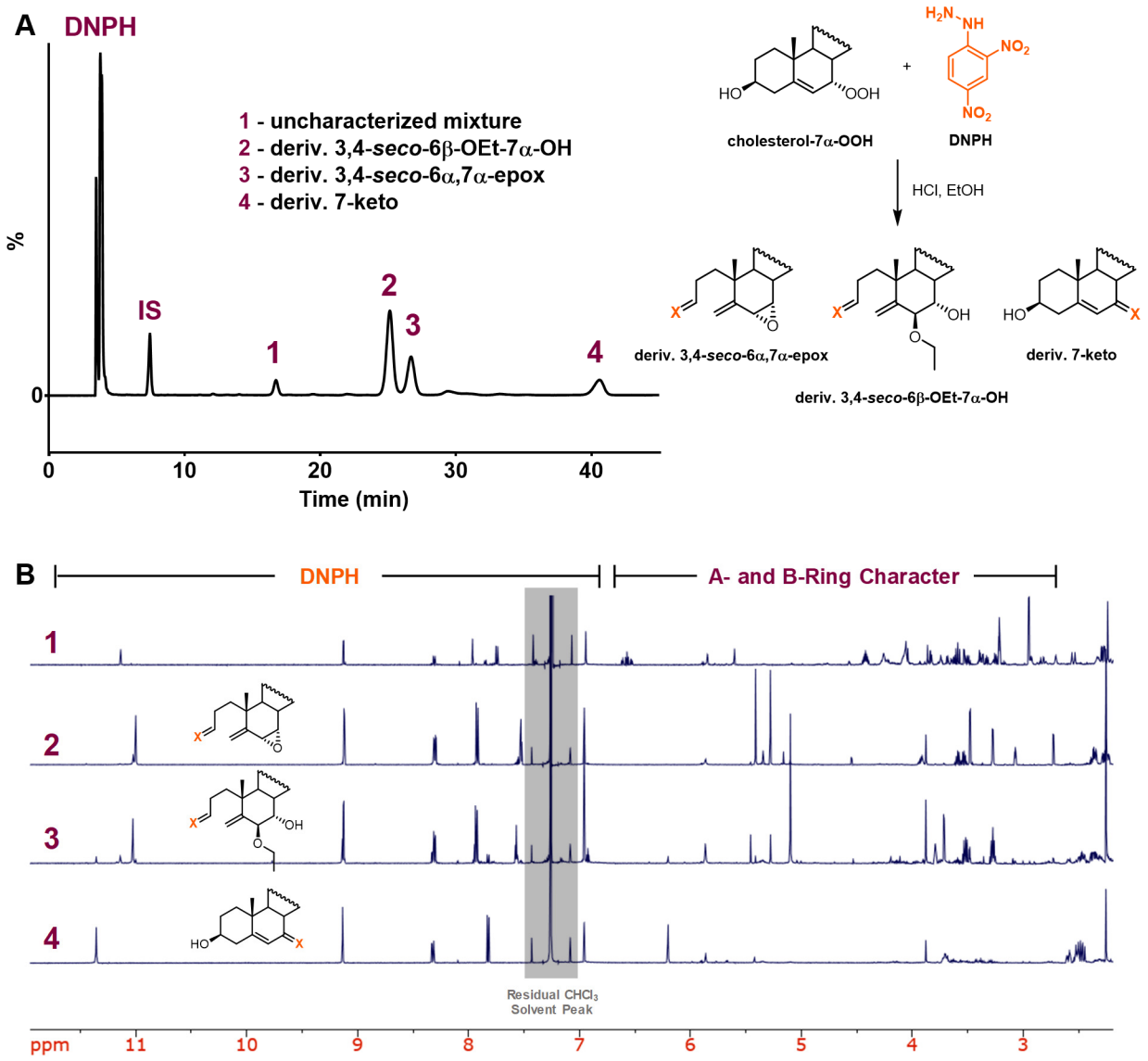

Figure 3.13 Representative HPLC chromatogram of a mixture of cholesterol-7α-OOH Hock fragmentation products with their proposed identification (**A**) and the ^{1}H NMR spectra obtained upon separation and characterization of the isolated products (**B**). 500 µL of a chol-7α-OOH Hock fragmentation mixture was injected onto a reverse-phase Waters XBridge Prep C18 5 µM column (19 × 150 mm) and separated isocratically with 75:20:5 ACN:MeOH:H_2O at a flow rate of 7 mL/min. Visualized with UV-Vis detection at 360 nm. Spectra were recorded at 600 MHz relative to chloroform-*d*. DNPH hydrazone of testosterone was used as an internal standard (IS).

Although the compound that elutes after 18 minutes (**1**) is of similar retention time, we do not observe any peaks that correspond to that of the DNPH hydrazone of secA upon direct

comparison of their ^{1}H NMR spectra. Unfortunately, upon inspection of the convoluted spectra obtained upon isolation of this peak, we were unable to characterize any DNPH hydrazones within the mixture definitively. It is interesting to note that we can clearly identify two large peaks at 3.21 and 2.95 ppm that correspond to the 5β-OH epoxide species, however, these epoxide species do not undergo DNPH derivatization under the conditions in which we have performed this reaction.

As expected, the ^{1}H NMR spectra of the compound eluting at 40 minutes (**4**) does indeed correspond to the DNPH hydrazone of 7-ketocholesterol as suggested by the HPLC co-injection performed of the authentic standard shown in **Figure 3.12**. Perhaps most surprisingly was the ultimate characterization assigned for the compounds eluting at 24 and 26 minutes (**2** and **3**, respectively) as the spectra obtained did not correspond to either the DNPH hydrazone of secB or the 3,4-*seco*-6β,7α-diol upon direct comparison of their ^{1}H NMR spectra.

Interestingly, the peak at 24 minutes (**2**) corresponding to the major product appears to exhibit spectroscopic "roofing" epoxydic character despite our expectation that it may correspond to derivatized 3,4-*seco*-6β,7α-diol or secB based upon their co-elution. Interestingly, we had fortuitously noticed similar character in our attempts to purify the underivatized 3,4-*seco*-6β,7α-diol preparatively on silica gel - a consequence of what we proposed as the dehydrating nature of silica gel. This becomes clear upon direct comparison of the underivatized 3,4-*seco*-6β,7α-diol and 3,4-*seco*-6α,7α-epoxide and corresponding DNPH hydrazones, as shown in **Figure 3.14**.

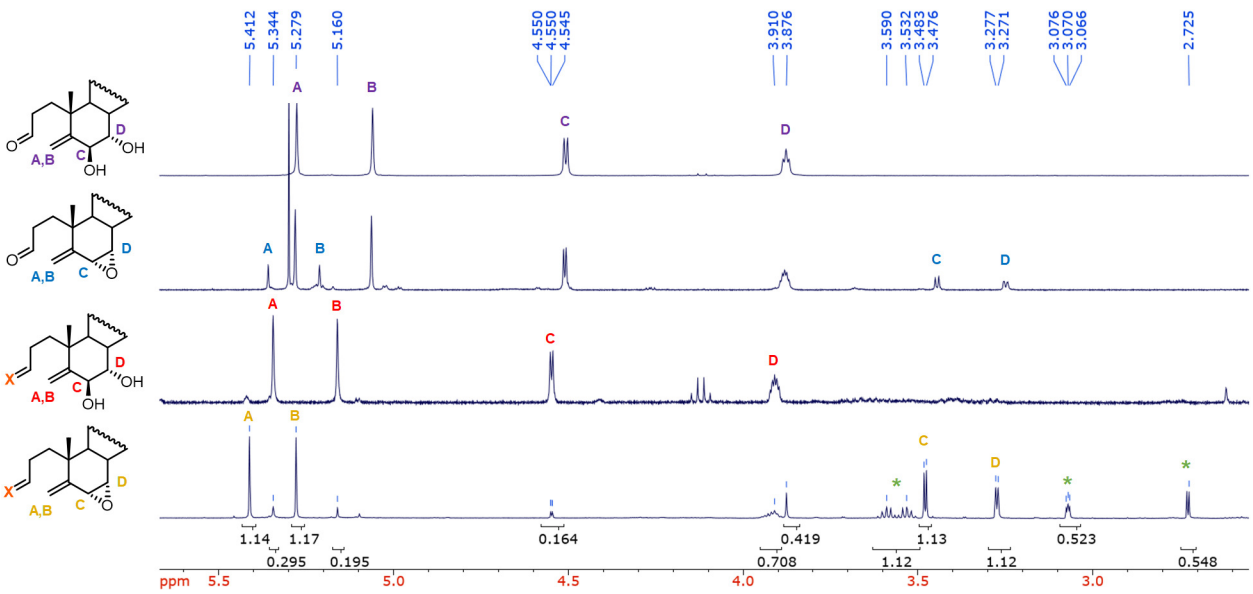

Figure 3.14 Representative ^{1}H NMR spectra of the DNPH hydrazone of 3,4-*seco*-6α,7α-epoxide (yellow) overlaid with spectra of the underivatized 3,4-*seco*-6β,7α-diol (purple), underivatized 3,4-*seco*-6α,7α-epoxide (blue), and DNPH hydrazone of the 3,4-*seco*-6β,7α-diol (red) for comparison. Region of 2.5-5.5 ppm displayed for clarity, excluding regions corresponding to DNPH and cholesterol hydrocarbon scaffold. Peaks marked with an asterisk (*) are proposed to correspond to 5β-ethoxy-6α,7α-epoxide. Spectra were recorded at 400 or 600 MHz relative to chloroform-*d*.

Additionally, the peak at 27 minutes (**3**) also exhibits character of similar to that of the 3,4-*seco*-6β,7α-diol. This compound appears to be the DNPH hydrazone of the 3,4-*seco*-6β-ethoxy-7α-ol that results from opening of the aforementioned epoxide with ethanol, or equilibrium exchange of one of the hydroxy groups of the DNPH hydrazone of the 3,4-*seco*-6β,7α-diol. This was fortuitously supported by the observation that upon incubation of derivatized 3,4-*seco*-6β,7α-diol in ethanol for ~ 1 month, the peak at 27 minutes (**3**) evolves. By ^{1}H NMR, it was apparent that equilibrium exchange of the hydroxy group for the ethoxy must have occurred, as we clearly observed peaks corresponding to the DNPH hydrazone of 3,4-*seco*-6β-ethoxy-7α-ol, as illustrated in **Figure 3.15**.

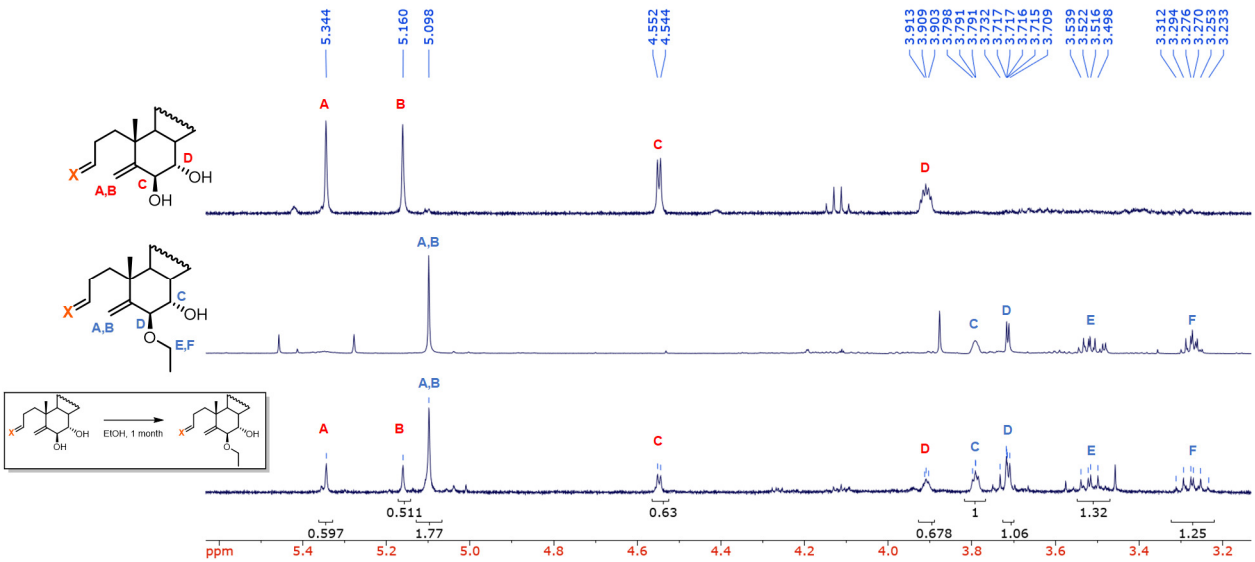

Figure 3.15 Representative ^{1}H NMR spectra of the DNPH hydrazone of 3,4-*seco*-6β-ethoxy-7α-ol (middle, blue) compared against the DNPH hydrazone of the 3,4-*seco*-6β,7α-diol (top, red) and the resultant ^{1}H spectra of the DNPH hydrazone of the 3,4-*seco*-6β,7α-diol after a month dissolved in ethanol (bottom). Region of 3.1-5.6 ppm displayed for clarity, excluding regions corresponding to DNPH and cholesterol hydrocarbon scaffold. Spectra were recorded at 600 MHz relative to chloroform-*d*.

To illustrate that the product distribution of the reaction is also dependent upon acid concentration in the presence of DNPH, we performed the reaction at different concentrations of HCl. Previous reactions were performed at 1 M HCl to promote the most efficient time-course for the reaction and subsequent preparative isolation of the resulting species, however, typical DNPH derivatization conditions utilize 0.1 M HCl and 200 µM DNPH. For monitoring of the resulting characterized compounds by UV-Vis, we utilized a larger equivalent of DNPH to match the amount of chol-7α-OOH required for visualization.

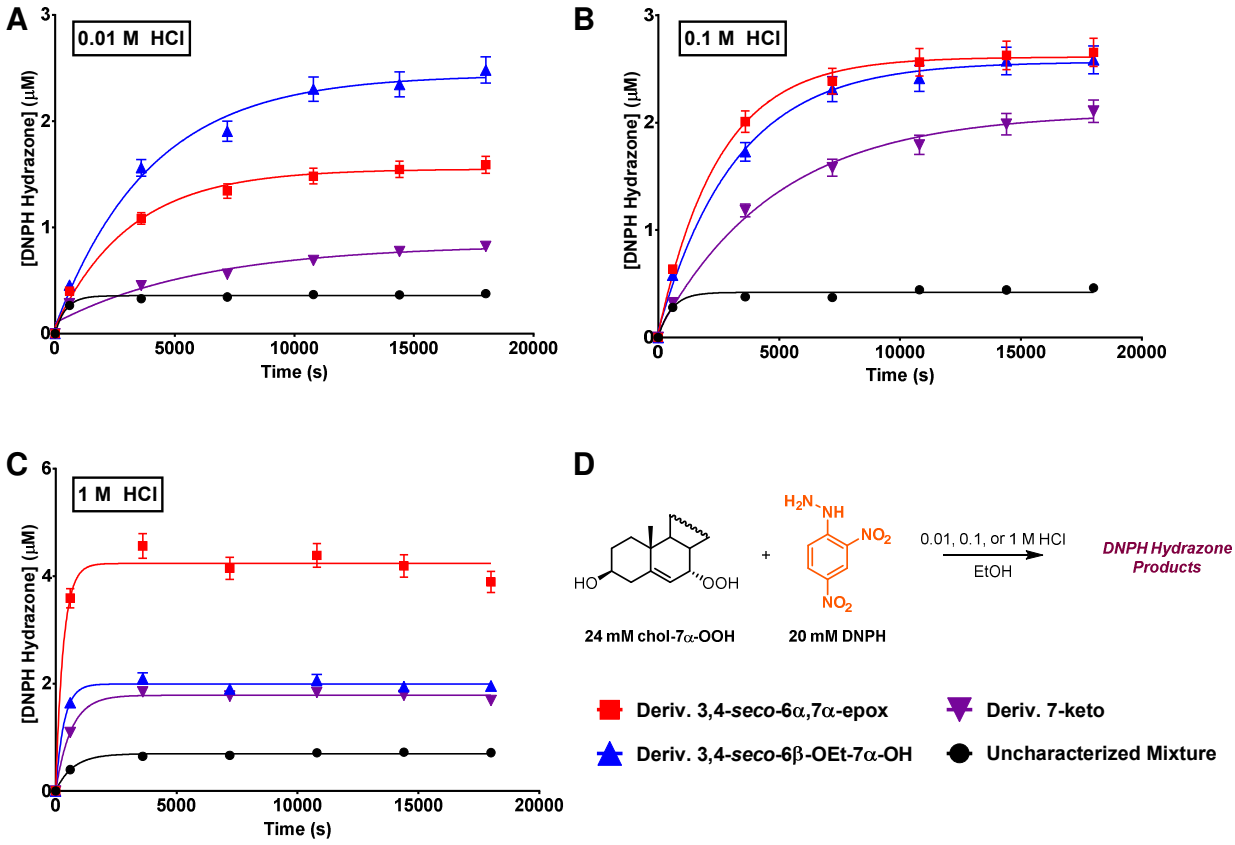

Figure 3.16 HPLC/UV-Vis monitoring of the evolution of DNPH hydrazone products resulting from subjection of cholesterol-7α-OOH to DNPH derivatization conditions at 0.01 (**A**), 0.1 (**B**), and 1 M HCl (**C**). Product evolution of the DNPH hydrazones of 3,4-*seco*-6α,7α-epox (■), 3,4-*seco*-6β-OEt-7α-OH (▲), 7-keto (▼), and the uncharacterized mixture (**1** from Figure 3.13; ●) were quantified by UV-Vis detection at 360 nm relative to the DNPH hydrazone of testosterone as an internal standard (**D**). 5 μL of each sample in ethanol was injected onto a 4.6 × 150 mm Atlantis C18 reverse-phase HPLC column and separated with 75:20:5 ACN:MeOH:H_2O at a flow rate of 1 mL/min.

Interestingly, the rate of the reaction appears to be dependent on the [HCl], analogous to the reactions performed in the absence of DNPH. Additionally, we observed a trend in product distribution that was perhaps counter-intuitive; as we increased the concentration of acid, more deriv. 3,4-*seco*-6α,7α-epox appeared to evolve relative to deriv. 3,4-*seco*-6β-OEt-7α-OH. As the ethoxy product was presumed to form as a result of epoxide opening or exchange of the hydroxy group of the open-epoxide diol compound, combined with the acidic stability of the epoxide

species at such high concentration of acid, we were puzzled by this observation. Interestingly, the product ratio of deriv. 3,4-*seco*-6α,7α-epox to deriv. 3,4-*seco*-6β-OEt-7α-OH compound is near 1:1 in 0.1 M HCl - the same acid concentration utilized for the classic DNPH derivatization conditions. It is also clear that the uncharacterized mixture (**1** from **Figure 3.13**) does not contribute to a large portion of the overall product distribution under any of the acid concentrations assessed.

3.2.6 Deconvolution of the DNPH Hydrazones Resulting from Derivatization of Sterol Extracts: Products of Cholesterol-7α-Hydroperoxide Hock Fragmentation or Otherwise?

Given that the hydrazone product profile arising from subjection of chol-7α-OOH to standard DNPH derivatization conditions is similar to that obtained from derivatization of cholesterol ozonolysis mixtures, we sought to determine whether secA and secB may have been erroneously identified in tissue extracts, and consequently, ozone erroneously implicated in the formation of secA and secB. In order to improve sensitivity, such that products could be determined from lipid extracts of liposomal membranes, cells and/or tissues, we carried out analyses by LC/MS.

In consideration of this, we sought to evaluate the DNPH hydrazones afforded from subjecting chol-7α-OOH to typical DNPH derivatization conditions as aforementioned and evaluate the products by ESI-MS. As illustrated in **Figure 3.17A**, the total ion chromatogram (TIC) presents a much more diverse product distribution than what had been observed simply using UV detection alone; this was not surprising considering that non-derivatized products would not absorb at this 360 nm, reflecting the aforementioned diverse product distribution afforded from chol-7α-OOH Hock fragmentation in the absence of DNPH.

As shown in **Figure 3.17A**, we highlighted specific points of interest in the TIC for closer observation of the mass scan based upon the points of highest intensity absorbance in the UV chromatogram or the points of highest intensity in the TIC. Analysis of these mass scans, shown in **Figure 3.17B**, appeared to support what we had predicted based upon characterization of the material obtained from preparative HPLC separation of the products. Peaks **C** (19.2 min), **E** (20.4 min), and **G** (31.5 min) picked for their high intensity in the UV absorbance chromatogram exhibit their expected $[M-H]^-$ ions corresponding to derivatized 3,4-*seco*-6α,7α-epoxide (*m/z* = 579), 3,4-*seco*-6β-OEt-7α-OH (*m/z* = 625), and 7-ketocholesterol (*m/z* = 579), respectively. Interestingly, although we were unable to characterize the mixture eluting at 12.3 minutes (peak **1** in **Figure 3.13**), thr corresponding MS scan predominantly exhibits signal for *m/z* = 597; this is notably similar to both the retention time and *m/*z observed for aforementioned derivatized secA. Peaks picked due to their high intensity in the TIC (**B**, **D**, and **F**) exhibit very similar spectroscopic characteristics to their neighbouring picked peaks; however, it is of interest to note the observation of signal for *m/z* = 597 (albeit low intensity) at 19.7 minutes (**D**) at the same retention time as authentic derivatized 3,4-*seco*-6β,7α-diol and derivatized secB have been observed.

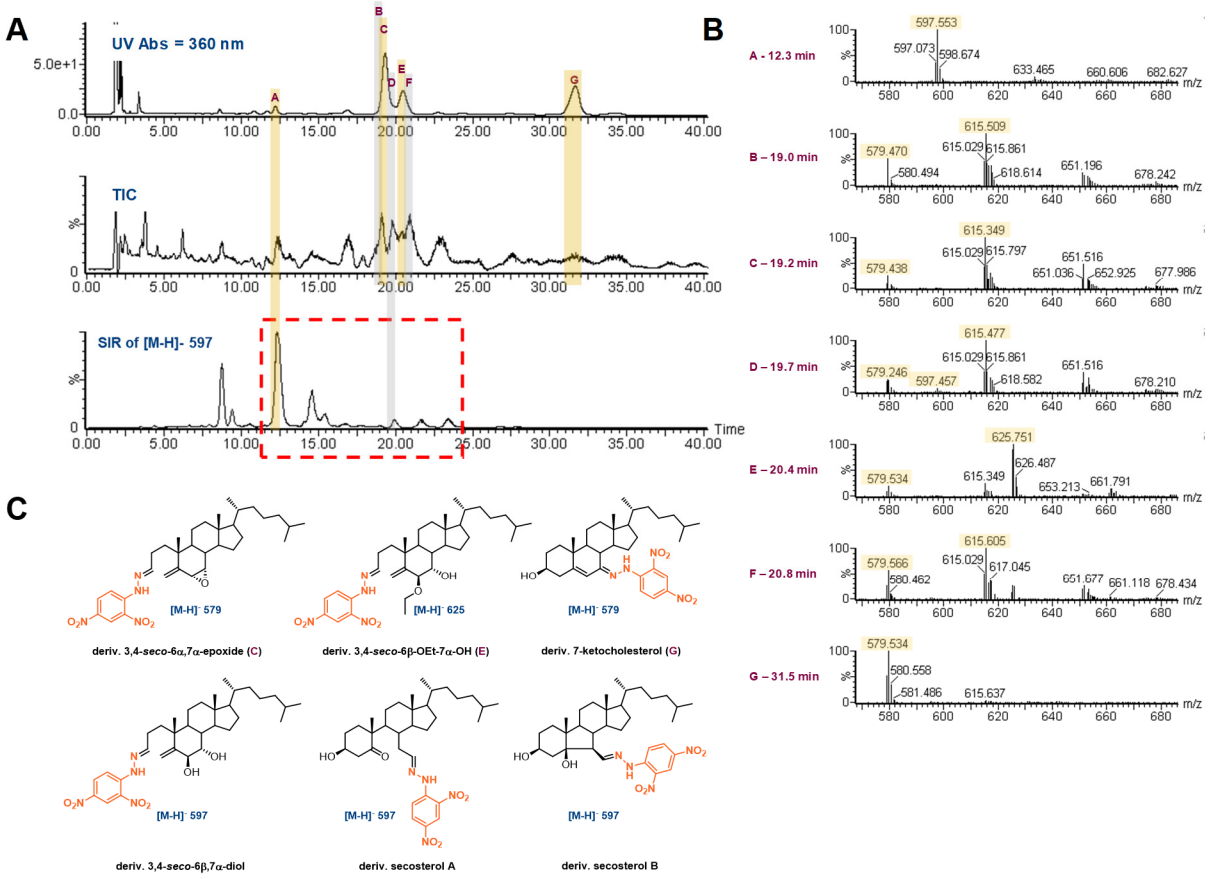

Figure 3.17 Comparison of representative chromatograms used to monitor UV absorbance at 360 nm and the total ion chromatogram scan for the same sample (**A**) relative to the mass ions of interest (**B**) compounds most likely to represent these mass ions (**C**) based upon our previous characterizations. 5 µL of a mixture of chol-7α-OOH subjected to DNPH derivatization conditions in ethanol was injected onto a 4.6 × 150 mm Atlantis C18 reverse-phase HPLC column with a flow rate of 1 mL/min of 75:20:5 ACN:MeOH:H_2O.

It is important to recognize the significant lack of signal for *m/z* = 597 in the mass ion scans obtained for compounds eluting around 20 minutes and the dominance of signal for *m/z* = 615. Although this mass ion is not consistent with any of the expected structures presented in **Figure 3.17C**, it is possible that this signal is representative of the hydrated hydrazone species, however, we were unable to find examples in the literature that provide evidence for similar species.

To support the mass scans obtained from the TIC of the LC/MS separation of products, we used direct infusion ESI-MS to obtain mass spectra of the authentic DNPH hydrazones of each

compound synthesized independently or isolated preparatively. As shown in **Figure 3.18**, direct infusion of derivatized secA and B afforded the expected $[M-H]^-$ for *m/z* 597 and this same signal is observed for direct infusion of the uncharacterized mixture (**1** from **Figure 3.13**) derived from chol-7α-OOH Hock fragmentation that elutes with the same retention time as derivatized secA. Interestingly, authentic derivatized 3,4-*seco*-6α,7α-epoxide and 3,4-*seco*-6β-OEt-7α-OH exhibit their expected *m/z* of 579 and 625, respectively, but also exhibit a signal for *m/z* 597, as shown in **Figure 3.18**. This is not surprising considering the ^{1}H NMR spectra for authentic derivatized 3,4-*seco*-6α,7α-epoxide indicated that some derivatized 3,4-*seco*-6β,7α-diol had co-eluted upon preparative separation from a chol-7α-OOH DNPH-Hock mixture, previously shown in **Figure 3.14**. Additionally, derivatized 3,4-*seco*-6β,7α-diol appears to undergo exchange with alcoholic solvent to afford the analogous derivatized 3,4-*seco*-6β-OEt-7α-OH in ethanol, previously shown in **Figure 3.15.** Since the anticipated $[M-H]^-$ of derivatized 3,4-*seco*-6β,7α-diol would correspond to *m/z* 597, this DNPH hydrazone appeared to be the most likely explanation for the apparent signal**.** Unexpectedly, direct infusion of authentic derivatized 3,4-*seco*-6β,7α-diol, material prepared from DNPH derivatization of authentic 3,4-*seco*-6β,7α-diol followed by purification and characterization (^{1}H NMR shown in **Figure 3.14**), does not exhibit a strong signal for its expected *m/z* of 597, but instead for *m/z* 579 and 615, as shown in **Figure 3.18**, suggesting that both dehydration and hydration of this species takes place in the ion source.

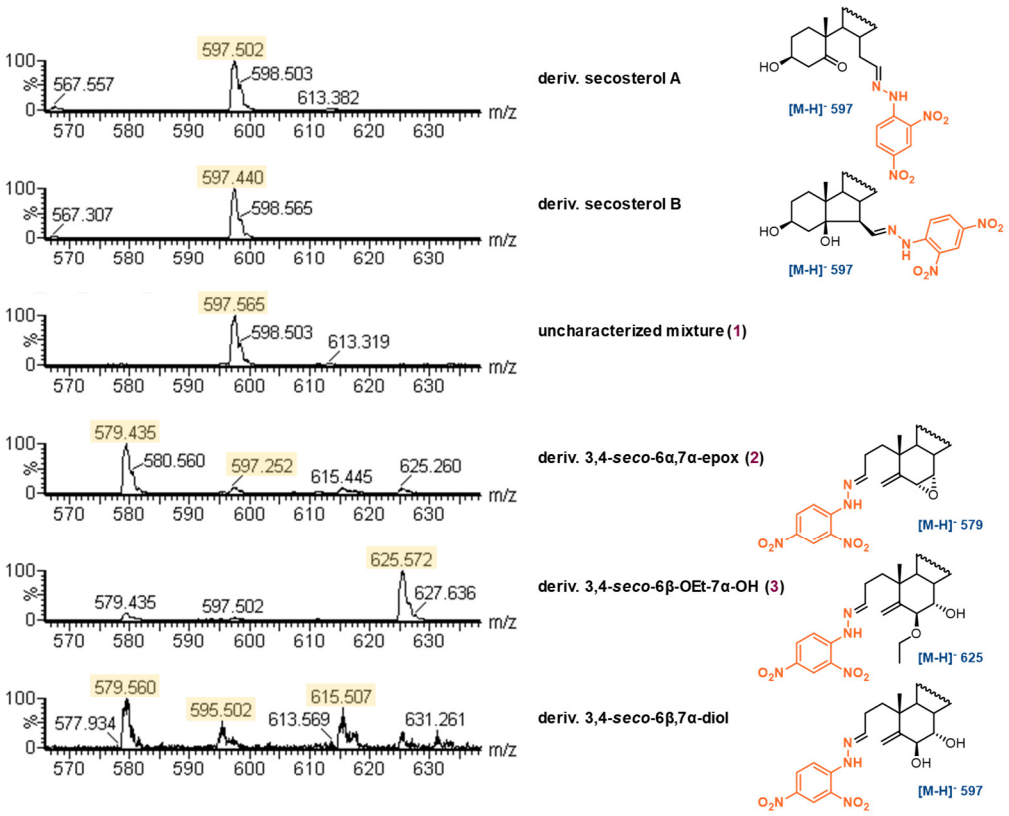

Figure 3.18 Mass spectra obtained upon direct infusion of the authentic DNPH hydrazone species. Samples were dissolved in methanol (5 mM) prior to detection by negative-mode ESI-MS.

We sought to investigate this further upon fortuitous discovery that the *m/z* = 597 signal increases in intensity at the retention time expected for derivatized secB and derivatized 3,4-*seco*-6β,7α-diol upon dilution of a chol-7α-OOH DNPH-Hock mixture. Foregoing experiments have shown that both derivatized secB and the chol-7α-OOH Hock-derived secosterols elute around the same retention time at ~ 20 minutes. To delineate secosterols derived from Hock fragmentation of chol-7α-OOH and cholesterol ozonolysis products, we increased the polarity of the mobile phase (from 75:20:5 to 75:15:10 ACN:MeOH:H_2O) to enable separation of the products. Interestingly, this did permit the separation of derivatized secB (new RT = 46 minutes) from 3,4-*seco*-6α,7α-epox and 3,4-*seco*-6β-OEt-7α-OH (new RT = ~ 53 minutes). Considering that derivatized secB is

not observed as a product of chol-7α-OOH Hock fragmentation under DNPH derivatization conditions (*vide supra*), the observed increase in intensity for the product of chol-7α-OOH DNPH-Hock fragmentation eluting at 46 minutes is expected to be the derivatized 3,4-*seco*-6β,7α-diol, and the increase in intensity upon dilution is possibly due to the aforementioned hydration that is causing ion suppression for this signal at higher concentrations, as shown in **Figure 3.19**. Interestingly, while co-injection of derivatized secB with this diluted chol-7α-OOH DNPH-Hock mixture expectedly increases the signal at this retention time, co-injection of derivatized 3,4-*seco*-6α,7α-epoxide or 3,4-*seco*-6β-OEt-7α-OH, compounds expected to contain some of the 3,4-*seco*-6β,7α-diol or have the capacity to form that compound, suppress the signal, as also shown in **Figure 3.19**.

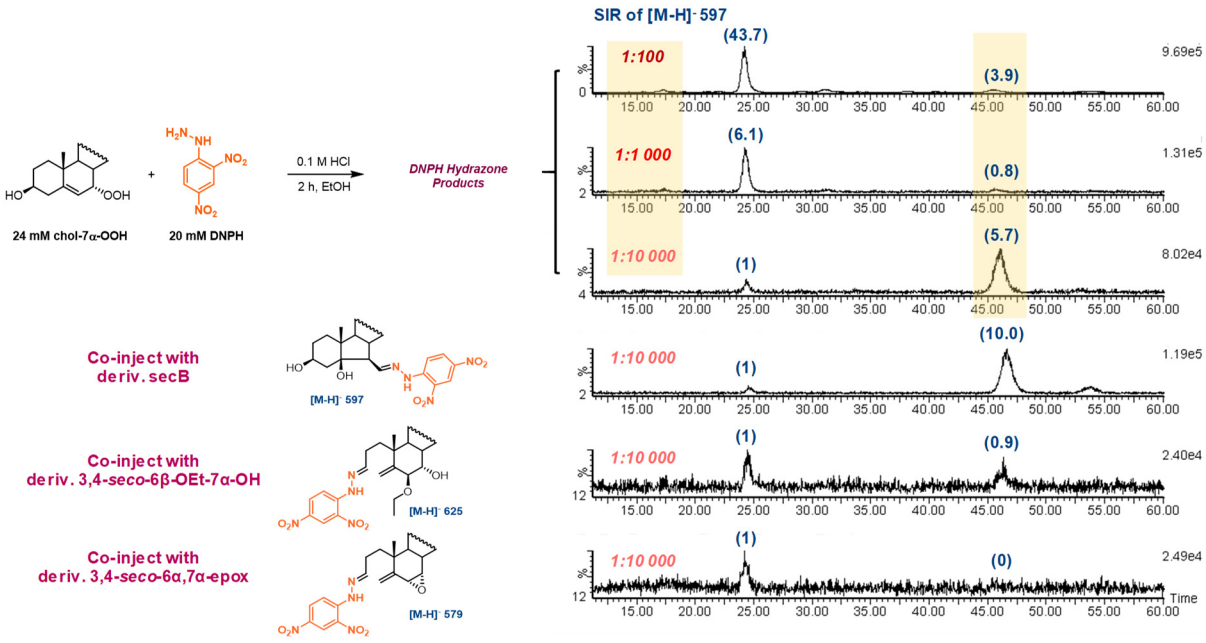

Figure 3.19 Effect of diluting the mixture resulting from subjecting chol-7α-OOH to DNPH derivatization conditions monitored by SIR of $[M-H]^-$ 597. Co-injections of authentic sample DNPH hydrazones are shown with the Hock mixture diluted 1:10 000 times relative to the initial concentration. 5 µL of each sample was injected onto a 4.6 × 150 mm Atlantis C18 reverse-phase HPLC column with a flow rate of 1 mL/min of 75:15:10 ACN:MeOH:H_2O. Relative intensities of the SIR *m/z* 597 signal are shown above the corresponding peak in blue for reference to the consistent intensity of the peak for the uncharacterized mixture (**1** from Figure 3.13) at 24 minutes.

3.2.7 The Biological Relevance (If Any) of Secosterols and Other Electrophilic Oxysterols

With the chromatographic and spectroscopic characteristics determined for chol-7α-OOH Hock fragmentation products, we sought to evaluate the product profile upon DNPH derivatization of sterol extracts obtained from various physiologically relevant sources. Initially, we investigated DNPH derivatization of products afforded from cholesterol autoxidation in a lipid bilayer analogous to the experiments we had previously described in Chapter 2. With a known predominance of chol-7α- and β-OOH, we expected that we would likely observe similar product distribution to the those experiments we had performed on neat chol-7α-OOH, but at a concentration more representative of that obtained upon sterol extraction from a biological source. Autoxidations of cholesterol were performed incorporated in egg-PC liposomes as previously described and the resulting sterol extract was subjected to typical DNPH derivatization conditions; the results are shown in Figure 3.20.

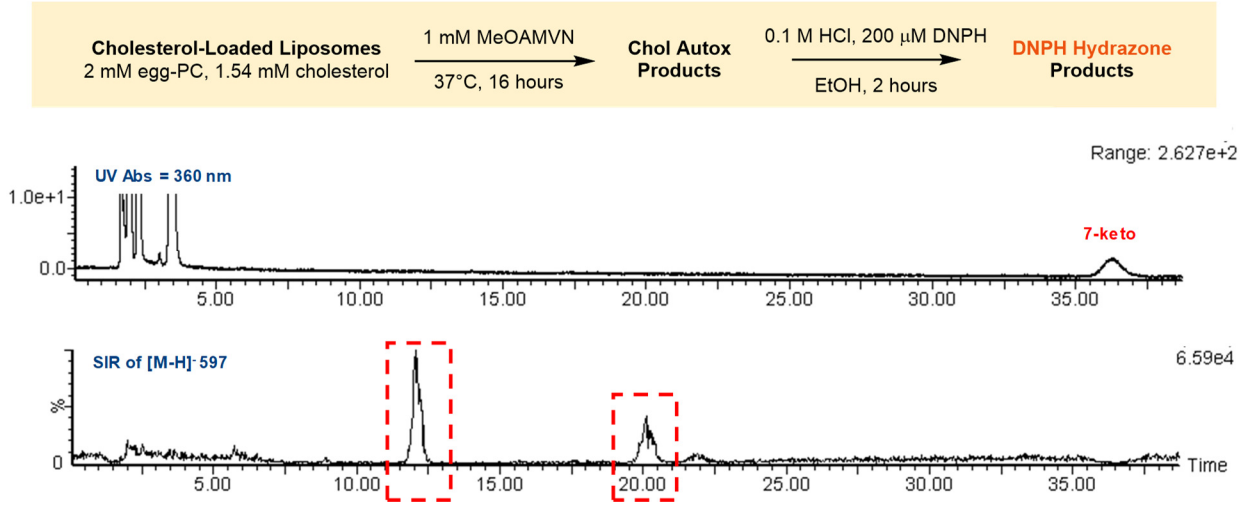

Figure 3.20 DNPH derivatization of cholesterol autoxidation products extracted from egg-PC liposomes. Autoxidations were initiated with 1 mM MeOAMVN at 37°C in the presence of atmospheric O_2 for 16 hours. Upon completion, samples are quenched and reduced to their corresponding alcohols and are extracted using a modified Bligh-Dyer method. Following extraction, the sterol residue was derivatized using DNPH (200 μM) under acidic conditions (0.1 M HCl) in ethanol for 2 hours. 5 μL of the resulting mixture was injected onto a 4.6 × 150 mm

Atlantis C18 reverse-phase HPLC column with a flow rate of 1 mL/min of 75:20:5 ACN:MeOH:H_2O. Representative chromatograms for UV absorbance at 360 nm and negative-mode ESI-MS SIR of $[M-H]^-$ 597 are illustrated.

LDL was oxidized under similar conditions to those used for our aforementioned cholesterol-loaded liposome experiments using the azo-initiator MeOAMVN. The oxidation products were then extracted following the same protocol utilized for sterol extraction from liposomes and subsequently derivatized under typical DNPH derivatization conditions. Upon analysis of the products, we observe three predominant peaks by UV absorbance, one of which corresponds to derivatized 7-keto, and two signals in the SIR of *m/z* 597 at 12.5 and 20 minutes, as shown in **Figure 3.21**, near identical to the chromatographic profile observed upon derivatization of extracted cholesterol autoxidation products in **Figure 3.20**.

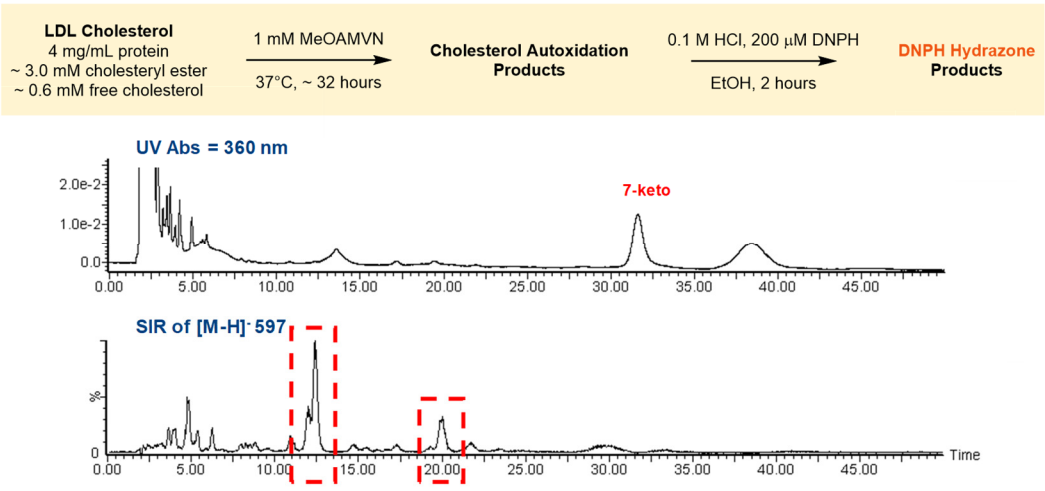

Figure 3.21 DNPH derivatization of sterol extracts obtained from oxidized LDL cholesterol. Oxidation of LDL (4 mg/ml protein in PBS) is initiated with the azo-initiator MeOAMVN (1 mM) at 37°C for 32 hours. Autoxidation products were extracted and the resulting residue was derivatized using DNPH (200 µM) under acidic conditions (0.1 M HCl) in ethanol for 2 hours. 5 µL of the resulting mixture was injected onto a 4.6 × 150 mm Atlantis C18 reverse-phase HPLC column with a flow rate of 1 mL/min of 75:20:5 ACN:MeOH:H_2O. Representative chromatograms for UV absorbance at 360 nm and negative-mode ESI-MS SIR of $[M-H]^-$ 597 are illustrated.

Analogous experiments were conducted using mammalian cells with the intention of using a model in which free cholesterol is more predominant that its esterified form. Similar to our

experiments attempting to assess product distribution of cholesterol autoxidation products (see Chapter 2), we utilized a covalent GPX4 inhibitor, (1*S*,3*R*)-RSL3, to promote accumulation of cholesterol hydroperoxide species through inhibition of their reduction to cholesterol alcohols. Additionally, HEK 293 cells were supplemented with exogenous cholesterol for several hours prior to induction of ferroptosis to enhance the potential for sufficient extraction of oxidation products for detection. Cells were harvested following 6 hours of incubation with RSL3 at which point cell viability was ~ 20 %. Upon extraction, the mammalian cell sterol extracts were subjected to typical DNPH derivatization conditions and once again signals were detected by SIR for *m/z* 597 at retention times expected for chol-7α-OOH derived secosterols, as shown in **Figure 3.22** (changes in retention time due to use of 75:15:10 ACN:MeOH:H_2O mobile phase). We also observed several other predominant masses in the individual scans obtained from the TIC, however we were unable to make assignments of these masses based upon compounds characterized thus far.

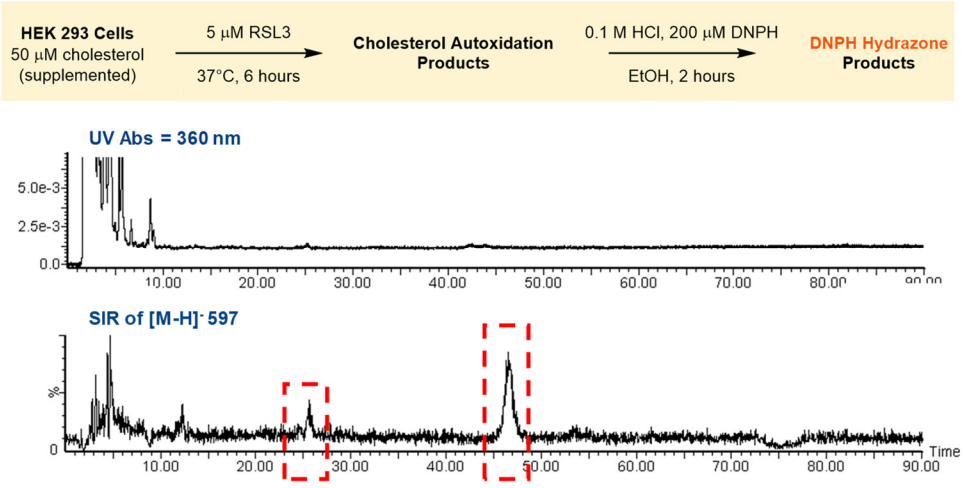

Figure 3.22 DNPH derivatization of sterol extracts from obtained from HEK 293 cells subjected to RSL3-induced ferroptotic cell death. HEK 293 cells were supplemented with exogenous cholesterol (50 μM) and ferroptosis was induced with (1*S*,3*R*)-RSL3 (5 μM) incubated at 37°C for 6 hours. Cells were harvested after 6 hours and the resulting autoxidation products were extracted. Sterol extracts were derivatized using DNPH (200 μM) under acidic conditions (0.1 M HCl) in

ethanol for 2 hours. 5 µL of the resulting mixture was injected onto a 4.6 × 150 mm Atlantis C18 reverse-phase HPLC column with a flow rate of 1 mL/min of 75:15:10 ACN:MeOH:H_2O. Representative chromatograms for UV absorbance at 360 nm and negative-mode ESI-MS SIR *m/z* = 597 are illustrated.

Interestingly, we once again observe apparent ion suppression upon co-injection of derivatized 3,4-*seco*-6β,7α-diol with the derivatized mammalian cell extracts that is not observed upon co-injection with the same concentration of derivatized secB, as shown in **Figure 3.23**. Although it is apparent that this issue of ion suppression occurs with high concentration of the derivatized 3,4-*seco*-6β,7α-diol, further investigation is required to fully understand to optimal conditions for clear delineation of derivatized secB and the secosterols derived from chol-7α-OOH DNPH Hock fragmentation – namely derivatized 3,4-*seco*-6β,7α-diol.

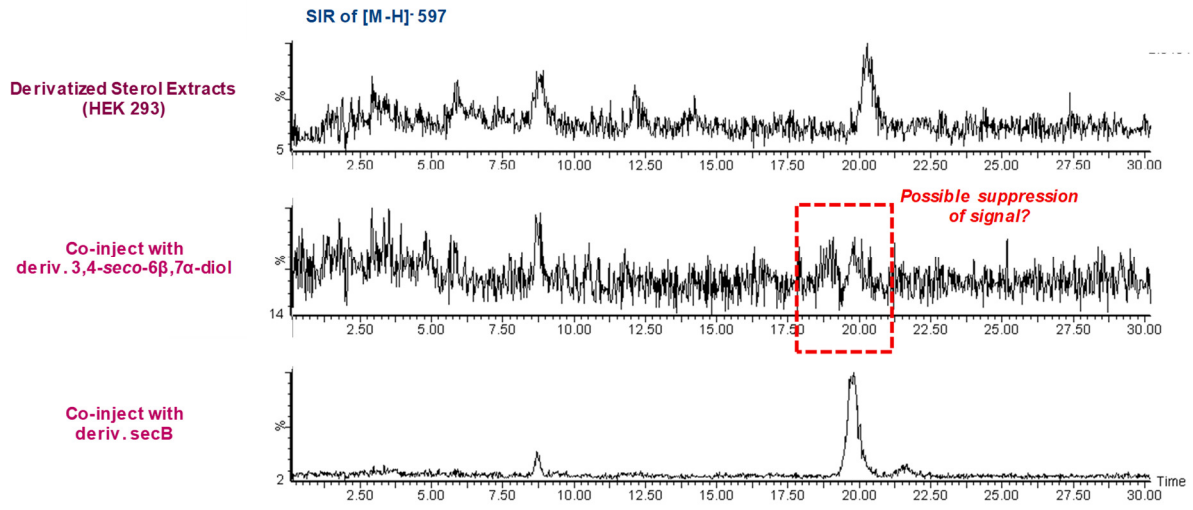

Figure 3.23 Co-injections of derivatized 3,4-*seco*-6β,7α-diol and derivatized secB (2.5 mM) with the DNPH hydrazone products obtained from HEK 293 cell sterol extracts. 5 µL of each sample was injected onto a 4.6 × 150 mm Atlantis C18 reverse-phase HPLC column with a flow rate of 1 mL/min of 75:20:5 ACN:MeOH:H_2O. Representative chromatograms for SIR at *m/z* = 597 are illustrated.

We also sought to investigate the potential toxicity of the underivatized secosterol species relative to other known oxysterol compounds in the event these compounds are generated through

Hock fragmentation *in vivo*. Thus, we assessed the cytotoxicity of 3,4-*seco*-6β,7α-diol and 5β-OH-epoxide in Pfa1 MEFs and compared them to other oxysterol compounds, including sec A and B, as shown in **Figure 3.24**.

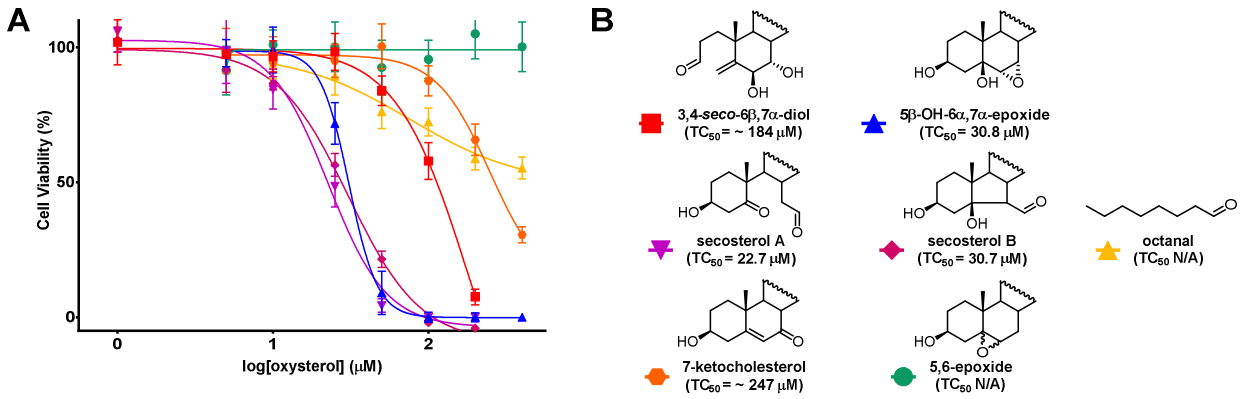

Figure 3.24 Cytotoxicity of electrophilic compounds of interest in Pfa1 MEFs. Compounds evaluated included 3,4-*seco*-6β,7α-diol (■), 5β-OH epoxide (▲), secA (▼), secB (◆), 7-keto (⬣), 5,6-epoxide (●), and octanal (▲). Cytotoxicity was assessed after 5 hours by AquaBluer assay.

Interestingly, the 3,4-*seco*-6β,7α-diol and 5β-OH-epoxide both exhibited enhanced toxicity relative to oxysterol compounds of similar nature (i.e. 5,6-epoxycholesterol and 7-keto), and exhibit similar toxicity to that of secA and B particularly for the 5β-OH-epoxide. Compounds exhibiting aldehydic moieties were compared to the cytotoxicity of a simple aldehyde, octanal, to assess the reactivity of a less sterically-encumbered and highly labile electrophile in culture medium.

3.3 Discussion

Initially, our mechanistic hypothesis for Hock fragmentation of cholesterol 7-hydroperoxide followed the traditional mechanism in which upon protonation of the hydroperoxide species, B-

ring expansion occurs to form an O-vinyl oxocarbenium intermediate which could be immediately trapped with water and subsequently collapse to afford a dialdehyde secosterol species, however, initial investigations performed in participating alcoholic solvent afford 6,7-epoxycholesterol species as the major product, suggesting formation of an α-epoxy carbenium ion instead.[29] Mechanistic investigations we have since carried out in non-participating solvent support formation of an α-epoxy carbenium ion based upon the evolution of both 5α/β-OH-6α,7α-epoxycholesterol and a novel aldehydic product, 3,4-*seco*-6β,7α-diol. Identification of 3,4-*seco*-6β,7α-diol is, to our knowledge, the first report of A-ring cleavage of the sterol scaffold of cholesterol that may possibly be formed under physiological conditions; naturally-occurring A-ring cleavage products have never been observed and have only been synthesized or proposed as a result of harsh MS fragmentation or oxidation conditions.[35–37] 3,4-*seco*-6β,7α-diol is an extremely interesting compound as it contains a potent electrophilic aldehyde moiety. Our proposed mechanism also serves as the most direct evidence to date of an α-epoxy carbenium intermediate in Hock fragmentation.

Scheme 3.5 Revised mechanism for acid-promoted Hock fragmentation of cholesterol 7α-hydroperoxide in non-participating solvent or potentially physiological conditions.

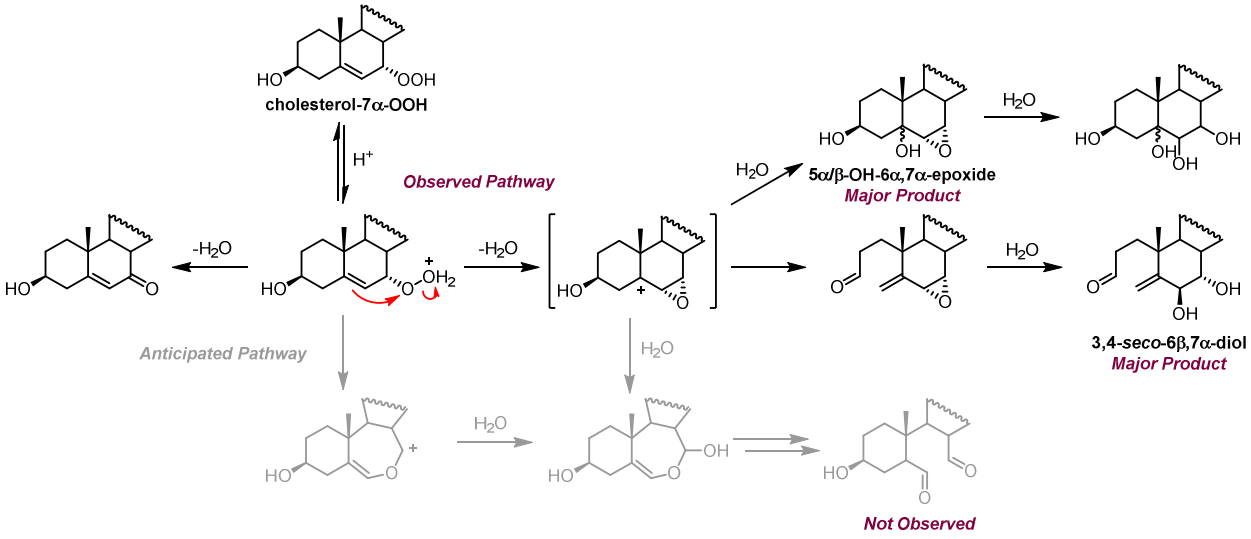

Interestingly, a similar α-epoxy carbenium intermediate has been proposed in the acid-catalyzed decomposition of a linoleate-derived hydroperoxide upon observation of an α-epoxy hydroxyl product, however, further cleavage to afford hexanal was below the detection limit of their assay.[10] When compared directly to the α-epoxy carbenium ion generated from chol-7α-OOH Hock fragmentation, the resonance-stabilized allylic cation formed during linoleate-derived hydroperoxide cleavage and absence of a nearby hydroxyl group make it difficult to facilitate cleavage to afford aldehydic products, and so quenching of the allylic carbocation cation by water is favoured. The tertiary α-epoxy carbenium ion generated from chol-7α-OOH Hock cleavage is stabilized by hyperconjugation, but is also flanked by the 3β-OH which is primed to facilitate A-ring cleavage to quench the carbocation; in an H-bonding medium, such as the phospholipid membrane, H-bonding of the 3β-OH is likely to facilitate cleavage of the A-ring.

Scheme 3.6 Comparison of α-epoxy carbenium intermediate formation between acid-promoted cleavage of linoleate-derived hydroperoxide and cholesterol 7α-hydroperoxide.

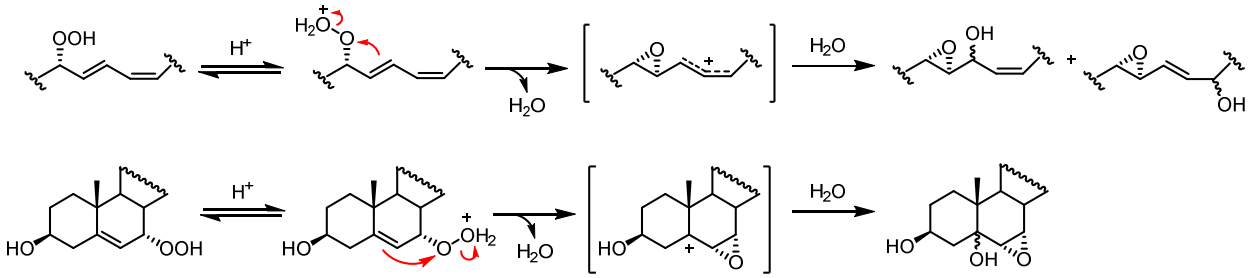

Interestingly, Hock fragmentation of cholesteryl-7α-OOH acetate does not yield significant amounts of the 3,4-*seco*-6β,7α-diol product, as shown in **Figure 3.11**, supporting the hypothesis that H-bonding of the 3β-OH is required to facilitate A-ring cleavage.

We believe it is likely that all products formed from chol-7α-OOH Hock fragmentation funnel exclusively through this α-epoxy oxocarbenium intermediate. None of the products characterized from the resultant Hock mixture exhibited character of the O-vinyl oxocarbenium

intermediate expected to arise upon migration of the sp^2 carbon as is generally invoked in the Hock fragmentation mechanism. Although oxocarbeniums are generally more stable than tertiary carbocations, epoxide formation requires less reorganization, which is particularly important for a rigid system, and is therefore favoured kinetically.

Although we were unable to account for all of the products using ^{1}H NMR as our method of detection due to convolution of the spectrum, we were able to decisively account for approximately half of the products generated, and can confidently speculate about the identity of the remaining products. Remarkably, the most interesting and potentially deleterious product, 3,4-*seco*-6β,7α-diol, was found consistently as the major product in all non-participating solvents assayed, typically composing ~ 30 mol % of the total products formed. The remaining mass balance definitively characterized consisted of ~ 6 mol % 5β-OH epoxide and ~ 4 mol % 5α-OH epoxide; the 5β-OH epoxide is presumed to dominate due to the steric repulsion experienced between 5α-OH and 6α,7α-epoxide, disfavouring this isomer.

Scheme 3.7 Comparative structural conformations of 5β- and 5α-OH-6α,7α-epoxide.

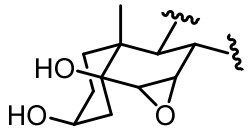

5β-OH-6α,7α-epoxide (6 mol %)

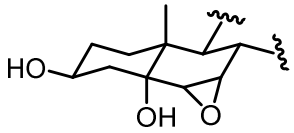

5α-OH-6α,7α-epoxide (4 mol %)

The remaining mass balance appears to consist of unresolvable polyhydroxy products resulting from hydrolysis of the 6α,7α-epoxide; this was supported by the appearance of peaks in the 3.0-4.5 ppm region of the ^{1}H NMR spectra upon subjection of the authentic 5β-OH-epoxide to the same acidic conditions used in our original analysis (0.1 M HCl). We expected that some of the mass balance may also be accounted for by hemiacetal products of hydrolysis of the aldehydic

moiety of the 3,4-*seco*-6β,7α-diol, however, we were unable to identify the corresponding hemi-acetal in non-participating solvent. However, we were able to identify the dimethoxy acetal products afforded when the reaction if performed in methanol, suggesting that this likely occurs in non-participating solvent as well.

Interestingly, we fortuitously identified the 3,4-*seco*-6α,7α-epoxide upon incubation of the 3,4-*seco*-6β,7α-diol in silica which presumably served as a desiccant to promote epoxide formation. Although we had suspected that we must generate the 3,4-*seco*-6α,7α-epoxide as a precursor to 3,4-*seco*-6β,7α-diol, we had not isolated this species from our preparative Hock fragmentation mixtures. However, it is likely that the 6,7-epoxide is hydrolyzed so rapidly to the diol that the existence of this product is fleeting. This does speak to the inherent electrophilicity of the products generated from the α-epoxy oxocarbenium ion, particularly their lability upon initial generation; the electrophilic intermediates generated are positioned such that they are available to react extremely rapidly with the closest nucleophilic source within a phospholipid bilayer, whether that be water or a protein-based nucleophile to facilitate covalent modification. Considering the neighbouring electron-withdrawing exomethylene moiety to the 6α,7α-epoxide of this structure, it is easy to understand why the existence of this epoxide moiety is relatively fleeting. Additionally, Michael-type addition at the exomethylene of the α/β-unsaturated epoxide moiety may serve to increase the lability of this compound. Quenching of the α-epoxy carbenium ion itself upon generation *in situ* would also likely be rapid with nearby amines or thiols, additionally leading to covalent modification of a nearby protein.

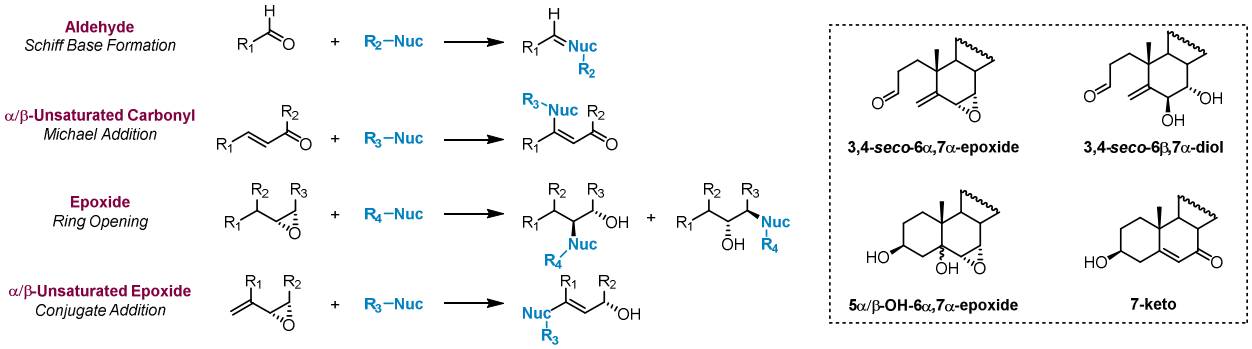

Figure 3.25 Proposed reactivity of potent electrophiles generated via Hock fragmentation of cholesterol-7α-OOH with biological nucleophiles.

Toxicity of reactive intermediates afforded from chol-7α-OOH Hock fragmentation are relatively difficult to definitively assess, however, the relative rates of formation and nature of the compounds detected speak to their potency upon generation *in situ*, as suggested in **Figure 3.25**. This may also serve to explain the unexpected results observed in our cytotoxicity assays relative to the expected electrophilicity of the compounds assayed. The intact epoxide species, 5β-OH epoxide, exhibits toxicity within the same range as secA and B at TC_{50} = ~ 30 μM whilst the 3,4-*seco*-6β,7α-diol exhibits a TC_{50} = ~ 180 μM. We were initially surprised by this result based upon the potential electrophilicity of the highly accessible aldehyde, however, it is likely that it reacts directly with components of the culture medium to lower its apparent toxicity. The low cytotoxicity of octanal, a similarly accessible aldehydic moiety, is indicative of this presumption. Nevertheless, it is likely that *in situ* generation of the 3,4-*seco*-6α,7α-epoxide would result in a more potent effect rather than its hydrolyzed diol analogue. It is interesting to contrast the reactivity of the 6,7-epoxide species to the reports of non-reactivity of the 5,6-epoxycholesterol with biological nucleophiles under normal S_N2 conditions;[38] 5,6-epoxycholesterol exhibits relatively hindered and electron poor epoxide with 3° and 2° substitution at the C5 and C6 positions, respectively. Additionally, this is also supported by the lack of toxicity of the 5,6-epoxycholesterol in our assay.

When comparing the foregoing toxicity values of the secondary autoxidation products to the TC_{50} value of 7.8 μM for their parent primary hydroperoxide, chol-7α-OOH (reported in Chapter 2, performed under same conditions in Pfa1 cells), aforementioned *in situ* generation of reactive intermediates such as the α-epoxy carbenium ion or the 3,4-*seco*-6α,7α-epoxide and immediate adduction of biological nucleophiles serve as an explanation for the markedly high toxicity of the hydroperoxide product. Considering the putative fates of cholesterol hydroperoxide species, or of any lipid hydroperoxide species for that matter, it is interesting to observe such potent cytotoxicity for the parent hydroperoxide compound. Hydroperoxides are either detoxified to their relatively non-toxic corresponding alcohols by GPX4, undergo Fe^{2+}-reduction to alkoxyl radicals via Fenton chemistry that contribute to propagation of the free-radical chain reaction, undergo dehydration to their corresponding ketones, or undergo acid-promoted Hock fragmentation to generate potent electrophilic species. Of these pathways, only Hock fragmentation appears to suggest a source of electrophilic species that could induce such severe toxicity upon treatment of cells with chol-7α-OOH. Interestingly, products resulting from Fe^{2+}-catalyzed reduction of cholesterol hydroperoxides to alkoxyl radicals and their subsequent decomposition has yet to be explored, aside from the amplification of propagation upon generation of the alkoxyl radical. One could propose decomposition of the alkoxyl radical to form two electrophilic products of interest: 5α/β-OH-epoxide via 3-*exo* radical cyclization, similar to that previously suggested for 4-HNE formation the Fe^{2+}-catalyzed reduction of linoleate-derived hydroperoxides,[11,39] or even secB via 5-*endo* radical cyclization. Our attempts to investigate the decomposition products of this reaction have yet to be explored, however, it is possible that these products also contribute to the apparent toxicity of cholesterol 7α-hydroperoxide.

Scheme 3.8 Proposed decomposition pathway of a cholesterol-7α-OOH derived alkoxyl radical generated upon one-electron reduction by Fe^{2+}.

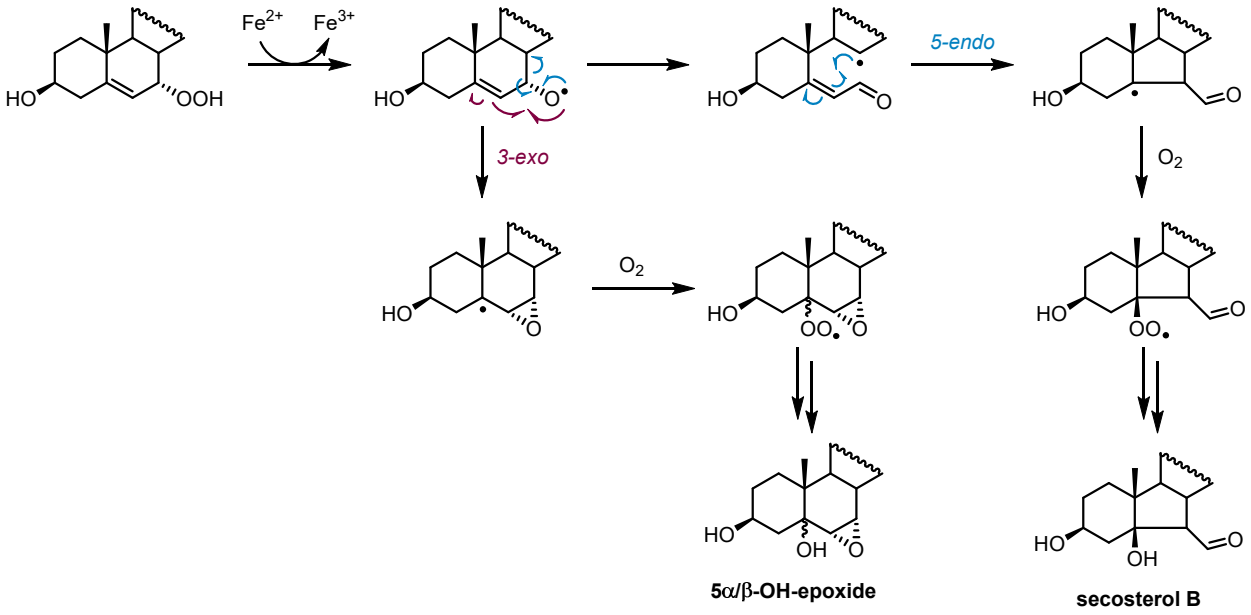

Upon characterization of the products generated upon acid-promoted Hock fragmentation cholesterol-7α-OOH, we sought to determine if these species were formed under physiological conditions, and if they may provide an alternative explanation for the extracted ozone-derived secosterol species identified in disease arterial plaque.[13] We hypothesized that cholesterol autoxidation and subsequent acid-promoted Hock cleavage of the most predominant product, cholesterol 7-hydroperoxide, may serve as the source of the secosterol products extracted was predicated on the similarity in chromatographic and spectroscopic characteristics (i.e. retention time and mass ionization) for the resulting DNPH hydrazones upon analysis by HPLC/ESI-MS. Remarkably, we observed a mixture of four predominant products for which two peaks exhibited near-identical retention times to those observed for authentic standards of the species previously identified in plaque extract - derivatized secA and B. Using a combination of characterization of by negative-mode ESI-MS and ^{1}H NMR, we were able to identify four products of interest and speculate about their probable mechanism of formation, as outlined in **Scheme 3.9**.

Scheme 3.9 Proposed mechanism for cholesterol 7α-hydroperoxide Hock fragmentation under acidic DNPH derivatization conditions based upon isolation and characterization of resulting products.

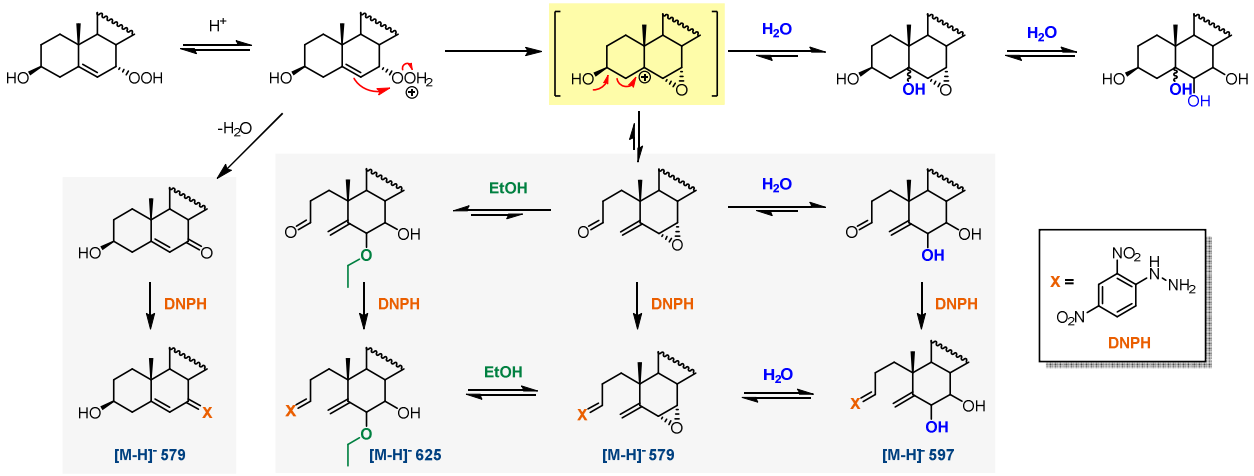

The majority of the products characterized exhibited aldehydic moieties, with the exception of the DNPH hydrazone of 7-ketocholesterol. As expected based upon previous work,[29] we did not observe any DNPH hydrazones derived from the 6,7-epoxide species. This is surprising considering the perceived electrophilicity of the 6,7-epoxide moiety, however, our ^{1}H NMR characterization of the 3,4-*seco*-6β,7α-diol suggests that epoxide hydrolysis occurs at the C6 position based upon the ^{3}J coupling of ~ 3 Hz for the protons at C6 and C7, suggesting that DNPH is too sterically encumbered compared to the small solvent molecules to facilitate epoxide hydrolysis. Hydrolysis at the C6 position by ethanol also appears to occur to generate derivatized 3,4-*seco*-6β-OEt-7α-OH, which we have also shown to form from incubation of 3,4-*seco*-6β,7α-diol in ethanol. An equilibrium appears to exist between these compounds and upon increasing acid concentration, the product distribution is affected; at high concentrations of acid (1 M HCl) the derivatized 3,4-*seco*-6α,7α-epoxide appears to predominate, whilst at low concentrations derivatized 3,4-*seco*-6β-OEt-7α-OH predominates (0.01 M HCl). This result initially seems counter-intuitive as one may expect that high concentrations of acid would promote epoxide

hydrolysis; however, we hypothesize that this increase is likely due to the hydrolysis of the epoxide by water to generate derivatized 3,4-*seco*-6β,7α-diol. This became a point of contention throughout our studies as we never isolated significant amounts of the derivatized 3,4-*seco*-6β,7α-diol upon preparative separation of a Hock mixture and later experienced difficulties observing the compound by ESI-MS. This will be detailed later in the forthcoming discussion.

Co-injection of authentic derivatized secA and B both exhibited co-elution with compounds explicitly derived from chol-7α-OOH Hock fragmentation. Unfortunately, we were unable to characterize the mixture of derivatized compounds preparatively isolated from the Hock mixture at the same retention time as derivatized secA, however, direct comparison of their ^{1}H NMR spectra confirms the absence of peaks corresponding to derivatized secA in this mixture. Remarkably, this uncharacterized mixture (**1** from **Figure 3.13**) exhibits the same SIR of $[M-H]^-$ *m/z* = 597 as observed for derivatized secA. Fortunately, we were able to identify all of the compounds with similar retention time to that of derivatized secB and each compound identified was a 3,4-secosterol analogue. Both the derivatized 3,4-*seco*-6α,7α-epoxide and derivatized 3,4-*seco*-6β-OEt-7α-OH share a near-identical retention time with derivatized secB, however, they do not share the same $[M-H]^-$ signal of *m/z* = 597. It was of great interest to explore the existence of the derivatized 3,4-*seco*-6β,7α-diol in greater detail as the authentic standard appeared to co-elute by HPLC-UVVis and should share the same molecular weight as derivatized secB, however, we were still experiencing issues identifying the derivatized 3,4-*seco*-6β,7α-diol by ESI-MS.

As outlined by dilution of the samples prior to analysis, difficulties observing derivatized 3,4-*seco*-6β,7α-diol appear to be rooted in ionization of the compound at high concentrations in ethanol or the mobile phase used to separate the compounds by HPLC (75:20:5 ACN:MeOH:H_2O). Upon direct infusion of the authentic derivatized 3,4-*seco*-6β,7α-diol and compounds identified to

contain some of the derivatized 3,4-*seco*-6β,7α-diol by ^{1}H NMR, the predominant mass ion observed typically appears to be *m/z* = 615 – a mass ion that can only be explained by solvation of water to form a stable adduct. Additionally, when signal for *m/z* = 597 is observed at low concentration, the signal becomes suppressed upon co-injection of derivatized 3,4-*seco*-6β,7α-diol, however, co-injection of the same amount of derivatized secB appears to exhibit an additive effect; this suggests that the issue resides in high concentrations of the diol product particularly. We hypothesize that dilution of the stock solution prevents formation of water adducts, therefore facilitating detection of the mass ion by SIR of *m/z* = 597, however, the reasoning for this is still unclear. Water adducts by negative-mode ESI-MS are not particularly common and therefore we are tentative in our proposal of this hypothesis, however lack an alternative explanation.

With the necessity of dilute concentrations for the detection of the derivatized 3,4-*seco*-6β,7α-diol in mind, we carried forward our assessment of the compounds extracted from biological sources upon DNPH derivatization. Our efforts began with attempts to replicate our cholesterol autoxidation experiments in liposomes in which cholesterol 7-hydroperoxide isomers are the major products. Remarkably, treatment of these sterol extracts with 0.1 M HCl and 200 μM DNPH appeared to generate two predominant products observed by SIR of *m/z* = 597: one corresponding to the uncharacterized mixture (**1** from **Figure 3.13**) that co-elutes with derivatized secA, and the other derivatized 3,4-*seco*-6β,7α-diol which co-elutes with derivatized secB. It is important to note that we have yet to study the products of cholesterol 7β-OOH Hock fragmentation as that is the other predominant autoxidation product yielded from cholesterol autoxidation, however, it is possible that fragmentation of this hydroperoxide may also product the same products, or those of similar character. Unfortunately, we were unable to investigate these products due to difficulties encountered in obtaining preparative amounts of the material; the only reported method of

synthesizing chol-7β-OOH affords the compound via epimerization of chol-7α-OOH,[30] however, the rate of epimerization is relatively slow and chol-7α-OOH begins to dehydrate under the suggested conditions, affording a mixture of chol-7α-OOH, chol-7α-OH, 7-keto, and a very small amount of chol-7β-OOH. Current investigations in our laboratory are seeking optimization of this synthesis to avoid generation of side products.

Remarkably, sterol extracts obtained from oxidized LDL and HEK 293 cells subjected to ferroptotic cell death conditions also both exhibited evidence for signal by SIR of *m/z* = 597 at similar retention times shared by derivatized secA and B and the products derived from chol-7α-OOH DNPH-Hock fragmentation. In LDL, we subjected the particles to autoxidation using the same conditions utilized for oxidation of cholesterol-loaded liposomes, and in HEK 293 cells we induced ferroptosis through covalent modification of GPX4 to prevent reduction of hydroperoxides to their corresponding alcohols and promote hydroperoxide accumulation – both of these experimental conditions promote cholesterol autoxidation and are not partial to the inflammatory model conditions in which endogenous ozone has been proposed to evolve. This suggests that the products generated and observed are likely those derived from cholesterol 7-hydroperoxide Hock fragmentation *in lieu* of cholesterol ozonolysis by endogenous ozone considering the experimental conditions aforementioned and comparisons to authentic standards of each derivatized species. Although we have provided thorough characterization data and well-documented attempts to troubleshoot our issues with detection of the 3,4-*seco*-6β,7α-diol at high concentrations, it is still difficult to unambiguously distinguish between derivatized secB or 3,4-*seco*-6β,7α-diol. Forthcoming suggestions and descriptions of our current investigations will describe how we intend to ameliorate this issue.

The most important consideration remains, is there potential for Hock fragmentation to occur under the acidic conditions of physiological environments, or do these compounds simply serve as an alternative explanation for ozone-derived secosterols (i.e. they are artefacts of the derivatization procedure used in analysis of biological samples)? As Hock fragmentation currently serves as a mechanistic explanation for the formation of 4-HNE, it is an important fundamental question to address. Considering that under the non-participating reaction conditions utilized for this assay the reaction require at least 0.005 M HCl to afford any product, it is difficult to argue that this reaction would occur *in vivo*. It is important to note that although the non-participating acetone/H_2O system may be reflective of the character of products observed, this system is not "water-like" and may not necessarily reflect the dynamics of *in vivo* acid decomposition. Our group has previously assessed the decomposition of chol-7α-OOH under acid-catalyzed conditions in methanol which is likely to serve as a better system to study this type of reaction.[29] In this case, we observed that Hock fragmentation of chol-7α-OOH is acid-catalyzed, however product evaluation in this system is not reflective of what may be observed *in vivo* due to the participating nature of methanol.

For this reaction to occur under physiological conditions, it is clear that the reaction clearly requires a pH of ~ 4, to evolve electrophilic species in significant amounts. Interestingly, uptake of oxidized LDL by macrophages and subsequent oxidation and decomposition within the acidic environment of a lysosome[40] may be one of the few instances in which cholesterol 7-hydroperoxide would exist in an acidic enough environment to facilitate Hock cleavage; the environment of a lysosome exists at an extremely acidic physiological pH ~ 4.5. It is important to consider, however, the limitation on A-ring cleavage when cholesterol predominantly exists in its esterified form in LDL particles. Illustrated by our foregoing results, subjecting cholesteryl

acetate-7α-OOH to acidic conditions exhibited predominantly 6,7-epoxide products and little evidence for A-ring cleavage. This does not completely eliminate the possibility for the A-ring cleavage to form secosterol products from cholesterol 7-hydroperoxide as free cholesterol does exist within the membrane, and to some extent the core, of LDL particles. In fact, upon acetylation, oxidized LDL transports cholesterol hydroperoxide products in both their free and esterified form to LDL receptors on macrophages for rapid uptake and internalization by endocytosis;[41] free or esterified cholesterol is then delivered to lysosomes within which they are subjected to a relatively acidic environment for hydrolysis of cholesterol esters to free cholesterol by acid lipase; cholesterol hydroperoxides existing as free cholesterol in the lysosome have ample opportunity to undergo Hock fragmentation condition under these conditions. Oxidized free cholesterol then effluxes to the cytoplasm in which it is either exported via high-density lipoproteins (HDL) or is deposited upon re-esterification by acyl-CoA:cholesterol acyltransferase (ACAT).[42]

Scheme 3.10 Macrophage uptake and metabolism of cholesteryl esters via a two-compartment system. Adapted from Brown, Ho, and Goldstein.[42]

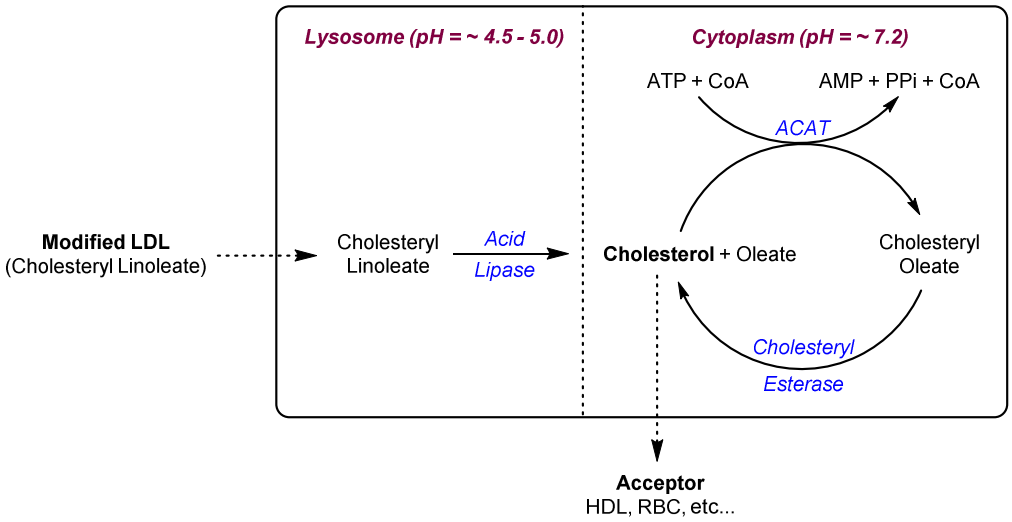

This is the most likely scenario in which cholesterol 7-hydroperoxide would undergo acid-promoted Hock fragmentation and provides several opportunities in which these potent cholesterol-derived electrophiles may encounter protein-based nucleophiles.

Comparisons of cholesterol 7-hydroperoxide-derived 3,4-secosterol and 6,7-epoxide products can naturally be made with the several subsequent studies on the proatherogenicity of the ozone-derived 5,6-secosterols. Currently, the mechanism by which cholesterol oxidation products exacerbate atherosclerosis is poorly understood, particularly pertaining to their involvement in foam cell generation. Although proatherogenic effects have been attributed to treatment with 5,6-secosterols, including foam cell generation, no chemical mechanism has ever been described.[13,14] Uptake of oxidized LDL leading to foam cell formation and ultimate deposition in arterial walls is the expected pathology of macrophages in development of atherosclerotic plaque, however, apart from the oxidation of LDL triggering binding to scavenger receptors, little is known about the mechanism by which lipid-derived electrophiles contribute to the pathogenesis of atherosclerosis. In contrast, the mechanism by which lipid-derived electrophiles, particularly the 5,6-secosterols, are implicated in neurodegenerative diseases is much more intuitive. Following alleged identification of these 5,6-secosterols in brain tissue,[15] these electrophiles are proposed to covalently modify protein-based nucleophiles through Schiff-base formation, triggering protein aggregation and misfolding.[15,36,43] It is likely that covalent modification of protein-based nucleophiles central to the potential role of any cholesterol-derived electrophile in foam cell formation, however, it is currently unclear.

Interestingly, almost all of the work performed to implicate 5,6-secosterol species in the pathogenesis of disease could, in principle, be performed analogously for any of the cholesterol 7-hydroperoxide-derived electrophiles we have identified, however, importance lies in their

unambiguous identification upon extraction from biological sources. We intend to develop conditions for the separation and ionization of these compounds in the absence of derivatization such that consequential products are not characterized fortuitously. Thus far, we have successfully shown that both the 3,4-*seco*-6β,7α-diol and secB ionize efficiently using the same APCI$^+$-MS conditions utilized for the analysis of the corresponding alcohols of the cholesterol hydroperoxides (see Chapter 2). Investigations are currently underway to develop conditions which will enable separation of these secosterol species by normal-phase chromatography.

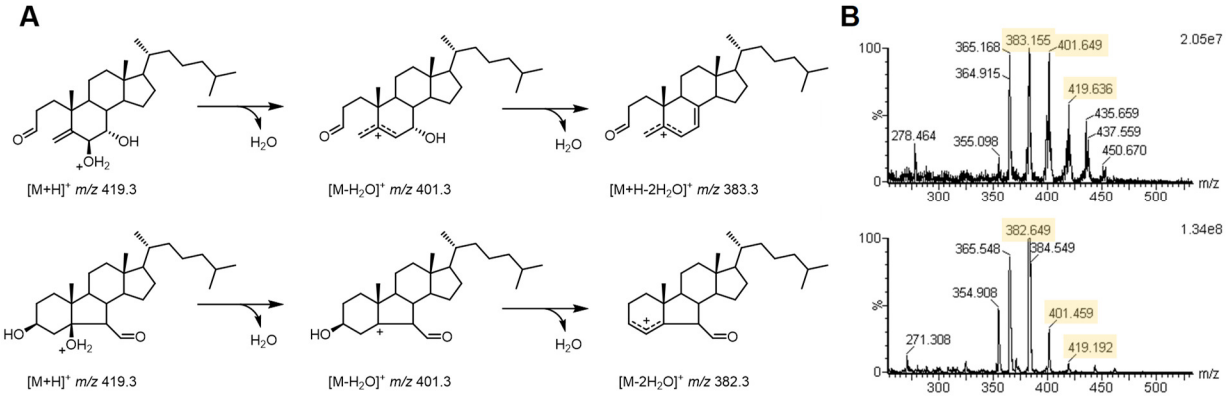

Figure 3.26 APCI$^+$-MS transitions of underivatized secosterols derived from autoxidation (3,4-*seco*-6β,7α-diol, top) and ozonolysis (secosterol B, bottom) (**A**) and representative spectrum of the relevant transitions (**B**).

3.4 Conclusions

In summary, herein we have described the investigation of a mechanism that may serve to aid in our understanding of the role of primary cholesterol autoxidation products in the deleterious effects of lipid peroxidation as well as to provide an alternative mechanism for controversial proposition that endogenous ozone is the source of proposed proatherogenic secosterol products. Generally, few investigations have been explicitly performed to understand the mechanism of Hock fragmentation *in vivo* despite the abundance of lipid-derived hydroperoxides in diseased states. Lipid-derived electrophiles such as 4-HNE, MDA, and acrolein have since been identified as likely products of acid-catalyzed fragmentation of linoleate hydroperoxides, however, similar investigations had never been performed for cholesterol hydroperoxides. Our studies towards development of a mechanism for Hock fragmentation of the major cholesterol autoxidation product, cholesterol 7-hydroperoxide, proved contrary to the traditional Hock fragmentation mechanism; based upon thorough isolation and characterization of the products evolved, we elucidated a mechanism that invokes a novel α-epoxy carbenium intermediate that facilitates unprecedented cleavage of the A-ring of the sterol scaffold. Products generated from this mechanism were shown to be potent electrophiles by character with the possession of epoxide, exomethylene, and aldehydic moieties. Cytotoxicity assays illustrated that the resulting compounds all exhibited relative toxicity values similar to, if not more potent than, other common oxysterol biomarkers, and were of similar toxicity upon exogenous administration to the secosterol compounds previously implicated in the pathogenesis of several diseases, termed “atheronals”. As expected, upon DNPH derivatization of cholesterol 7α-hydroperoxide, these compounds also exhibited near-identical chromatographic and spectroscopic character to the ozonolysis-derived atheronals, suggesting that primary cholesterol autoxidation products were simply obtained upon

processing of diseased plaque extracts and the electrophilic secondary products were observed as a consequence of the acidic derivatization conditions. This was further supported by our own sterol extractions performed on oxidized LDL and mammalian cells undergoing ferroptotic cell death. To completely and unambiguously identify the nature of these compounds in future assays of biological samples, it is likely necessary to develop a method for quantification of these compounds in the absence of derivatization – a methodology that is currently under investigation by our group. Development of this method would not only serve to unambiguously identify the origin of the secosterols, but it would also facilitate investigation of the decomposition of primary cholesterol hydroperoxide products in an effort to understand the mechanism by which lipid peroxidation, specific to ubiquitous cholesterol autoxidation, impacts cell viability and contributes to the pathogenesis of disease.

3.5 Experimental

All chemicals and solvents were purchased from Sigma Aldrich Co. LLC and used as received, unless otherwise stated. Cholesterol (92%) was purified to >99% by the well precedented method of bromination/debromination to remove other sterol impurities.[44] The >99% cholesterol was then freshly recrystallized from methanol prior to each experiment to remove trace oxidation product impurities. 2,2'-Azobis (4-methoxy-2,4-dimethylvaleronitrile) (MeOAMVN)[45] was purchased from Wako Pure Chemical Industries, Ltd. and used as received. 2,4-dinitrophenylhydrazine (DNPH) was recrystallized from acetonitrile prior to use. All HPLC/UV-Vis experiments are carried out on a Waters 2996 Separations Module with PDA detection or a Waters Acquity UPLC with TQ detector. (1*R*,3*S*)-RSL3 was synthesized according to literature procedures.[46,47] MEM media with/without phenol red, Dulbecco's phosphate buffered saline (DPBS), fetal bovine serum (FBS), penicillin-streptomycin, and AquaBluer were purchased from commercial sources and used as received.

Synthesis of cholesterol-7α-hydroperoxide (chol-7α-OOH): Prepared as previously reported.[30] Cholesterol (5.0 g, 12.9 mmol) and rose bengal (70 mg, 0.07 mmol) were dissolved in 75 mL of pyridine and oxygen was bubbled through the solution for 16 hours at 4°C while irradiated by a HPS 400 W sodium lamp (Apollo Horticulture) at a distance of 5 cm. Upon completion, the pyridine was removed by rotary evaporation with residual solvent removed *in vacuo* to obtain the crude chol-5α-OOH. The crude material was then reconstituted in $CHCl_3$ and left to stir for 8 hours at room temperature to facilitate rearrangement to the 7α-OOH; completion assessed by crude NMR. The product was purified by silica gel flash column (30% EtOAc in hexanes) and compared to previously reported characterization.[30] White solid; 85% yield. ^{1}H-NMR (400 MHz; CDCl3): δ 7.53 (s, 1H), 5.72 (dd, J = 5.1, 1.8 Hz, 1H), 4.16 (td, J = 4.6, 1.6 Hz, 1H), 3.62 (td, J = 11.3, 4.5

Hz, 1H), 2.41 (ddd, J = 13.0, 4.9, 2.3 Hz, 1H), 2.34 (dt, J = 11.2, 2.0 Hz, 1H), 1.98 (dt, J = 13.6, 3.9 Hz, 2H), 1.89-1.83 (m, 4H), 1.55-1.12 (m, 35H), 0.99 (s, 4H), 0.92 (d, J = 6.5 Hz, 4H), 0.86 (dd, J = 6.6, 1.9 Hz, 8H), 0.68 (s, 1H), 0.66 (s, 3H).

Preparative scale Hock fragmentation of cholesterol-7α-OOH to 3,4-seco-6β,7α-diol and cholesterol-5α/β-hydroxy-6α,7α-epoxide: Chol-7α-OOH (1.0 g, 2.3 mmol) was dissolved in 50 mL of acetone followed by addition of ~ 2 mL of H_2O until the solution was saturated whilst maintaining solubility of chol-7α-OOH. 200 µL of concentrated HCl (44 mM) was then added and the reaction mixture was stirred vigorously at room temperature for 6 hours. Upon completion, the reaction was quenched with water and the organic layer was extracted using DCM and brine, dried over $MgSO_4$, filtered, and concentrated *in vacuo*. The products were isolated and purified from a diverse mixture of products by silica gel flash column (30% EtOAc in hexanes). **3,4-*seco*-6β,7α-diol:** White solid; 35% yield. ^{1}H-NMR (600 MHz; $CDCl_3$): δ 9.79 (t, J = 1.3 Hz, 1H), 5.28 (s, 1H), 5.06 (s, 1H), 4.51 (d, J = 3.0 Hz, 1H), 3.88 (t, J = 3.0 Hz, 1H), 2.48-2.38 (m, 2H), 2.09-2.04 (m, 2H), 2.00 (dt, J = 12.8, 3.3 Hz, 2H), 1.88 (dtd, J = 13.3, 9.5, 5.9 Hz, 3H), 1.75 (ddd, J = 15.3, 10.0, 6.3 Hz, 2H), 1.64 (dddd, J = 12.2, 9.7, 7.2, 2.7 Hz, 3H), 1.54-1.48 (m, 5H), 1.45 (dt, J = 15.7, 5.2 Hz, 4H), 1.39-1.25 (m, 19H), 1.18-1.09 (m, 15H), 1.03-0.96 (m, 3H), 0.91 (d, J = 6.5 Hz, 6H), 0.87 (d, J = 2.6 Hz, 6H), 0.86 (d, J = 2.5 Hz, 6H), 0.74 (s, 3H); ^{13}C NMR (151 MHz; $CDCl_3$): δ 202.3, 148.6, 118.5, 72.8, 64.5, 56.2, 50.4, 42.6, 41.5, 39.65, 39.48, 39.2, 37.2, 36.3, 35.9, 33.7, 28.9, 28.30, 28.17, 26.9, 23.88, 23.78, 23.0, 22.7, 21.2, 18.8, 11.9; HRMS (EI): calculated for $C_{27}H_{46}O_3$ 418.3447, found 418.3437. **cholesterol-5β-hydroxy-6α,7α-epoxide:** ^{1}H-NMR (400 MHz; $CDCl_3$): δ 4.20 (broad m, 1H), 3.75 (broad m, 1H), 3.10 (dd, J = 3.7, 2.0 Hz, 1H), 2.93 (d, J = 3.8 Hz, 1H), 2.21 (s, 1H), 2.11 (dd, J = 15.5, 3.1 Hz, 1H), 2.02-1.96 (m, 2H), 1.93 (d, J = 2.4 Hz, 2H), 1.79-1.71 (m, 4H), 1.55-1.50 (m, 5H), 1.34 (d, J = 16.4 Hz, 11H), 1.12 (dd, J = 9.4, 2.9

Hz, 6H), 1.02 (d, J = 10.0 Hz, 3H), 0.90 (d, J = 6.5 Hz, 3H), 0.87 (d, J = 1.8 Hz, 3H), 0.85 (d, J = 2.1 Hz, 6H), 0.70 (s, 3H). ^{13}C NMR (101 MHz; $CDCl_3$): δ 72.8, 67.5, 59.2, 56.0, 55.3, 51.9, 43.2, 39.9, 39.6, 38.7, 36.29, 36.18, 35.92, 35.75, 35.5, 28.6, 28.1, 27.8, 25.0, 23.9, 23.6, 22.9, 22.7, 21.0, 18.81, 18.77, 12.1. Crystal data and structure refinement obtained at 200 K at a wavelength of 0.71073 Å with an orthorhombic crystal system (see Appendix). Consistent with previous characterization.[31] **cholesterol-5α-hydroxy-6α,7α-epoxide:** ^{1}H-NMR (400 MHz; CDCl3): δ 4.43 (tt, J = 10.8, 5.6 Hz, 1H), 3.23 (t, J = 3.0 Hz, 1H), 2.96 (d, J = 3.4 Hz, 1H), 2.29 (dd, J = 13.1, 5.4 Hz, 1H), 1.95 (t, J = 11.6 Hz, 6H), 1.78-1.73 (m, 4H), 1.55-1.48 (m, 12H), 1.33-1.11 (m, 22H), 1.00 (s, 3H), 0.90 (d, J = 6.5 Hz, 4H), 0.86 (dd, J = 6.6, 1.9 Hz, 9H), 0.70 (s, 3H). ^{13}C NMR (101 MHz; $CDCl_3$): δ 79.6, 67.3, 57.5, 57.2, 55.8, 51.4, 43.5, 42.9, 39.79, 39.60, 39.58, 36.2, 36.0, 29.8, 28.57, 28.55, 28.14, 28.11, 23.9, 23.4, 22.9, 22.7, 20.9, 18.7, 16.3, 12.3. Consistent with previous characterization.[32]

Synthesis of 2,2,4,4-d_4-cholesterol (d_4-chol): Synthesis adapted from a previous report.[35] To a flame dried flask, Δ^4-cholesten-3-one (1.7 g, 4.4 mmol) and potassium *tert*-butoxide (4.25 g, 37.9 mmol) were added. The flask was fitted with a septum and the atmosphere was evacuated *in vacuo* and replaced with N_2. *Tert*-butanol-OD (21.3 mL, 231.2 mmol) was added under N_2 atmosphere and the brown solution was left to stir at room temperature for 2 hours. The reaction was quenched with 10% acetic acid-OD in D_2O and extracted with dichloromethane. The organic layer was washed twice with water, dried over $MgSO_4$, filtered, and concentrated *in vacuo* to afford the crude 2,2,4,4-d_4-3-ketocholesterol. In preparation for reduction of the resulting ketocholesterol, lithium aluminum hydride (1.36 g, 35.9 mmol) was added to a flame dried flask and dissolved in 50 mL of THF followed by the dropwise addition of *tert*-butanol (6.8 mL, 391 mmol). The crude 2,2,4,4-d_4-3-ketocholesterol was reconstituted in 50 mL THF and added to the reaction. The reaction was

left to stir at 0°C for 30 minutes and was then left to stir for an additional 2 hours at room temperature. The reaction was quenched with 100 mL of 5% HCl and extracted with dichloromethane. The organic layer was washed twice with water, dried over $MgSO_4$, filtered, and concentrated *in vacuo.* The product stood overnight in a mixture of 1:1 15% HCl and conc. acetic acid. The following morning, the reaction was extracted with dichloromethane and washed twice with sat. Na_2CO_2 and twice with water, dried over $MgSO_4$, filtered, and concentrated *in vacuo.* The product was purified by silica gel flash column (30% EtOAc in hexanes). Note that the signals corresponding to C2 and C4 are not observed in the ^{13}C NMR presumably due to broadening caused by their coupling with two D-atoms each. White solid; 59% yield. ^1H-NMR (400 MHz; $CDCl_3$): δ 5.35 (dd, J = 5.3, 1.9 Hz, 1H), 3.51 (dd, J = 3.9, 0.3 Hz, 1H), 2.17 (s,), 1.99 (s, 2H), 1.83 (d, J = 13.3 Hz, 2H), 1.55 (s, 16H), 1.00 (s, 12H), 0.91 (d, J = 6.6 Hz, 4H), 0.86 (dd, J = 6.6, 1.8 Hz, 6H), 0.68 (s, 3H). ^{13}C NMR (101 MHz; $CDCl_3$): δ 140.9, 121.8, 100.1, 71.7, 56.9, 56.3, 50.3, 42.5, 39.9, 39.7, 37.2, 36.6, 36.3, 35.9, 32.1, 28.4, 28.2, 24.5, 24.0, 23.0, 22.7, 21.2, 19.5, 18.9, 12.0. HRMS (EI): calculated for $C_{27}H_{42}D_4O_2$ 420.3801, found 420.3800.

Synthesis of 2,2,4,4-d$_4$-cholesterol-7α-OOH (d$_4$-chol-7α-OOH): Prepared from d_4-chol as above for the transformation of chol to chol-7α-OOH.[30] ^1H NMR (400 MHz; $CDCl_3$): δ 7.95 (s, 1H), 5.72 (d, J = 4.9 Hz, 1H), 4.15 (t, J = 4.7 Hz, 1H), 3.60 (s, 1H), 2.39 (s,), 2.31-2.21 (m,), 1.99-1.95 (m, 1H), 1.85 (dd, J = 16.5, 10.6 Hz, 4H), 1.61 (td, J = 11.6, 4.5 Hz, 2H), 1.49 (ddt, J = 19.7, 12.8, 6.5 Hz, 5H), 1.34 (tdd, J = 20.3, 8.8, 6.5 Hz, 9H), 1.19-1.09 (m, 11H), 0.98 (s, 3H), 0.91 (d, J = 6.5 Hz, 4H), 0.86 (dd, J = 6.6, 1.9 Hz, 9H), 0.65 (s, 3H). ^{13}C NMR (101 MHz; $CDCl_3$): δ 148.8, 120.2, 78.6, 71.3, 55.9, 49.2, 43.7, 42.5, 39.7, 39.2, 37.5, 37.2, 36.7, 36.3, 35.9, 28.35, 28.16, 24.6, 23.9, 23.0, 22.7, 21.0, 18.9, 18.3, 11.5. HRMS (EI, $[M-H_2O]^+$): calculated for $C_{27}H_{40}D_4O_2$ 404.3580, found 404.3567.

Synthesis of d_4-3,4-seco-6β,7α-diol: Prepared from d_4-chol-7α-OOH as above for the transformation of cholesterol-7α-OOH to 3,4-*seco*-6β,7α-diol. White solid; 35% yield. ^{1}H NMR (400 MHz; $CDCl_3$): δ 9.78 (s, 1H), 5.25 (s, trace), 5.04 (s, trace), 4.50 (d, J = 2.9 Hz, 1H), 3.87 (t, J = 2.5 Hz, 1H), 2.38 (d, J = 10.7 Hz, 1H), 2.04 (d, J = 17.2 Hz, 4H), 1.87 (dd, J = 8.3, 4.8 Hz, 2H), 1.75-1.62 (m, 5H), 1.53-1.27 (m, 19H), 1.13 (t, J = 10.2 Hz, 9H), 1.01 (t, J = 9.2 Hz, 2H), 0.91 (d, J = 6.5 Hz, 4H), 0.86 (dd, J = 6.6, 1.7 Hz, 9H), 0.73 (s, 3H). ^{13}C NMR (101 MHz; $CDCl_3$): δ 202.5, 148.5, 72.7, 64.5, 56.2, 50.4, 42.6, 41.4, 39.64, 39.48, 37.2, 36.3, 35.9, 33.7, 28.8, 28.29, 28.15, 26.8, 23.88, 23.77, 22.9, 22.7, 21.2, 18.8, 11.9. HRMS (EI, $[M-H_2O]^+$): calculated for $C_{27}H_{40}D_4O_2$ 404.3580, found 404.3567.

Kinetic monitoring of acid-catalyzed Hock fragmentation by ^{1}H NMR: Chol-7α-OOH, chol-5β-OH-6α,7α-epoxide, and cholOAc-7α-OOH (~ 10 mg, 50 mM) was dissolved in 495 μL of chloroform-*d*, acetone-d_6, or methanol-d_4 containing 1 μL/mL TCE (11.1 mM) as an internal standard. A solution of HCl was prepared in D_2O depending upon the final concentration required for the experiment. Using a 300 MHz NMR, the sample was locked to the desired solvent, shimmed, and the probe was tuned prior to the addition of HCl. The sample was ejected from the instrument and 5 μL of the HCl solution was added to the NMR tube to achieve a final concentration of 0.001, 0.005, 0.01, 0.1, or 1 M HCl; the tube was inverted to mix and was immediately replaced within the instrument. ^{1}H NMR spectra were collected every 5 minutes for an hour and then every hour subsequently for the next 8 hours at 64 scans per spectra to monitor the reaction.

Hock fragmentation of cholesterol-7α-OOH under DNPH derivatization conditions: A 2 mM DNPH solution (4 mg, 0.020 mmol) in 9.1 mL of ethanol containing 1 M HCl (883 μL conc. HCl, 9.1 mmol) was prepared and 100 μL was added to chol-7α-OOH (3 mg, 0.007 mmol) dissolved in

900 µL of EtOH such that the final concentration of the solution was 200 µM DNPH, 0.1 M HCl, and 7 mM chol-7α-OOH. The homogenous solution is stirred for 2 hours at room temperature. Upon completion, the solution was filtered through a 0.2 µm PTFE syringe filter (Fisher Scientific). 5 µL of each sample in ethanol was injected onto a 4.6 x 150 mm Atlantis C18 reverse-phase HPLC column and was separated isocratically with a solvent composition 75:20:5 ACN:MeOH:H2O at a flow rate of 1 mL/min. Detected by UV-Vis absorbance at 360 nm and negative-mode ESI-MS using the following settings: corona current 1.2 µA; cone voltage 53 V; source temperature 250°C; ESI probe temperature 250°C; desolvation gas flow 500 L/hr; cone gas flow 50 L/hr.

Preparative Hock fragmentation of cholesterol-7α-OOH under DNPH derivatization conditions: Adapted from the procedure described above, chol-7α-OOH (10 mg, 0.024 mmol) was dissolved directly into a 20 mM DNPH solution (4 mg, 0.020 mmol) in 1.0 mL ethanol containing 1 M HCl (88.8 µL, 10.0 mmol). The solution was stirred for 2 hours at room temperature. Upon completion, the solution was filtered through a 0.2 µm PTFE syringe filter (Fisher Scientific) and was injected onto the HPLC. For preparative separation of the resulting DNPH hydrazones, 500 µL of the solution is injected onto a reverse-phase Waters XBridge Prep C18 5 µM column (19 x 150 mm) and was separated isocratically with a solvent composition of 75:20:5 ACN:MeOH:H_2O and a flow rate of 7 mL/min over the course of 60 minutes. Several injections are typically required to accumulate enough material for desired analysis and characterization. Separation affords the following compounds with reasonable purity (detailed in foregoing results section). **2,4-dinitrophenylhydrazone of 3,4-*seco*-6α,7α-epoxide:** ^{1}H-NMR (600 MHz; $CDCl_3$): δ 11.00 (s, 1H), 9.12-9.12 (m, 1H), 8.30 (dd, J = 9.6, 2.6 Hz, 1H), 7.92 (d, J = 9.6 Hz, 1H), 7.53 (s, 1H), 5.41 (s, 1H), 5.28 (s, 1H), 3.48 (d, J = 4.2 Hz, 1H), 3.27 (d, J = 4.1 Hz, 1H), 2.35 (dt, J = 10.8, 5.1 Hz,

1H), 2.28-2.25 (m, 3H), 2.02 (dt, J = 8.7, 4.0 Hz, 1H), 1.96-1.85 (m, 5H), 1.79 (q, J = 9.8 Hz, 3H), 1.66-1.59 (m, 2H), 1.54-1.46 (m, 10H), 1.38-1.32 (m, 25H), 1.15 (t, J = 10.0 Hz, 17H), 1.01 (s, 7H), 0.91 (t, J = 6.8 Hz, 6H), 0.87 (d, J = 3.4 Hz, 5H), 0.86 (t, J = 3.4 Hz, 9H), 0.84 (s, 3H), 0.72 (s, 4H), 0.69 (s, 3H). ^{13}C NMR (151 MHz; $CDCl_3$): δ 152.8, 130.1, 123.7, 118.0, 116.7, 77.2, 67.3, 56.0, 55.8, 55.24, 55.10, 52.2, 51.5, 43.5, 43.0, 39.66, 39.65, 39.62, 36.3, 35.9, 35.5, 34.6, 33.3, 30.1, 28.5, 28.2, 27.2, 25.8, 24.0, 23.0, 22.7, 18.8, 11.9 HRMS (EI): calculated for $C_{33}H_{48}N_4O_5$ 580.3613, found 580.3601. **2,4-dinitrophenylhydrazone of 3,4-*seco*-6β-OEt-7α-OH:** ^{1}H-NMR (600 MHz; $CDCl_3$): δ 11.03 (s, 1H), 9.13 (d, J = 2.6 Hz, 1H), 8.31 (dd, J = 9.1, 2.6 Hz, 1H), 7.93 (d, J = 9.6 Hz, 1H), 7.57 (t, J = 5.0 Hz, 1H), 6.96 (s, 2H), 5.87 (s, 1H), 5.10 (s, 2H), 3.79 (s (broad), 1H), 3.71 (d, J = 3.3 Hz, 1H), 3.54-3.48 (m, 2H), 3.27 (ddd, J = 11.1, 7.6, 4.1 Hz, 2H), 2.48 (dd, J = 20.6, 11.7 Hz, 2H), 2.34 (td, J = 19.8, 9.2 Hz, 3H), 2.25 (s, 3H), 2.03-1.87 (m, 10H), 1.73-1.60 (m, 7H), 1.55-1.48 (m, 20H), 1.38-1.23 (m, 42H), 1.17-1.15 (m, 25H), 1.01 (s, 2H), 0.91 (d, J = 6.5 Hz, 6H), 0.87 (d, J = 2.6 Hz, 7H), 0.86 (d, J = 2.6 Hz, 6H), 0.74 (s, 3H). ^{13}C NMR (151 MHz; $CDCl_3$): δ 152.7, 130.1, 129.0, 126.5, 123.7, 116.7, 85.4, 71.5, 63.0, 56.3, 50.6, 42.6, 41.7, 39.7, 38.5, 36.3, 35.9, 35.1, 34.5, 33.6, 30.1, 28.4, 28.17, 28.16, 27.5, 23.89, 23.80, 23.62, 23.0, 22.7, 21.4, 21.0, 18.8, 15.1, 12.1. HRMS (EI; $[M\text{-}OH]^+$): calculated for $C_{35}H_{53}N_4O_5$ 609.4009, found 609.4002.

Synthesis of the 2,4-dinitrophenylhydrazone of 3,4-seco-6β,7α-diol: 2,4-dinitrophenylhyradzine (DNPH; 25 mg, 0.126 mmol) was dissolved in a mixture of 30 mL of acetonitrile and 20 mL of DCM containing 0.3 mM *p*-toluenesulfonic acid (PTSA; 1 mg, 0.006 mmol) and stirred for ~ 20 minutes at RT to ensure complete solubilization of DNPH. 3,4-*seco*-6β,7α-diol (30 mg, 0.072 mmol) was then added to the DNPH solution and was stirred at RT for an additional 2 hours. Upon completion, the reaction was quenched with water and the organic layer was extracted using DCM

and brine, dried over $MgSO_4$, filtered, and concentrated *in vacuo*. The products were isolated and purified from a diverse mixture of products by silica gel flash column (30% EtOAc in hexanes). ^{1}H-NMR (400 MHz; $CDCl_3$): δ 11.02 (s, 1H), 9.12 (d, J = 2.6 Hz, 1H), 8.31 (ddd, J = 9.6, 2.6, 0.6 Hz, 1H), 7.92 (d, J = 9.5 Hz, 1H), 7.55 (t, J = 4.9 Hz, 1H), 5.34 (s, 1H), 5.16 (s, 1H), 4.55 (d, J = 3.0 Hz, 1H), 3.91 (dt, J = 4.9, 2.5 Hz, 1H), 2.39 (ddd, J = 21.8, 11.1, 5.0 Hz, 3H), 2.11 (t, J = 9.7 Hz, 1H), 2.05 (s, 3H), 1.83 (t, J = 15.0 Hz, 4H), 1.73-1.60 (m, 2H), 1.54-1.46 (m, 11H), 1.30 (d, J = 23.1 Hz, 14H), 1.15 (dt, J = 10.2, 5.2 Hz, 12H), 1.04-0.98 (m, 4H), 0.92 (d, J = 6.5 Hz, 4H), 0.87 (dd, J = 6.6, 1.7 Hz, 9H), 0.76 (s, 3H). ^{13}C NMR (101 MHz; $CDCl_3$): δ 152.4, 148.7, 145.2, 138.0, 130.1, 129.0, 123.7, 118.3, 116.6, 72.8, 64.6, 56.3, 42.58, 42.57, 41.9, 39.64, 39.54, 37.1, 36.3, 35.9, 33.79, 33.66, 28.28, 28.16, 27.3, 26.9, 23.89, 23.79, 22.9, 22.7, 21.3, 18.8, 12.0. HRMS (EI; $[M\text{-}OH]^+$): calculated for $C_{33}H_{49}N_4O_5$ 581.3679, found 589.3655.

Preparation of Egg-PC Liposomes: Performed as described previously (see Chapter 2). ***Autoxidation of Cholesterol-Loaded Liposomes:*** Performed as described previously (see Chapter 2).

Oxidation of LDL: 4 mg/mL solution of LDL (Alfa Aesar; human plasma) is prepared in 1 mL of PBS (pH = 7.4). To initiate oxidation, 20 μL of a 100 mM stock of MeOAMVN in benzene is added. The vial was loosely capped and incubated at 37°C for 32 hours with stirring. Upon completion, each solution is quenched with 2 mL of 4 mM BHT and 4 mM PPh_3 in 2:1 $CHCl_3$:MeOH in preparation for extraction.

Sterol Extraction from Egg-PC Liposomes and LDL: Performed as described previously (see Chapter 2); LDL extraction procedure performed analogous to that of extraction from chol-loaded egg-PC liposomes.

Cell culture: Both HEK 293 and Pfa1 cell lines were cultured at 37 °C in a 5% CO_2 atmosphere. HEK 293 cells were cultured in MEM with 10% FBS, 1% 100 × non-essential amino acid solution, 1 mM sodium pyruvate and 1% penicillin-streptomycin. Cells were passaged by dissociation with 0.05% trypsin and 0.2% EDTA every two to three days. Pfa1 cells were cultured in DMEM with 10% FBS, 1% 100 × non-essential amino acid solution, 1 mM sodium pyruvate and 1% penicillin-streptomycin. All cell experiments were carried out at a minimum of three biological replicates.

Generation of cholesterol hydroperoxides in mammalian cells under ferroptotic cell death conditions: Performed as described previously (see Chapter 2).

Sterol extraction from HEK 293 mammalian cells: Performed as described previously (see Chapter 2).

Analysis of sterol extracts from cholesterol-loaded egg-PC liposomes, HEK 293 cells, and LDL: A 2 mM DNPH solution (4 mg, 0.020 mmol) in 9.1 mL of ethanol containing 1 M HCl (883 μL conc. HCl, 9.1 mmol) was prepared and 100 μL was added to each sterol extract sample dissolved in 900 μL of EtOH such that the final concentration of the solution was 200 μM DNPH and 0.1 M HCl. Remaining portion of procedure performed as described above (see "Hock fragmentation of cholesterol-7α-OOH under DNPH derivatization conditions").

Cytotoxicity of lipid-derived electrophiles in Pfa1 cells: Pfa1 cells (3,000 in 100 μL) were seeded in 96-well plates and cultured overnight. The next day the media was removed, the cells were washed with PBS and the cells were suspended in new media containing varied concentrations of the desired lipid-derived electrophilic species dissolved in EtOH (total EtOH conc < 1%). Control experiments in which PFa1 cells were treated with the same concentration of EtOH as administered showed no inherent toxicity. Cell viability was assessed ~ 5 hours later using the AquaBluer assay

(MultiTarget Pharmaceuticals, LLC) according to the manufacturer's instructions. Cell viability was calculated by normalizing the data to untreated controls. Experiments are carried out with six-technical replicates (n = 6 wells of a 96-well plate) and performed independently with a minimum of three biological replicates.

3.6 References

(1) Porter, N. A.; Mills, K. A.; Carter, R. L. *J. Am. Chem. Soc.* **1994**, *116* (15), 6690–6696.

(2) Porter, N. A.; Weber, B. A.; Weenen, H.; Khan, J. A. *J. Am. Chem. Soc.* **1980**, *102* (17), 5597–5601.

(3) Porter, N. A.; Lehman, L. S.; Weber, B. A.; Smith, K. J. *J. Am. Chem. Soc.* **1981**, *103* (21), 6447–6455.

(4) Zielinski, Z. A. M.; Pratt, D. A. *J. Am. Chem. Soc.* **2016**, *138* (22), 6932–6935.

(5) Zielinski, Z. A. M.; Pratt, D. A. *J. Am. Chem. Soc.* **2019**, *141* (7), 3047–3051.

(6) Xu, L.; Korade, Z.; Porter, N. A. *J. Am. Chem. Soc.* **2010**, *132* (7), 2222–2232.

(7) Thomas, J. P.; Geiger, P. G.; Maiorino, M.; Ursini, F.; Girotti, A. W. *Biochim. Biophys. Acta* **1990**, *1045*, 252–260.

(8) Schneider, C.; Tallman, K. A.; Porter, N. A.; Brash, A. R. *J. Biol. Chem.* **2001**, *276* (24), 20831–20838.

(9) Schneider, C.; Boeglin, W. E.; Yin, H.; Stec, D. F.; Hachey, D. L.; Porter, N. A.; Brash, A. R. *Lipids* **2005**, *40* (11), 1155–1162.

(10) Gardner, H. W.; Weisleder, D.; Nelson, E. C. *J. Org. Chem.* **1984**, *49* (3), 508–515.

(11) Wilcox, A. L.; Marnett, L. J. *Chem. Res. Toxicol.* **1993**, *6* (4), 413–416.

(12) Brinkhorst, J.; Nara, S. J. and; Pratt, D. A. *J. Am. Chem. Soc.* **2008**, *130* (37), 12224–12225.

(13) Wentworth Jr., P.; Nieva, J.; Takeuchi, C.; Galve, R.; Wentworth, A. D.; Dilley, R. B.; DeLaria, G. A.; Saven, A.; Babior, B. M.; Janda, K. D.; Eschenmoser, A.; Lerner, R. A. *Science* **2003**, *302* (5647), 1053–1056.

(14) Takeuchi, C.; Galvé, R.; Nieva, J.; Witter, D. P.; Wentworth, A. D.; Troseth, R. P.; Lerner, R. A.; Wentworth, P. *Biochemistry* **2006**, *45* (23), 7162–7170.

(15) Bosco, D. A.; Fowler, D. M.; Zhang, Q.; Nieva, J.; Powers, E. T.; Wentworth, P.; Lerner, R. A.; Kelly, J. W. *Nat. Chem. Biol.* **2006**, *2*, 249–253.

(16) Wentworth, A. D.; Song, B.; Nieva, J.; Shafton, A. *Chem. Commun.* **2009**, 3098–3100.

(17) Mansano, F. V; Kazaoka, R. M. A.; Ronsein, G. E.; Prado, F. M.; Genaro-Mattos, T. C.; Uemi, M.; Di Mascio, P.; Miyamoto, S. *Anal. Chem.* **2010**, *82* (16), 6775–6781.

(18) Windsor, K.; Genaro-Mattos, T. C.; Miyamoto, S.; Stec, D. F.; Kim, H.-Y. H.; Tallman, K. A.; Porter, N. A. *Chem. Res. Toxicol.* **2014**, *27* (10), 1757–1768.

(19) Dantas, L. S.; Chaves-Filho, A. B.; Coelho, F. R.; Genaro-Mattos, T. C.; Tallman, K. A.; Porter, N. A.; Augusto, O.; Miyamoto, S. *Redox Biol.* **2018**, *19*, 105–115.

(20) Brown, A. J.; Leong, S.-L.; Dean, R. T.; Jessup, W. *J. Lipid Res.* **1997**, *38* (9), 1730–1745.

(21) Smith, L. L. *Chem. Phys. Lipids* **1987**, *44*, 87–125.

(22) Sevanian, A.; McLeod, L. L. *Lipids* **1987**, *22* (9), 627–636.

(23) Lund, E.; Diczfalusy, U.; Bjoerkhem, I. *J. Biol. Chem.* **1992**, *267* (18), 12462–12467.

(24) Chisolm, G. M.; Ma, G.; Irwin, K. C.; Martin, L. L.; Gunderson, K. G.; Linberg, L. F.; Morel, D. W.; DiCorleto, P. E. *Proc. Natl. Acad. Sci. U. S. A.* **1994**, *91* (24), 11452–11456.

(25) Sevanian, A.; Peterson, A. R. *Food Chem. Toxicol.* **1986**, *24* (10–11), 1103–1110.

(26) Lizard, G.; Deckert, V.; Dubrez, L.; Moisant, M.; Gambert, P.; Lagrost, L. *Am. J. Pathol.* **1996**, *148* (5), 1625–1638.

(27) Colles, S. M.; Irwin, K. C.; Chisolm, G. M. *J. Lipid Res.* **1996**, *37* (9), 2018–2028.

(28) Luchetti, F.; Canonico, B.; Cesarini, E.; Betti, M.; Galluzzi, L.; Galli, L.; Tippins, J.; Zerbinati, C.; Papa, S.; Iuliano, L. *Steroids* **2015**, *99* (Part_B), 204–211.

(29) Nadia Zopyrus. On the Origin of Secosterols upon Oxidation of Cholesterol, University of Ottawa, 2017.

(30) Beckwith, A. L. J.; Davies, A. G.; Davidson, I. G. E.; Maccoll, A.; Mruzek, M. H. *J. Chem Soc. Perkin Trans. II* **1989**, *1* (4), 815–824.

(31) Glotter, E.; Zviely, M. *J. Chem. Soc. Perkin Trans. 1* **1986**, No. 0, 321–325.

(32) Adam, W.; Staab, E. *Liebigs Ann. der Chemie* **1988**, 757–760.

(33) Nyberg, N. T.; Duus, J. O.; Sorensen, O. W. *J. Am. Chem. Soc.* **2005**, *127* (17), 6154–6155.

(34) Foroozandeh, M.; Adams, R. W.; Meharry, N. J.; Jeannerat, D.; Nilsson, M.; Morris, G. A. *Angew. Chemie, Int. Ed.* **2014**, *53* (27), 6990–6992.

(35) Diekman, J.; Djerassi, C. **1967**, *32* (4), 1005–1012.

(36) Zhang, Q.; Powers, E. T.; Nieva, J.; Huff, M. E.; Dendle, M. A.; Bieschke, J.; Glabe, C. G.; Eschenmoser, A.; Wentworth Jr., P.; Lerner, R. A.; Kelly, J. W. *Proc. Natl. Acad. Sci. U. S. A.* **2004**, *101* (14), 4752–4757.

(37) Westphal, D.; Zbiral, E. *Justus Liebigs Ann. Chem.* **1975**, 2038–2052.

(38) Paillasse, M. R.; Saffon, N.; Gornitzka, H.; Silvente-Poirot, S.; Poirot, M.; de Medina, P. *J. Lipid Res.* **2012**, *53* (4), 718–725.

(39) Pryor, W. A.; Porter, N. A. *Free Radic. Biol. Med.* **1990**, *8* (6), 541–543.

(40) Satchell, L.; Leake, D. S. *Biochemistry* **2012**, *51* (18), 3767–3775.

(41) Goldstein, J. L.; Ho, Y. K.; Basu, S. K.; Brown, M. S. *Proc. Natl. Acad. Sci. U. S. A.* **1979**,

76 (1), 333–337.

(42) Brown, M. S.; Ho, Y. K.; Goldstein, J. L. *J. Biol. Chem.* **1980**, *255* (19), 9344–9352.

(43) Bieschke, J.; Zhang, Q.; Bosco, D. A.; Lerner, R. A.; Powers, E. T.; Wentworth Jr., P.; Kelly, J. W. *Acc. Chem. Res.* **2006**, *39* (9), 611–619.

(44) Fieser, L. F. *J. Am. Chem. Soc.* **1953**, *75*, 542l – 2.

(45) Noguchi, N.; Yamashita, H.; Gotoh, N.; Yamamoto, Y.; Numano, R.; Niki, E. *Free Radic. Biol. Med.* **1997**, *24* (2), 259–268.

(46) Friedmann Angeli, J. P.; Schneider, M.; Proneth, B.; Tyurina, Y. Y.; Tyurin, V. A.; Hammond, V. J.; Herbach, N.; Aichler, M.; Walch, A.; Eggenhofer, E.; Basavarajappa, D.; Radmark, O.; Kobayashi, S.; Seibt, T.; Beck, H.; Neff, F.; Esposito, I.; Wanke, R.; Foerster, H.; Yefremova, O.; Heinrichmeyer, M.; Bornkamm, G. W.; Geissler, E. K.; Thomas, S. B.; Stockwell, B. R.; O'Donnell, V. B.; Kagan, V. E.; Schick, J. A.; Conrad, M. *Nat. Cell Biol.* **2014**, *16* (12), 1180–1191.

(47) Yang, W. S.; SriRamaratnam, R.; Welsch, M. E.; Shimada, K.; Skouta, R.; Viswanathan, V. S.; Cheah, J. H.; Clemons, P. A.; Shamji, A. F.; Clish, C. B.; Brown, L. M.; Girotti, A. W.; Cornish, V. W.; Schreiber, S. L.; Stockwell, B. R. *Cell* **2014**, *156* (1), 317–331.

3.7 Appendix

3.7.1 Full Characterization of 3,4-seco-6β,7α-diol

^{1}H NMR (400 MHz, $CDCl_3$)

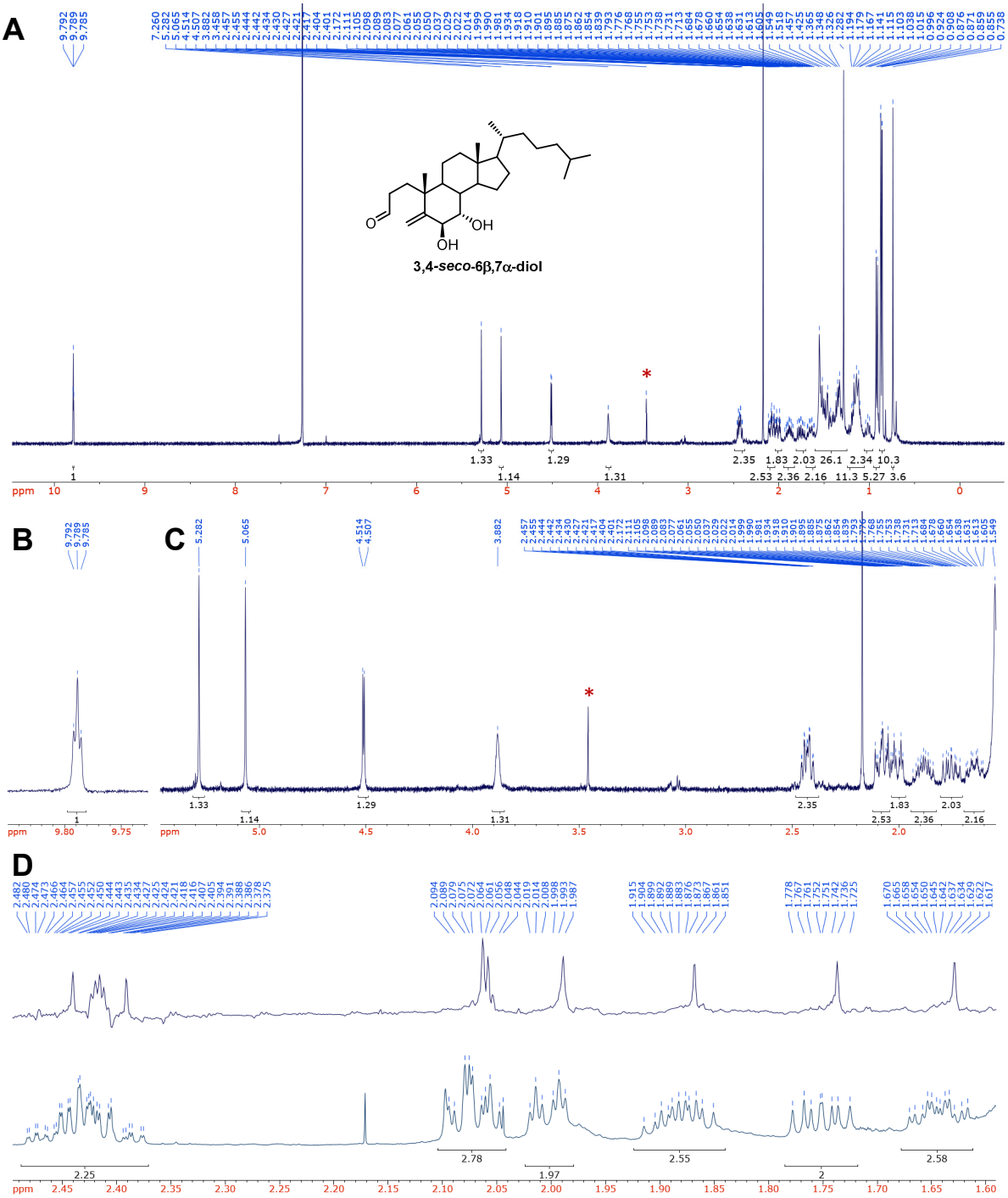

Figure 3.27 ^{1}H NMR spectrum of 3,4-*seco*-6β,7α-diol (**A**) and expansions of 9.78-9.80 ppm (**B**) and 1.0-6.0 ppm (**C**). Expansion of 1.60-2.50 ppm shows overlay of PSYCHE suppression of homonuclear coupling (**D**). Peaks corresponding to residual MeOH indicated with an asterisk (*).

^{13}C NMR (151 MHz, $CDCl_3$)

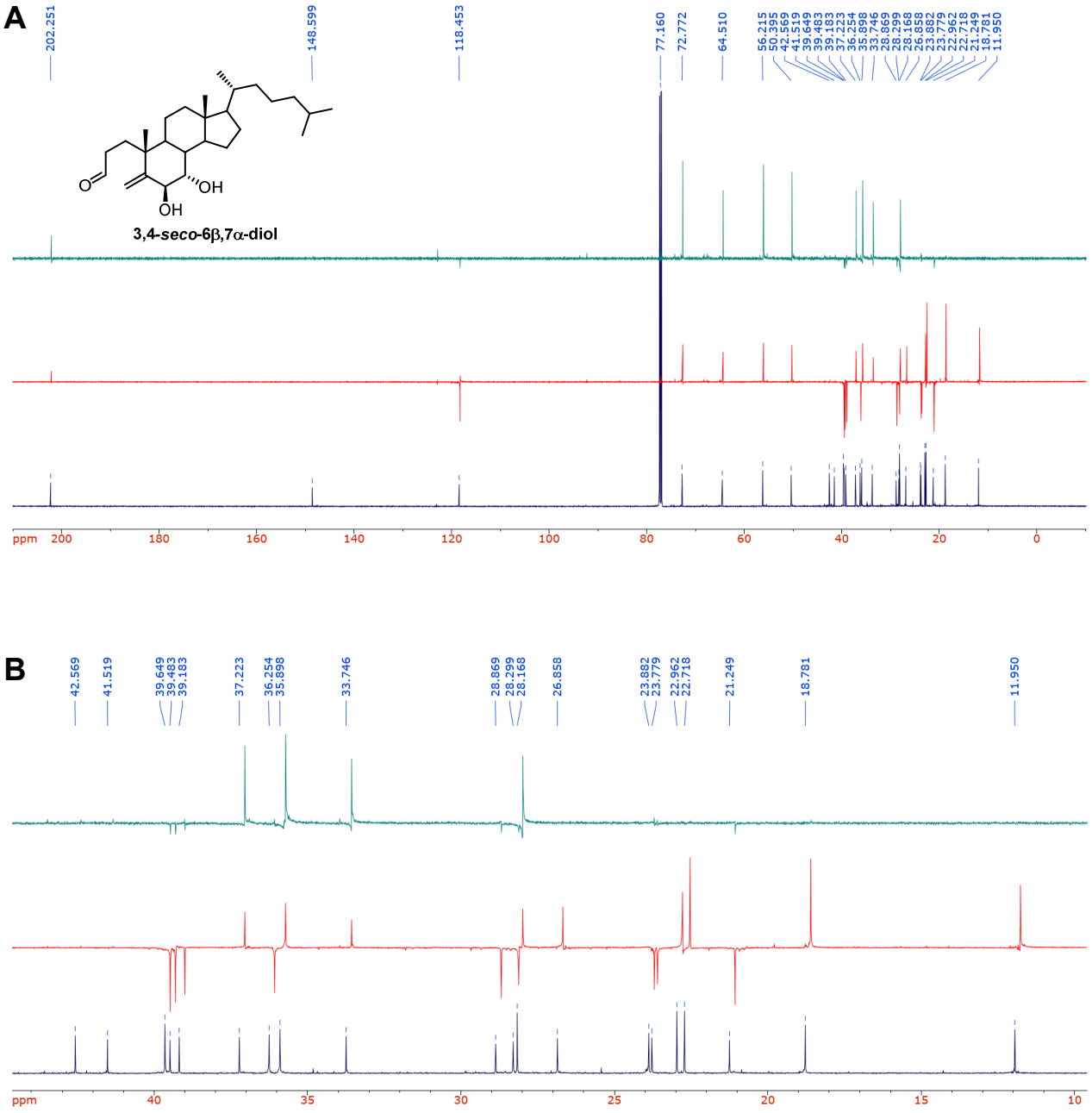

Figure 3.28 ^{13}C NMR spectra of 3,4-*seco*-6β,7α-diol (**A**) and an expansion of 10-45 ppm (**B**). DEPT-135 (red) and DEPT-90 (green) spectra are overlaid for comparison to the proton decoupled spectra.

^{1}H-^{1}H COSY (600 MHz, $CDCl_3$)

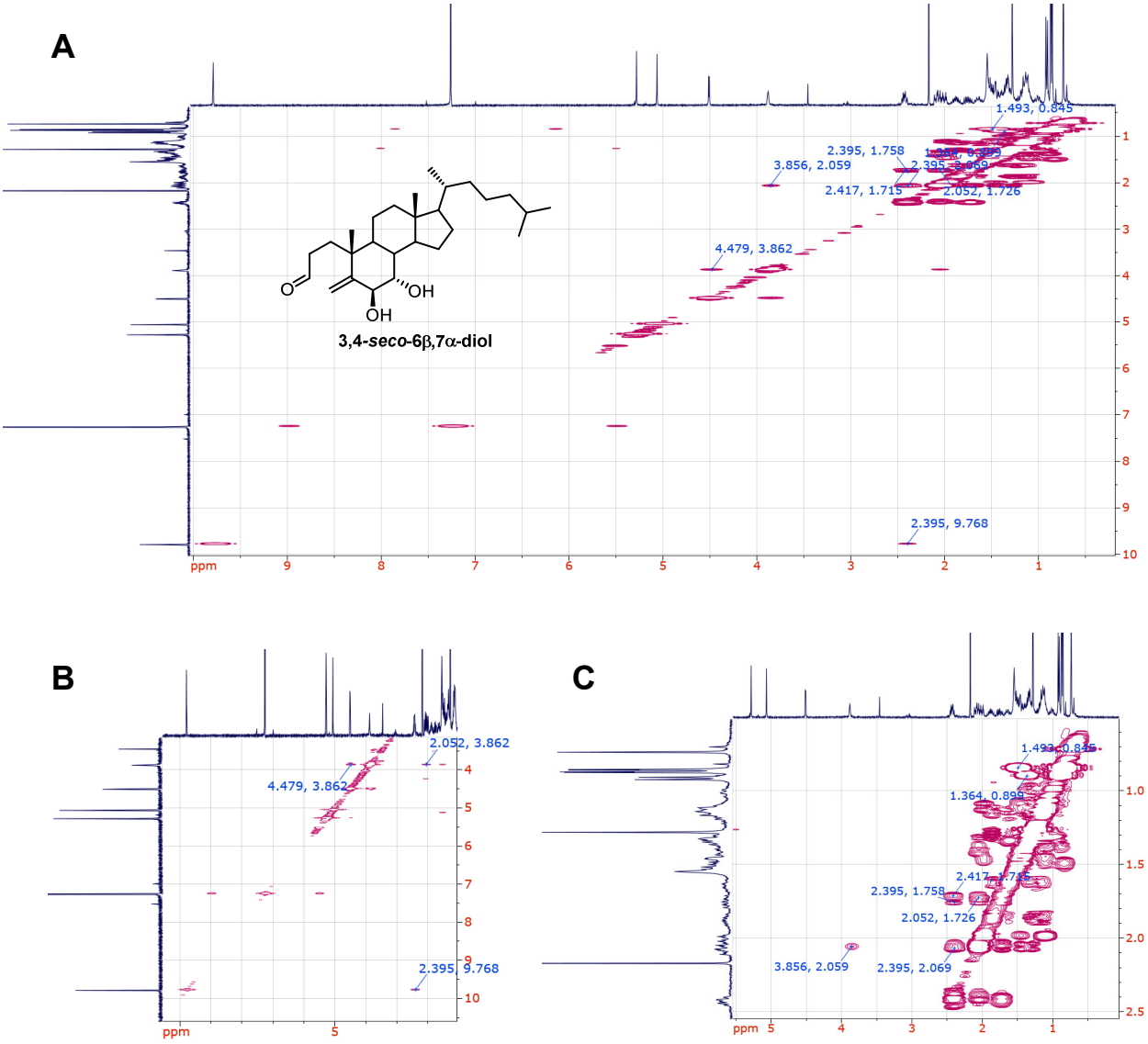

Figure 3.29 ^{1}H-^{1}H COSY spectra of 3,4-*seco*-6β,7α-diol (**A**) and expansions of 4.0-6.0 x 3.0-10.0 ppm (**B**) and 0.0-5.5 x 0.5-2.5 ppm (**C**).

^{1}H-^{13}C HSQC (600 MHz, 151 MHz, $CDCl_3$)

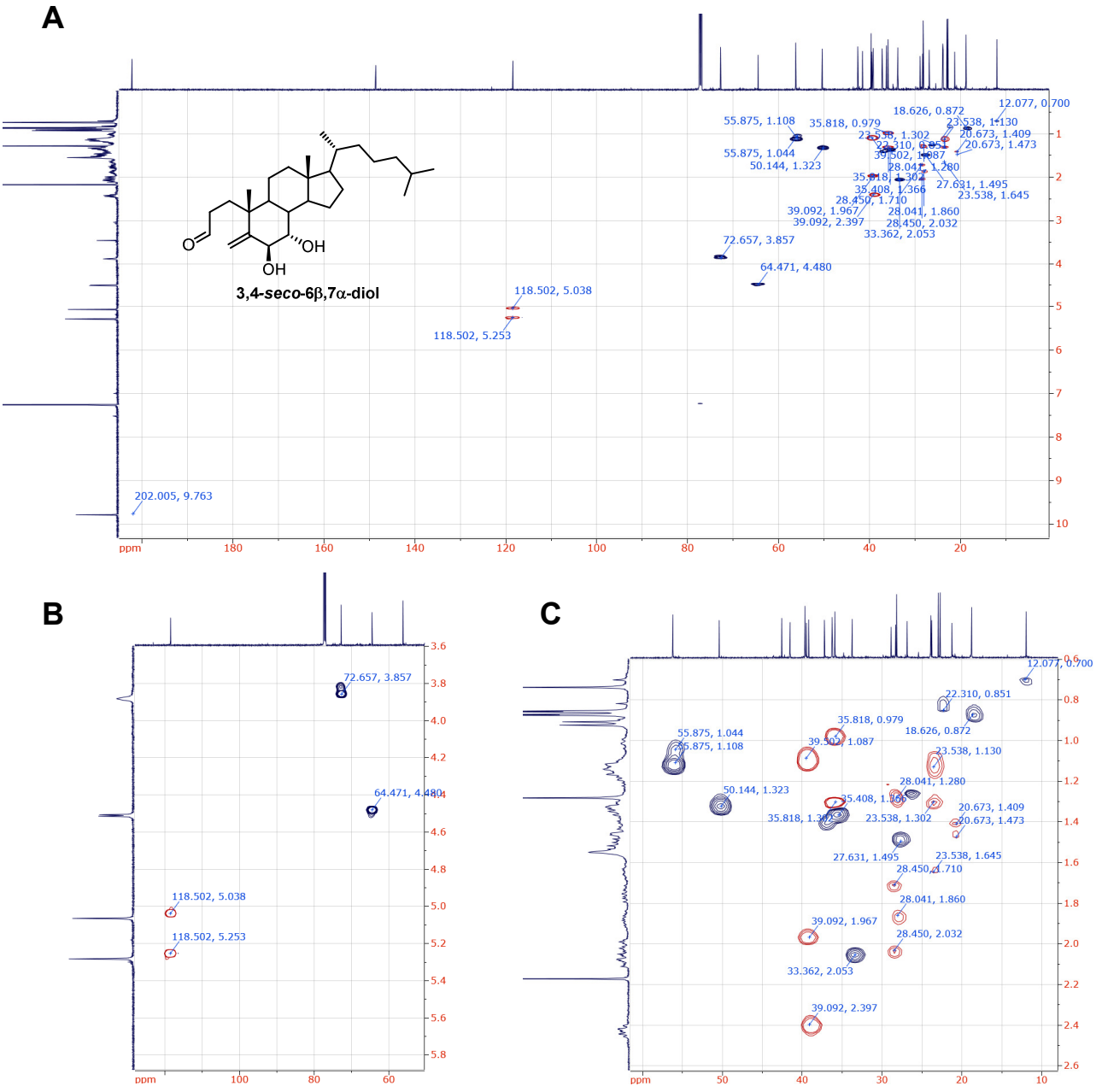

Figure 3.30 ^{1}H-^{13}C HSQC spectra of 3,4-*seco*-6β,7α-diol (**A**) and expansions of 50-130 x 3.6-5.9 ppm (**B**) and 10-60 x 0.6-2.6 ppm (**C**).

^{1}H-^{13}C HMBC (600 MHz, 151 MHz, $CDCl_3$)

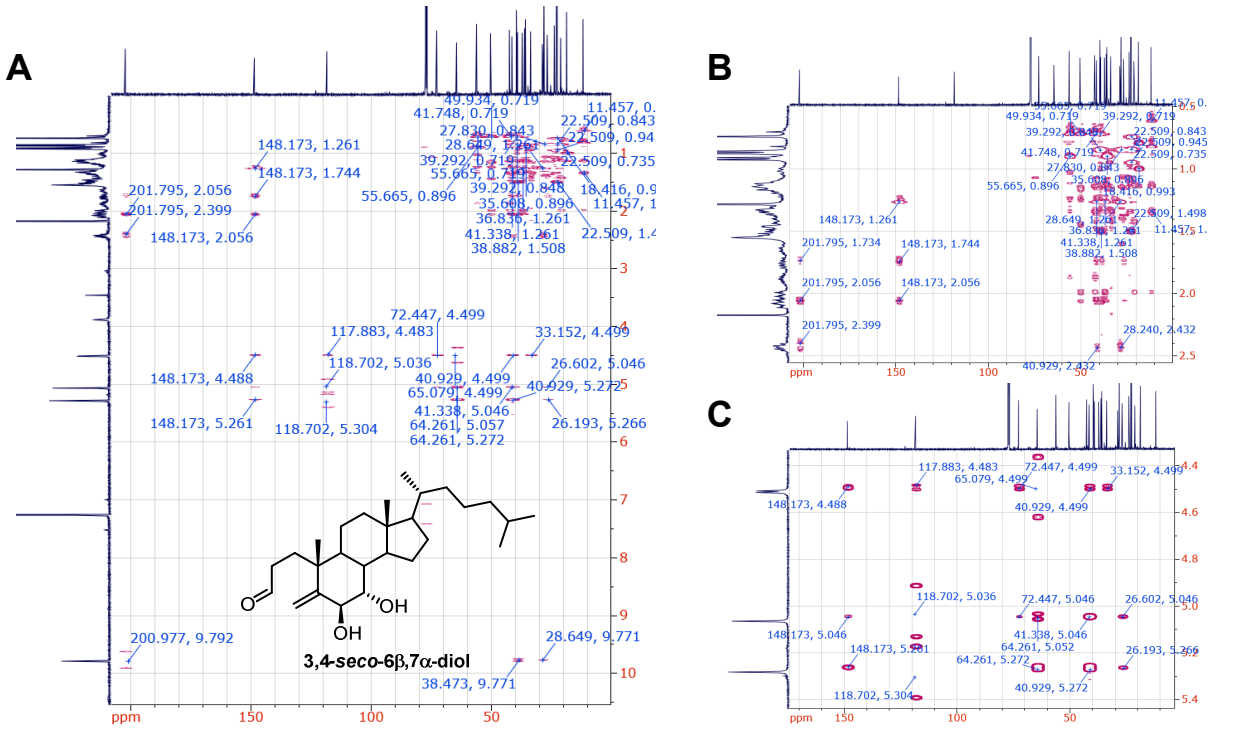

Figure 3.31 ^{1}H-^{13}C HMBC spectra of 3,4-*seco*-6β,7α-diol (**A**) and expansions of 0-200 x 0.5-2.5 ppm (**B**) and 0-175 x 4.4-5.4 ppm (**C**).

^{1}H-^{13}C H2BC (600 MHz, 151 MHz, $CDCl_3$)

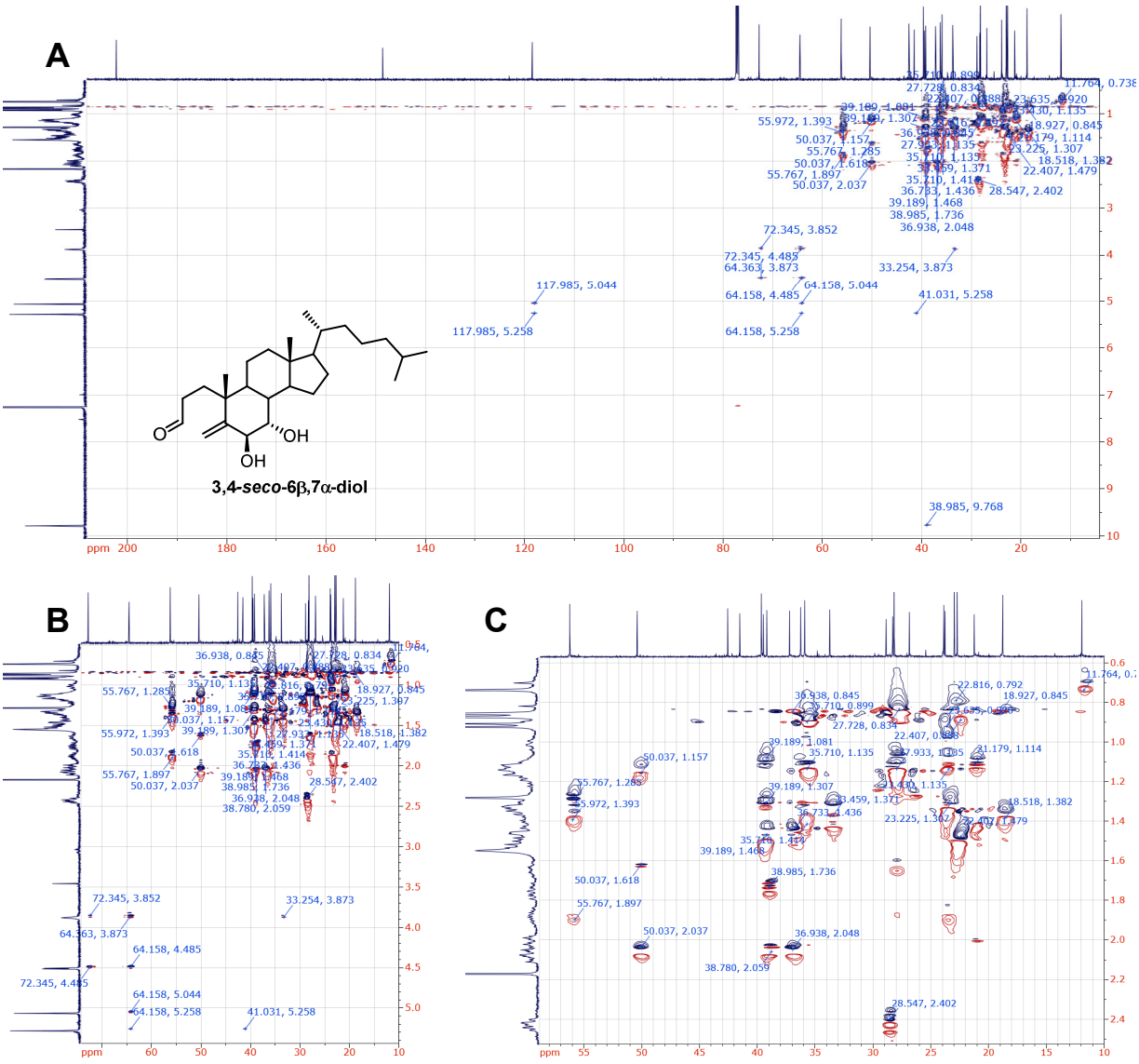

Figure 3.32 ^{1}H-^{13}C HMBC spectra of 3,4-*seco*-6β,7α-diol (**A**) and expansions of 10-70 x 0.5-5.5 ppm (**B**) and 10-60 x 0.6-2.5 ppm (**C**).

^{1}H-^{1}H NOESY (600 MHz, $CDCl_3$)

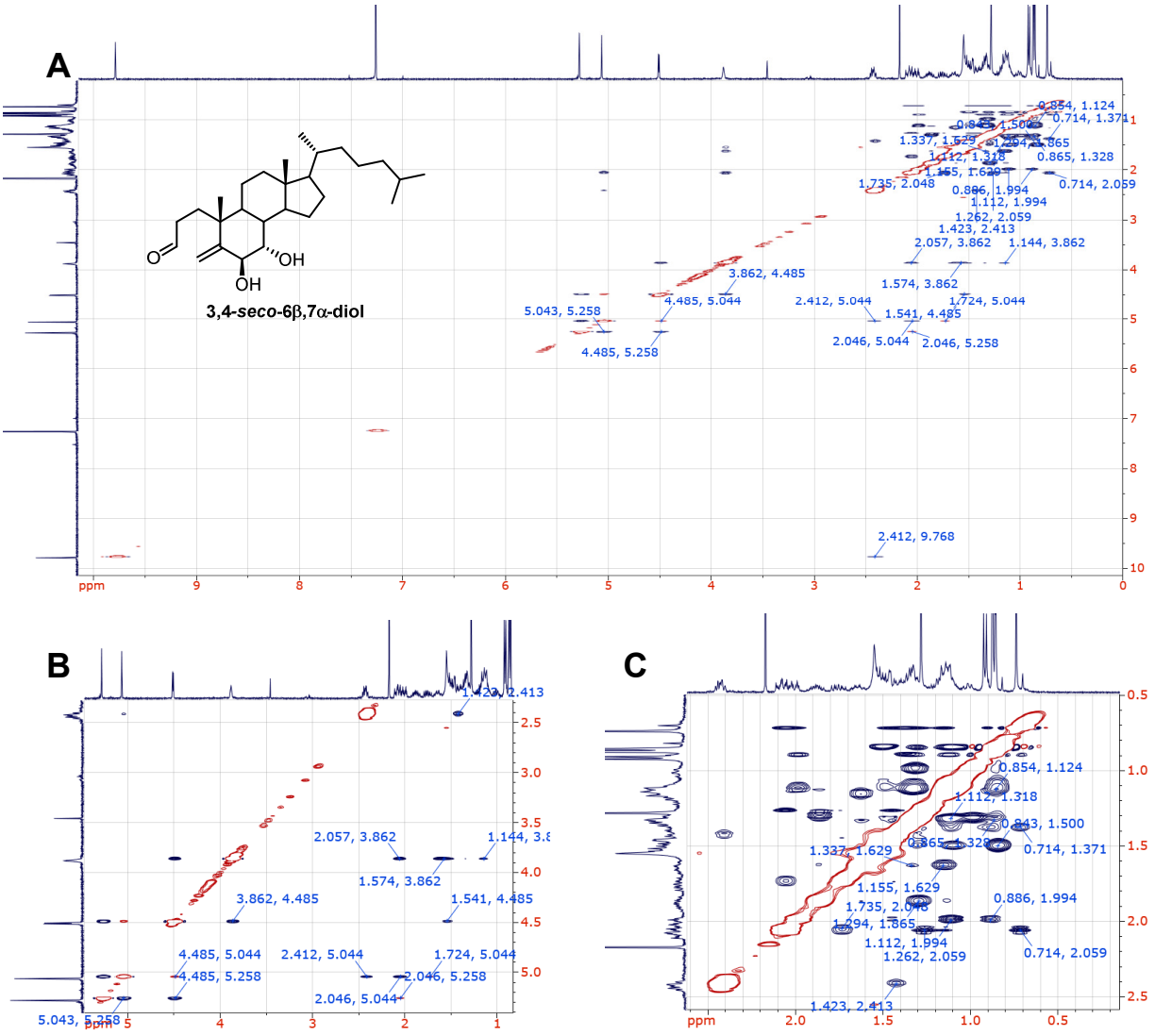

Figure 3.33 ^{1}H-^{1}H COSY spectra of 3,4-*seco*-6β,7α-diol (**A**) and expansions of 1.0-5.5 x 2.0-5.5 ppm (**B**) and 0.0-2.5 x 0.5-2.5 ppm (**C**).

3.7.2 NMR Spectra of d_4-cholesterol, d_4-cholesterol-7α-OOH, and d_4-3,4-seco-6β,7α-diol

^{1}H NMR (400 MHz, $CDCl_3$)

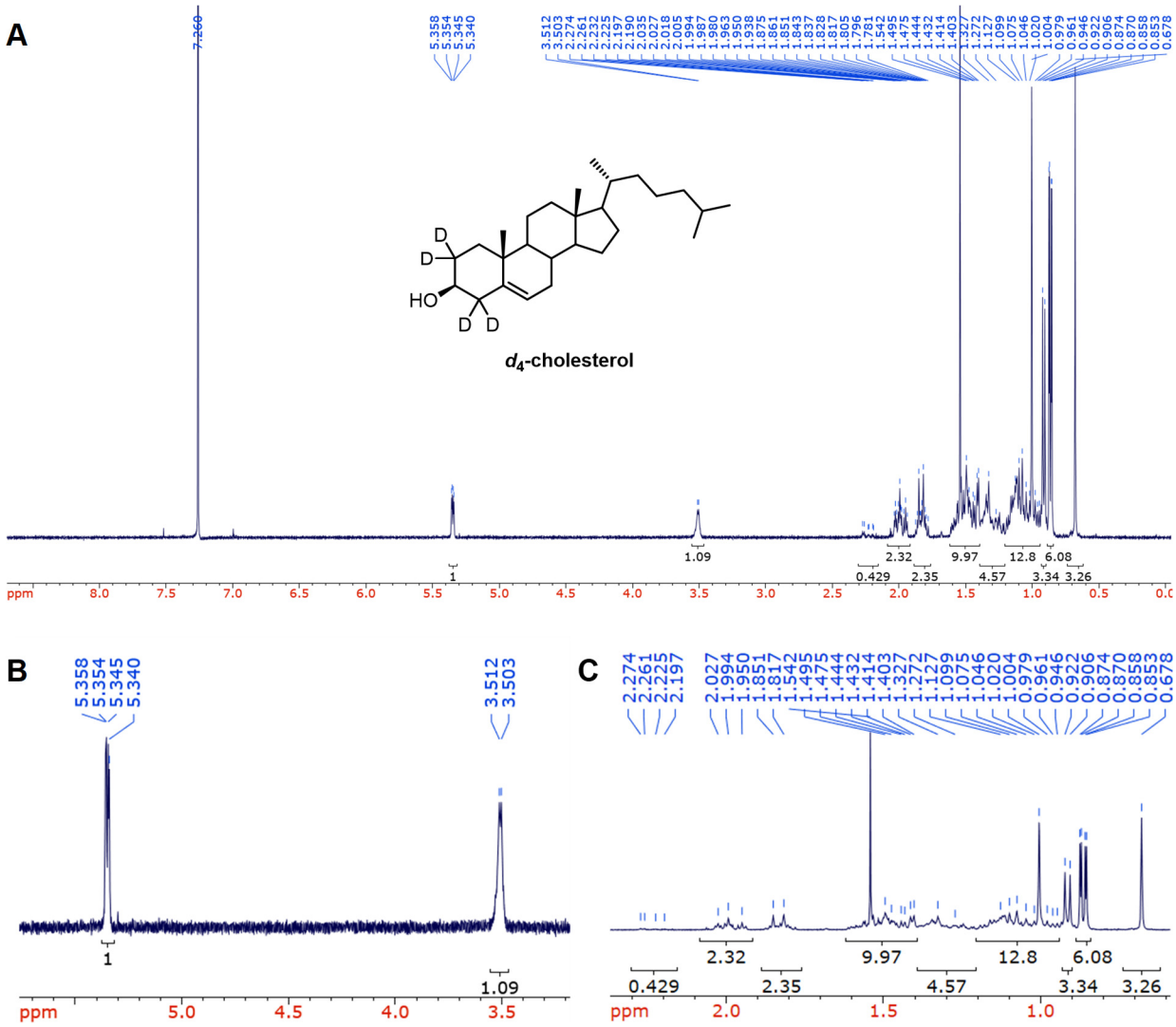

Figure 3.34 ^{1}H NMR spectrum of 2,2,4,4-d_4-cholesterol (**A**) and expansions of 3.0-6.5 ppm (**B**) and 0.5-2.5 ppm (**C**).

^{13}C NMR (101 MHz, $CDCl_3$)

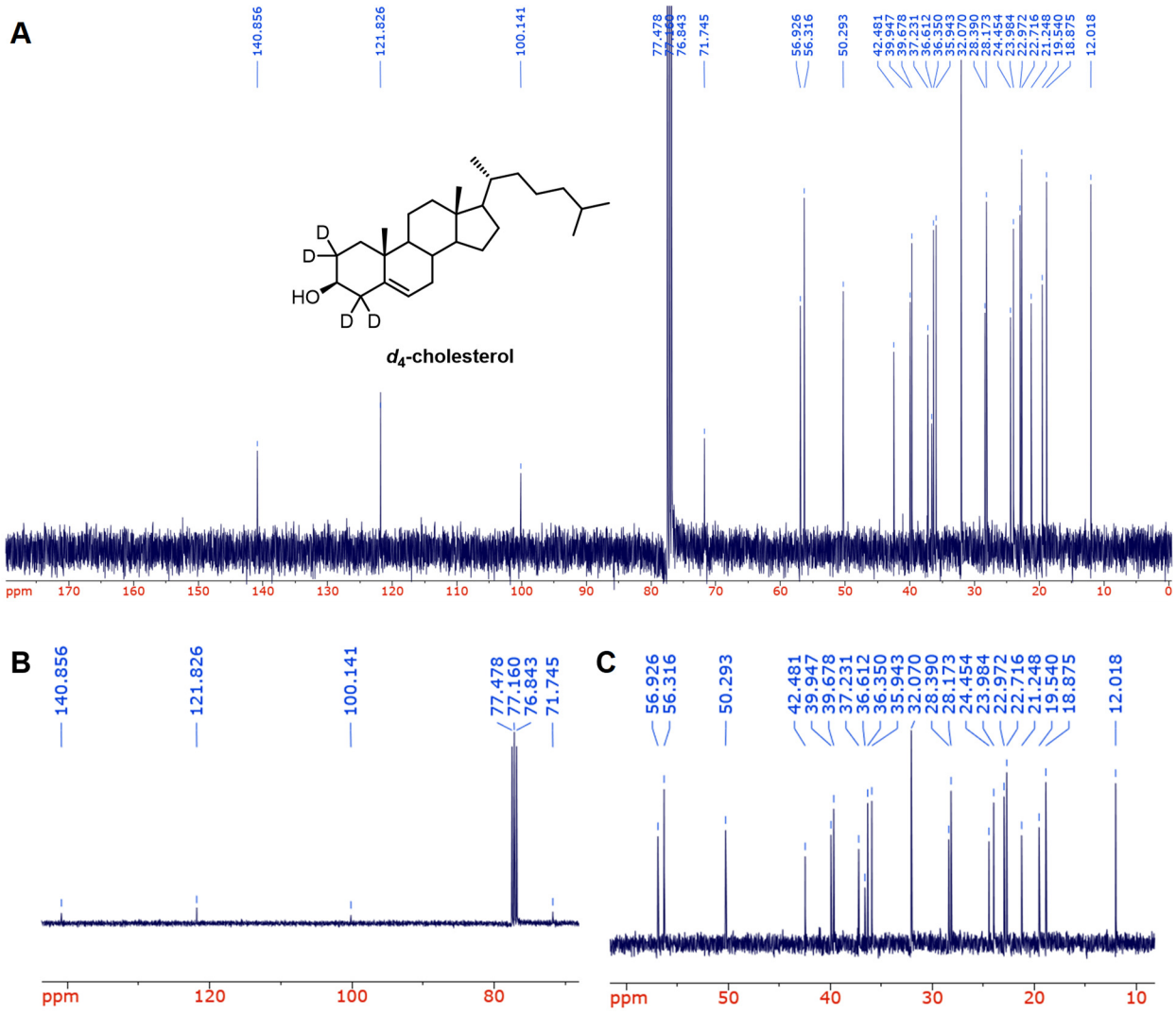

Figure 3.35 ^{13}C NMR spectrum of 2,2,4,4-d_4-cholesterol (**A**) and expansions of 70-145 ppm (**B**) and 10-60 ppm (**C**).

^{1}H NMR (400 MHz, $CDCl_3$)

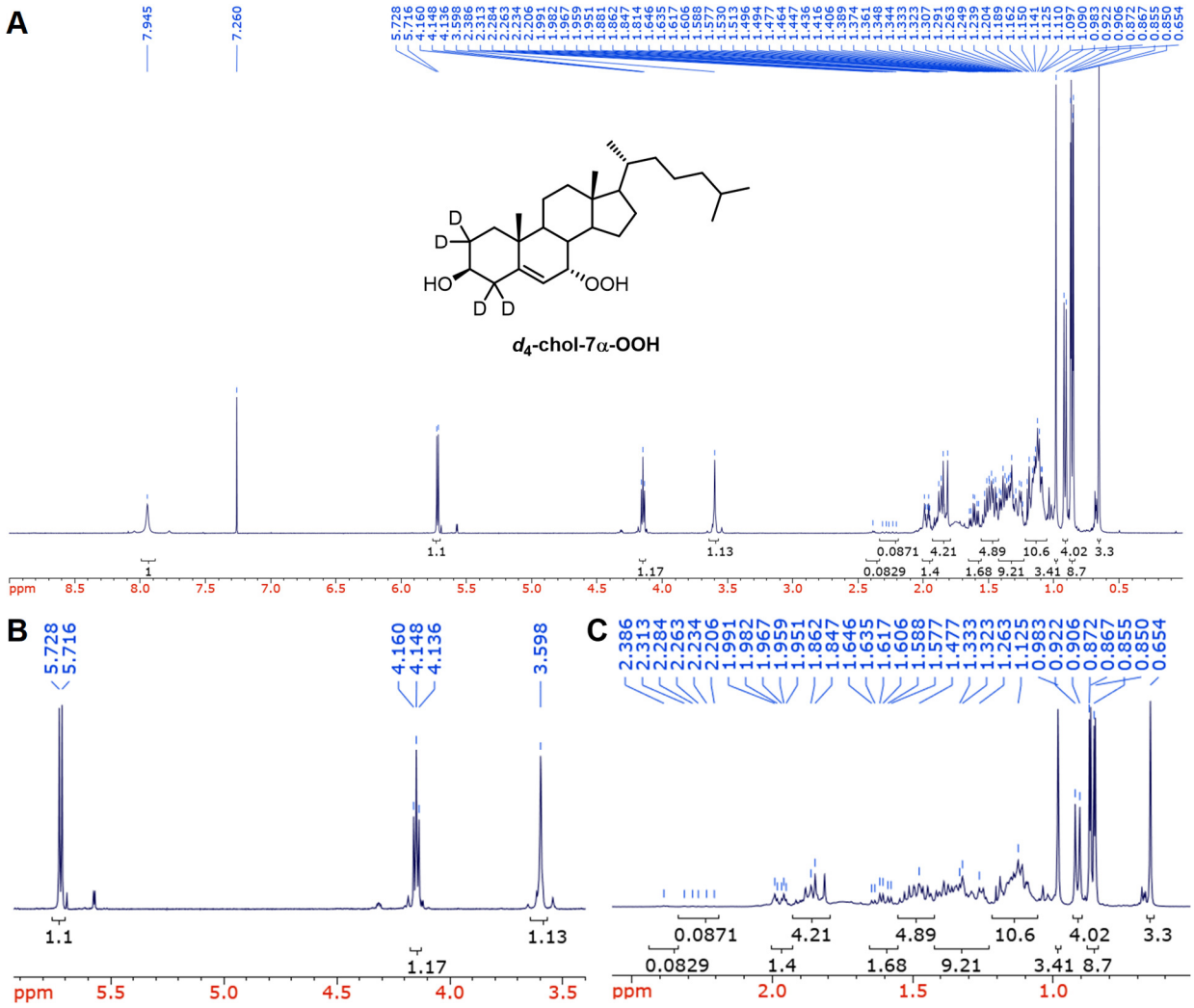

Figure 3.36 ^{1}H NMR spectrum of 2,2,4,4-d_4-chol-7α-OOH (**A**) and expansions of 3.5-6.0 ppm (**B**) and 0.0-3.0 ppm (**C**).

^{13}C NMR (101 MHz, $CDCl_3$)

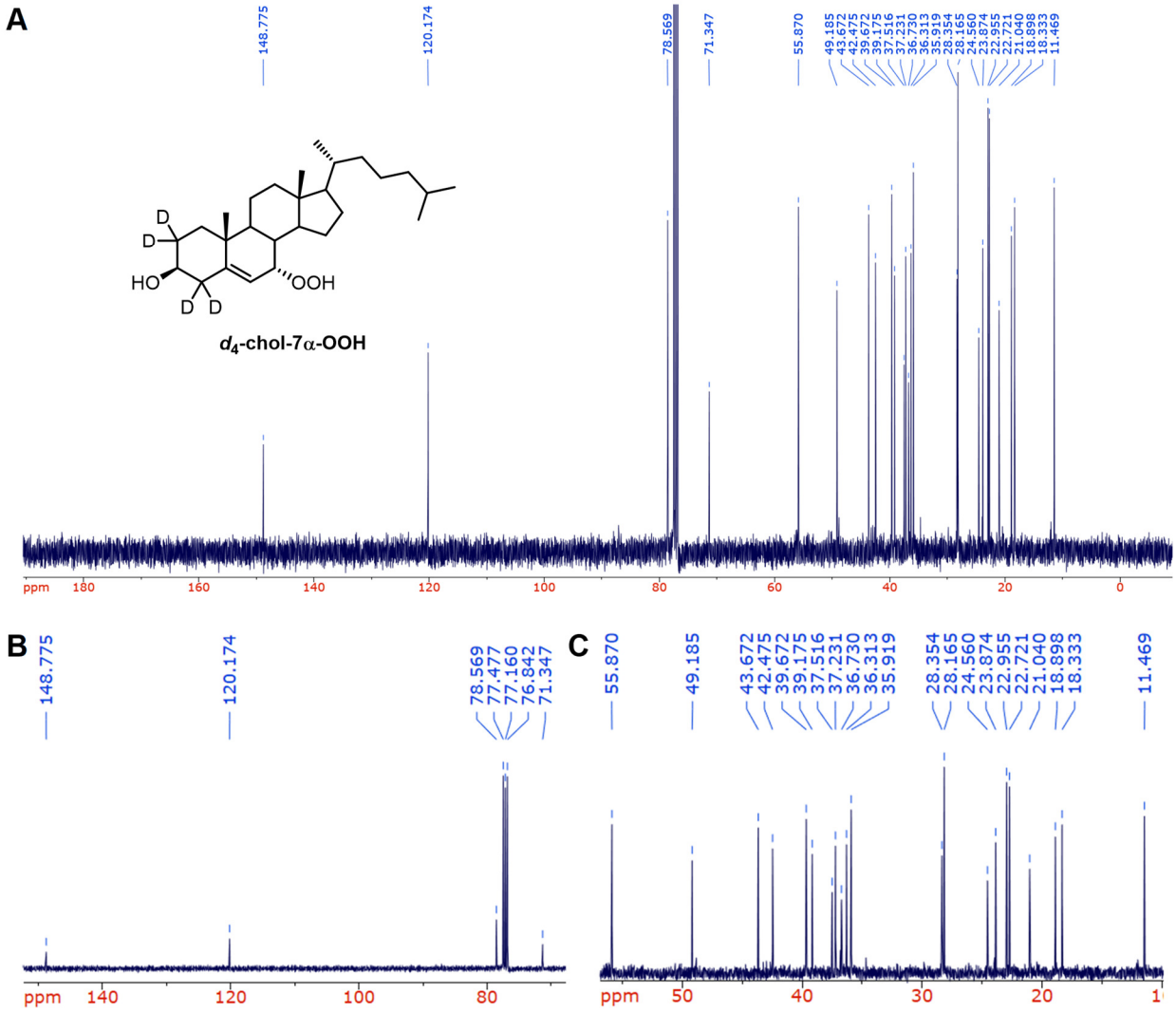

Figure 3.37 ^{13}C NMR spectrum of 2,2,4,4-d_4-chol-7α-OOH (**A**) and expansions of 70-150 ppm (**B**) and 10-60 ppm (**C**).

^{1}H NMR (400 MHz, $CDCl_3$)

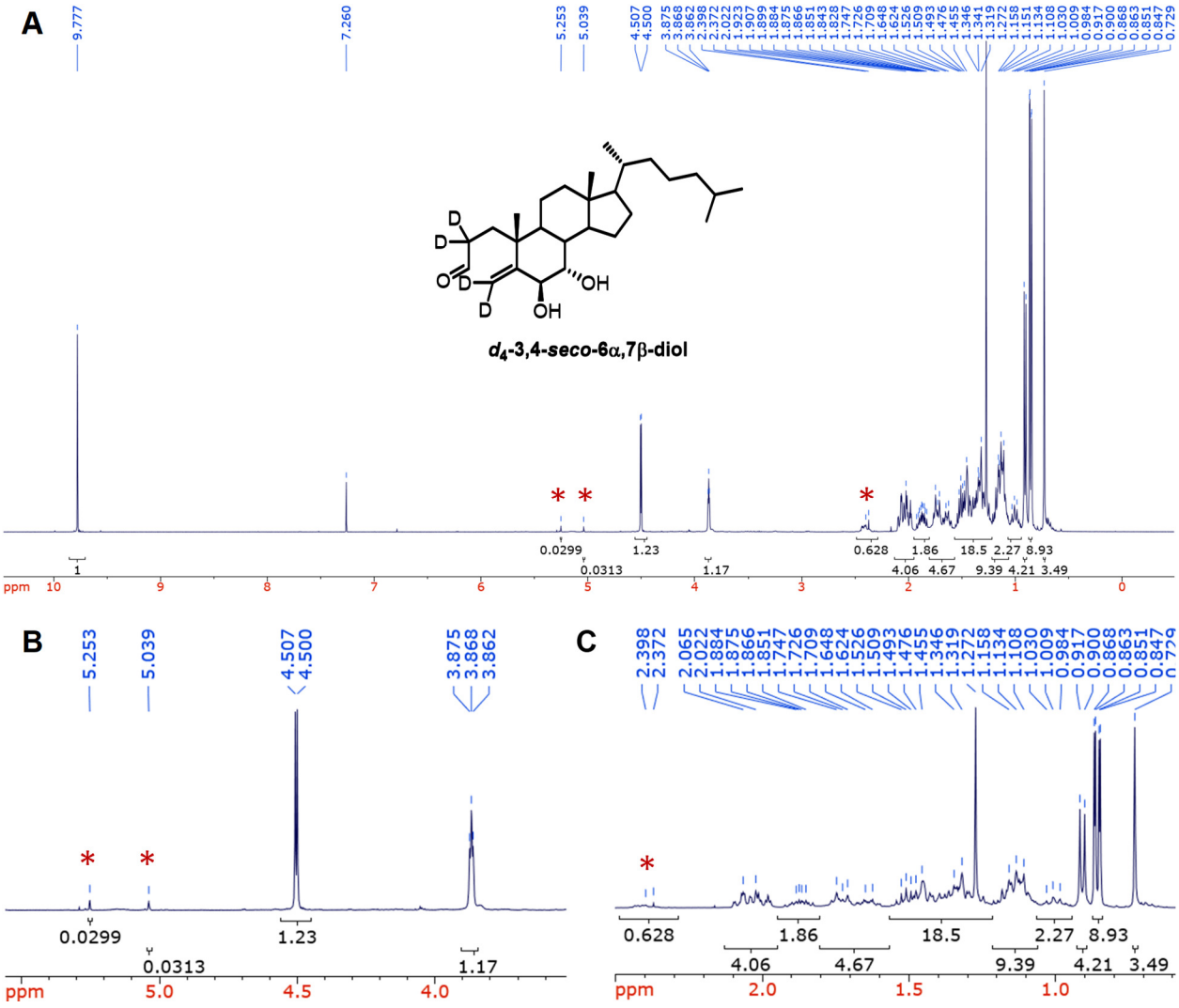

Figure 3.38 ^{1}H NMR spectrum of d_4-3,4-*seco*-6α,7β-diol (**A**) and expansions of 3.5-5.5 ppm (**B**) and 0.5-2.5 ppm (**C**). Peaks corresponding to residual protiated compound are indicated with an asterisk (*).

^{13}C NMR (101 MHz, $CDCl_3$)

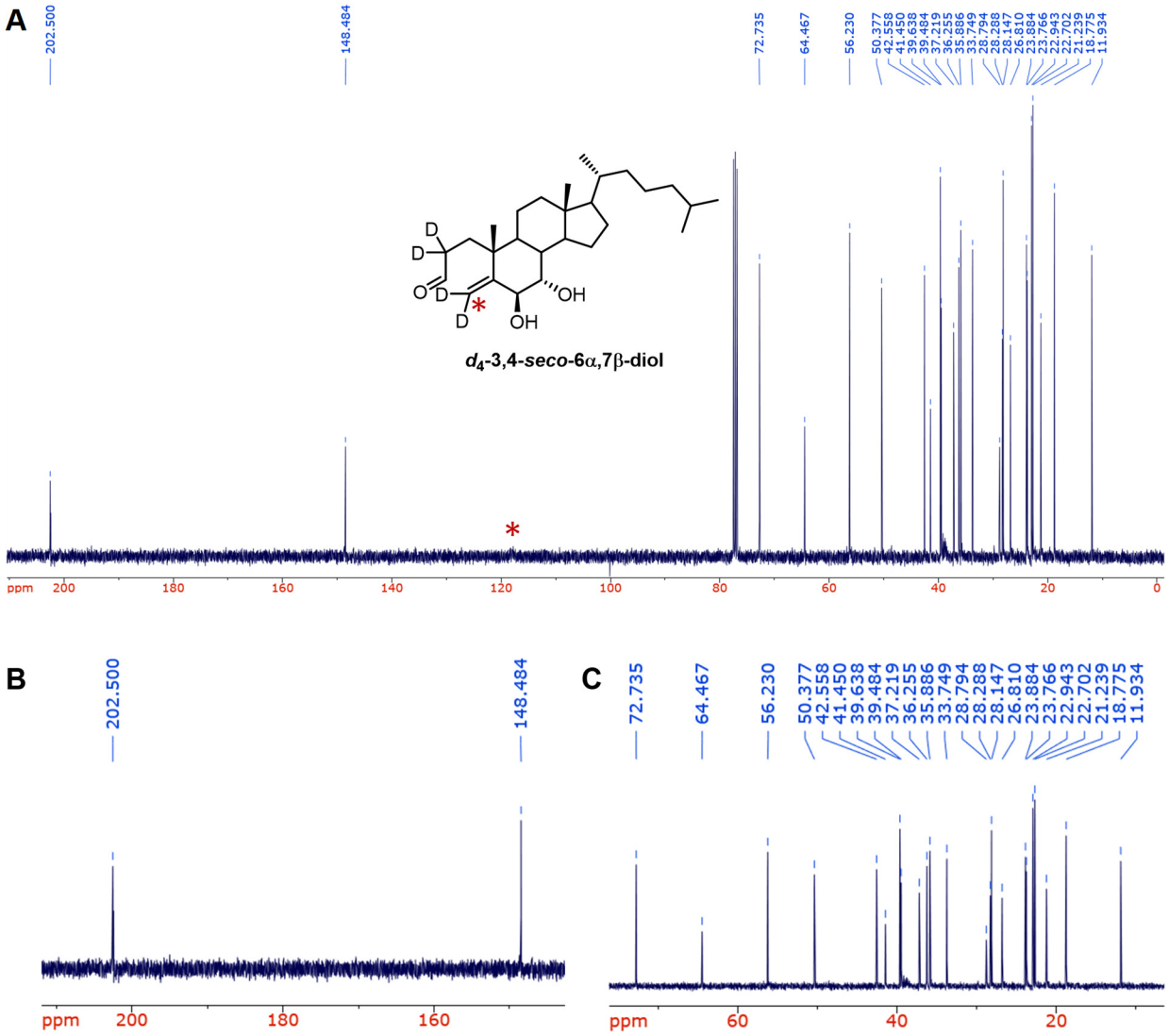

Figure 3.39 ^{13}C NMR spectrum of d_4-3,4-*seco*-6α,7β-diol (**A**) and expansions of 140-210 ppm (**B**) and 10-75 ppm (**C**). The peak corresponding to the exomethylene is indicated with an asterisk (*), however, resolution with acquired material was too low to resolve the C-D coupling of the quintet.

3.7.3 Characterization Data for Cholesterol-5α- and 5β-hydroxy-6α,7α-epoxide

^{1}H NMR (400 MHz, $CDCl_3$)

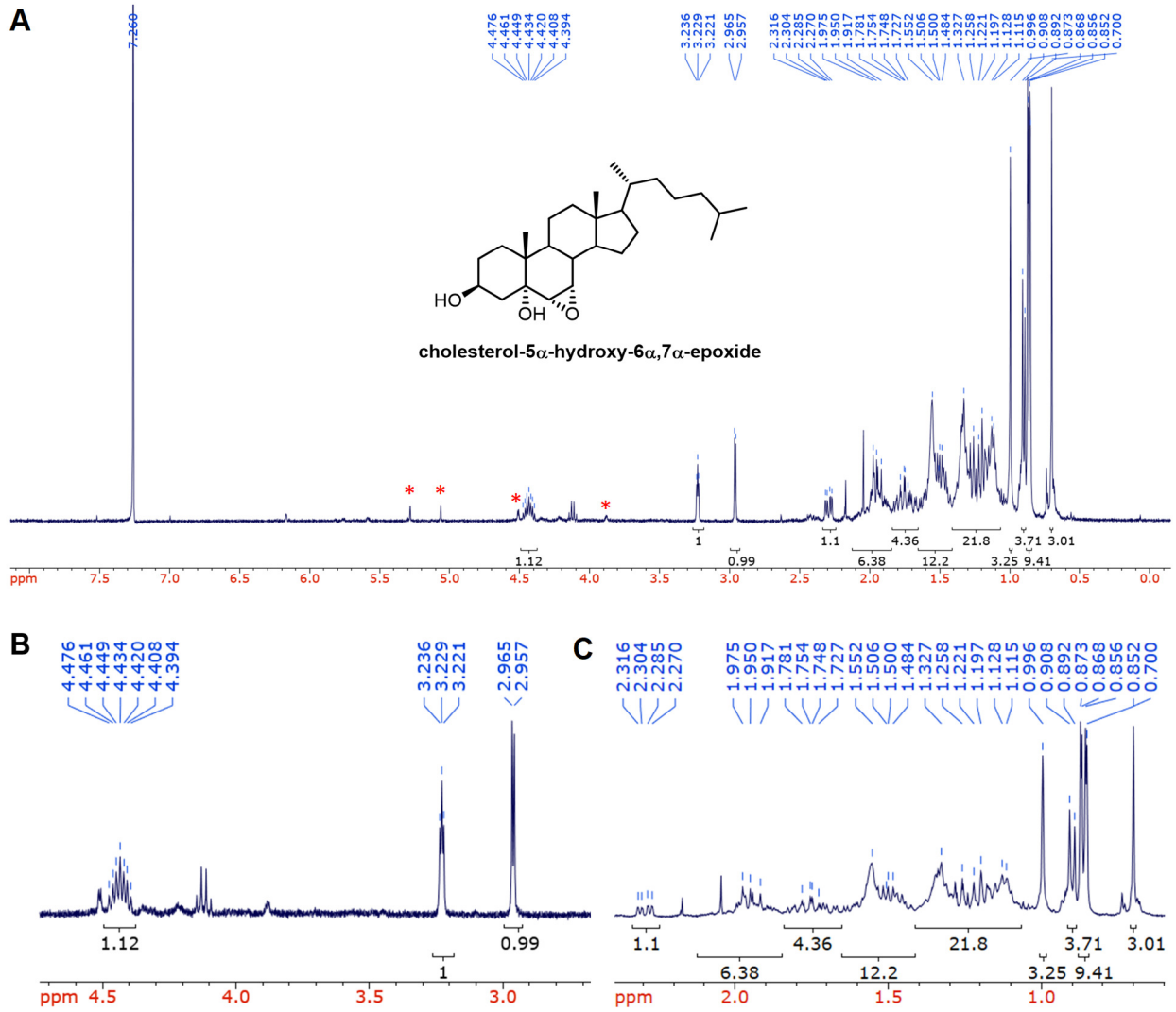

Figure 3.40 ^{1}H NMR spectrum of cholesterol-5α-hydroxy-6α,7α-epoxide (**A**) and expansions of 2.5-4.7 ppm (**B**) and 0.5-2.5 ppm (**C**).

^{13}C NMR (101 MHz, $CDCl_3$)

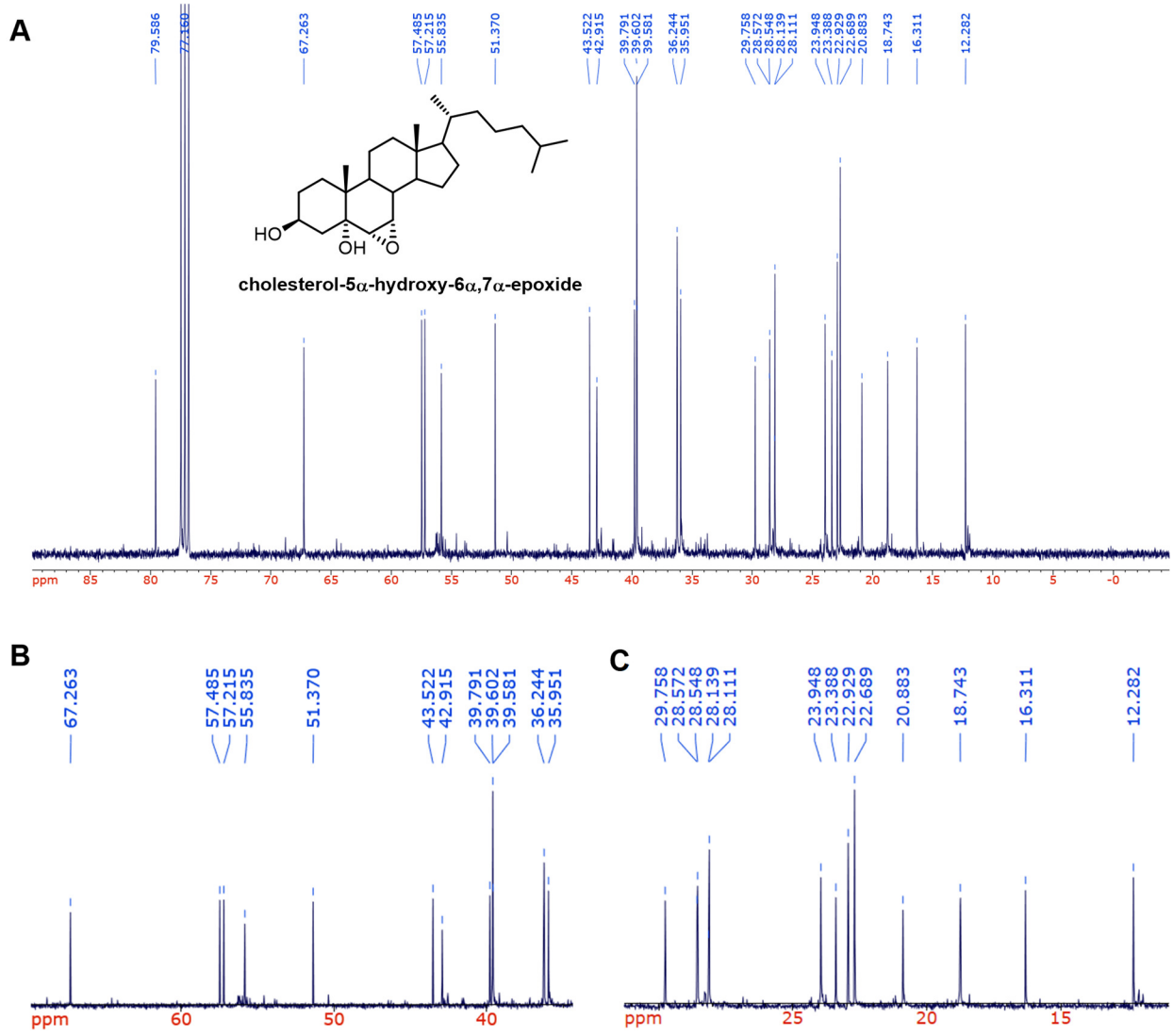

Figure 3.41 ^{13}C NMR spectrum of cholesterol-5α-hydroxy-6α,7α-epoxide (**A**) and expansions of 35.0-70.0 ppm (**B**) and 10.0-30.0 ppm (**C**).

^{1}H NMR (400 MHz, $CDCl_3$)

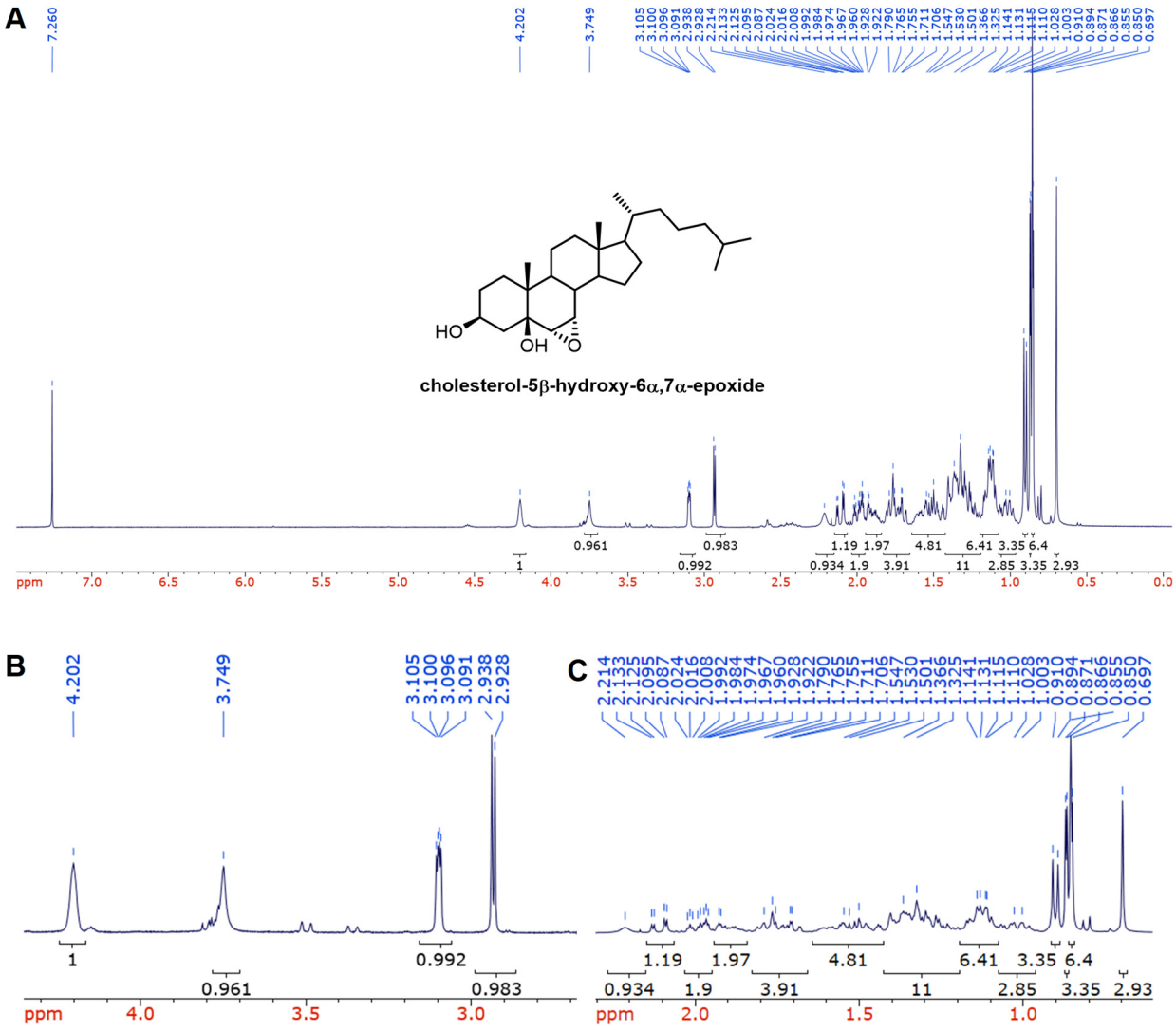

Figure 3.42 ^{1}H NMR spectrum of cholesterol-5β-hydroxy-6α,7α-epoxide (**A**) and expansions of 2.5-4.5 ppm (**B**) and 0.5-2.5 ppm (**C**).

^{13}C NMR (101 MHz, $CDCl_3$)

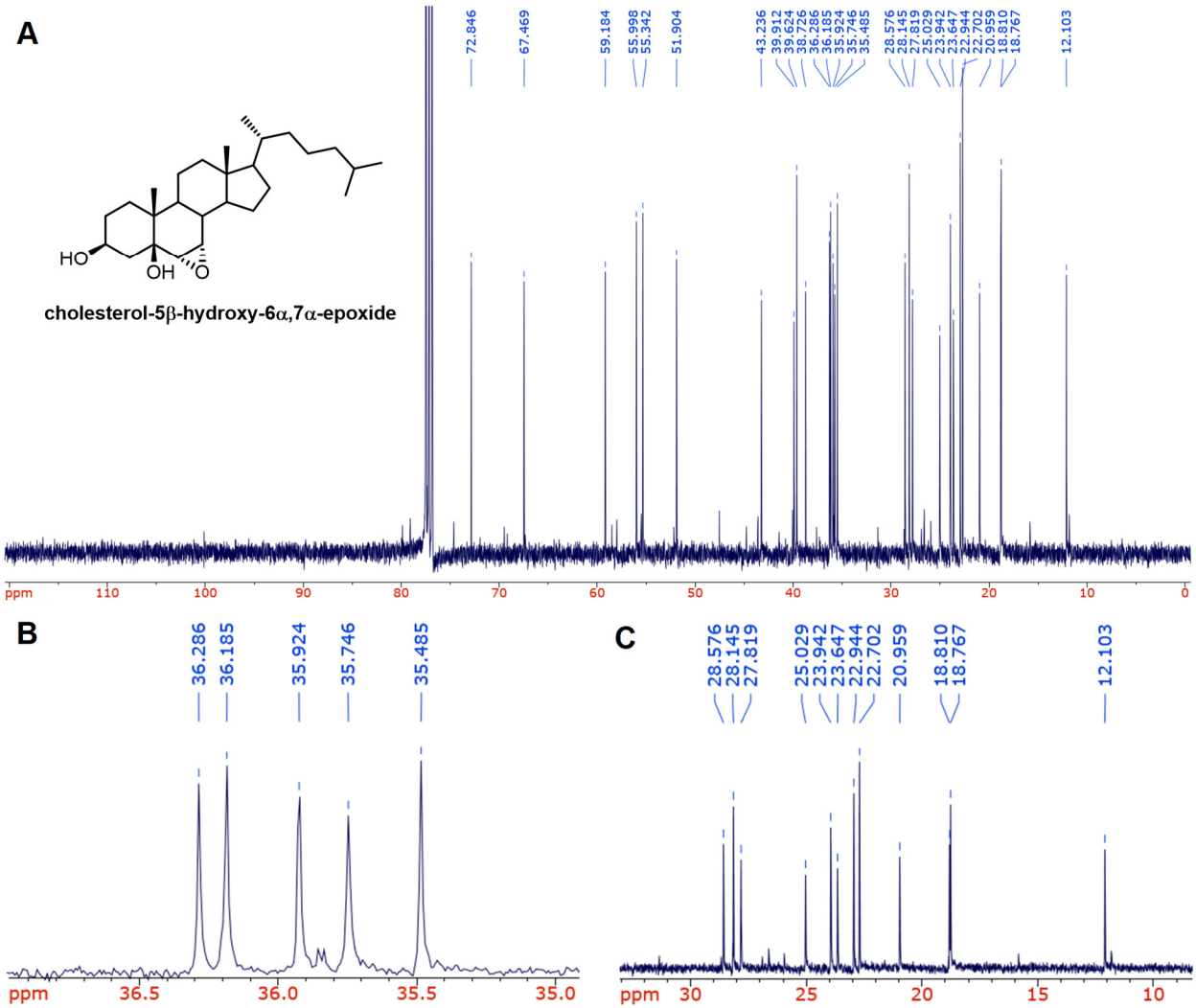

Figure 3.43 ^{13}C NMR spectrum of cholesterol-5β-hydroxy-6α,7α-epoxide (**A**) and expansions of 35.0-37.0 ppm (**B**) and 5.0-35.0 ppm (**C**).

Table 3.1 X-ray crystal data and structure refinement for chol-5β-hydroxy-6α,7α-epoxide.

Identification code	shelx	
Empirical formula	C28 H50 O4	
Formula weight	450.68	
Temperature	296(2) K	
Wavelength	0.71073 Å	
Crystal system	Orthorhombic	
Space group	P 21 21 2	
Unit cell dimensions	a = 19.41(2) Å	α = 90°
	b = 36.04(4) Å	β = 90°
	c = 7.560(9) Å	γ = 90°
Volume	5289(10) $Å^3$	
Z	8	
Density (calculated)	1.132 Mg/m^3	
Absorption coefficient	0.073 mm^{-1}	
F(000)	2000	
Crystal size	0.665 x 0.117 x 0.068 mm^3	
Theta range for data collection	1.191 to 25.249°.	
Index ranges	-23<=h<=21, -34<=k<=43, -9<=l<=9	
Reflections collected	32131	
Independent reflections	9457 [R(int) = 0.1870]	
Completeness to theta = 25.242°	99.7 %	
Refinement method	Full-matrix least-squares on F^2	
Data / restraints / parameters	9457 / 0 / 592	
Goodness-of-fit on F^2	1.070	
Final R indices [I>2sigma(I)]	R1 = 0.0938, wR2 = 0.2160	
R indices (all data)	R1 = 0.2611, wR2 = 0.3380	
Absolute structure parameter	-1.6(10)	
Extinction coefficient	n/a	
Largest diff. peak and hole	0.266 and -0.238 $e.Å^{-3}$	

3.7.4 Characterization Data for Dinitrophenylhydrazine Derivatized Secosterol Species

^{1}H NMR (400 MHz, $CDCl_3$)

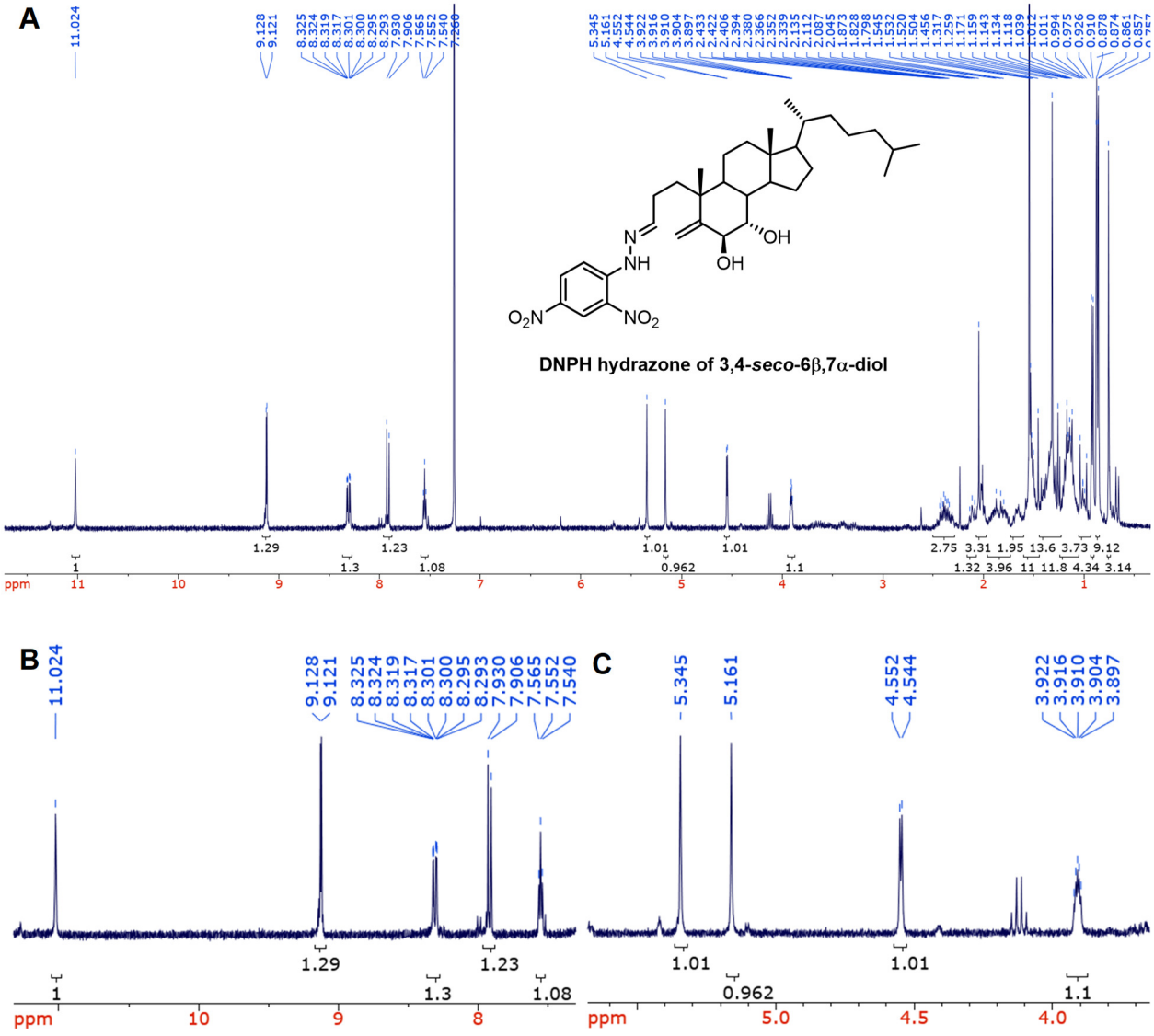

Figure 3.44 ^{1}H NMR spectrum of the DNPH hydrazone of 3,4-*seco*-6β,7α-diol (**A**) and expansions of 7.5-11.0 ppm (**B**) and 3.5-6.0 ppm (**C**).

^{13}C NMR (151 MHz, $CDCl_3$)

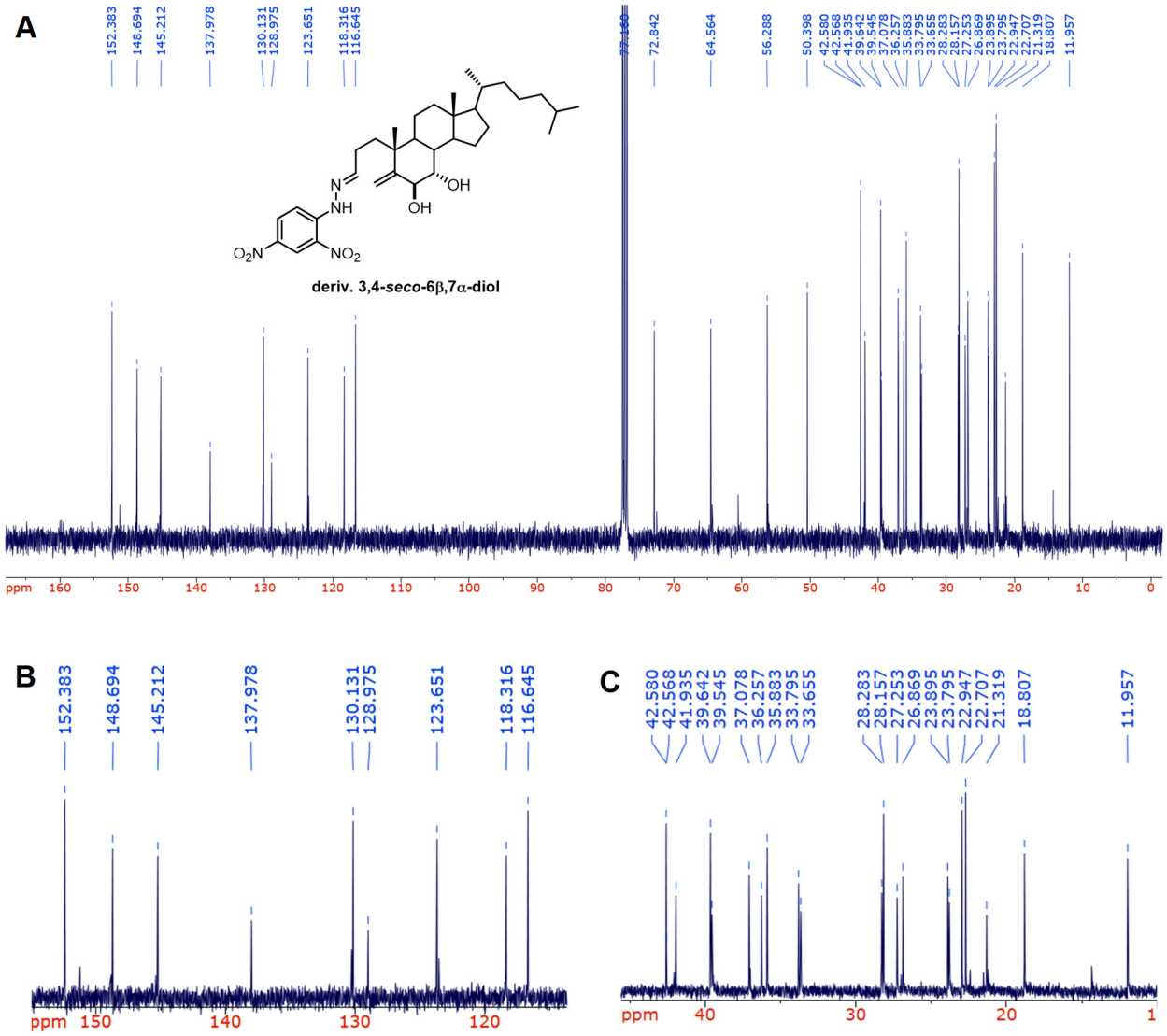

Figure 3.45 ^{13}C NMR spectrum of the DNPH hydrazone of 3,4-*seco*-6β,7α-diol (**A**) and expansions of 115-155 ppm (**B**) and 10-45 ppm (**C**).

^{1}H NMR (600 MHz, $CDCl_3$)

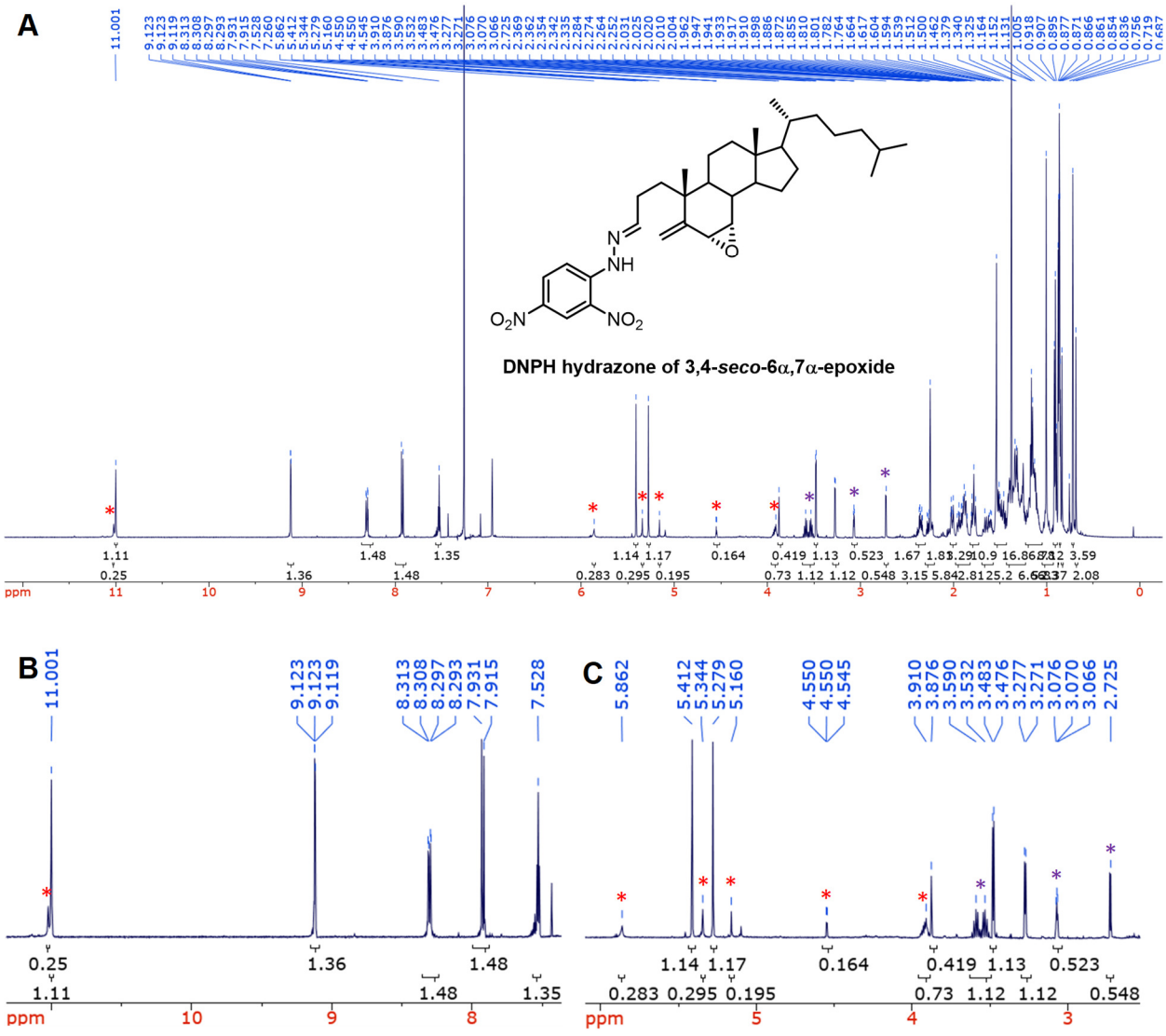

Figure 3.46 ^{1}H NMR spectrum of the DNPH hydrazone of 3,4-*seco*-6α,7α-epoxide (**A**) and expansions of 7.5-11.0 ppm (**B**) and 2.5-6.0 ppm (**C**). DNPH hydrazone of 3,4-*seco*-6β,7α-diol is indicated with red asterisks (*) and the proposed 5β-ethoxy-6α,7α-epoxide is indicated with purple asterisks (*).

^{13}C NMR (151 MHz, $CDCl_3$)

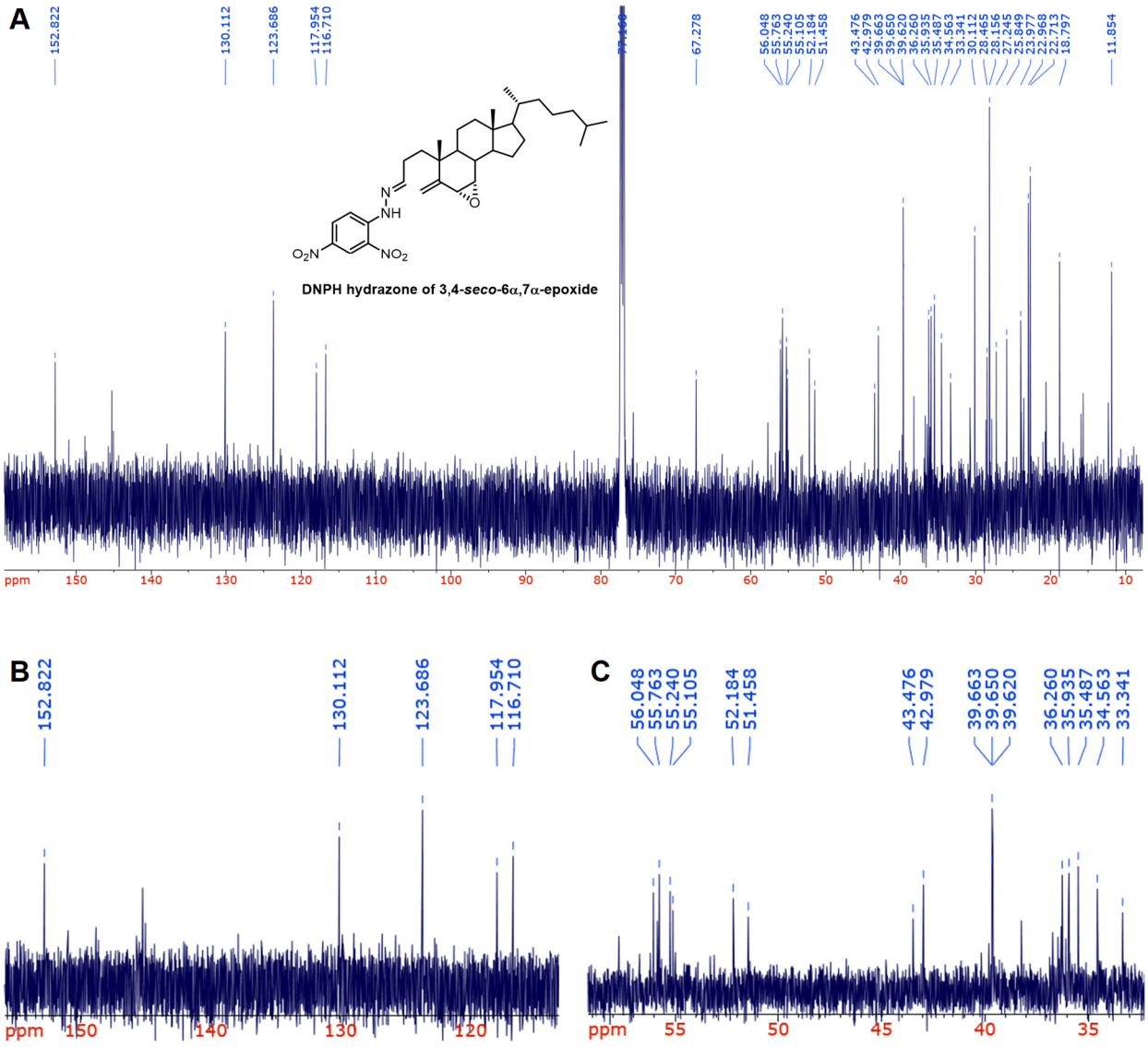

Figure 3.47 ^{13}C NMR spectrum of the DNPH hydrazone of 3,4-*seco*-6α,7α-epoxide (**A**) and expansions of 115-155 ppm (**B**) and 30-60 ppm (**C**). Peaks proposed to correspond to the DNPH hydrazone of 3,4-*seco*-6α,7α-epoxide are picked whilst the contaminants identified in **Figure 3.46** are left unpicked.

^{1}H NMR (600 MHz, $CDCl_3$)

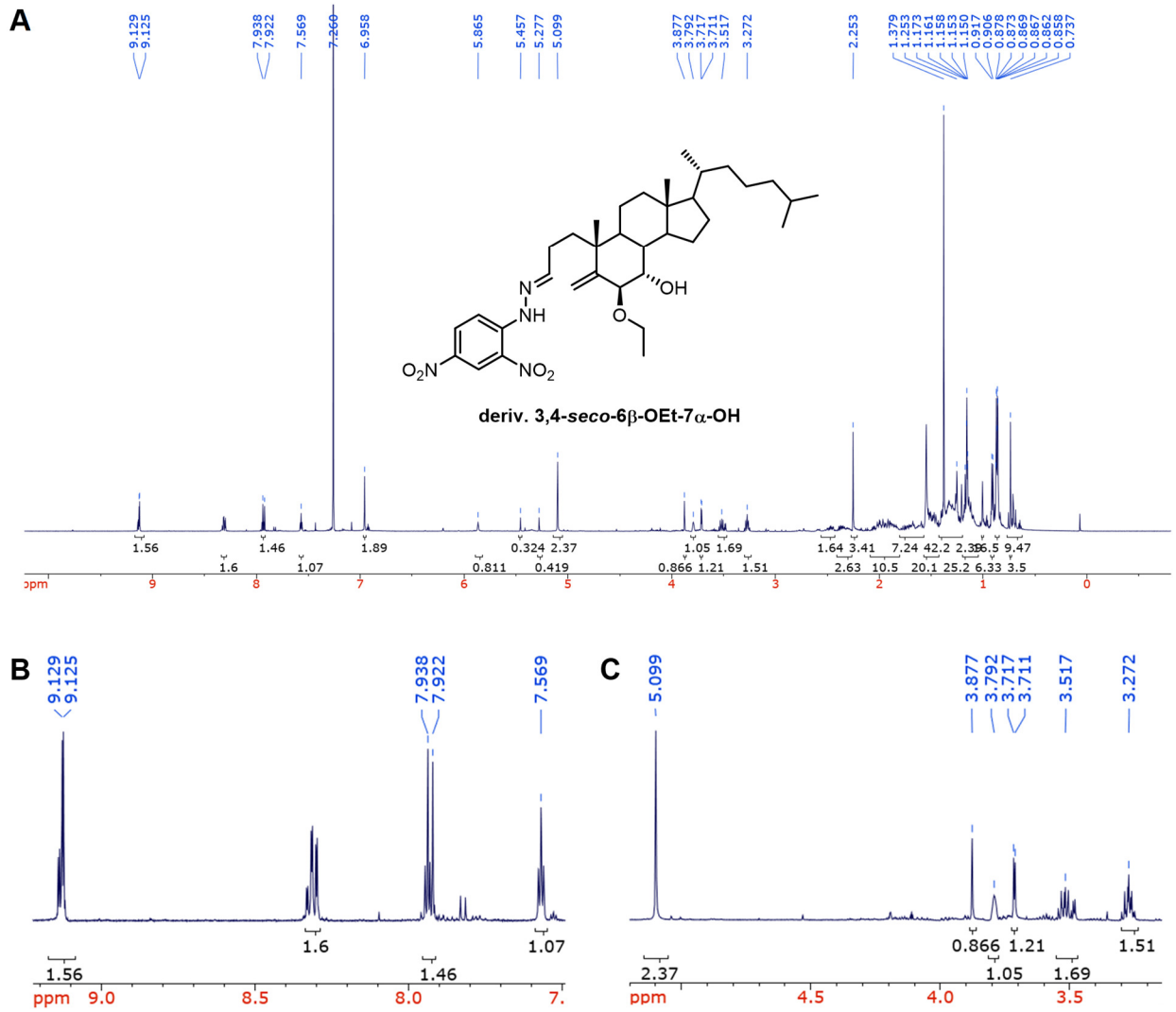

Figure 3.48 ^{1}H NMR spectrum of the DNPH hydrazone of 3,4-*seco*-6β-OEt-7α-OH (**A**) and expansions of 7.5-9.5 ppm (**B**) and 3.0-5.0 ppm (**C**).

^{13}C NMR (151 MHz, $CDCl_3$)

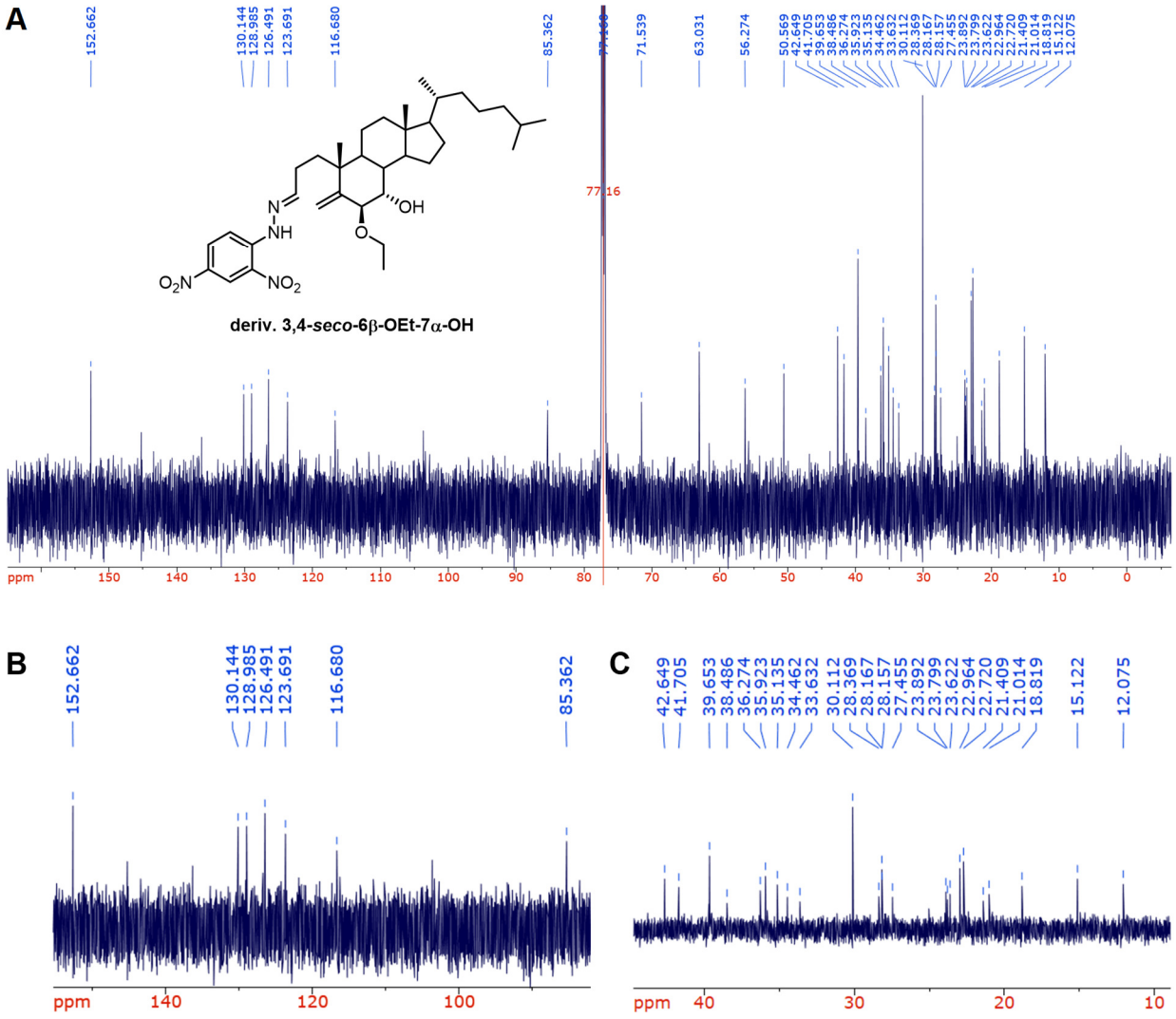

Figure 3.49 ^{13}C NMR spectrum of the DNPH hydrazone of 3,4-*seco*-6β-OEt-7α-OH (**A**) and expansions of 95-150 ppm (**B**) and 10-45 ppm (**C**).